

CLAY FLUID INTERACTIONS IN MONTMORILLONITE SWELLING CLAYS: A
MOLECULAR DYNAMICS AND EXPERIMENTAL STUDY

A Thesis
Submitted to the Graduate Faculty
of the
North Dakota State University
of Agriculture and Applied Science

By

Md Zillur Rahman Patwary

In Partial Fulfillment
for the Degree of
MASTER OF SCIENCE

Major Department: Civil Engineering

March 2012

Fargo, North Dakota

North Dakota State University
Graduate School

Title

Clay Fluid Interactions in Montmorillonite Swelling Clays:
A Molecular Dynamics and Experimental Study.

By

Md Zillur Rahman Patwary

The Supervisory Committee certifies that this *disquisition* complies with North Dakota State University's regulations and meets the accepted standards for the degree of

MASTER OF SCIENCE
In Civil Engineering

SUPERVISORY COMMITTEE:

Dr. Dinesh Katti

Chair

Dr. Kalpana Katti

Dr. Bernhardt Saini-Eidukat

Dr. Achintya N. Bezbaruah

Approved:

July 06, 2012

Date

Dr. Eakalak Khan

Department Chair

ABSTRACT

Swelling clays cause tremendous amounts of damage to infrastructure. For the effective prevention of detrimental effects of these clays, and to optimize the beneficial properties for industrial applications it is necessary to clearly understand the fundamental mechanisms of swelling of clays.

We studied the effect of fluid polarity on swelling and flow properties of swelling clays using molecular modeling and experimental technique for bridging the molecular level phenomenon of these clays with microstructure change, particle breakdown and macro scale swelling and flow properties. A wide range of fluids (Dielectric Constant 110 to 2.4) were used, those are also commonly present in landfill leachates. We were able to tie the properties of swelling clays at different length scales. Then, we simulated the solvation of clay sheets, studied the effect of discrete charge distribution, contribution of edge charges on swelling clays and discussed some fundamental assumptions associated with double layer theories.

ACKNOWLEDGEMENTS

Among the numerous contributors to this achievement, the person who comes to my mind before anybody else is my advisor, Dr. Dinesh Katti. Without his intellectual efforts and continuous guidance I would have not have reached to this stage of getting my MS degree. Besides academics I have learnt from him innumerable things which will be help guiding in rest of my life. Next, I would like to acknowledge my sincere thanks to my co-advisor, Dr. Kalpana Katti, for her guidance in experiments as well as modeling works and research methods pertaining to my MS. She has been extremely helpful in all respects throughout the period of my master's program. I very much appreciate having the opportunity to work with Dr. Katti's research group.

I thank to Department of Civil Engineering of North Dakota State University for supporting me with teaching and research assistantship. My sincere thanks to Dr. Saini Eidukat and Dr. Achintya Bezbaruah, my thesis supervisory committee members.

I acknowledge Dr. Greg Wettstein of NDSU Center for High Performance Computing (CHPC) for proving constant support for computational resources used in this research. I would also like to acknowledge NCSA-TERAGRID for providing me access to National supercomputer facilities at University of Illinois at Urbana Champaign.

I thank to my group members, Shashindra, Raviprasad, Laxmikanth, Avinash, Chunju, Scott, Anurag and Kristin for being wonderfully cooperative and helpful. I thank to everyone especially Shashindra, Raviprasad and Laxmikanth for helpful discussions.

Finally, I thank my proud family members especially my mother (Shefali Begum) for boundless inspiration, encouragement, sacrifice and blessings.

TABLE OF CONTENTS

ABSTRACT.....	iii
ACKNOWLEDGEMENTS.....	iv
LIST OF TABLES.....	x
LIST OF FIGURES.....	xi
LIST OF ABBREVIATIONS.....	xvi
CHAPTER 1. INTRODUCTION.....	1
1.1 Justification.....	1
1.2 Original Contribution.....	6
1.3 Summary of Literature Review.....	7
1.4 Summary of Chapters.....	7
1.5 References.....	9
CHAPTER 2. LITERATURE REVIEW.....	10
2.1 Clay Mineralogy.....	10
2.2 Structure of Clay Minerals.....	11
2.3 Cation Exchange Capacity.....	15
2.4 Types of Clay Minerals.....	16
2.4.1 Kaolinite.....	16
2.4.2 Pyrophyllite-Talc Group.....	17
2.4.3 Mica-like Clay Minerals.....	17
2.4.3.1 Illite.....	17
2.4.3.2 Vermiculite.....	18
2.4.3.3 Chlorite.....	18

2.4.4 Smectite Minerals.....	19
2.5 Na-MMT Structure.....	23
2.6 Forces in Clay Fluid Colloidal System.....	25
2.6.1 Van der Waals Forces (VDW).....	26
2.6.2 Gravity.....	27
2.7 Polarity and Dielectric Constant.....	27
2.8 References.....	29
CHAPTER 3. MULTI SCALE EXPERIMENTAL AND MODELING TECHNIQUES FOR THE STUDY OF SWELLING CLAYS.....	32
3.1 Introduction.....	32
3.2 Experimental Techniques.....	32
3.2.1 FTIR (Fourier Transform Infrared Spectroscopy).....	32
3.2.1.1 Physical Principles.....	34
3.2.1.2 FTIR Studies on Swelling Clays	36
3.2.2 X-ray Diffraction Technique (XRD).....	39
3.2.3 Microstructure Analysis of Swelling Clay Using Scanning Electron Microscope (SEM).....	42
3.2.4 Macroscale Testing on Clays.....	47
3.2.4.1 Permeability.....	48
3.2.4.2 Triaxial Consolidation Tests of Na-Montmorillonite Clays.....	50
3.3 Modeling Techniques for Study of Swelling Clays.....	55
3.3.1 Discrete Element Models (DEM).....	55
3.3.2 Molecular Dynamics Simulations.....	58
3.3.2.1 Force Fields.....	59

3.3.2.2 Molecular Dynamics.....	63
3.3.3 Molecular Dynamic Study on Swelling Clays.....	65
3.4 References.....	74
CHAPTER 4. EFFECT OF FLUID POLARITY ON PERMEABILITY AND CONSOLIDATION CHARACTERISTICS OF Na-MONTMORILLONITE SWELLING CLAY	80
4.1 Introduction.....	80
4.2 Permeability Measuring Techniques	83
4.3 Types of Permeability Cells.....	84
4.3.1 Rigid Wall Permeameter.....	84
4.3.2 Flexible Wall Permeameter.....	85
4.4 New Integrated Porous Rigid Wall and Flexible Wall Permeameter.....	86
4.5 Permeability Testing Procedure.....	90
4.6 Materials and Method.....	91
4.7 Permeability Test Results.....	92
4.8 References.....	96
CHAPTER 5. ROLE OF MOLECULAR INTERACTIONS AND EFFECT OF FLUID POLARITY ON SWELLING AND FLOW PROPERTIES OF SWELLING CLAYS: A MOLECULAR DYNAMICS STUDY.....	98
5.1 Introduction.....	98
5.2 Modeling Approach.....	99
5.3 Model Construction.....	101
5.4 Force Field Parameters.....	104
5.5 Simulation Details.....	104
5.6 Results and Discussion.....	106

5.7	Conclusion.....	119
5.8	References.....	120
CHAPTER 6. STUDY THE DOUBLE LAYER THEORY FOR SWELLING CLAYS.....		124
6.1	Introduction.....	124
6.2	Double Layer Theory.....	126
6.3	Helmholtz Double Layer Theory.....	128
6.4	Gouy-Chapman Double Layer Theory.....	130
6.5	Stern Theory.....	132
6.6	Triple Layer Theory.....	132
6.7	Zeta Potential(ζ).....	134
6.7.1	Effect of Electrolyte Concentrations on Zeta Potential.....	134
6.8	Double Layer Thickness.....	135
6.9	DLVO Theory.....	139
6.9.1	Potential Energy Due to Two Interacting Double Layers.....	139
6.9.2	Potential Energy Due to Van der Waals Forces Between Two Particles.....	141
6.9.3	Total Potential Energy.....	142
6.9.4	Hamaker Constant.....	143
6.10	Application and Limitations of DLVO Theory.....	144
6.11	References.....	145
CHAPTER 7. SOLVATION OF NA-MONTMORILLONITE (NA-MMT) CLAYS: EFFECT OF ATOMS AT THE EDGE AND DISCRETE CHARGE DISTRIBUTION IN CLAYSHEET.....		150
7.1	Introduction.....	150
7.2	Modeling Approach.....	152

7.3	Simulation Details.....	153
7.4	Results and Discussions.....	155
7.5	Conclusion.....	164
7.6	References.....	164
CHAPTER 8. SUMMARY AND CONCLUSIONS.....		167
8.1	Summary and Conclusions	167
8.2	References.....	175
CHAPTER 9. FUTURE WORKS.....		188
9.1	Experimental Works.....	188
9.2	Computational Works.....	188
CHAPTER 10. APPENDICES.....		189
10.1	Configuration Files in NAMD for Molecular Dynamics Simulation.....	189
10.2	NAMD Generated Coordinate File (Shown Part Only).....	192
10.3	Part of a NAMD Generated Velocity File (Shown Part Only).....	194
10.4	NAMD Generated PSF Structure File (Shown Part Only).....	196
10.5	Part of a NAMD Constrain File (Shown Part Only).....	198
10.6	CHARMm Force Field Parameter File.....	200
10.7	Topology File.....	203

LIST OF TABLES

<u>Table</u>	<u>Page</u>
2.1: Smectite group minerals.....	22
4.1: Calculation of permeability of clays in formamide-clay sample	93
4.2: Permeability of sodium montmorillonite clays with different polarity solvents	94
5.1: d_{001} spacing from experiments and molecular dynamics simulations.....	108
6.1: Effect of electrolyte concentration and ion valences on double layer thickness	136

LIST OF FIGURES

<u>Figure</u>	<u>Page</u>
1.1: Extent of clay mineral deposits in United States.....	1
2.1: (a) Silicon tetrahedron and hexagonal sheet of silica tetrahedrons, (b) Aluminum octahedral unit and sheet of octahedral units.....	12
2.2: (a) Trioctahedral structure and (b) dioctahedral structure.....	13
2.3: Types of clay minerals.....	16
2.4: Montmorillonite structure.....	24
2.5: Schematic diagram of clay structure.....	24
2.6: Atomic organization within the unit cell of 2:1 layer mineral.....	25
2.7: Surface symmetry of (a) ditrigonal and (b) regular hexagonal montmorillonite.....	26
2.8: Dipole moment of water.....	28
3.1: Schematic diagram of principal components of FTIR spectrometer.....	33
3.2: FTIR spectrum of clay-water sample showing shift in H-O-H bending with increasing clay-water interaction time.....	33
3.3: Michelson interferometer.....	35
3.4: Reflectance spectra of MMT-formamide sample shows that shift in Si-O stretching bands with clay-fluid interaction time as more and more formamide molecules enter into the interlayer.....	37
3.5: MMT-methanol sample reflectance spectra showing the change in HOH bending with clay-methanol interaction time.....	38
3.6: Reflectance spectra of MMT-toluene sample showing no significant changes in HOH bending with time which indicates the low molecular interactions between clay and toluene.....	38
3.7: Relative shift in HOH bending for different fluids showing higher the polarity of fluids greater the shift in HOH band.....	39
3.8: Schematic of X-ray reflection from clay surfaces.....	41

<u>Figure</u>	<u>Page</u>
3.9: X-ray diffraction pattern for different clay-fluid systems showing higher value of d001 spacing for high polar fluids.....	41
3.10: Change in swelling pressure from dry state to increasing clay-water interaction time.....	43
3.11: Change in swelling pressure and void ration with different percent swelling.....	44
3.12: Scanning electron micrograph for clay-water sample at 0% swelling (a), 50% swelling (b) and 75% swelling (c). From the micrograph we see that clay particles break down into smaller sizes with increasing swelling.....	45
3.13: Change in particle size with swelling and relative swelling pressure.....	46
3.14: Scanning Electron Micrograph (SEM) image of dry Na-MMT clay and different clay-fluid samples.....	47
3.15: Constant head (bottom) and falling head (top) permeability testing device.....	49
3.16: Permeability Vs dielectric constants graph, showing higher permeability for low polar fluids.....	51
3.17: Void ration (e) Vs \sqrt{t} , consolidation test at 186.15 KPa effective stress.....	52
3.18: Coefficient of consolidation (Cv) Vs effective stress.....	52
3.19: Coefficient of consolidation (Cv) Vs effective stress for different solvents.....	53
3.20: Void ratio Vs effective stress.....	54
3.21: The change in void ratio due to effective consolidation pressure for different clay-fluid samples.....	54
3.22: Discrete Element Model (DEM) showing evolution of microstructure in montmorillonite, particles decrease in size with increasing swelling	57
3.23: For different particle subdivision volume changes relative to volume at zero stress and no subdivision	57
3.24: Potential energy curve for a diatomic molecule.....	59
3.25: Graphical representation of the interactions that described by equations in CHARMM force field: (a) bond stretching, (b) angle bending, (c) dihedral angle bending, and (d) improper angle deformation.....	61

<u>Figure</u>	<u>Page</u>
3.26: Mechanical response of phyllophillite upon applied stress.....	72
3.27: (a) Molecular model of sodium montmorillonite interlayer with two layers of water, (b) Stress Vs interlayer spacing for different water content in clays.....	73
4.1: Different type of clay liners, (a) Needle-punched (b) adhesive-bonded (c) stitched bonded (d) composite GCL.....	82
4.2: Constant head (bottom) and falling head permeability measuring device (top).....	84
4.3: Rigid wall permeability meter cell.....	85
4.4: Flexible wall permeability meter cell.....	86
4.5: Complete set up of new integrated porous rigid wall and flexible wall permeameter.....	88
4.6: Components of newly designed permeameter (1a) Porous stone cylinder (2a) Stainless steel porous stone holding cap (2c) porous stone with clamped holding cap.....	89
4.7: Design details of new permeameter.....	89
4.8: Molecular structures and dielectric constant values of solvents used in this study.....	91
4.9: Amount of water absorbed by the sample over time.....	92
4.10: Permeability Vs dielectric constant graph showing higher permeability for low polar fluids.....	94
4.11: Schematic of landfill.....	95
5.1: T-O-T structure and different components of Na-Montmorillonite model has been shown in 6x3 (with 18 unit cell) model used in this study.....	99
5.2: Molecular structures and dielectric constants of the solvents used in this study.....	100
5.3: 4x2 Na-Montmorillonite model (with 8 unit cell) used in our previous study.....	102
5.4: 6x3 Na-Montmorillonite model (with 18 unit cell) used in this study.....	102
5.5: Na-MMT with (a) 40 wt% interlayer formamide (b) 20% Water (c) 20% Methanol and (d) 10% Acetone (After Equilibration). Total thirteen models were prepared with 10%, 20%, 30%, 35% and 40% interlayer different fluids.....	103
5.6: Correlation of fluid polarity, amount of interlayer fluid and permeability of fluids.....	107

<u>Figure</u>	<u>Page</u>
5.7: Na-MMT with 10% toluene (conformation).....	108
5.8: Interaction Energies between clay-claybound fluid, Na ⁺ -sodiumbound fluids and clay-clay at experimental condition.....	110
5.9: Interaction Energy between two clay sheets for 10 wt% different polarity fluids.....	111
5.10: Interaction Energy between two clay sheets for 20 wt% different polarity fluids.....	111
5.11: Interaction Energy between two clay sheets at experimental condition for different polarity fluids	112
5.12: Interaction Energy between clay sheets and sodium ions for 10 wt% different polarity fluids	112
5.13: Interaction Energy between clay sheets and sodium ions for 20 wt% different polarity fluids.....	113
5.14: Na-MMT with 10% water (After Equilibration).....	114
5.15: Dipole moment direction of clay bound water.....	115
5.16: Dipole moment direction of clay bound formamide.....	115
5.17: Dipole moment direction of clay bound fluids.....	116
5.18: Perspective view of Na-MMT with 20% formamide (conformation).....	117
5.19: Perspective view of Na-MMT with 20% methanol (conformation).....	117
5.20: Perspective view of Na-MMT with 10% methanol (conformation).....	118
5.21: Perspective view of Na-MMT with 40% formamide (conformation).....	118
6.1: Distribution of ions from clay surface according to diffused double layer theory.....	128
6.2: Graphical representation or Potential distribution according to Helmholtz double layer theory.....	129
6.3: Graphical representation or Potential distribution according to Gouy-Chapman double layer theory.....	131
6.4: Potential and ion distribution according to Stern double layer theory.....	133

<u>Figure</u>	<u>Page</u>
6.5: Schematic of diffuse double layer and Triple layer model.....	134
6.6: Potential distribution at different electrolyte concentration showing lower the concentration, greater the thickness of double layer.....	136
6.7: Potential Vs distance plot for montmorillonite with different electrolyte concentration showing potential decreases with increasing cation concentration.....	137
6.8: Potential vs. distance curves for Na and Ca montmorillonites showing potential decreases with increasing cation valence.....	137
6.9: Zeta potential Vs characteristics of ions. (a) Ion-exchange capacity and (b) ionic radius...	138
6.10: Effect of pore fluid dielectric constant on the thickness of double layer.....	138
6.11: Charge distribution in interacting double layers between two plates.....	139
6.12: Schematic for repulsion between two interacting charged plates.....	140
7.1: 6x3 claysheet (18 unit cell) and solvation model (left); 4x2 claysheet (8 unit cell) and solvation model (right).....	155
7.2: Relative density of water molecules at different distance from clay sheet for 6x3 solvation model (left) and 4x2 solvation model (right).....	159
7.3: Conformation in water molecules near clay surface shown for solvation model with 4x2 claysheet (a,b,d) and in 6x3 claysheet (c). Figure shows that a higher concentration of water molecules at the zones of isomorphous substitutions (purple atom represents Mg).....	160
7.4: Interaction energies between water molecules and per unit cell of claysheet.....	161
7.5: Dipole moment direction showing near clay surface water molecules strongly oriented towards claysheet, as we go away from claysheet orientation of water molecules decreases.....	162
7.6: Distribution of 1st and 2nd layer of water molecules on claysheet.....	163

LIST OF ABBREVIATIONS

Å.....	Angstrom
AFM.....	Atomic Force Microscope
FEA.....	Finite Element Analysis
FEM.....	Finite Element Method
FTIR.....	Fourier Transform Infrared Spectroscopy
GPa.....	Gigapascal
K.....	Kelvin
K^A	Angle Constant
K^B	Bond Constant
MD.....	Molecular Dynamics
MMT.....	Montmorillonite
MPa.....	Megapascal
NPT.....	Constant Number, Particle and Temperature
PBC.....	Periodic Boundary Condition
PME.....	Particle Mesh Ewald
pN.....	PicoNewton
ps.....	PicoSecond
r_o	Equilibrium bond length
θ_o	Equilibrium angel
SMD.....	Steered Molecular Dynamics
SEM.....	Scanning Electron Microscope
TEM.....	Transmission Electron Microscopy

VDW.....Van der Waals
XRD.....X-Ray

CHAPTER 1. INTRODUCTION

1.1 Justification

Swelling clays cause tremendous amounts of damage to infrastructure in the United States and around the world due to swelling and swelling pressure. The extent of swelling clay deposits is significant in the United States and many other countries in the world. Figure 1.1 shows areas of expansive clays in the United States. The red region in the map shows the areas with abundant deposits of swelling clays with high swelling potential and the blue region shows the areas with less than 50% swelling clays but have high swelling potential. The orange region represents areas with less than 50% swelling clays with moderate swelling potential.

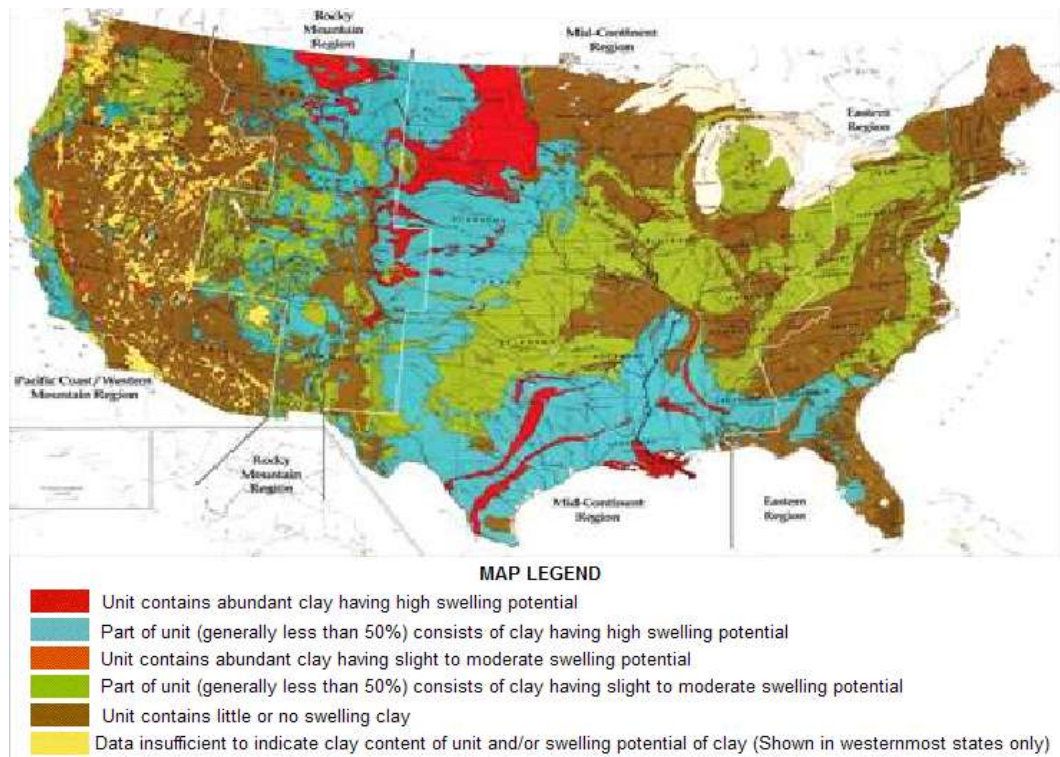


Figure. 1.1: Extent of clay mineral deposits in United States (Ref: U.S. Geological Survey publication, 1989; W.W. Olive, 1989).

These clays have many beneficial applications such as barrier materials in landfill liners and as drilling mud in the drilling industry. These clays are also used in clay based composites, in petroleum industry as drilling mud and catalyst, and also in pharmaceutical and biomedical applications. For the effective prevention of detrimental effects of these clays, and to optimize or tailor the beneficial properties for industrial applications it is necessary to clearly understand the fundamental mechanisms of swelling relating to molecular interactions, evolution of microstructure, particle breakdown to macro scale swelling and flow properties of these clays. Swelling and flow properties of these clays with different solvents are not clearly understood, which are important for many applications, especially for the use of these clays in barrier applications.

The term clay refer to particle size and clay mineral has implication for both particle size and composition (Cornelis and Dutrow, 2007). Clay mineral crystals have sheet like structures that are stacked one upon another, forming clay layers. A single clay particle has lateral dimensions from 0.1 μm to 100 μm and a thickness of approximately 1nm. According to the AIPEA (International Association for the Study of Clays) nomenclature and CMS (Clay Mineral Society) nomenclature committee's report clay mineral is defined as "a naturally occurring material composed primarily of fine grained minerals, which is generally plastic at appropriate water contents and will harden when dried or fired. Although clay usually contains phyllosilicates, it may contain other materials that impart plasticity and harden when dried or fired. Associated phases in clay may include materials that do not impart plasticity and organic matter" (Guggenheim and Martin, 1995). Clay minerals are aluminum phyllosilicates, with basic building blocks of Silicon tetrahedral (T) and Aluminium octahedral (O), sometimes with variable amounts of iron, magnesium, alkali metals, alkaline earths and other cations.

Montmorillonite belongs to the smectite type of 2:1 clay with two T-O-T layers and interlayer cations. The charge developed in the clay sheet due to isomorphic substitution is balanced by the interlayer cations.

Mineralogical organization of components of clay mineral, nature of interlayer counter ions and isomorphic substitution greatly determines the properties of these clays. When these clays come in contact with solvents, interactions of solvent molecules with different components of clay particle become a significant factor. Although many studies had been performed on swelling clays by number of researchers the mechanism of swelling still needs to be understood. It is important to understand how molecular level interactions affect the microstructure and macro scale swelling and flow properties. Moreover, most of the studies in the literature are on hydration of swelling clays and very few studies had been performed on clay with humic substances. The behavior of swelling clays with different types of fluids is vital for many engineering applications. We undertook a systematic approach to study the behavior of these clays with different polarity fluids. Our study combines the mineralogical understanding of clay along with the study of molecular level interactions, change in microstructure and their influence on macro scale swelling and flow properties. The fundamental understandings of this study will lead to better methodologies for the barrier design, the disposal and containment of hazardous and nuclear waste, and the protection of ground water.

For the application of these materials in the most efficient way, understanding the mechanism of swelling, relating molecular level interactions, change in microstructure and macroscopic scale swelling and flow properties is necessary. Previously, many researchers have attempted to explain the interactions between clay and solvent in terms of double layer theories (Helmholtz, Gouy, Chapman, Stern double layer theory). These theories have significant

limitations and cannot accurately describe the interlayer expansion in swelling clays (Jo, et al., 2001). The double layer theory is based on the fundamental assumptions as described below (M. Elimelech, 1998, Tan, 1998):

- a. An infinite, flat impenetrable interface.
- b. Ions in solution are point charges, able to approach right up to the interface.
- c. The surface charge and potential is considered to be evenly distributed over the surface (charge density σ).
- d. The solvent is uniform medium with properties (especially permittivity) independent of distance from the surface.
- e. The electrochemical potential is the maximum at colloidal surface and drops linearly with increasing distance (χ) from the surface within the double layer. This is because the value for σ is decreases very fast with distance from the surface, and reaches zero at the border of the double layer.

Most of these assumptions are questionable and some of the assumptions have been modified in newer versions of the double layer theory (Stern-Gouy-Chapman; Triple layer theory). Gouy-Chapman double layer theory also known as the diffused double layer theory described the counter ions as dispersed in the liquid layer similar to the gas molecules in the earth's atmosphere. For this reason it is called diffused double layer theory. According to the Gouy-Chapman double layer theory, the concentration distribution in the liquid zone follows the Boltzmann equation. $C_x = C_x^0 \exp(-ze\psi/KT)$. The initial electric potential at the colloidal surface is the maximum and decreases exponentially with distance from the surface as follows according to the equation: $\Psi_x = \Psi_0 \exp(-K_x)$. One of the major limitations is that the counter ions were assumed to be point charges therefore occupy no spaces; they may reach excessively high

concentrations at the liquid interface. In Stern's modification (1924) of double layer theory, finite size of ions are considered, therefore, they cannot approach more closely than allowed by their effective radii. Another problem associated with the Gouy-Chapman double layer theory is that it assumes that ions distribution follows the Boltzman's equation. Boltzman's distribution considers the activity as equal to the molar concentration, which may be considerable for bulk solution but cannot be true near a charged surface. Another problem is experimentally observed double layer thickness by a number of researchers has been found to be somewhat greater than that calculated by the theory. The error may be associated with the assumption of activity equal to molar concentration, as of when using the Boltzman distribution (Chemistry lab, New Mexico State University).

Montmorillonite shows great extent of swelling starting with crystalline swelling followed by osmotic swelling. Crystalline swelling is due to surface hydration which is reported between 17-20 Å in different literature. DLVO theory (Derjaguin, Landau, Verwey, and Overbeek) described as able to explain the colloidal stability over 20Å (Verwey and Overbeek, 1948). But this theory cannot explain the interlayer swelling at smaller interlayer spacing. It is also found recently that the water molecules confined into the interlayer are different from bulk water (Delville, 1991, Delville, 1992). Another problem with the DLVO theory is mean field approximation which will be valid only when width of the pore largely exceeds the size of the solvents molecule (Delville and Sokolowski, 1993). Therefore, to accurately describe the swelling phenomenon and solvent organization at the clay interfaces molecular model is necessary.

1.2 Original Contribution

This research consists of two parts, 1) the effect of fluid polarity on clay fluid interactions using molecular dynamics simulations, 2) the effect of discrete charge distribution and edge charge of clay particles on water molecules conformations that provide a commentary on the double layer theory, its applications and limitations in explaining swelling mechanism was also discussed. The first part of the research includes both molecular simulations and experimental studies. Twelve clay-fluid models were prepared with Na-Montmorillonite clay and four different interlayer fluids with a wide range of polarities (dielectric constant from 1 to 2.4). Molecular dynamics simulations were performed and the results from molecular simulations were validated with similar experimental studies. Analysis includes calculation of interaction energies and conformational analysis. In the models, fluid molecules were allowed to move freely in three dimensions and actual complete molecular structures were modeled to mimic the reality. Permeability tests for the formamide-clay system were conducted using a newly designed permeameter (Katti et al. US patent 2008) which is capable of accurate measurement of permeability for swelling clays. The permeability test for clay-formamide system took 1.3 years. For the second part of the research, molecular simulations for solvation of single clay sheet were conducted. Three solvation models were prepared with box size $100 \times 100 \times 100 \text{ \AA}$, $50 \times 50 \times 50 \text{ \AA}$ and clay sheet with 8 unit cells (4x2) and 18 unit cells (6x3). Extensive theoretical study along with molecular dynamics simulation was conducted to investigate the applicability of double layer theories for swelling clays. Two different sized models of clay sheet allowed us to study the particle size effects and edge charge effects on the clay-water interactions. Lastly and most significantly, important correlation has been developed between properties of swelling clays at different length scale; this study along with systematic researches over a decade provides an

insight into molecular mechanism, evolution of particle breakdown and macroscale behavior of swelling clays.

1.3 Summary of Literature Review

An extensive literature review was undertaken as part of this research. Literature review was multidisciplinary which includes papers, books and literature in the field of civil engineering, soil science, geosciences, physics and chemistry. The review incorporates literatures from studies at different length scales from macroscopic to microscopic level to the molecular level. Experimental methods such as X-ray diffraction, electron microscopy and spectroscopy are included. Theoretical and computational works including molecular dynamics and double layer theories are included. The fundamental state of knowledge from mineralogy, physics and colloidal chemistry are also incorporated.

1.4 Summary of Chapters

Chapter 2 is a literature survey of the current knowledge in swelling clays. This chapter includes the areas of clay mineralogy, and theories of swelling and hydration of clays, laboratory testing for clays, colloid science, surface chemistry, microstructure evaluation, and spectroscopic studies in swelling clays.

Chapter 3 includes the basic introduction on the experimental and modeling techniques which has been utilized for the study of swelling clays by the group over a decade. Current states of art applications of these techniques in civil engineering also have been discussed.

Chapter 4 describes the effect of fluid polarity on permeability characteristics in Na-montmorillonite swelling clays. This chapter provides a brief discussion on different

permeability testing methods and describes the newly designed permeameter developed in the group. Interesting results of permeability experiments using the new device also are presented in this chapter.

Chapter 5 discusses the results and findings of the first part of the research from both molecular modeling and experimental results. This chapter incorporates the results of experimental and modeling study performed in this study and provides a shed of light on the role of molecular interactions and effect of fluid polarity on swelling and flow properties of swelling clays. This chapter mainly focuses on effect of fluid polarity on swelling characteristics of Na-MMT clays and molecular mechanism that lead to macroscale swelling behaviors.

Chapter 6 includes the study of double layer theories for swelling as another part of this thesis. This chapter includes basic understanding on double layer theories, assumptions associated with those theories, limitations and their efficiency to explain behavior of swelling clays.

Chapter 7 describes the results of solvation study of Na-montmorillonite (Na-MMT) clays using molecular dynamics. This chapter introduces the effect of broken bonds at the edge and discrete charge distribution in claysheet that has been ignored in all the existing theories. Mathematically and through molecular dynamics simulation we were able to show how effects of broken bonds dominant with increasing particle breakdown.

Chapter 8 lists the summary of the study, conclusions and contribution of the research.

Chapter 9 provides recommendation for future works.

1.5 References

- [1] W.W. Olive, A. F. C., C.W. Frahme, Julius Schlocker, R.R. Schneider, and R.L. Shuster, 1989, "Swelling Clays Map Of The Conterminous United States," U. S. G. S. publication, ed.
- [2] Cornelis, K., and Dutrow, B., 2007, Manual of Mineral Science, John Wiley & Sons, Inc.
- [3] Guggenheim, S., and Martin, R. T., 1995, "Definition of clay and clay mineral - joint report of the aipea and cms nomenclature committees," Clay Minerals, 30(3), pp. 257-259.
- [4] Jo, H. Y., Katsumi, T., Benson, C. H., and Edil, T. B., 2001, "Hydraulic conductivity and swelling of nonprehydrated GCLs permeated with single-species salt solutions," Journal of Geotechnical and Geoenvironmental Engineering, 127(7), pp. 557-567.
- [5] M. Elimelech, J. G., Xiadong Jia, Richard Williams, 1998, Particle deposition and aggregation: measurement, modelling and simulation, Butterworth-Heinemann.
- [6] Tan, K. H., 1998, Principles of soil chemistry, Marcel Dekker, Inc.
- [7] Overbeek, V. a. J. T. G., 1948, "Theory of the Stability of Lyophobic Colloids," Elsevier, Amsterdam.
- [8] Delville, A., 1991, "Modeling the clay water interface," Langmuir, 7(3), pp. 547-555.
- [9] Delville, A., 1992, "structure of liquids at a solid interface - an application to the swelling of clay by water," Langmuir, 8(7), pp. 1796-1805.
- [10] Delville, A., and Sokolowski, S., 1993, "Adsorption of vapor at a solid interface - a molecular-model of clay wetting," Journal of Physical Chemistry, 97(23), pp. 6261-6271.

CHAPTER 2. LITERATURE REVIEW

2.1 Clay Mineralogy

Clay and clay minerals are closely related terms; clay refers to particle size, on the other hand clay mineral has implication for both particle size and composition (Cornelis and Dutrow, 2007). For engineering applications the clay size refers to all particles smaller than 0.002 mm (2 μm). According to the AIPEA (International Association for the Study of Clays) nomenclature and CMS (Clay Mineral Society) nomenclature committee's report clay mineral defined as, "The term "clay" refers to a naturally occurring material composed primarily of fine-grained minerals, which is generally plastic at appropriate water contents and will harden with dried or fired. Although clay usually contains phyllosilicates, it may contain other materials that impart plasticity and harden when dried or fired. Associated phases in clay may include materials that do not impart plasticity and organic matter" (Guggenheim and Martin, 1995). This clay minerals are aluminum phyllosilicates, with basic building blocks of Silicon tetrahedral (T) and Aluminium octahedral (O), sometimes with variable amounts of iron, magnesium, alkali metals, alkaline earths and other cations. The fundamental building blocks of clay minerals are these tetrahedral and octahedral sheets. Depending on the arrangements of these sheets and nature of interlayer counter ions clay minerals can be divided into different groups.

The clay minerals have a sheet like structure and hence exhibit more surface area than cubic or rectangular shape. Length to thickness ratios of these sheet shaped clay minerals is nearly twenty times, making the surface area of a clay particle nearly three times that of a cube with the same volume (Velde, 1995). The charge developed in the clay sheet due to isomorphic substitution is balanced by the interlayer cations. The behavior of a particular soil is dominated by the clay minerals although their proportion may not be very high. The layered configuration,

cation exchange capacity, high surface area to volume ratio, and nature of counter ions present gives the clay minerals unique properties such as swelling and evolution of microstructure as seen in smectite (with surface area around $700\text{m}^2/\text{g}$) (Schmidt, 2005). Montmorillonite belongs to the smectite type of 2:1 clay with two T-O-T layers and interlayer cations shows significant amount of swelling behaviors.

2.2 Structure of Clay Minerals

Clay minerals belong to the family of minerals called phyllosilicates, or layer silicates. Layer silicates are made of combination of silicon tetrahedral sheets and aluminum octahedral sheets. Clay structure is characterized by the stacking arrangements of these basic sheets. Tetrahedral and octahedral sheets are joined together by mutual sharing of oxygen ions, forming the crystal structure of the clay minerals (Birkeland, 1999). In some clay minerals a net negative charge is developed in these sheets due to substitution of Si^{+4} in the tetrahedral sheet and Al^{+3} in the octahedral sheet that are replaced by other cations which is known as isomorphic substitution. The negative layer charge developed due to isomorphous substitution is called structural or permanent charge (Bleam, 1993). This excess negative charge is compensated by the absorption of the same amount (charge) of cations. In the presence of water, these cations can easily be exchanged or replaced by another cation and, therefore, are called exchangeable cations (Van Olphen, 1979, Mitchell, 1993). This crystal structure is known as a layer. The space between adjacent layers is called the interlayer. The layers plus the interlayer is referred to as a unit structure. Depending on type and amount of isomorphous substitution and arrangement of basic sheets clay minerals are classified into different groups.

The silicon tetrahedron is the basic unit of the tetrahedral sheets which consist of one silicon ion surrounded by four oxygen ions. These silicon tetrahedrons share three of the four

oxygen ions forming a hexagonal net as shown in Figure 2.1. The chemical composition of silicon tetrahedral sheet is $(\text{Si}_4\text{O}_{10})^{4-}$. The basic unit of the octahedral sheet is aluminum octahedron. The octahedrons consist of magnesium or aluminum octahedrally coordinated by six oxygen and hydroxyls (Birkeland, 1999, Mitchell, 1993). These octahedrons are interconnected forming the octahedral sheet as shown in Figure 2.2 (Mitchell, 1993, Mitchell, 1993).

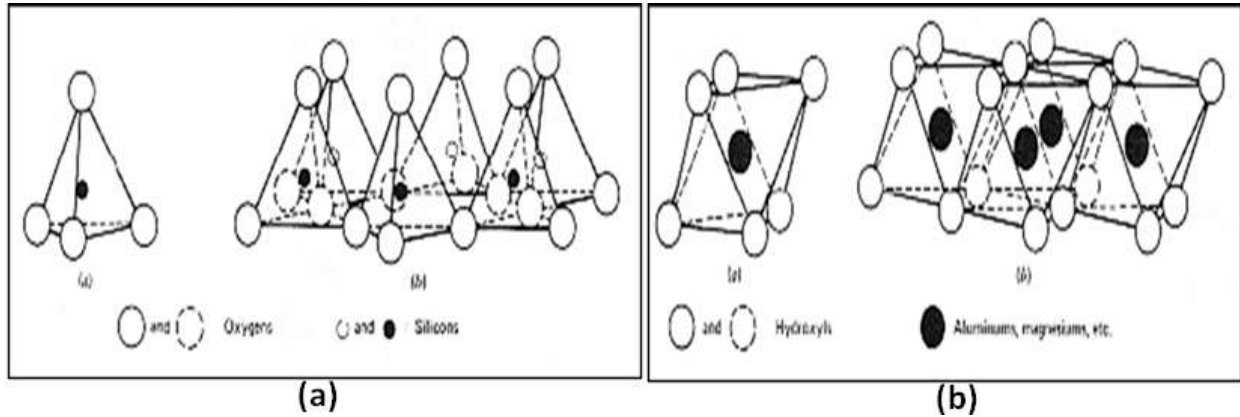


Figure 2.1: (a) Silicon tetrahedron and hexagonal sheet of silica tetrahedrons, (b) Aluminum octahedral unit and sheet of octahedral units (Grim, 1968, as cited by Mitchell, 1993).

In the case of trivalent octahedral cations, two thirds of the possible spaces are filled and the structure is called dioctahedral. For example, for aluminum the composition will be $\text{Al}_2(\text{OH})_6$ which is known as gibbsite structure or as gibbsite sheets. In case of divalent octahedral cations, all the possible spaces are filled and the structure is called trioctahedral. Figure 2.3 shows the structure of dioctahedral and trioctahedral sheets.

Clay minerals are classified according to layer types, arrangement of tetrahedral and octahedral sheets and isomorphic substitution and the resulting layer charge (Birkeland, 1999, Sposito, et al., 1999). Clay minerals are classified into three main groups called 1:1, 2:1 and 2:1:1. The 1:1 type clay mineral consists of one tetrahedral and one octahedral sheet. Kaolinites belong to 1:1 group of clay. In this group, octahedral sheet is usually dioctahedral type and no

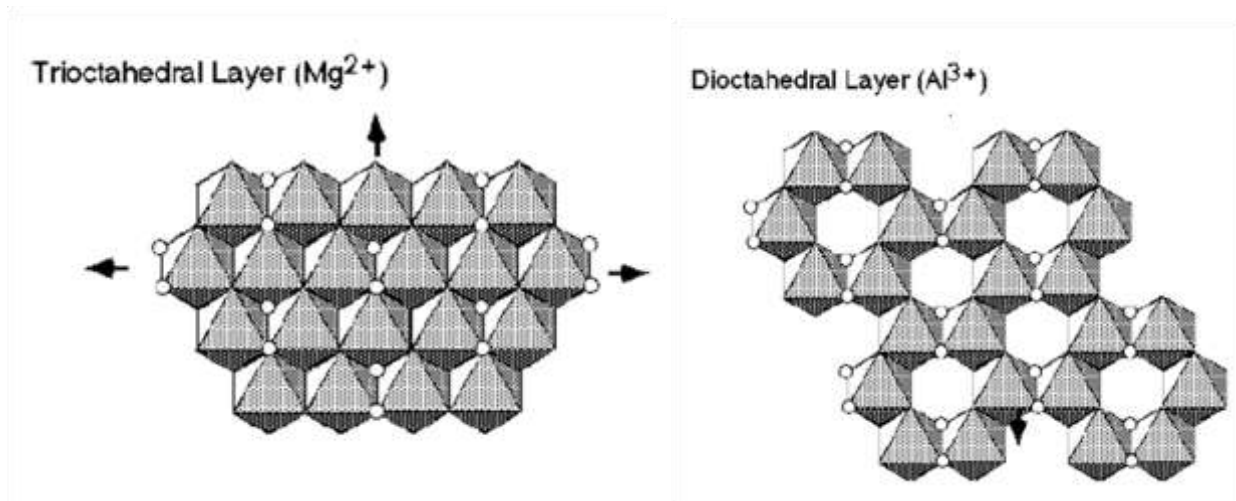


Figure 2.2: (a) Trioctahedral structure and (b) dioctahedral structure (unknown source as presented by (Schmidt, 2005)).

isomorphous substitution occurs in the Si tetrahedron or aluminum octahedron. Therefore, no net negative charge develops in the clay sheets and hence do not have interlayer cations. The 2:1 type structure called T-O-T structure i.e. two tetrahedral sheets arranged in a sandwich pattern on both sides of octahedral sheets. Three clay minerals illite, vermiculite and smectite belong to 2:1 group. The main interest of this research is Na-Montmorillonite which belongs to smectite group under 2:1 group with interlayer sodium ions. In 2:1:1 group an additional octahedral sheet lies between two 2:1 layers (Birkeland, 1999). Chlorite clay mineral group belong to 2:1:1 type.

The layers in the clay minerals are stacked in the c-direction. Depending on the presence and type of isomorphous substitution, nature of cations and surface characteristics bonding mechanism between layers may be different. One of the mechanisms may be sharing of hydrogen between oxygen of both layers. Hydrogen bonding can occur between polar solvent molecules and two adjacent clay layers. Another mechanism can be isomorphous substitution. Due to isomorphous substitution, a net negative charge arises in the clay sheets which can be compensated by introducing interlayer cations. These interlayer cations can bond the two clay

layers especially as the clay layer contains surface oxygen. Isomorphic substitutions can occur either in octahedral or tetrahedral layer of the T-O-T structures. If the substitution occurs in the octahedral layer, bonding between layers is relatively loose as the distance is greater. On the other hand, if the substitution occurs in the tetrahedral layer, bonding between layers is relatively strong as the distance is smaller. Due to substitution in tetrahedral layers clay can absorb the cations and solvent molecules more strongly. Due to these substitutions a highly reactive site is found on the clay surface called hexagonal cavity. The charge distribution and hexagonal cavity determines the reactivity of clay surface. The diameter of cavity was reported as 2.6 Å by (Schmidt, 2005) and is bordered by six oxygen atoms and a hydroxyl group at the bottom in the octahedral sheet. The edge of clay sheets also show strong charged sites but the effect of edge charge is still not well understood (Sposito, et al., 1999).

The c-dimension of clay minerals is not fixed. Water and other solvent molecules can go into the interlayer causing expansion of the lattice. The d_{001} spacing of clay minerals can be very low (9.6Å) at the dry state to complete exfoliation upon significant hydration. Depending on the nature of interlayer cations clay minerals show different swelling behavior. For example, Na-MMT shows a stepwise increase in d_{001} spacing until complete exfoliation, while Ca-MMT shows no swelling after 18 Å. Again Mg^{2+} -MMT and K-MMT shows very limited amount of swelling (Grim, 1968).

The dimension of tetrahedral and octahedral sheet is a little different and commonly lateral dimension of tetrahedral sheet is more than octahedral sheet. Thus, a structural misfit occurs. Isomorphic substitution further aggravates this misfit. For an ideal octahedral sheet containing only Mg^{2+} or Al^{3+} and tetrahedral sheet containing only Si^{+4} the misfit is 3-5% (Schmidt, 2005).

2.3 Cation Exchange Capacity

Negative charges develop on soil surfaces due to isomorphous substitution. Interlayer cations counter the charge imbalance developed due to isomorphous substitutions. These cations are attracted by the surface charge. Ions can be adsorbed on the exterior surface and interlayer surfaces. The adsorbed cations are often solvated by water or solvent molecules, causing the clay to expand. Cation Exchange Capacity (CEC) is the total sum of exchangeable cations that a soil can absorb. This amount of exchangeable cations or CEC is a measure of nutrient reserve available to plant roots in soil science. This CEC is also sometimes described as the measure of reactivity of the soil. Cation exchange capacity (CEC) depends on soil texture and organic matter content. CEC varies with different types of clays. Smectite has the highest value of CEC (80-150 milliequivalents 100 g^{-1}), then the illites (15-40 meq 100 g^{-1}) and kaolinites (3-15 meq 100 g^{-1}) (Cornelis and Dutrow, 2007). The attraction of the cations on the surfaces depends on the ion types (Velde, 1995). So, if two cations are added to soil solution in equal amounts, the clay may adsorb one of the ions more than the other. The surface charge density, size of the cations and presence of adsorbed water are some of the factors that determine the CEC. Higher the charge of the cations and smaller the atomic radius, greater the preference for that cation to be adsorbed (Velde, 1995). The concentration of the ions in solution is another important factor for attraction of cations onto clay sites.

Smectite consists of broken bonds at their edge which also contribute to the CEC. The charge due to broken O bonds and OH⁻ bonds is called pH-dependent charge (Dixon, 1989 as cited by Schmidt, 2005). As the particle size is decreased, the number of broken bonds and consequently CEC, will increase. In smectites and vermiculites broken bonds are responsible for

approximately 20% of the CEC (Katti, et al., 2005). Charge imbalance due to isomorphous substitution contributes to the rest of the CEC.

2.4. Types of Clay Minerals

Clay Mineral can be divided into different groups according to the type and combination of octahedral and tetrahedral layers, also based on isomorphous substitution. The three main groups of clay minerals are 1:1, 2:1 and 2:1:1. The 1:1 type clay mineral consists of one tetrahedral and one octahedral sheet, 2:1 clay mineral contains two tetrahedral sheets arranged in a sandwich pattern on both sides of octahedral sheets forming a T-O-T structure. Illite, vermiculite and smectite are the members of 2:1 group. The main interest of this research Na-Montmorillonite belongs to smectite group under 2:1 group with interlayer sodium ions. 2:1:1 group of clay mineral contains an additional octahedral sheet between two 2:1 layers (Birkeland, 1999). Chlorite clay mineral group belongs to 2:1:1 type.

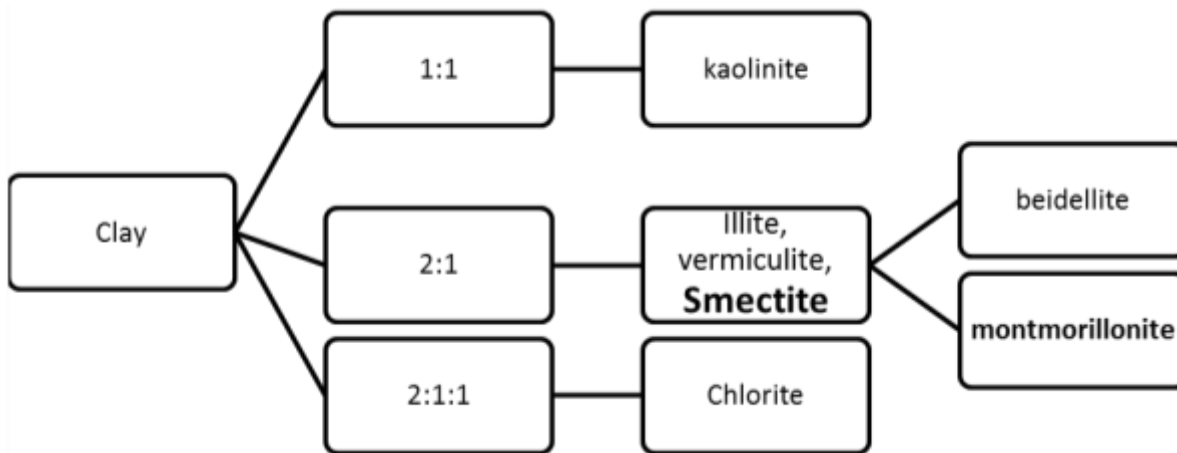


Figure 2.3: Types of clay minerals.

2.4.1. Kaolinite

The 1:1 layer arrangement that is one tetrahedral and one octahedral sheet combination can form two mineral types called lizardite and kaolinite. The dioctahedral group of 1:1 mineral is referred to as the kaolinite group. Kaolinite shows a low shrink-swell capacity when it comes

in contact with water and has a low cation exchange capacity. In kaolinite bonding between two layers is mainly electrostatic although there may be some Van der Waals attraction due to hydrogen bonding between hydroxyl ions and hydrogen of the layers. Kaolinite group do not consist any interlayer cations (Van Olphen, 1979). The dimensions of kaolinite sheet are 0.1 to 4 μm and thickness between 0.05 to 2 μm (Mitchell, 1993).

2.4.2. Pyrophyllite-Talc Group

Electrically neutral 2:1 clay minerals are grouped as Talc and pyrophyllite. The main difference between Pyrophyllite and Talc is Pyrophyllite consists of dioctahedral structure while Talc consists of trioctahedral structure. The composition of Pyrophyllite and Talc are $\text{Al}_4\text{Si}_8\text{O}_{20}(\text{OH})_4$ and $\text{Mg}_6\text{Si}_8\text{O}_{20}(\text{OH})_4$ respectively (Newman, 1987 as cited by Schmidt, 2005). Pyrophyllite and Talc are usually found in the areas of little weathering. In XRD experiment, Pyrophyllite shows specific peak (d_{001}) at 9.19 \AA , while the peak in talc is found at 9.4 \AA (Dixon and Weed, 1989 as cited by Schmidt, 2005).

2.4.3. Mica-like Clay Minerals

2.4.3.1. Illite

Illite, member of mica group, is a nonexpanding 2:1 clay mineral. Illite is named for a series of dioctahedral interlayer-deficient materials within Mica Group, with no end members defined. Illite is distinguished from smectite by the non-swelling behavior when comes in contact with water. Substitutions in illite mainly occur in tetrahedral sheets with non-exchangeable potassium ions in the interlayer. Exfoliation (separation of layers) does not occur due to solvation by water, electrostatic interactions between potassium ions and clay layers hold together. Although a compositional range is provided by mindat.org as $\text{K}_{0.65}\text{Al}_{2.0}[\text{Al}_{0.65}\text{Si}_{3.35}\text{O}_{10}](\text{OH})_2$, the name is for a series in the Mica Group, not an individual species. With the

development of our knowledge the series will be better defined and will possibly be divided into two or more species names. The cation exchange capacity is 10 to 40 meq/100 g, so may show limited inter layer swelling as CEC values greater than 10 to 15 meq/100 g is an indication for some swelling. The interlayer spacing remains at 10 Å even in the presence of polar liquids due to the strong interlayer bonding. Illites are usually small flaky shape particles, hexagonal if well crystallized, mixed with other clay and non-clay materials. The dimension of long axis in illite may be from 0.1 µm to several micrometers while the thickness may be as small as 30 Å. The specific surface area is about 65 to 100 m²/g (Mitchell, 1993).

2.4.3.2. Vermiculite

Vermiculite is a 2:1 type clay mineral that contains both dioctahedral and trioctahedral type of sheets. The empirical formula for vermiculite is $Mg_{1.8}Fe^{2+}_{0.9}Al_{4.3}SiO_{10}(OH)_2 \cdot 4(H_2O)$. Isomorphous substitutions occur at tetrahedral sheet in vermiculite. Due to the strong bond between the adjacent layers, vermiculite exhibits limited amount of swelling (Birkeland, 1999). The cation exchange capacity (CEC) of vermiculite is between 100 to 150 meq/100g, the higher CEC is due to the exchange capacity of cations. The charge deficiency ranges from 1 to 1.4 (Schmidt, 2005, Smith, et al., 2004). The d_{001} spacing for vermiculite is between 10.5 to 12.2 Å depending on type of cation exchange and hydration of the mineral. Specific surface area without the interlayer is about 40 to 80 m²/g and interlayer surface area could be up to 870 m²/g (Mitchell, 1993).

2.4.3.3. Chlorite

Chlorite is a group of triclinic and monoclinic micaceous 2:1 phyllosilicate minerals with a T-O-T layered structure. In chlorite, silicon tetrahedral apices of two layers points towards each other, separated by an interlayer. The interlayer may be octahedrally coordinated cations or may

have a brucite-like layer of two sheets of closely packed OH groups (www.mindat.org).

Electrostatic and hydrogen bond forces are responsible for bonding of the T-O-T layers and interlayer in chlorites. Chlorite mineral groups can be stated with general formula as $A_{5-6}T_4Z_{18}$, where A = Al, Fe²⁺, Fe³⁺, Li, Mg, Mn, or Ni, where T = Al, Fe³⁺, Si, or can be a combination of them, and Z = O and/or OH (www.mindat.org).

Isomorphous substitutions in chlorite are mainly at the tetrahedral sheet with Al⁺³ for Si⁺⁴ results in a net negative charge. Due to the strong bond between two oppositely charged layers no expansion occurs in chlorite (Birkeland, 1999). So, chlorite shows fixed d₀₀₁ spacing at 14 Å. The cation exchange capacity of chlorite is about 10 to 40meq/100g.

2.4.4. Smectite Minerals

Due to the extensive isomorphous substitutions, smectite group shows maximum swelling behavior. Depending on these isomorphous substitutions in the tetrahedral and octahedral sheets smectite exhibits different composition which used to classify smectites (Dixon and Weed, 1989 as cited by (Schmidt, 2005). Substitution can be of two types, substitution of ions of the same valence and Substitutions by ions of lesser charge. Substitutions of ions of the same valence usually occur in the octahedral sheet while substitutions by ions of lesser charge can be occurred in both tetrahedral and octahedral sheets. Due to the smaller size, these ions can replace the Si⁺⁴ and Al⁺³ atoms. Al⁺³ can be replaced upto 15% by Fe⁺³ may replace up to 15% in the tetrahedral sheet while Al⁺³ in the octahedral sheet may be replaced by Mg⁺², Fe⁺³, Fe⁺², Cr⁺², Zn⁺², Ni⁺², Li⁺¹, or other cations (Van Olphen, 1979); (Mitchell, 1993); (Birkeland, 1999) ; Brindely and Brown, 1980, Newman, 1987 as cited by Schmidt, 2009).

Smectite group consists of both dioctahedral and tri-octahedral minerals.

Montmorillonite, beidellite, and nontronite are the dioctahedral smectite minerals while hectorite

(Li-rich), saponite (Mg-rich), and saunonite (Zn-rich) are the trioctahedral members of smectite group. The layers of smectite are continuous in horizontal directions and stacked vertically. Due to the excessive cleavage and weak bonds between the layers, water and other fluid molecules can enter into the interlayer causing expansion in the vertical direction (Grim, 1968).

Smectite usually occurs from the weathering of basic rocks. Mild slope terrains, slightly alkaline (for example marine condition), having high Si and Mg potentials with poor drainage is a favorable condition for smectite formation (Borchardt, 1977 as cited by (Schmidt, 2005). Poor drainage is very important for smectite formation as otherwise water can leach away ions (e.g. Mg) freed due to the alteration reactions.

The characteristic feature of smectite is its X-ray diffraction pattern varies with moisture content, nature of exchangeable cations, heat treatment and exposure to certain organic molecules (Wilson, 1987 as cited by (Schmidt, 2005). Some of the characteristic features for example includes collapse of d_{001} spacing to 10 Å if heated to 400°C, if saturated with ethylene glycol will swell to about 17 Å (U. S. Geological Survey Open-File Report 01-041). Members of smectite can be differentiated by nature of cations or higher order peaks. For example, 060 reflections for dioctahedral smectite at 1.50-1.52 Å while for trioctahedral smectite at 1.53-1.54 Å and Li saturation sometimes can be used to differentiate some montmorillonites from beidellite (Schultz, 1969), 1969 as cited in U. S. Geological Survey Open-File Report 01-041).

Smectite also can be characterized by negative charge in the range of 0.5 to 1.20. Commonly for a formula unit of $O_{20}(OH)_4$ the charge is about 0.7 and 1.0 (Schmidt, 2005). Among the dioctahedral smectite montmorillonite consists only octahedral substitutions, whereas beidellite, ideally consist of tetrahedral substitutions only. Chemical composition and thermal properties can be used to differentiate between smectites. For example, Wyoming type smectite

has a layer charge less than 0.85 per $O_{20}(OH)_4$ formula unit and tetrahedral substitution are responsible for 15 to 50% of the total charge in the layer, whereas Otay type smectite has a layer charge greater than 0.85 per unit formula and less than 15% of the charge comes from the tetrahedral substitution. On the other hand, Tatatila and Chambers type of smectite has a layer charge greater than 0.85 with 15 to 50% of charge contribution from tetrahedral substitution. Beidellite type has a layer charge greater than 0.85 with more than 50% of the charge in the layer comes from the contribution of tetrahedral substitution (Newman, 1987 as cited by (Schmidt, 2005).

Different smectite group minerals, their formula and source of isomorphic substitution are shown in Table 2.1 as presented by (Mitchell, 1993). The formulas provided here are not absolute as a number of combination and proportion are possible for each of the minerals.

Montmorillonite and beidellite are two very important smectite types of clay minerals. Due to the negative charge and swelling behavior when comes in contact with water and other fluids, these minerals can cause excessive amount of expansion. These minerals cause shrinkage and swelling with change in moisture content at different periods of the year. These minerals cause tremendous damage to engineering infrastructure and are also responsible for landslides. In particular, despite being smaller in percentage, these minerals significantly control the behavior of soils. Although the shear strength of soils containing smectite are higher than soils containing other minerals at dry condition, smectite can adsorb much higher amount of water (Dixon and Weed, 1989 as cited by Schmidt, 2005). (Katti, et al., 2003) have shown that significant reduction of shear strength occurs due to swelling. Smectite together with vermiculite have the maximum cation exchange capacity (CEC) which is very useful for plant growth, organic

compound adsorptions, pesticides and herbicides (Dixon and Weed, 1989 as cited by (Schmidt, 2005).

Table 2.1: Smectite group minerals (Mitchell, 1993)

Mineral	Tetrahedral Sheet Substitutions	Octahedral Sheet Substitutions	Formula/Unit Cell ^a
Dioctahedral, Smectites or Montmorillonites			
Montmorillonite	None	1 Mg ²⁺ for every sixth Al ²⁺	(OH) ₄ Si ₈ (Al _{3.34} Mg _{0.66}) O ₂₀ ↓ Na _{0.66}
Beidellite	Al for Si	None	(OH) ₄ (Si _{6.34} Al _{1.66}) Al _{4.34} O ₂₀ ↓ Na _{1.66}
Nontronite	Al for Si	Fe ²⁺ for Al	(OH) ₄ (Si _{7.34} Al _{0.66}) Fe _{4.34} O ₂₂ ↓ Na _{0.66}
Trioctahedral, Smectites or Saponites			
Hectorite	None	Li for Mg	(OH) ₄ Si ₈ (Mg _{5.34} Li _{0.66}) O ₂₀ ↓ Na _{0.66}
Saponite	Al for Si	Fe ²⁺ for Mg	(OH) ₄ Si _{7.34} Al _{0.66}) Mg ₈ O ₂₂ ↓ Na _{1.66}
Sauconite	Al for Si	Zn for Mg	(OH) ₄ (Si _{7.34} Al _{0.66})(Zn ₂₋₂ Mg ₂) O ₂₀ ↓ Na _{1.66}

^a Two formula units are needed to give one unit cell.
After Ross and Hendricks (1945); Marshall (1964); and Warshaw and Roy (1961).

Smectite shows maximum amount of swelling property due to high surface to weight ratio, negatively charged layered structure and smaller size. Different researchers tried to explain this phenomenon in different ways. One of the explanations can be due to hydration induced free mobility of cations. Another possible argument is water molecules directly interact with clay surface (Dixon and Weed, 1989 as cited by Schmidt, 2005). Although the complete mechanism of swelling is still known many researchers supports that the dominating factor for swelling is the balance of attractive and repulsive forces between two adjacent clay layers and counter ions. The main contributing attractive force is the attraction between negatively charged clay sheets and positively charged counter ions (Schmidt, 2005). Our current study suggests that the

interaction between two clay sheets could be positive, neutral and negative depending on the separation distance. This is may be due to the complex charge distribution within the clay sheets. The magnitudes of this force greatly vary between mineral to mineral and depends on several factors including isomorphous substitution, charge density, separation distance, between negative and positive charges etc. in case of small separation distance Van der Waals forces also will play role. The source of repulsive force is the solvation of interlayer cations and clay sheets (intercalation of surface oxygen). Solvation of clay sheets is not sufficient for clay swelling as the attractive forces due to Van der Waals and electrostatic attraction is much higher. This may be the reason for non-swelling behavior of pyrophyllite. Hydrogen of the hydroxyl group linked with octahedral cations also contributes repulsive force with interlayer cations. The magnitude of this repulsion depends on the position of the hydroxyl hydrogen relative to interlayer cations (Newman, 1987). In engineering practice, expansive clays are treated with lime and other chemicals although the mechanism is poorly understood. Lime produces Ca-Al silicate cementing agents, thus decrease the plasticity index or lime could be present as a monolayer on the clay surfaces (Dixon, 1989). The tremendous amount of swelling properties of smectites may be due to the combination of several factors including huge amount of isomorphous substitution, cation exchange capacity, high aspect ratio provides high specific surface area; thickness of clay sheet is 10\AA where particle size may be up to $1\text{-}2\ \mu\text{m}$, surface area can be up to $840\ \text{m}^2/\text{g}$ as cited by Mitchell, 1993.

2.5 Na-MMT Structure

The structure of smectite minerals consist of two tetrahedral sheets and in between one octahedral sheet forming a T-O-T structure as shown in Figure 2.4 and 2.5. The oxygen of the

tetrahedral sheet is shared with the octahedral sheet and hydroxyl ions of the octahedral sheet arranged directly above and below the hexagonal cavity of silica tetrahedrons (Mitchell, 1993).

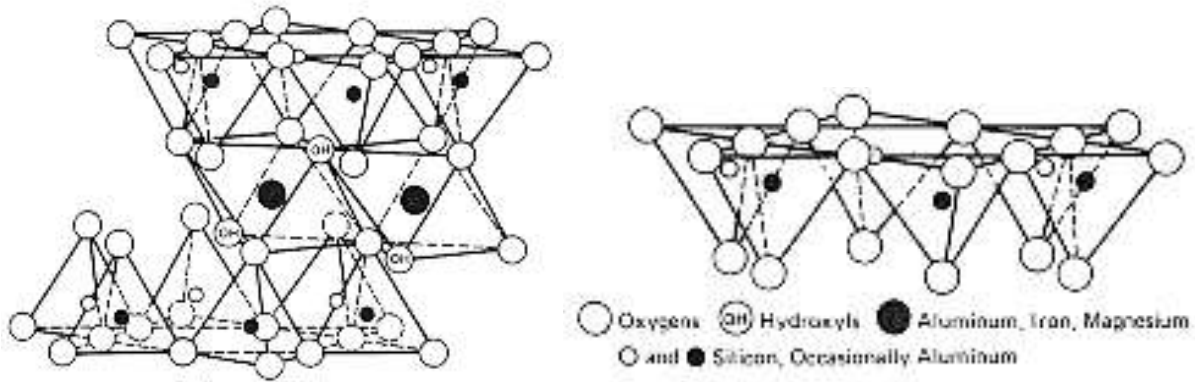


Figure 2.4: Montmorillonite structure (Grim, 1968, as cited by Mitchell, 1993).

The smectite clay layers are continuous in x and y directions and stacked one above another in z direction. Interlayer cations stay between the spaces of the adjacent layers. The interlayer spacing is highly variable and depends on nature of interlayer exchangeable cations, amount of isomorphic substitutions at the clay layer, nature and amount of fluid present in the interlayer. The interlayer spacing for MMT is highly variable ranging from 9.6 Å for dry case to complete separation (Mitchell, 1993). The unit cell dimensions are 5.28 Å x 9.14 Å x 6.56 Å as

shown in Figure 2.6

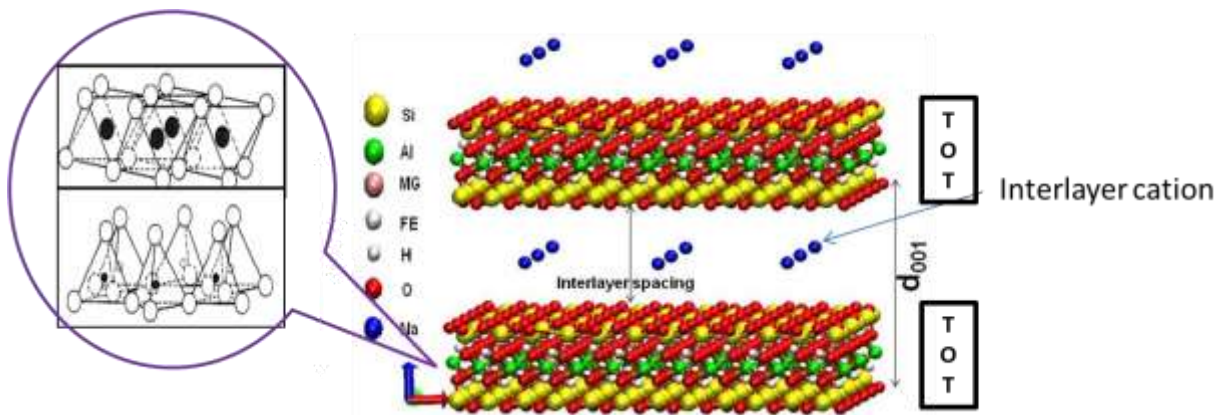


Figure 2.5: Schematic diagram of clay structure.

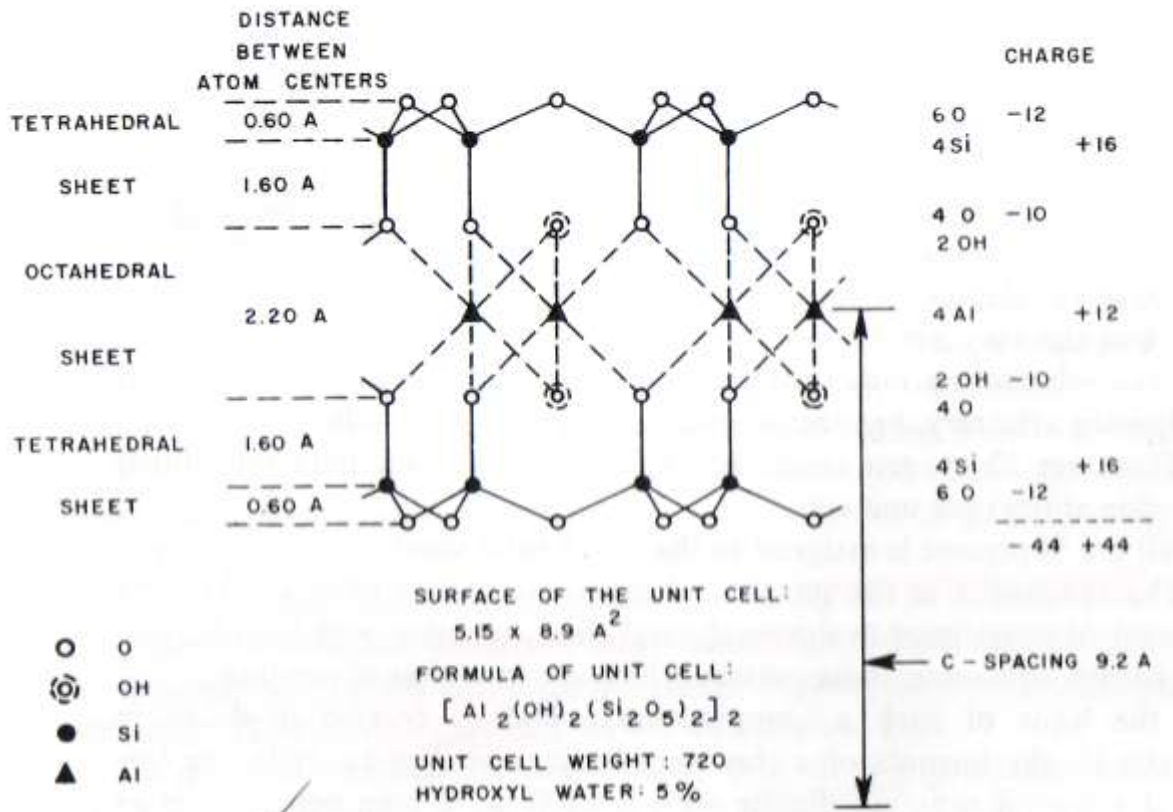


Figure 2.6: Atomic organization within the unit cell of 2:1 layer mineral (Van Olphen, 1979).

The tetragonal sheets of clay sheet are larger than the octahedral sheet which is balanced by alternative counterclockwise and clockwise rotation of the tetrahedron about the vertical axis. This results a di-trigonal symmetry as shown in Figure 2.7. Isomorphic substitution further exaggerates the dimension mismatch between tetrahedral and octahedral sheets as the substituted ions have different size than native ions.

2.6 Forces in Clay Fluid Colloidal System

The dominating forces in a clay fluid colloidal system are electrostatic interactions between oppositely charged constituents, Van der Waals force and gravity. In terms of constituents, forces can be divided as interactions between clay particles, clay with fluids, clay with interlayer cations, fluids with interlayer cations and fluid-fluid interactions.

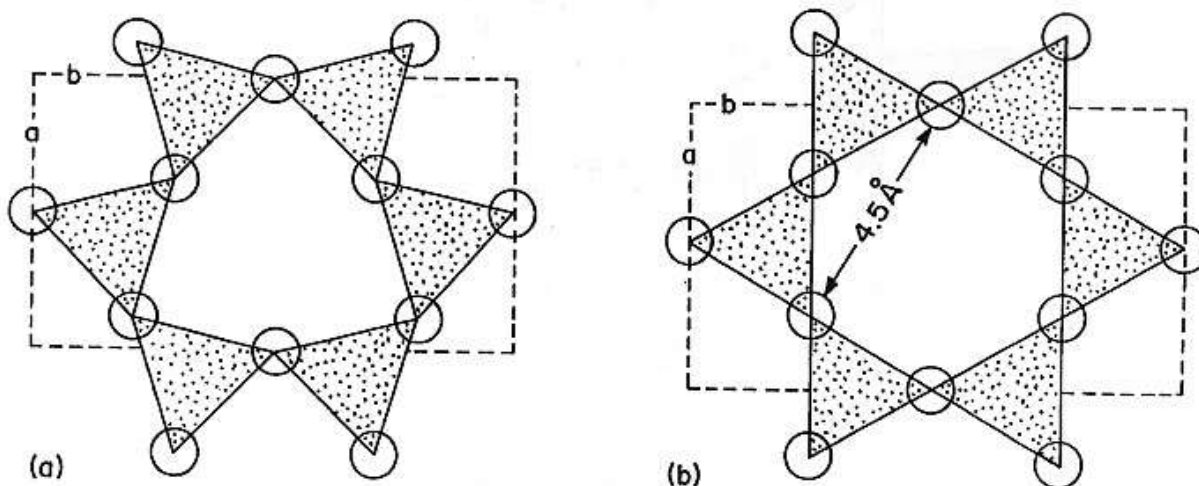


Figure 2.7: Surface symmetry of (a) ditrigonal and (b) regular hexagonal montmorillonite (Low, 1973).

2.6.1 Van der Waals Forces (VDW)

Attractive forces between neutral atoms had been first explained by Van der Waals in 1873 (Overbeek, 1952 as cited by (Schmidt, 2005)). As in an atom, the electrons continuously rotate around the positive nucleus at a very high frequency which results net charge intensity at a particular location at a specific moment. This charge intensity causes a fluctuating dipole moment. According to Overbeek, (1952) this fluctuating dipole are capable of polarizing neighboring atom and consequently the two atoms starts attracting each other. The time average of dipole moment for a nonpolar atom is zero. Depending on the instantaneous positions of the electrons about the nucleus a finite dipole moment always exists. This instantaneous dipole creates an electric field that polarizes neighboring neutral atoms. These two dipoles attract each other and cause an attractive force between the two atoms (Israelachvili, 1985).

Van der Waals force is a significant contributor along with other forces for numerous important physical properties for example strength of materials, properties of gas, liquids, proteins and other biomolecules. The Van der Waals forces between two particles of similar

material in fluid are always attractive as there is no noticeable orientation of the fluid molecules. Van der Waals forces are a very short ranged force in the order of atomic dimensions and decay rapidly with a small atomic separation. But colloid particles can act over much longer distances (Overbeek, 1952). Van der Waals attraction between two atoms is attractive and the total attraction between clay particles having a large number of atoms is the sum of the attractive force between each of the particles, hence the summation leads to a huge force and occur rapid decay with increasing distance.

2.6.2 Gravity

For large celestial body gravity is the main contributing force, but for atomic and colloidal system the contribution of gravitational force is negligible. Gravitational force on colloidal particles exceeds the attraction between two colloids for a separation distance larger than 200 nm due to very small diameter or size. Even, for small separation distance Van der Waals force is the greater contributor, can be thousand times of gravitational forces between particles (Anandarajah, 1997).

2.7 Polarity and Dielectric Constant

Dielectric constant also sometimes termed as relative permittivity is a measure to characterize solvents. Mathematically it is the ratio of electric field strength in vacuum to that in the material (Smith 1955 as cited by (Amarasinghe, 2009)). In a laboratory setup, dielectric constant is measured by inserting the desired solvents between two charged plates and electric field strength (E_0) is monitored. The electric field strength is lower than when the plates are in vacuum (E_0) and the ration E_0/E is called dielectric constant value.

If the solvent molecules consist of permanent dipoles, these molecules are forced to an ordered pattern due the electric field, thus reduction in the strength of the electric field. The

higher the dipole moment value of the molecules, greater is the polarization. Hence, greater reduction in field strength occurs and the material has a higher dielectric constant. The larger the dipole moment of molecules, greater the dielectric constant and depending on the capability to be organized in to arranged pattern causing reduction of electric field strength of the plates.

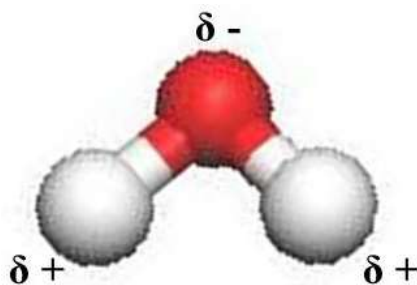


Figure 2.8: Dipole moment of water.

Dipole moment is a directional force that results due to asymmetrical charge distribution between atoms within a molecule. If q_1 and q_2 are the charges of two oppositely charged atoms within a molecule separated by a distance l , then the dipole moment $\mu = (q_1 \times q_2) \times l$. Solvents having molecules with permanent dipoles are called polar or dipolar solvents while solvents whose molecules do not possess permanent dipoles are called nonpolar solvents.

In water molecules, one oxygen atom is covalently bonded with two hydrogen atoms. Due to greater electronegativity of oxygen, the shared electrons cloud stay more towards oxygen results a slightly net negative charge in oxygen and slight positive charge in hydrogen. Due to this unbalanced charge distribution, dipole moment develops in water molecules.

Hydrogen bond formation occurs in polar molecules. When covalently bonded hydrogen atom forms second bond with other atom, the second bond is termed as hydrogen bond. Hydrogen bond can occur between molecules or within the molecules. Hydrogen bonds are responsible for high boiling/melting points and other properties of many polar fluids.

2.8 References

- [1] Cornelis, K., and Dutrow, B., 2007, Manual of Mineral Science, John Wiley & Sons, Inc.
- [2] Guggenheim, S., and Martin, R. T., 1995, "Definition of clay and clay mineral - joint report of the aipea and cms nomenclature committees," Clay Minerals, 30(3), pp. 257-259.
- [3] Velde, B., 1995, "Use of the smectite to illite conversion reaction model - effects of order of magnitude," Bulletin Des Centres De Recherches Exploration-Production Elf Aquitaine, 19(1), pp. 235-242.
- [4] Schmidt, S. R., 2005, "Evaluation of clay-water interactions : a quantitative determination of clayinterlayer forces with varying hydration by steered molecular dynamics," MS, North Dakota State University,, ND, USA.
- [5] Birkeland, P. W., 1999, Soils and geomorphology, Oxford University Press, New York.
- [6] Bleam, W. F., 1993, "Atomic theories of phyllosilicates - quantum-chemistry, statistical-mechanics, electrostatic theory, and crystal-chemistry," Reviews of Geophysics, 31(1), pp. 51-73.
- [7] Van Olphen, H. a. F., J. J, 1979, Data handbook for clay materials and other non-metallic minerals, Pergamon Press, New York.
- [8] Mitchell, J. K., 1993, Fundamentals of Soil Behavior, Second Edition, John Wiley Sons, Inc.
- [9] Mitchell, J., 1993, Fundamentals of Soil Behavior, Second Edition, John Wiley & Sons, Inc., New York.
- [10] Grim, R., 1968, Clay mineralogy, 2nd Edition, McGraw-Hill, New York.

- [11] Sposito, G., Skipper, N. T., Sutton, R., Park, S. H., Soper, A. K., and Greathouse, J. A., 1999, "Surface geochemistry of the clay minerals," *Proceedings of the National Academy of Sciences of the United States of America*, 96(7), pp. 3358-3364.
- [12] Dixon, J. a. W., SB, 1989, *Minerals in Soil Environments*, 2nd Edition, Soil Science Society of America, Madison, WI.
- [13] Katti, D. R., Schmidt, S. R., Ghosh, P., and Katti, K. S., 2005, "Modeling the response of pyrophyllite interlayer to applied stress using steered molecular dynamics," *Clays and Clay Minerals*, 53(2), pp. 171-178.
- [14] Smith, D. E., Wang, Y., and Whitley, H. D., 2004, "Molecular simulations of hydration and swelling in clay minerals," *Fluid Phase Equilibria*, 222, pp. 189-194.
- [15] Schultz, L. G., 1969, "Lithium and potassium absorption, dehydroxylation temperature, and structural water content of aluminous smectites," *Clays and Clay Minerals*, 17(3), pp. 115-&.
- [16] Katti, D. R., Tang, J. P., and Yazdani, S., 2003, "Undrained response of clays to varying strain rate," *Journal of Geotechnical and Geoenvironmental Engineering*, 129(3), pp. 278-282.
- [17] Newman, A. C. D., 1987, *Chemistry of Clays and Clay Minerals*. Mineralogical Society Monograph, Longman Scientific and Technical, Harlow, Essex, England.
- [18] Low, P. F., "Fundamental mechanisms involved in the extension of clays and shales in highway design and construction," *Proc. Workshop on expansive clays and shales in highway design and construction*.
- [19] Israelachvili, J. N., 1985, *Intermolecular and Surface Forces*, Academic Press: London.
- [20] Overbeek, J. T. G., 1952, "Electrokinetic phenomena," *Colloidal Science*, Vol 1, Elsevier, Amsterdam, Netherlands, 1952.

[21] Anandarajah, A., 1997, "Influence of particle orientation on one-dimensional compression of montmorillonite," *Journal of Colloid and Interface Science*, 194(1), pp. 44-52.

[22] Amarasinghe, P. M., 2009, "Role of clay-fluid molecular interactions on fluid flow and mechanical behavior of swelling clays," PhD, North Dakota State University, ND, USA.

www.mindat.org

CHAPTER 3. MULTI SCALE EXPERIMENTAL AND MODELING TECHNIQUES FOR THE STUDY OF SWELLING CLAYS

3.1 Introduction

Swelling mechanism of clays has been a mystery for many years. Many researchers have attempted to investigate the reason for swelling using different experimental and modeling techniques. An individual experimental or modeling study at a particular length scale may trigger some phenomenon of swelling clays but complete understanding of swelling mechanism is not possible. We know that material properties vary significantly at different length scale. For the complete understanding of swelling mechanism, bridging the properties at different length scale is necessary. In this study along with different modeling and experimental studies at different length scale in previous studies by our group, we are able to bridge properties at different length scale. We are able to provide a quantitative link between swelling, swelling pressure, particle breakdown, and evaluation of microstructure and flow properties of swelling clays. Following are some of the experimental and modeling techniques that can be effectively used for the study of swelling clays.

3.2 Experimental Techniques

3.2.1 FTIR (Fourier Transform Infrared Spectroscopy)

FTIR (Fourier Transform Infrared Spectroscopy) is a powerful technique for determining the chemical bonds present in a molecule. FTIR produces distinct infrared absorption spectrum which can be compared as a molecular "fingerprint".

FTIR is a very useful tool for identifying both organic and inorganic chemicals. FTIR can identify the chemical bonds or functional groups present in a material from the characteristic IR spectrum. Pure compounds show very unique FTIR spectra and can be compared as a molecular

"fingerprint". Usually organic compound shows detailed spectra while inorganic compounds have much simple spectra. Spectrum of an unknown material for common materials can be interpreted by comparing with the existing database of known compounds. IR spectra can be used along with nuclear magnetic resonance, X-ray diffraction, emission spectroscopy, mass spectrometry, and/or other techniques for the analysis of less common materials. FTIR is also to some extent provides valuable quantitative estimation as the strength or intensity of absorption spectra is proportional to the concentration.

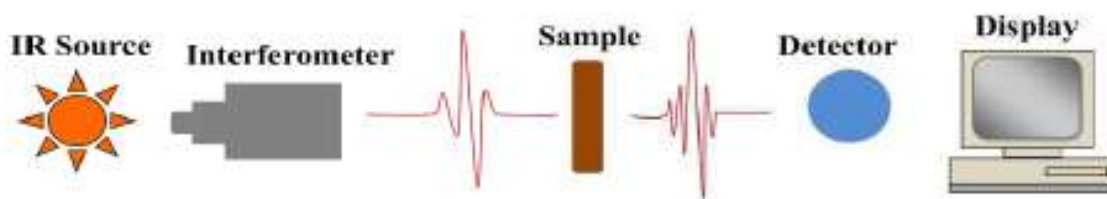


Figure 3.1: Schematic diagram of principal components of FTIR spectrometer (Amarasinghe, 2009).

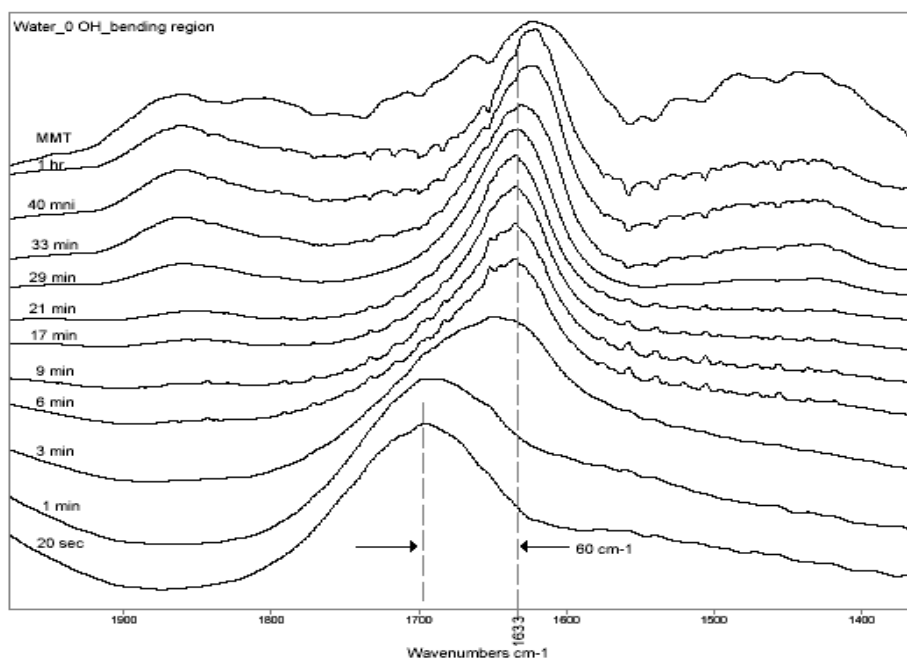


Figure 3.2: FTIR spectrum of clay-water sample showing shift in H-O-H bending with increasing clay-water interaction time (Amarasinghe, 2009).

3.2.1.1 Physical Principles

Molecular bonds exhibit vibration, at distinct frequencies based on the presence of elements and types of bonds. The bond between any two atoms can vibrate at different frequencies. For example, O-H bond vibration frequency in organic compounds is different from that when in inorganic compounds. The lowest frequency is called ground state in quantum mechanics, while several excited states are possible. When infrared light passes through the material it absorbs the energy and causes an increase of molecular vibration frequency. When this increase overcomes the transition of one state to another state, the light energy (which is determined by the wavelength) is the same as the energy difference between the two states which is usually ground state (E_0) and first excited state (E_1). The magnitudes of the energy between two vibrational states are 1 to 10 Kcal/mol, which is in the range of infrared light in the electromagnetic spectrum.

Difference between two Energy States = Energy of absorbed light

$$\Delta E = hc/\lambda$$

$$E_1 - E_0 = hc/\lambda$$

Where, h = Plank Constant

c = speed of light

λ = wavelength of light

The interactions of infrared light with materials are energy absorption processes. When a molecular system is exposed to infrared radiation the total energy is from a multi-atom molecule and consists of rotational, vibrational, electronic and transitional energy. Each of these energies can be measured individually,

$$E_{\text{total}} = E_{\text{rotational}} + E_{\text{vibrational}} + E_{\text{electronic}} + E_{\text{transitional}}$$

Where, $E_{\text{rotational}}$ is due to the rotation of molecules, $E_{\text{vibrational}}$ is due to vibration of molecules, $E_{\text{electronic}}$ is due to electrons movements and $E_{\text{transitional}}$ is due to transition of molecules. Infrared spectroscopy (IR) measures the vibration energy of molecules. The usual range of vibration energy ranges from 10^2 cm^{-1} to 10^4 cm^{-1} (Urban, 1993as cited by (Amarasinghe, 2009); (Essig, et al., 1993). When exposed to electromagnetic radiation, molecules absorb energy according to the vibration energy of the molecules. Another criteria must be met which is molecules should be able to change the direction of dipole moments. These molecules are called IR active molecules and suitable for infrared spectroscopy. The degree of change in dipole moments controls the intensity of absorption or emission.

$$I_k = A \left(\frac{\partial \mu_d}{\partial x} \right)^2$$

Where, μ_d = Dipole moment x = Displacement

The main components of an FTIR are a source of electromagnetic radiation, interferometer, detector and display as shown in Figure 3.1

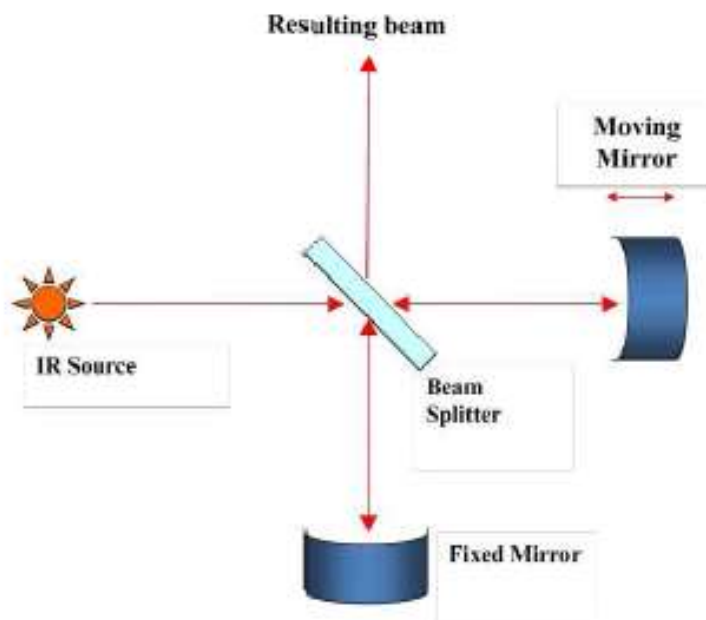


Figure 3.3: Michelson interferometer (Amarasinghe, 2009).

Infrared beam from an IR source hits the beam splitter (usually made of KBr) and diverts into two beams. Half of the beam divert off the beam splitter while the other half goes through the beam splitter. These two diverted infrared lights then reflect on the mirror and form constructive or destructive interference depending on the position of the mirror. The resulting beam is translated by a mathematical formulation known as Fourier transformation, and provides an intensity Vs frequency spectrum known as interferogram (West Coast Analytical Service).

Samples preparation is very important for good FTIR results. The easiest method for liquid sample preparation is placing a drop of sample between two salt plates (sodium chloride) as salt is infrared transparent. A thin film of liquid sample forms between the salt plates. Solid samples is usually powdered with potassium bromide (KBr) compressed to form a thin pellet for FTIR study. KBr is also infrared transparent. Solid samples can also be dissolved to prepare solution and use the technique for liquid samples using salt plate. Then the solvent gets evaporated off and leaves a thin film of the original sample on the salt plate. This technique is known as cast film techniques and widely used in polymer identification.

3.2.1.2 FTIR Studies on Swelling Clays

Infrared spectroscopy is a powerful technique for composition and structural analysis of minerals. It also can be used for the study of molecular interactions of clay fluid system. Si-O is the most prominent bands in clay. (Katti and Katti, 2006) observed four distinct types of Si-O vibrations, three in plane vibration and one out of plane vibration in the range of 1200 to 900 cm^{-1} . Bending vibrations of Al-Fe-OH, Al-Al-OH, and AlMgOH are some other bands observed in clay which is in the range of 900 to 800 cm^{-1} (Madeja et al. 2002 as cited by (Amarasinghe, 2009). Interlayer water in clay shows stretching vibration in the range of 3500 to 3000 cm^{-1} and bending vibration at around 1632 cm^{-1} (Johnston and Premachandra, 2001); Madeja et al. 2003

as cited by Amarasinghe 2009). This H-O-H bending and stretching vibration has been studied by various researchers as an indication for clay swelling. Hydration behavior of exchangeable cations of montmorillonite and effect of temperature on hydration of clays was tried to understand studying the H-O-H bending-stretching bands (Leonard, 1970), (Sposito and Anderson, 1975).

In our previous work, clay-fluid molecular interactions have been investigated using a wide range of polarity fluids. Characteristic H-O-H bending vibrations of interlayer water, Si-O stretching of clay sheet, and some other band like C-O and C=O stretching has been studied as an attempt to understand molecular interactions as high polarity to low polarity fluids enter into the interlayer. Transmission and reflectance FTIR techniques had been used.

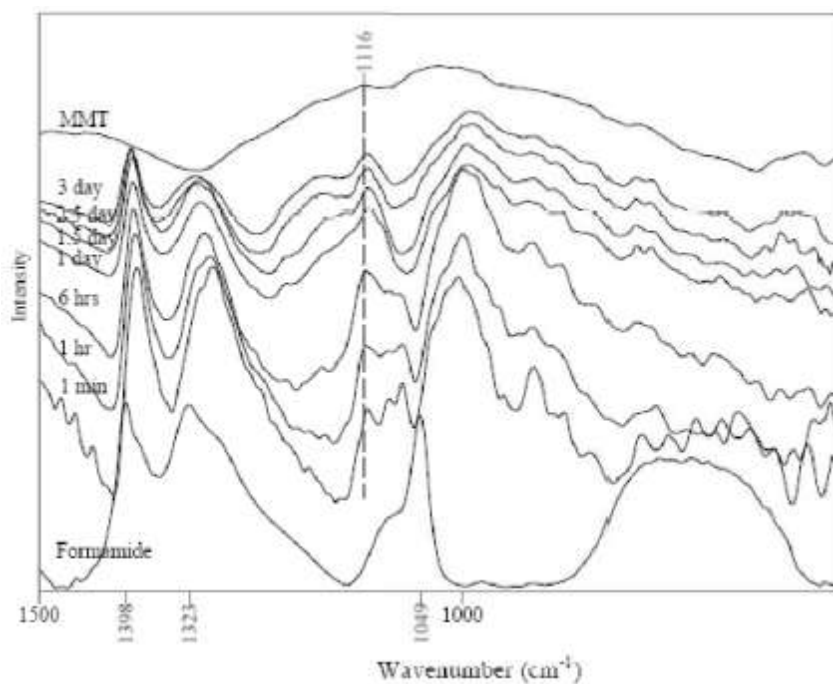


Figure 3.4: Reflectance spectra of MMT-formamide sample shows that shift in Si-O stretching bands with clay-fluid interaction time as more and more formamide molecules enter into the interlayer (Amarasinghe, 2009).

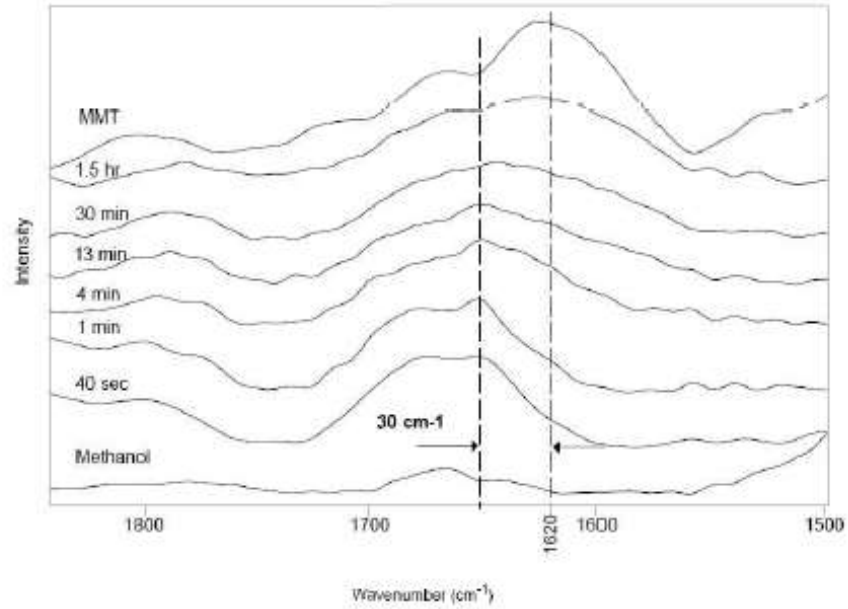


Figure 3.5: MMT-methanol sample reflectance spectra showing the change in HOH bending with clay-methanol interaction time (Amarasinghe, 2009).

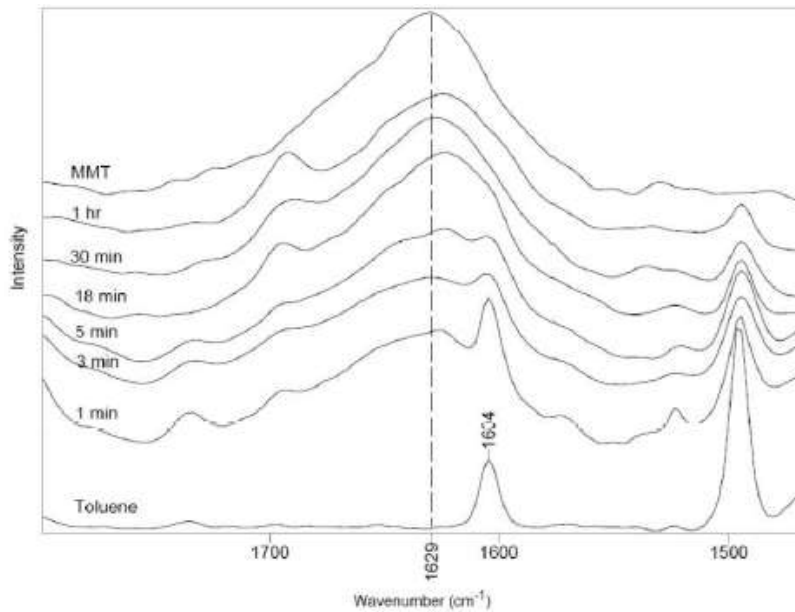


Figure 3.6: Reflectance spectra of MMT-toluene sample showing no significant changes in HOH bending with time which indicates the low molecular interactions between clay and toluene (Amarasinghe, 2009).

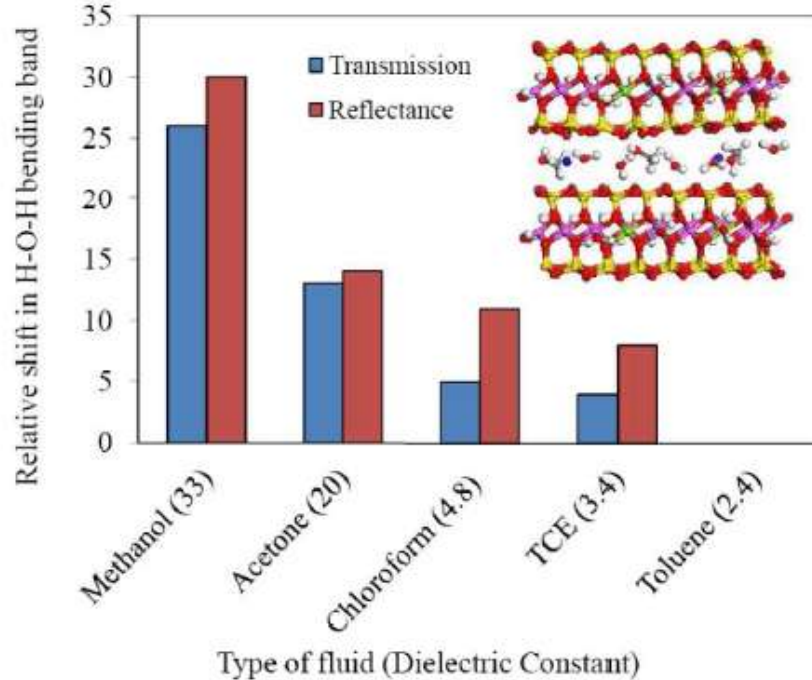


Figure 3.7: Relative shift in HOH bending for different fluids showing higher the polarity of fluids. greater the shift in HOH band (Amarasinghe, 2009).

Any shift in HOH bending is considered as the indication of molecular interactions. So, we qualitatively see that high polar fluids show greater amount of molecular interactions with fluids. Consistent results had been observed from both transmission and reflectance FTIR studies (Amarasinghe, 2009).

Our previous FTIR study shows some promising results indicating higher amounts of molecular interactions for high polar fluids. From scanning electron microscopy study we observe a greater amount of particle breakdown occurs for high polar fluids. In our present study, we used molecular modeling techniques to get a quantitative estimation of molecular interactions and amount of interlayer fluids at a particular level of swelling.

3.2.2 X-ray Diffraction Technique (XRD)

X-ray diffraction is a popular technique in mineralogy. X-rays are electromagnetic radiation with wavelength in the range of 10^{-1} to 10^{-5} nm and energies range of 100 eV - 100

keV. X-ray used for diffraction applications are usually of short wavelength with 0.1 or few angstrom (1 keV - 120 keV).

The primary source of X-ray in laboratory is X-ray tube. X-rays are produced when electron beam across a high voltage field bombard a target of interested element usually copper, tungsten, and molybdenum metal target. Electron from outer or inner shells of target material can be ejected depending on the energy of hitting electrons; consequently X-ray with characteristic energy is emitted. Cu and Mo target produces x-ray with an energy of 8 keV and 14 keV (wavelength of 1.54 Å and 0.8 Å) (Materials Research Laboratory, UC Santa Barbara). The energy associated with an x-ray photon can be represented as $E = hc/\lambda$, where h is Planck's constant and c the speed of light. If the transition of electron occurs from M shell to K shell, associated X-ray is called K_{β} radiation and if the transition occurs from L shell to K shell associated X-ray called K_{α} radiation. In XRD analysis only K_{α} radiation is used and K_{β} radiation is filtered out.

When x-ray hits the electrons of an atom, a portion of the x-ray beam deflects away. These diffracted waves travel different paths to interfere with each other and results in constructive or destructive interference. A sharp constructive interface (peak or maxima) of diffracted waves form in case of materials which consists of organized atomic pattern such as crystals. This peak resembles the symmetry of distribution of atoms as present in the material. So diffraction pattern can provide us useful information about distribution of atoms in a material or crystal structure.

The nature of peaks in x-ray diffraction depends on the atomic distances at different planes of a crystal structure. A constructive interference will form if the path difference between two waves is a multiple of wavelength, known as Bragg's law.

$$2d\sin\theta = n\lambda$$

Here n is an integer, λ wavelength; d is the distance between two planes.

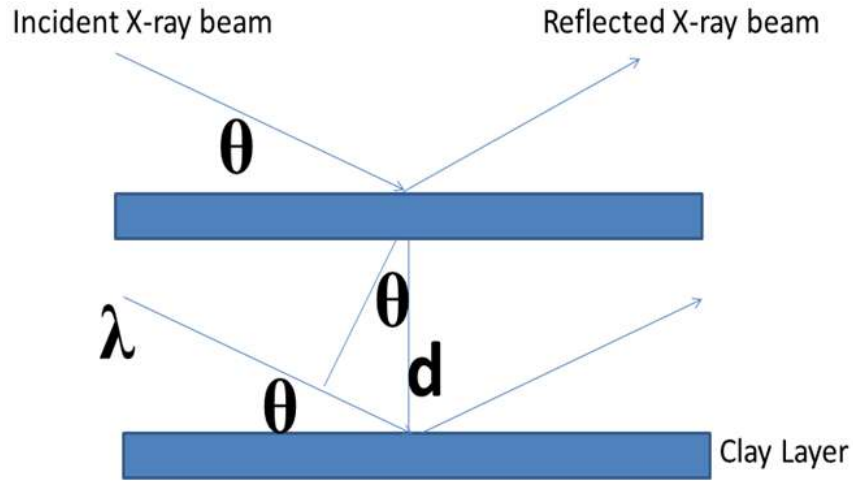


Figure 3.8: Schematic of X-ray reflection from clay surfaces.

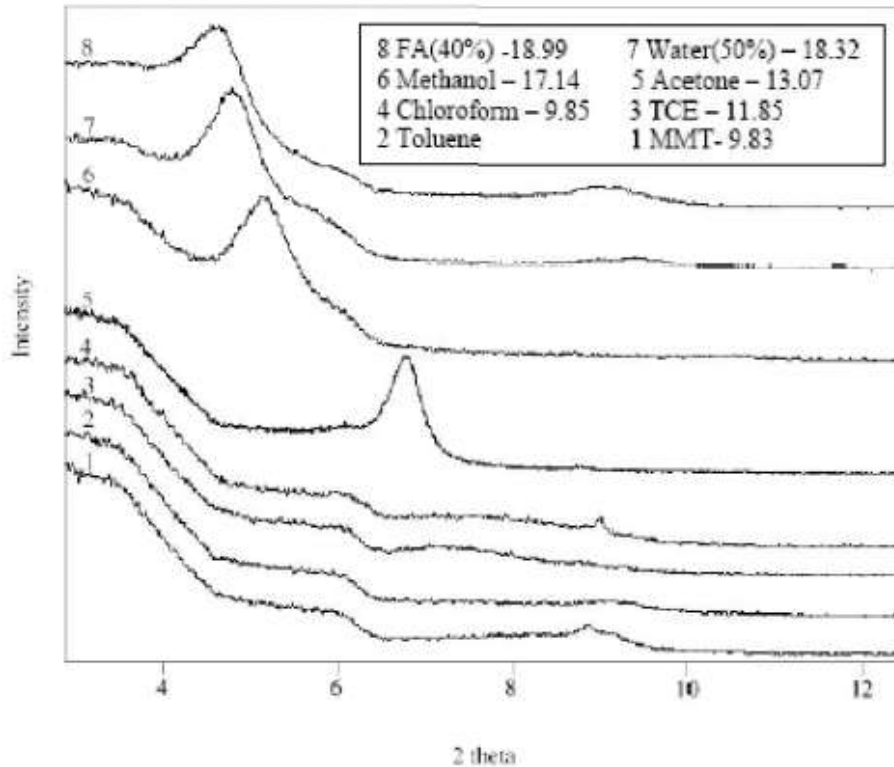


Figure 3.9: X-ray diffraction pattern for different clay-fluid systems showing higher value of d_{001} spacing for high polar fluids (Amarasinghe, 2009).

X-ray diffraction has been widely used in identification and structural studies of mineral. As the clay swells the interlayer space of swelling clays expands. XRD analysis can be used to accurately measure the d_{001} spacing of swelling clay minerals. Effect of modifier on clay had been investigated in our previous studies (Katti, et al., 2006, Sikdar, et al., 2006, Sikdar, et al., 2007, Sikdar, et al., 2009) which provided important information about clay based nano-composites. Influence of different interlayer cations on swelling behavior had been studied using XRD analysis (Olejnik et al. 1974 as cited by Amarasinghe, 2009). Time dependent swelling behavior has been studied in our previous studies (Amarasinghe 2009). Recent XRD studies of montmorillonite swelling clays with different polarity organic fluids reveal that high polarity fluids exhibits greater interlayer expansion thus greater swelling behavior. Our previous FTIR studies shows greater amount of clay fluid interactions in case of high polar fluids. Interesting results from our FTIR and XRD studies provide sufficient motivation for further experimental and modeling investigations.

3.2.3 Microstructure Analysis of Swelling Clay Using Scanning Electron Microscope (SEM)

Although significant studies have been performed on swelling clays, microstructure of clays had been overlooked. Continuum models of swelling clays overlooked the soil structure, mineralogy and interlayer cation type, thus not very successful in explaining swelling phenomenon. (Katti and Shanmugasundaram, 2001) revealed the effect of microstructure on macroscale mechanical, swelling and flow properties in swelling clays. Previous research successfully developed correlation between evolution of clay microstructure, swelling and swelling pressure. Swelling pressure of montmorillonite swelling clays had been measured with time using a controlled uniaxial swelling (CUS) device. The swelling pressure increase rapidly

for dry montmorillonite clays following a gradual increase and steady phase as presented in the Figure 3.10.

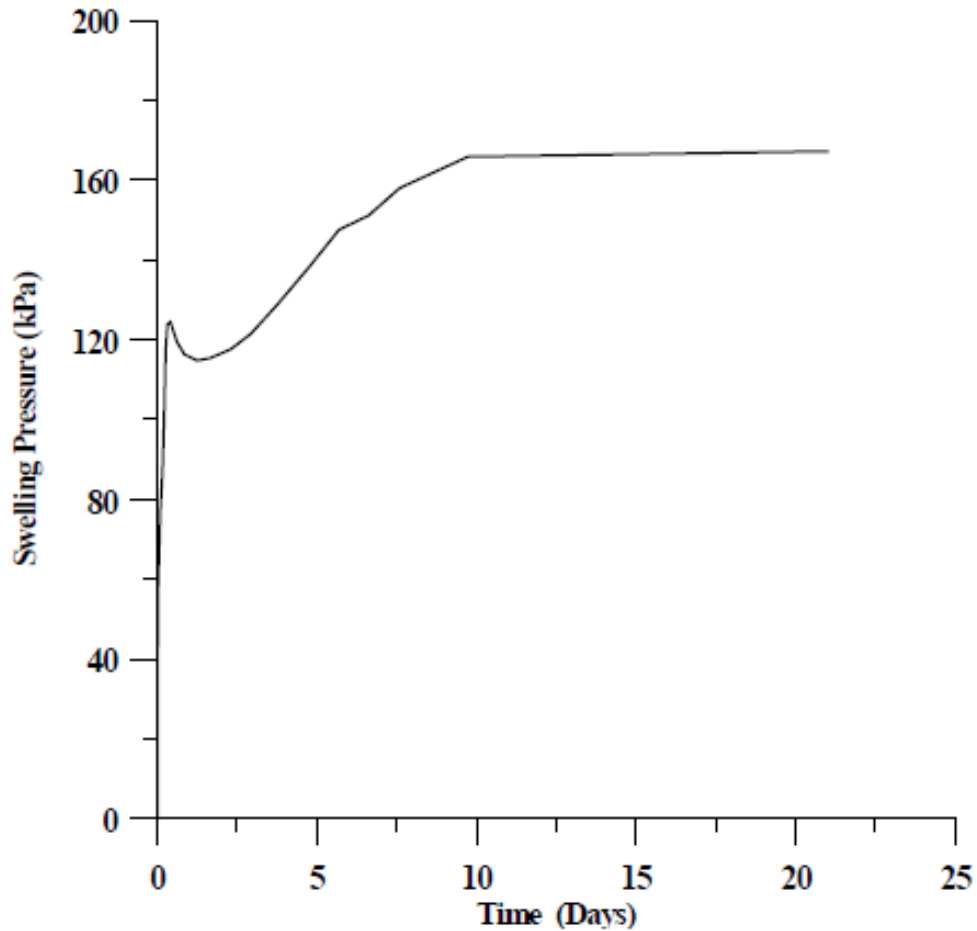


Figure 3.10: change in swelling pressure from dry state to increasing clay-water interaction time (Katti and Shanmugasundaram, 2001).

Swelling pressure had been recorded at different amount (0, 1, 2, 4, 10, 17.5, 25, 50, 75 and 100 percent) of swelling. Interesting correlation had been found that swelling pressure decreases with increasing amount of swelling as presented in Figure 3.11.

Effect of swelling and swelling pressure on clay microstructure has been studied using Scanning Electron Microscopy (SEM) imaging technique for 0%, 50%, and 75% (% by vol) swollen clays. Larger particle had been observed for zero swelling, comparatively smaller

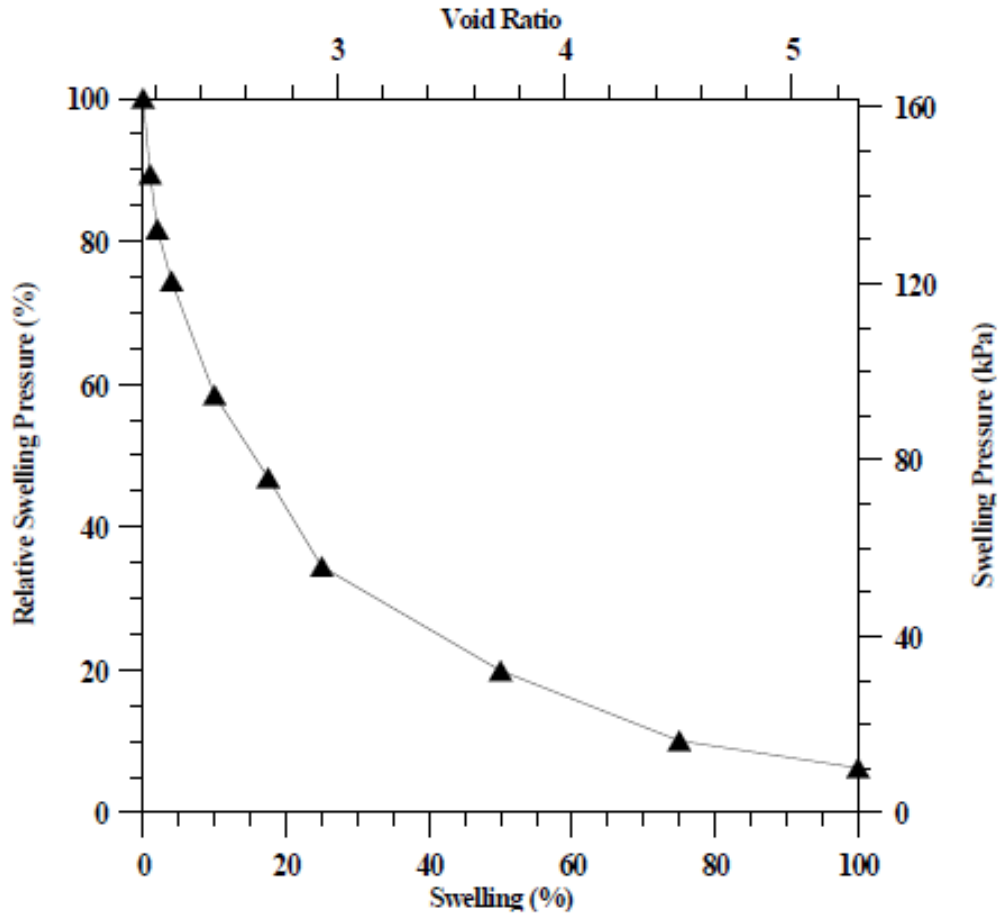


Figure 3.11: Change in swelling pressure and void ratio with different percent swelling (Katti and Shanmugasundaram, 2001).

particle size observed for 50% swelling clays and smallest particle size were observed 75% swollen clays. The observation was verified using image analysis software. Thus a very interesting phenomenon for swelling clays had been revealed which is as the clay swells, particles break down to smaller and smaller size (Katti and Shanmugasundaram, 2001).

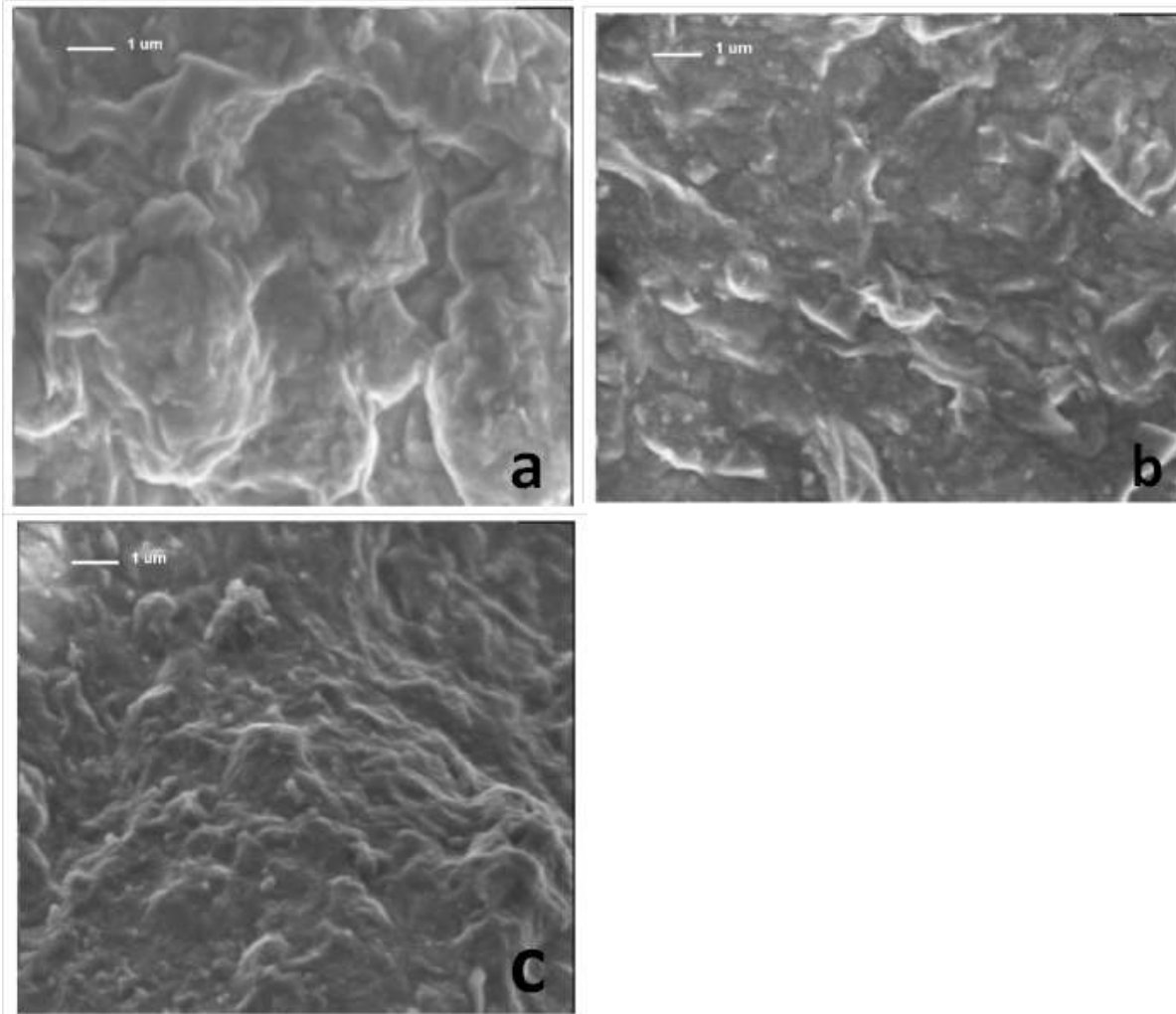


Figure 3.12: Scanning electron micrograph for clay-water sample at 0% swelling (a), 50% swelling (b) and 75% swelling (c). From the micrograph we see that clay particles break down into smaller sizes with increasing swelling (Katti and Shanmugasundaram, 2001).

Inspired by the interesting results with the clay-water system, the effects of fluid polarity on clay microstructure using Scanning Electron Microscope (SEM) were investigated.

Interestingly it has been seen that microstructure of clay with different organic fluid is significantly different. In the Figure 3.14 we see that for dry condition clay particle is large and have enough void spaces. For high polar water clay particles break down and we see very low void

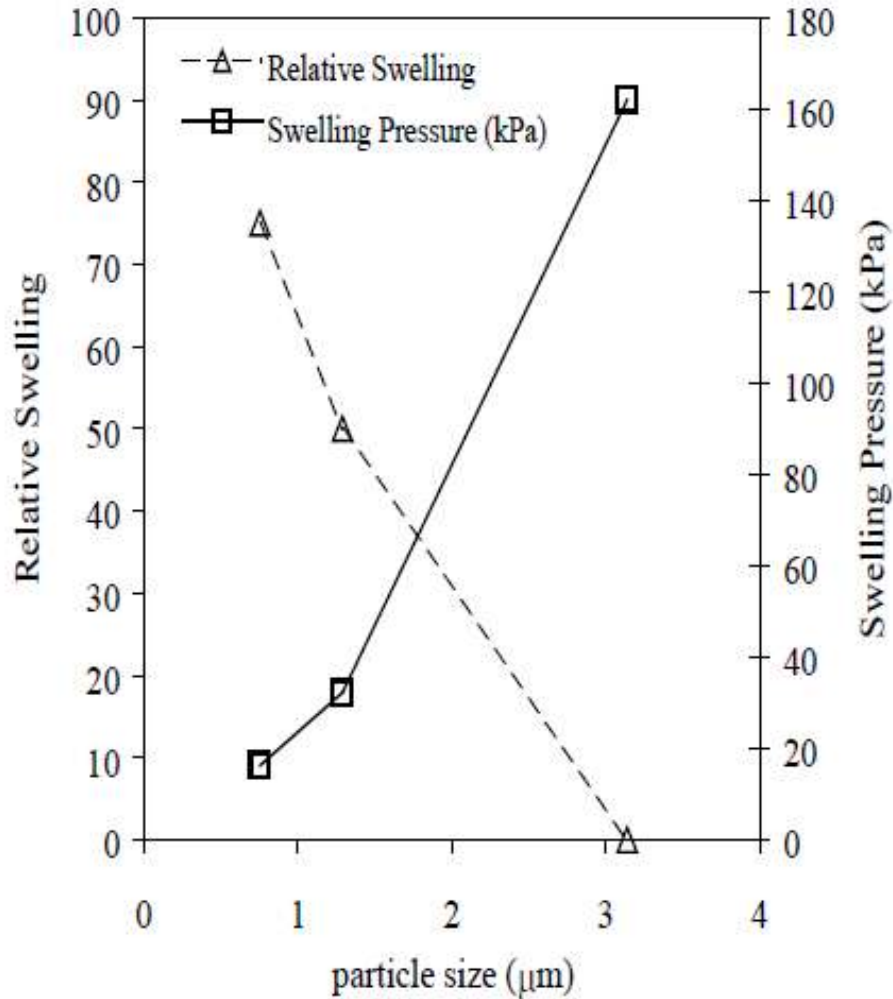


Figure 3.13: Change in particle size with swelling and relative swelling pressure (Katti and Shanmugasundaram, 2001).

spaces. For low polar fluids like TCE we see larger particles and void space, almost same as dry clay. For medium polarity methanol we see a behavior in between high and low polar fluids.

This indicates that high polar fluid causes greater amount of particle breakdown while low polar fluid have less influence on clay microstructure. Thus high polar fluids show greater swelling pressure. As the swelling occurs, for high polar fluids, clay particles breakdown into smaller particles resulting a decrease in void spaces which may be the reason for low permeability of high polar fluids. For low polar fluids since small amount of fluids enter into the

interlayer, less number of particles breakdown occurs, hence the pore size remains the same. This is may be the reason for high permeability for low polar fluids. Previous SEM studies were able to develop significant correlation between fluid polarity with change in microstructure and flow properties of swelling clays.

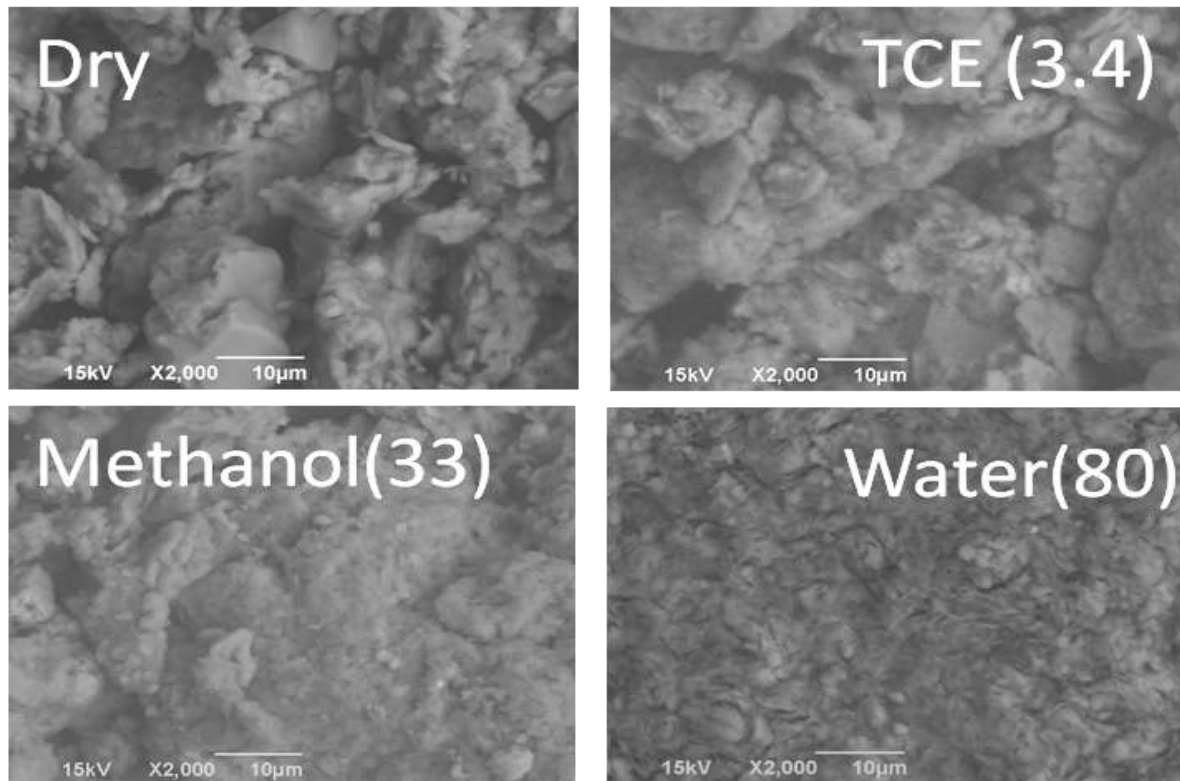


Figure 3.14: Scanning Electron Micrograph (SEM) image of dry Na-MMT clay and different clay-fluid samples (Amarasinghe, 2009).

3.2.4. Macroscale Testing on Clays

Correlation of molecular scale and microscale phenomenon with macroscale properties is necessary for complete understanding of swelling mechanism of clays. Among different macroscale testing for engineering applications permeability, consolidation and Atterberg Limit tests were conducted in our previous studies and attempted to develop a correlation of properties at different length scale.

3.2.4.1. Permeability Test

Permeability also termed as saturated hydraulic conductivity is the rate of fluid flow through a unit cross section of porous media at standard temperature and unit hydraulic gradient (ASTM D 5084). Mathematically hydraulic conductivity was presented by Darcy (1856) as

$$Q = k i A$$

Here, Q = rate of flow (cm^3/sec), k = coefficient of hydraulic conductivity (permeability), i = hydraulic gradient and A = cross sectional area.

Falling head and constant head methods are two most common laboratory tests for permeability measurement. Falling method is used for fine grained (clay) soil with low permeability while constant head method is appropriate for fine to coarse grained soil (silt and sand). In this method, hydraulic head is allowed to fall during experiments and recorded over time. If for a small period of time dt , change in hydraulic head is dh and discharge is dQ then,

$$dQ = - dh a = k (h/L) A dt \quad (\text{Tschebotarioff, 1951 as cited by Amarasinghe, 2009})$$

$$\text{So, } k = 2.3 (La/At) \log_e (h_1/h_2)$$

Here, K = coefficient of permeability, L = Length of the sample, a = cross sectional area of tube, A = cross sectional area of sample.

In constant head permeameter, hydraulic head are kept constant and volume of water is measured over time. The permeability for constant head permeameter can be expressed as

$$K = \Delta Q.L / (A.h.\Delta t)$$

Here, ΔQ = flow of fluid for a time interval Δt , A = cross sectional area of sample and h = avg head loss across the sample.

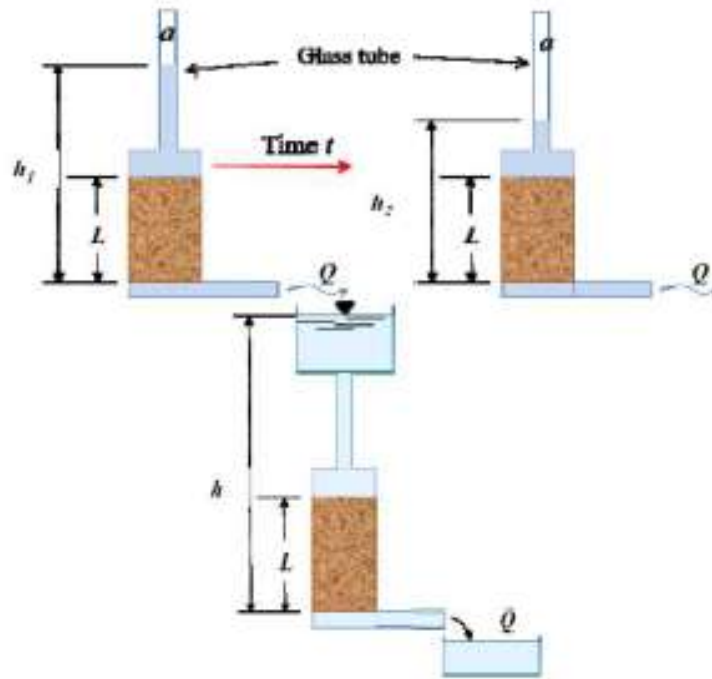


Figure 3.15: Constant head (bottom) and falling head (top) permeability testing device (Amarasinghe, 2009).

Our previous study suggests that swelling causes change in microstructure (Katti and Shanmugasundaram, 2001, Amarasinghe, et al., 2009) which makes the permeability test results inaccurate as the cross sectional area do not remain same. To solve the problem, a new permeability testing device was designed by the group and permeability of different polarity fluids was calculated. The test method ASTM D5084 (2003) were followed and standard test method for flexible wall cells were used. The sample saturation was confirmed during permeability tests. Interestingly, it took different amount of time for different polarity fluids to saturate the clays; almost six months for formamide, one month for water, less than a week for other fluids. The permeability test of Na-Montmorillonite with TCE, toluene, methanol and water were performed by previous PhD student Pryanthi Amarasinghe. Permeability of Na-Montmorillonite with formamide took more than one year while all other tests took almost one

year. From our experiment permeability of Na-Montmorillonite with water was found as 3.77×10^{-10} which is very much agreeable with the existing literature (Gleason, et al., 1997). In terms of magnitude, still our results represent more accurate value due to a newly designed device.

Our permeability test results indicate that the permeability of clay with toluene is 10^6 times greater than permeability of the same clay with water. Again, permeability of clay with formamide is 100 times lesser than permeability with water. So, we see that permeability of fluids through clays decreases with increasing polarity. These results provide a wonderful trigger for the reason behind landfill liner failure, a great concern for health, safety and environment. Since, permeability of low polar organic fluids can be million times greater than water, barrier system designed assuming water permeability is no longer adequate.

3.2.4.2. Triaxial Consolidation Tests of Na-Montmorillonite Clays

Consolidation characteristics of soil are very important for design and construction of structures. Despite the simplicity of odometer consolidation technique it does not mimic the real system as lateral confining stress cannot be applied. In our previous study, a new device had been designed and fabricated which capable of applying confining stress to mimic the field condition. Using the new device, confining stress was applied in the range from 27.58 KPa to 186.16 KPa and at each pressure volume change of the sample was monitored. The drainage was allowed in both sides of the sample.

Coefficient of consolidation (C_v) was calculated using the equation-

$$C_v = T_v H^2 / (4t_{90})$$

Here, T_v is the time factor $t_{90} = 0.848$, t_{90} is the 90% primary consolidation time, and H is the max drainage length.

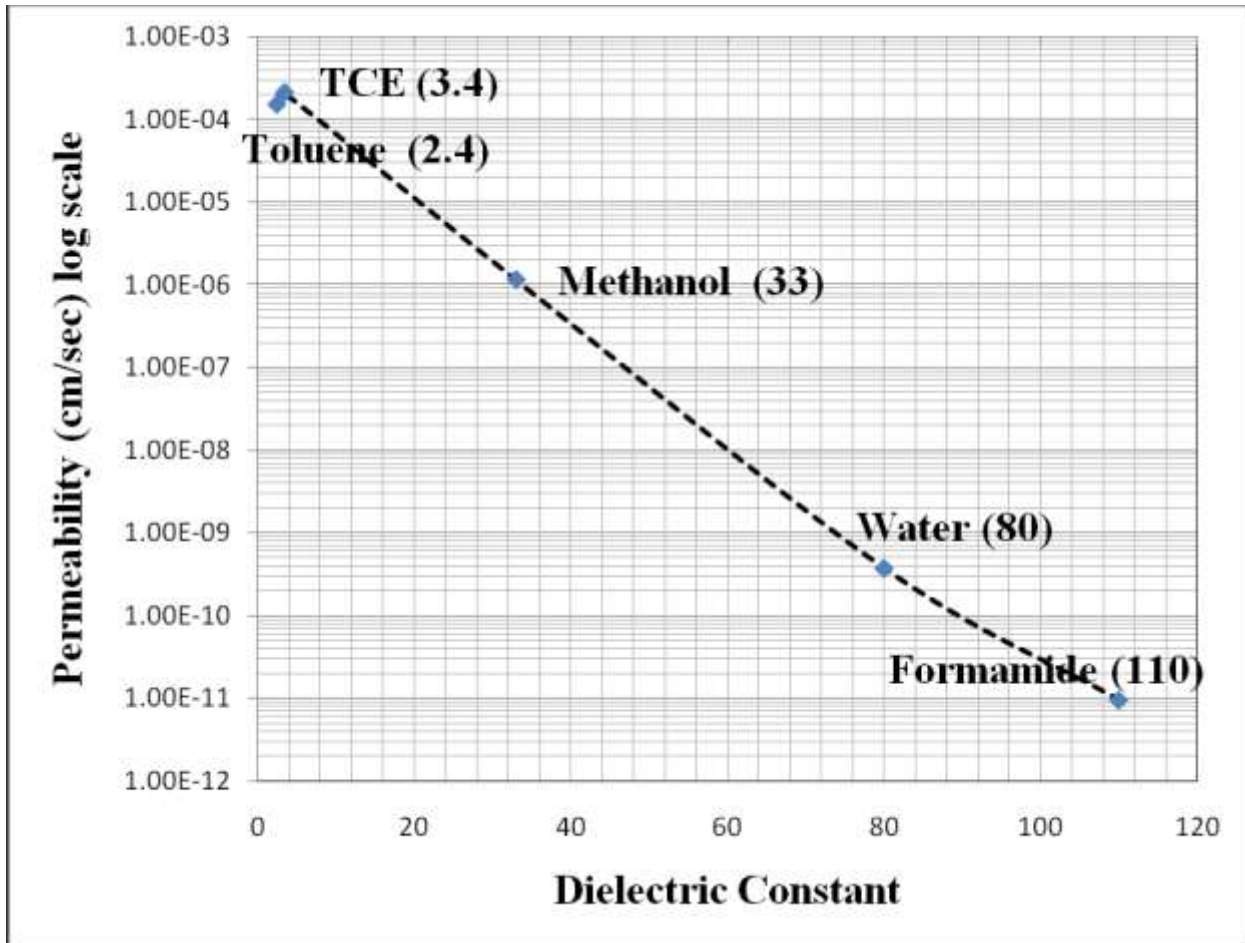


Figure 3.16: Permeability Vs dielectric constants graph, showing higher permeability for low polar fluids.

We see from the graph that coefficient of consolidation (C_v) decreases with increase in effective stress. This is may be due to at low effective stress only loosely bound pore water expelled out where at high effective stress interlayer waters also possibly comes out. Again, similar to hydration of interlayer dehydration of clay interlayer is a slow process (Amarasinghe, 2009).

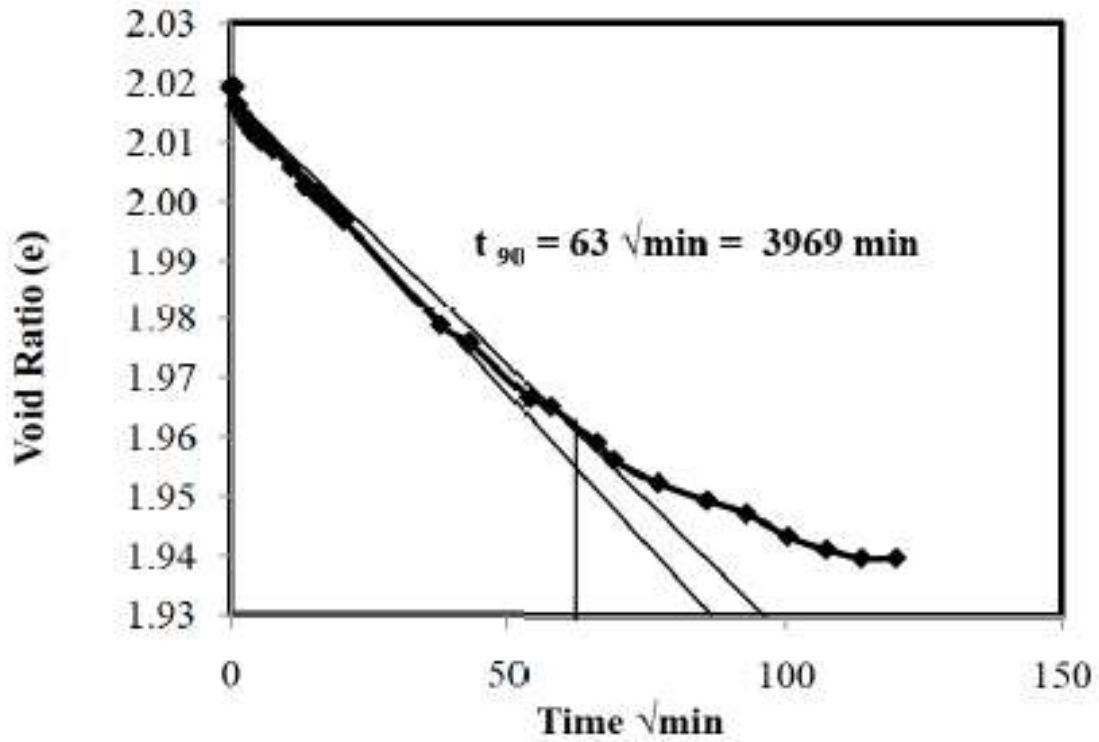


Figure 3.17: Void ratio (e) Vs \sqrt{t} , consolidation test at 186.15 KPa effective stress (Amarasinghe, 2009).

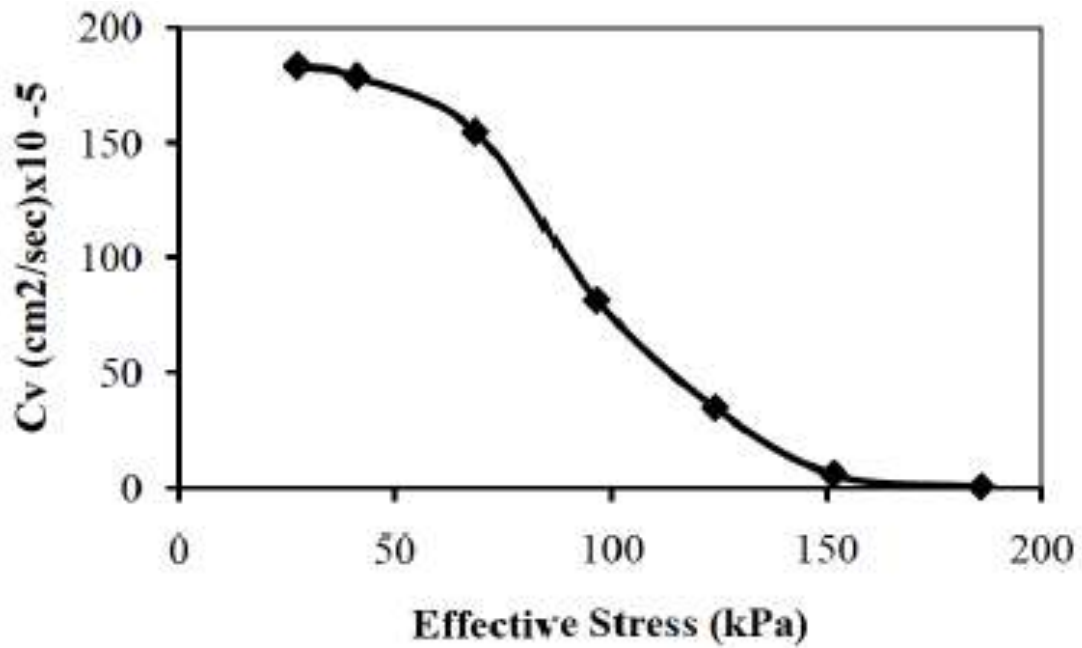


Figure 3.18: Coefficient of consolidation (C_v) Vs effective stress (Amarasinghe, 2009).

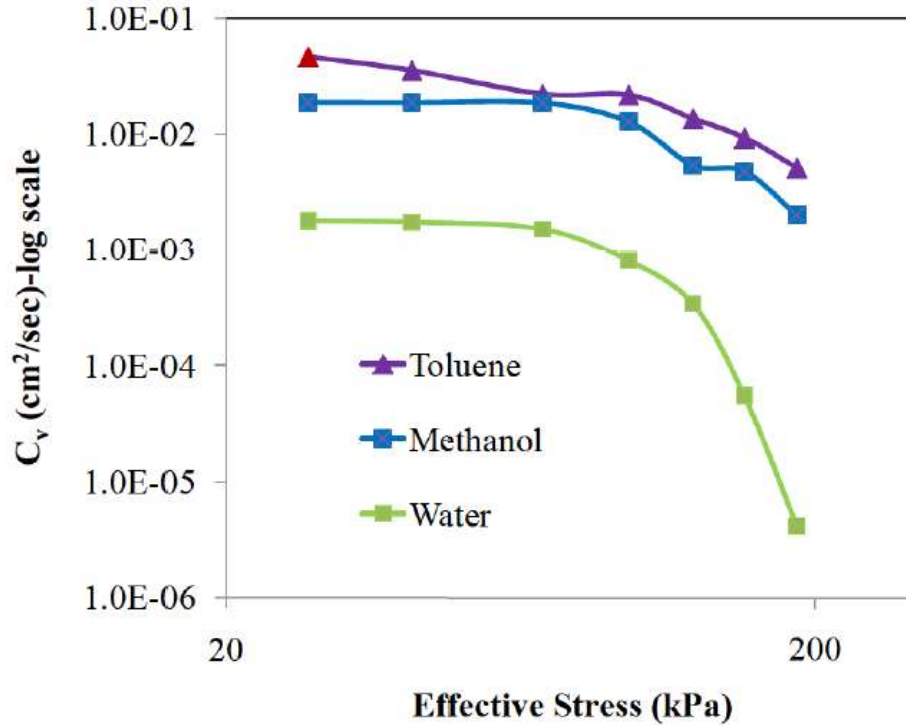


Figure 3.19: Coefficient of consolidation (C_v) Vs effective stress for different solvents (Amarasinghe, 2009).

From the C_v versus effective stress plots for different solvents although C_v decreases with increasing effective stress for every solvent, a significant variation between high polar water and other low polar organic solvents had been observed. This may be due to very low permeability of high polar solvents in taking longer time to expel out the solvents in comparison to nonpolar solvents with higher flow rate in clays. Again, coefficient of consolidation (C_v) had been observed to be even smaller when effective stress become greater than the swelling pressure of clays. This may be due to the decrease in void space or less mobility of clay bound water.

Compression index (C_c) had been determined by calculating the slope of the “void ratio Vs log (effective stress)” - curve (linear portion) using the following equation-

$$C_c = \frac{e_2 - e_1}{\log \frac{p_2}{p_1}}$$

Here, e_1, e_2 = void ratio of sample at effective stress P_1 and P_2 .

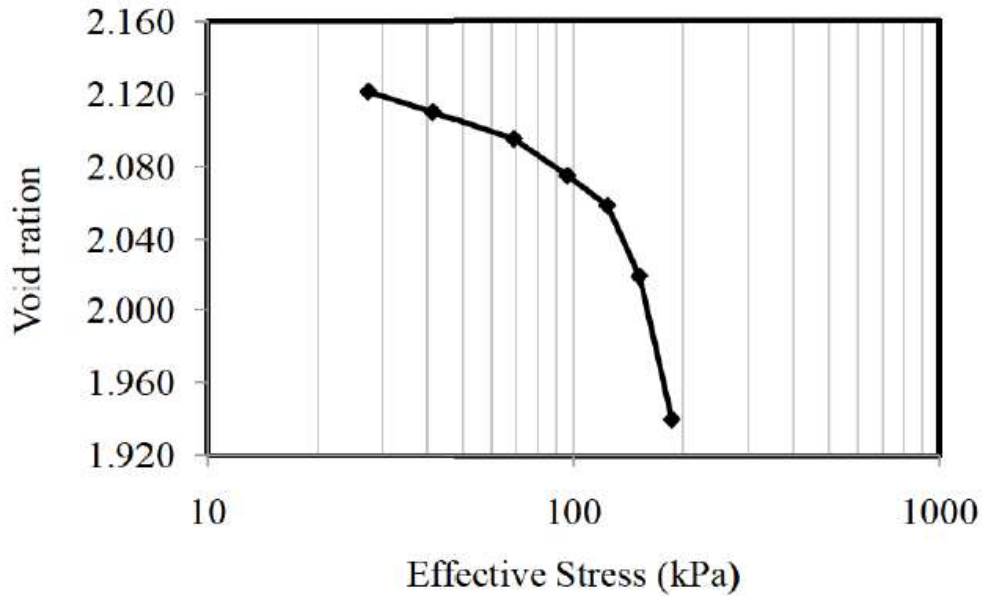


Figure 3.20: Void ratio Vs effective stress (Amarasinghe, 2009).

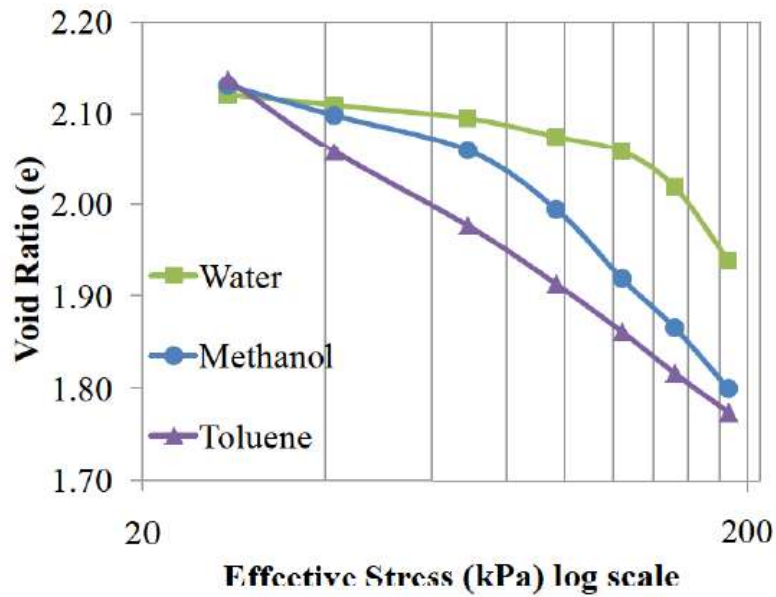


Figure 3.21: The change in void ratio due to effective consolidation pressure for different clay-fluid samples (Amarasinghe, 2009).

Clay had been observed to have a preconsolidation pressure of 70 KPa in case of water while no preconsolidation pressure was observed in case of toluene which is similar as behavior

of granular soil such as sand and silts. This observation had been suggesting that consolidation behavior of swelling clays changes from cohesive to cohesionless with a decrease in fluid polarity. Low preconsolidation pressure was observed in case of methanol, medium polarity fluid. It had been observed that compression index (C_c) of clay also depends on fluid polarity, higher the polarity of fluids larger the compression index.

3.3 Modeling Techniques for Study of Swelling Clays

3.3.1 Discrete Element Method (DEM)

Discrete Element Method (DEM) is a numerical technique to simulate behavior of a volume containing large number of particles. The method has been used in studying geomaterials such as soil, rock and concrete. In DEM, granular material is considered as an assembly of rigid particles and interactions among individual particles is considered explicitly. This method has successfully been able to simulate the behavior sands, silts and non-swelling clays. Mechanical and physical properties of clays depend on complex forces including body forces (friction, bouncy and gravity), microscopic interactions and inter particle forces.

(Anandarajah, 1997, Yao and Anandarajah, 2003) has studied the one dimensional compression for montmorillonite to investigate the influence of particle orientation. His study shows that clustered particle orientation or contacts has greater significance in stress-strain behavior than individual particle orientation of the entire assembly (Anandarajah, 2000). Later on, three dimensional discrete element technique had been used for the analysis of clays by (Yao and Anandarajah, 2003). Two dimensional DEM had been studied by Anderson and Lu (2001) to study the effect of microscopic force on volumetric behavior of clays. Although settling velocity and force equilibrium had been considered in this model, the swelling of clays had been ignored. Moreover, clay particles are not spherical as considered in the model rather platy shape in reality.

Another interesting experimental finding of our previous study shows that the particles break down into smaller size as clay swells. None of the state of art DEM models have addressed this phenomenon. To address the issue, in our previous study a modified discrete element method has been developed to simulate the breakdown of clay particle with increasing swelling (Katti, et al., 2009).

Properties of non-swelling clays and sands depends on soil fabric (Katti, et al., 2009). In case of swelling clays, soil fabric changes with swelling and microstructure controls the properties of swelling clays. Engineering properties of swelling clays such as shear strength, stress-strain behavior, permeability, swelling, and shrinkage phenomenon are determined by both inter particle and clay interlayer forces. With increasing moisture content as the water enters into the interlayer evolution of microstructure occurs in swelling clays. Discrete Element Method (DEM) models ignoring the change in microstructure with swelling may lead to an inaccurate conclusion. For the complete understanding of swelling clays, this important property need to be incorporated in DEM models, to accurately simulate the behavior of swelling clays. (Katti, et al., 2009) developed a modified discrete element method which incorporates evolution of microstructures. Figure 3.22 shows montmorillonite particles decrease in size with increasing swelling. Dissociation of clay layers associated with increasing hydration is the reason for this particle breakdown. A complete understanding of the different forces acting on the clay interlayer is necessary for the understanding of this phenomenon. Our previous molecular dynamics study on mechanical response of clay interlayer with increasing hydration provides important information on this phenomenon.



Figure 3.22: Discrete Element Model (DEM) showing evolution of microstructure in montmorillonite, particles decrease in size with increasing swelling (Katti et. al., 2009).

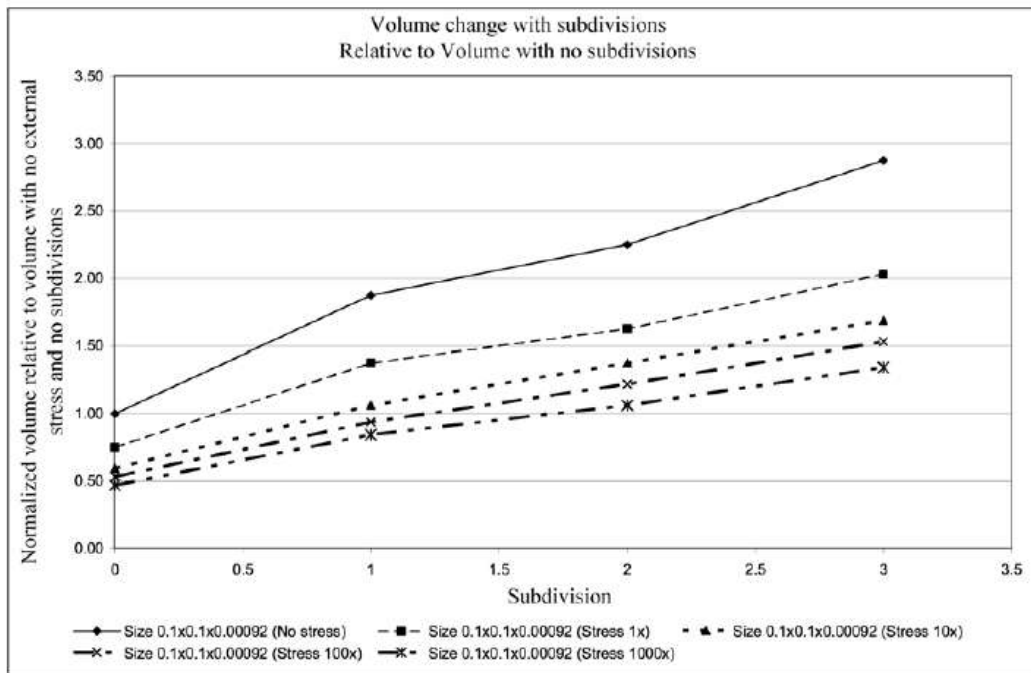


Figure 3.23: For different particle subdivision volume changes relative to volume at zero stress and no subdivision (Katti, et al., 2009).

3.3.2 Molecular Dynamics Simulations

Molecular modeling simulates the phenomenon of a molecular system by calculating the energy of the system. The energy of the system varies with the atomic and molecular arrangements. Monte Carlo (MC) and Molecular Dynamics (MD) methods are two common techniques for the calculation of energy. (Stillinger and Rahman, 1974) first used the Molecular dynamics technique to simulate liquid water (Schmidt, 2005).

In molecular mechanics, atoms are considered as Newtonian particles. Atomic interactions follow the potential energy function which depends on several factors such as bond length, angle, torsion angle and non-bonded interactions. Non-bonded interactions consist of electrostatic and Van der Waals interactions. The forces acting on an atom depends on its position in a molecular system, and its surrounding atoms. The potential energy function of a molecule depends on molecular structure (Hypercube, Inc. 1996 as cited by (Schmidt, 2005).

With change in position of atoms, bond length, angle and dihedral values of molecules potential energy of the system also changes. Figure 3.24 shows a typical potential energy curve for a diatomic molecule showing how the energy of the molecule changes with change in bond length. The potential distribution for multi-atomic molecules will certainly be more complex. The energy minimum of the curve at particular time represents the bond length between the atoms.

At infinite separation between two atoms, the attractive energy is constant and approaches near zero which is the energy of two individual atoms. When two atom approach close to each other, attractive forces increases up to a certain separation, which is the minimum energy separation and distance between the atoms is the stable bond length of the molecule. At distance closer than stable separation distance, repulsive force between the atoms sharply

increases to $+\infty$. Obviously, potential energy will be quite complex, depending on inter-atomic interactions between the atoms within the molecules. In a force field, empirically the potential energy curve is reproduced which requires several factors to be verified and depends on atom types, atomic charges, functional form of the energy equation, and parameters for the function terms (Molecular Simulations, Inc., 2000 as cited by Schmidt, 2005).

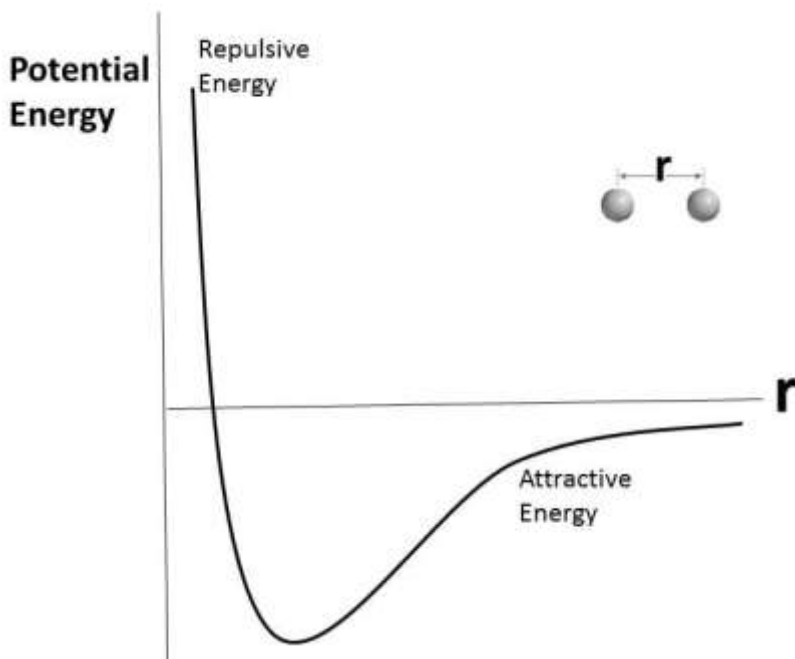


Figure 3.24: Potential energy curve for a diatomic molecule.

3.3.2.1 Force Fields

In a molecular system, position of atoms changes or vibrates with time. Therefore bond lengths, bond angles, and torsions changes with time, consequently Van der Waals and electrostatic interactions among atoms also changes. In molecular mechanics, this change is represented by a set of equations, known as force field and atoms are considered as charged particles bonded by a spring. Therefore, force field is the reproduction of molecular geometry and properties of tested structures by a set of equations and constants (NCSA NAMD Workshop 2002). Force field consists of equation sets for bonded and non-bonded interactions. Bond

distances, bond angles and torsion angle are used to represent the interactions between bonded atoms, while non-bonded interactions between atoms are described as Van derWaals and electrostatic interactions.

Force field is developed for a specific set of molecules at particular conditions and then optimized by a number of experimental and numerical methods. Force field developed for a particular situation may give poor or completely different results in another situation. For example, force field of a fluid can be different from its vapor condition. The energy of molecular interactions is described by bond stretching, bond angle bending, dihedral angle bending, improper dihedral deformation, and non-bonded interactions. Second generation force fields can promisingly simulate the real system by considering additional cross terms for bond or angle distortions caused by surrounding atoms. These cross terms may include stretch-stretch, stretch-bend-stretch, bend-bend, torsion-stretch, torsion-bend-bend, bend-torsion-bend, and stretch-torsion-stretch (Molecular Simulations, Inc., 2000 as presented by Schmidt, 2005).

With the advancement of modern computing system, molecular dynamics simulations become more and more popular in the scientific community. A number of commercially available and open source software is available. Each of these has particular competence and weakness. Consequently, a number of force field or potential functions have been developed to support these programs. Among many force field parameters CHARMM, Amber, CFF, UFF are some of the popular ones. In our simulations, CHARMM forcefield parameter and simulation software NAMD 2.7b2 were used. The energy functions as described in CHARMM (Brooks, et al., 1983) are as follows.

$$E = E_{\text{bond}} + E_{\text{angle}} + E_{\text{dihedral}} + E_{\text{nonbonded}}$$

$$E = k^B (r - r_0)^2 + k^A (\theta - \theta_0)^2 + V^D [1 + \cos(n\phi + \delta)] + \sum_{i \neq f} 4\epsilon_{if} \left[\left(\frac{\sigma_{if}}{r_{if}} \right)^{12} - \left(\frac{\sigma_{if}}{r_{if}} \right)^6 \right] + \frac{q_i q_f}{r_{if}}$$

The different terms of the CHARMM potential equation can be graphically presented as shown in Figure 3.25.

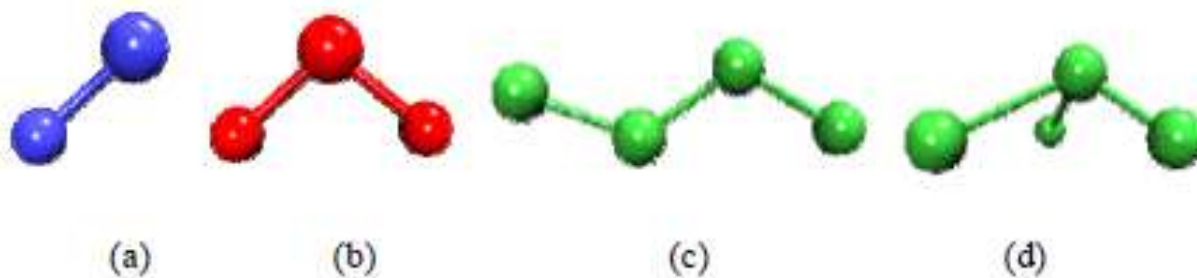


Figure 3.25: Graphical representation of the interactions that described by equations in CHARMM force field: (a) bond stretching, (b) angle bending, (c) dihedral angle bending, and (d) improper angle deformation (NCSA NAMD Workshop, 2002).

In the derivation of force field, bond between atoms are considered as analogous to two masses connected by a spring. The spring constant of the spring is calculated according to Hooke's law. In bonded terms of energy equations, K^B is the spring constant, r_0 is equilibrium distance between two atoms, and r is distance at any particular time. The r_0 value is the distance between two individual atoms, but not the same as when present in molecules. This value can be obtained from experimental observation. Mathematically, r_0 is the bond length of two atoms at a hypothetical unperturbed state where the bond is an isolated occurrence without the effect of any external forces and outside the molecule. However, in real molecular system neighboring atoms influences the stretching or compressing of a bond and never at a perturbed state. A higher value of spring constant k^B represents a stronger bond and the bond tends to remain at its reference length r_0 (Hypercube, Inc. 1996, NCSA NAMD Workshop, 2002 as cited by Schmidt, 2005).

The second term in the energy equation represents the deformation of a bond angle from its normal position. Similar to bonded term, here θ_0 represents the bending angle at a virtual unperturbed state. In a molecule, angle of bending can be significantly different from its

equilibrium value as a result of intermolecular restrains (Dinur and Hagler, 1990). The dihedral term represent the torsional potential around a middle plane.

The dihedral potential function in molecular mechanics is commonly given as a truncated Fourier series (Schmidt S., 2002).

$$E_{dihedral} = \sum_{dihedral} k_{\phi} [1 + \cos(n\phi + \delta)]$$

In the equation, k_{ϕ} = dihedral force constant, n = periodicity of the Fourier term, δ = phase angle, and ϕ = dihedral angle. The period of the interaction is $360/n$ and the phase angle δ represents the shifts of the curve to the left or right. Torsional energy is usually used as correcting term for rest of the energies rather representing an actual physical process. The amount of energy that needs to be added or subtracted from the cumulative bond, angle, and non-bonded energy terms to represent the actual total energy with experiment or quantum mechanical calculations is usually known as torsional energy (The NIH Guide to Molecular Modeling, 1996).

Interaction between atoms not connected by any physical bond, bending angle or sometimes dihedral are known as non-bonded interactions. Non-bonded interactions are possible between atoms within the same molecule or atoms of different molecules. Nonbonded interactions consist of two opposing forces, Van der walls repulsive force that keeps the atoms apart at close range and attractive force that bring them together at long range. The potential is referred to as a Lennard-Jones or 6–12 potential, and is summed over all nonbonded pairs of atoms i and j separated by a distance r_{ij} (Hypercube, Inc. 1996 as cited by Schmidt, 2009). The electrostatic interaction is strong and acts in a very short range usually at distance less than the sum of contact radii of interacting atoms. On the other hand, the attractive force is long range and due to the effect of induced dipoles or London dispersion.

3.3.2.2 Molecular Dynamics

The molecular dynamics (MD) simulation technique is based on the Newton's second law or the equation of motion, that is $F=ma$. Here, F = force on atom, m = mass, and a = acceleration. The bonding between two atoms is analogous to a spring connecting two masses and is calculated by Hooke's law. So, the acceleration of each atom of a system can be found if the force on each of the atom in the system is known. Newton's equation of motion can be correlated with the derivative of the potential energy to the changes in position as a function of time. The initial positions can be obtained from experimental studies, such as the x-ray crystal structure. Then by integrating the equations of motion, a trajectory of atoms that describes the positions, velocities, and accelerations of the atoms with time can be found ("Tutorial-Molecular Dynamics Simulation-CHARMm," 1999).

The force on an atom can be described by the change in energy, E with respect to its position vector, r_i . So,

$$-\frac{dE}{dr_1} = F_i$$

Here, E = potential energy and r_i = position of atom i . Again $F= ma$ where acceleration 'a' can be represent as the double derivate of position vector. Therefore the equation can be written as,

$$-\frac{dE}{dr_1} = m_i \frac{d^2r_i}{dt^2}$$

In case of constant acceleration, it can be expressed as; $a_i = \frac{dv_t}{dt}$ expression for the velocity can e obtained by after integration, $v_t = a_t t + v_0$

Again, velocity can be expressed as, $v_t = \frac{dr_t}{dt}$. By integrating the equation we can obtain the relation between velocity, time and position vector, $r_i = v_i t + r_0$

By combining this equations for velocity and position vectors we can obtain,

$$r_i = a_i t^2 + v_0 t + r_0$$

Therefore, a trajectory can be calculated using only the initial positions of the atoms, initial velocity distribution, and the acceleration. Initial position can be obtained from crystallographic study or ab initio calculations and acceleration can be obtained from the gradient of the potential energy function.

A typical molecular dynamics simulation usually consists of several steps. First step is the preparation of the model. Preparation of the molecular model requires the initial coordinates of molecule which usually can be obtained from X-ray crystal structure, and the bonds present within atoms in the molecule. Next step is the energy minimization of the model. Minimization is performed to get rid from any strong localized energy, may be due to the Van der waal interactions. Minimization diminishes if there is any localized energy present in the model, which is very important as it may cause local structural distortion or make the simulation unstable at later steps. Minimization is usually done by running the simulation appropriate number of iterations without assigning atomic velocities. Geometry of the structure become optimized during the minimization depending on the force field parameters has been used. The optimized structure after minimization can be termed as static (NCSA NAMD Workshop, 2002; Hypercube, Inc., 1996; "Tutorial-Molecular Dynamics Simulation-CHARMm," 1999).

The third step is raising the temperature of the system usually 0K to 300 or 298K. In this step, simulation is started with initial velocities at low temperature; consequently velocity is assigned with higher temperature. Usually raising temperature consists of several steps. Although temperature can be raised at a single steps, but multiple steps allows the system equilibrated at each time step (NCSA NAMD Workshop, 2002; Hypercube, Inc. 1996; "Tutorial-Molecular Dynamics Simulation-CHARMm," 1999). The next step is equilibration to make sure

that the system is stable. Usually after reaching the desired temperature the simulation is kept continued up to certain number of time steps while structure, pressure, temperature and energy of the system is monitored. The system is considered to be equilibrated when these properties of the system become stable over time. At this step, atoms interact with each other following the equation of motion and reach at the equilibrated velocities (NCSA NAMD Workshop, 2002; Hypercube, Inc. 1996; “Tutorial-Molecular Dynamics Simulation-CHARMm,” 1999). The fifth step is the simulation of the system at desired condition and data collection. The sixth and final steps of molecular dynamics simulation is the analysis of data. Data analysis can be trajectory, conformation, energy calculation or any other parameter of the system. As the molecular dynamics is a very dynamic process, time average of particular segment is frequently used depending on the size of the simulation length. Molecular simulation can be performed at different desired condition such as NPT, NVT, NVE, and NE. In NVT simulation temperature and volume remain constant, in NPT temperature and pressure remain constant, in NE is the constant energy and constant particle number simulation and NVE is the constant energy and constant volume simulation. The type of simulation is determined depending on the actual physical condition or scope of the simulation. NVT and NPT are most popular molecular dynamics simulation.

3.3.3 Molecular Dynamics Study on Swelling Clays

Molecular dynamics simulation had been used as an effective tool for the study of swelling clays. Although several researchers have attempted to study swelling phenomenon of clays using molecular dynamics simulation, there is still a lack of understanding the link between the molecular phenomenon with micro and macro scale properties. For complete understanding

of clay swelling mechanism, bridging the molecular level interactions with microstructure change and macro scale swelling and flow properties is necessary.

Molecular dynamics technique used for the study of structure and dynamics of interlayer fluids in swelling clays by (Skipper, et al., 2006). (Skipper, et al., 2006) considered confined aqueous and organic fluids within interlayer pores of 2:1 swelling clays as a 2 dimensional environments. Their study shows that local hydrogen bonding environment is remarkably resilient in comparison to bulk water and in the case of clay-water system. Confined interlayer water molecules are capable of forming hydrogen bonds with each other as well as with the clay surfaces.

The adsorption isotherms of water in Li, Na, and K montmorillonite had been used by (Hensen, et al., 2001) to study using Monte Carlo molecular simulation technique. They calculated the water adsorption isotherms for Li-, Na-, and K-montmorillonite considering at fixed d_{001} spacing of 12.0 Å. They described the water adsorption as two-step process: firstly at low concentration adsorption of water is dominated by the hydration of the interlayer cations, with time adsorption of water increases with greater extent of cation-water hydration energy. Although further confirmation is necessary, their study suggested that despite counter ions hydration being the main driving force for water adsorption, clay surface influence the configuration of the water molecules, which forces the water molecules to remain in the mid-plane with dipole vectors parallel to the surface of the claysheet. Secondly, at higher water concentration water molecules coordinate with the structural OH groups and are adsorbed at the clay surface.

The thermodynamic promotion effect of montmorillonite on methane hydrate formation surface has been studied by (Park and Sposito, 2003) using molecular simulations. Their studies

included 0.5, 1.0 and 2.25 methane per unit cell. Their study suggests that stable clathrate-like water structure around methane molecules and rest of the methane molecules adjacent to the hexagonal array of clay surface oxygen. Unstable hydrates were observed in case of 2.25 and 1 methane molecule per unit cell systems. Based on their molecular simulation results they proposed a new model for methane hydrate structure incorporating the involvement of 2:1 clay surface.

Adsorption of organic molecules on the clay surface had been studied by (Yu, et al., 2003, Yu, et al., 2000). They studied the interactions of clay with organic pollutants, pesticides, and dyes and observed three adsorption mechanisms. Formation of three distinct water layers had been observed, at excessive water contents a thin water layer formed near the clay surface while a bulk phase of water was observed at the center of the interlayer (Yu, et al., 2003).

Animated molecular dynamics simulations had been used by (Sutton and Sposito, 2002) to study the structure and dynamics of hydrated Cs-smectite interlayers. Their study describes the change in behavior of the interlayer cations and location of the charge sites with the amount of water content. They had been shown that more rapid movement occurs in the interlayer for both cesium ions and the water molecules at higher water contents which solvate them. The dynamics of the interlayer are dependent on the mineral charge patterns and predilection of the structural hydroxyl group towards water molecule shared by two cesium ions.

(Warne, et al., 2000) utilized molecular dynamics simulations for the study of kaolinite and amorphous silica. Rigid clay structure may be acceptable when studying the interlayer expansion during swelling is the only interest, but for the study of molecular adsorption process study flexible model for hydroxyl and other surface atoms are necessary (Warne, et al., 2000).

(Shroll and Smith, 1999) studied clay swelling with varying amount of water molecules using molecular dynamics simulations. Cs-montmorillonite had been studied for mono layer and two layers of hydration keeping the interlayer dimensions constant with basal spacing ranging from 12 to 18.5 Å. Swelling free-energy profile was integrated for minima of single and two layer hydrates. The Cs-montmorillonite clay model had been studied at different water content and significance of initial water content was reported. Disjoining pressure of clay had been calculated as a function of interlayer layer spacing, and stable spacing was observed when externally applied pressure match with the disjoining pressure. Oscillations observed in disjoining pressure which may be an indication of multiple stable spacing (Shroll and Smith, 1999). Distinct minima in free energy curve have been observed at the points where the disjoining pressure exceeds the externally applied pressure line with negative slope. Two minima at 12.7 and 15.3 Å in free energy curve was consistent with the spacing for single and two layer montmorillonite hydrates (Shroll and Smith, 1999).

(Hwang, et al., 2001) studied the interactions of organic molecules with kaolinite and pyrophyllite using molecular simulations. They allowed varying the partial charges of the atoms and calculated sorption energies and immersion enthalpies of clays into polar and nonpolar fluids (Hwang, et al., 2001). Cationic and anionic clays containing amino acids had been studied by (Newman, et al., 2002) using molecular modeling. In case of anionic clay the position of the interlayer anions had been assumed to be perpendicular with the longest axis of the hydroxide layers while cationic clay (montmorillonite) interlayer found to be oriented parallel to the clay layers. Electrochemical interactions of Wyoming montmorillonite with cationic metal compounds had been studied by (Park, et al., 1997) using molecular dynamics simulations and correlation was observed with experimental results.

Ab Initio Molecular Dynamics technique had been used by (Tunega, et al., 2002, Daniel Tunega*, 2004) for the study of monolayer water on octahedral and tetrahedral surfaces of kaolinite. Significant differences had been observed in behavior of water molecules for these two clay surfaces. A well-organized pattern had been observed in case of octahedral surfaces. Water molecules near octahedral surfaces tend to form as much as possible hydrogen bonds with surface hydroxyl groups as well as with water molecules themselves. Competition for forming hydrogen bonds among water molecules themselves and with surface hydroxyls creates certain disorders in octahedral surfaces (Tunega et al. 2004). Tetrahedral surface on the other hand shows that water molecules form a weak contact with the basal oxygen atom and clustering of water molecules occur as a result of hydrogen bonds among water molecules. The self-diffusion coefficients computed by Tunega et al. 2004 had been found to be smaller than that of bulk waters.

(Suter, et al., 2008) utilized ab initio molecular dynamics technique for the study of sodium ion adsorption on smectite clay. Their study found no preference of sodium ions for inner-sphere complex as reported in classical simulations. On the other hand preference was observed to reside at 6.1 Å separations from the center of clay layer and all bound oxygen atoms found to be located at same distance from Na⁺ ions (Suter, et al., 2008).

(Lock and Skipper, 2007) have investigated the structure and dynamics of phenol-water solutions in bulk and in two dimensional confined pores of sodium montmorillonite using Monte Carlo and molecular dynamics simulations. They used two clay systems with layer spacing 34Å and 17 Å (uncompact and compacted) and mimicked the temperature pressure conditions at surface and at depths of 3 and 6 km. Phenol molecules had been found able of forming donor hydrogen bond with clay surface. Again, phenolic –OH group were found to be solvated by three

water molecules (approx.) and was able to directly coordinate with interlayer sodium ions. By analyzing the various interactions Lock and Skipper (2007) concluded that phenol molecules were not strongly adsorbed on clay surfaces. Phenol ring had been observed to be solvated by 18 water molecules in compacted clay while solvated by 25 molecules in case of bulk solutions. Interlayer diffusion had been found to be increased for increase in temperature from 275K to 460K (Lock and Skipper, 2007).

Molecular mechanism of clay swelling hysteresis had been studied as a function of relative humidity by (Tambach, et al., 2006) using grand-canonical molecular simulations. Effect of different types of counter ions (Li^+ , Na^+ , and K^+) had been investigated at the experimental relative humidity regions of shrinkage or swelling occurrence (focused at the transition from one to two layer hydrate). (Tambach, et al., 2006) had shown that free-energy barrier separation of the layered hydrates is the thermodynamic initiator of hysteresis in swelling clays. Breaking and formation of hydrogen bonds between and within water layers dominates the free-energy barrier (Tambach, et al., 2006). Greater affinity for adsorption onto clay surface had been observed for relatively larger K^+ ions thus inhibits swelling and increases the free-energy barrier while smaller sized Li^+ ions well-placed in the water network capable of forming new swelling state (basal spacing approximately 13.5 Å). Types of counter ions and relative humidity determine the stability of layered hydrates. The location of the counter ions is determined by their size. Relatively larger K^+ ions desorb from the clay platelets as they get sufficient space in water network thus increase the free-energy barrier and may act as a swelling inhibitor (Tambach, et al., 2006).

(Pintore, et al., 2001) studied interlayer methanol with Ca and Na-saturated montmorillonite using molecular dynamics simulations. Their study shows that in a monolayer

Ca⁺ and Na⁺ ions clustered with four and two methanol ions. The formation of second and third layer occurs after complete fill-up of first layer; Ca⁺ and Na⁺ ions are coordinated with six and four methanol ions respectively at this stage. In our current study, from the experimental condition simulation for methanol we observed maximum only 20 wt % methanol can be present between interlayer.

Self-diffusion coefficient of methanol in montmorillonite had been found to be slower than water (Chang, et al., 1995) which agrees with our macro scale permeability results. Structure and dynamics of kaolinite interlayer had been studied by (Smirnov and Bougeard, 1999) using molecular dynamics simulations. Two different orientations of water molecules had been observed.

Molecular Steered dynamics model of sodium montmorillonite was first developed by (Schmidt, et al., 2005). The model developed by (Schmidt, et al., 2005) contains 8 unit cells (4x2). The unit cell coordinates are based on as proposed by (Skipper, et al., 1995). Atomic charges were obtained from (Teppen, et al., 1997). Later on (Katti, et al., 2006) developed larger clay sheet containing 18 unit cells (6x3) for the study of polymer clay nanocomposites. Na-MMT model used in the current study was developed by appropriate isomorphous substitution and charge balanced by inserting appropriate number of sodium atoms in model used by (Katti, et al., 2006). The size of the clay unit cell is 5.28 Å x 9.14 Å x 6.56 Å. The model used in this study contains 18 unit cells with total dimensions of 31.68Å x 27.42Å x 6.56 Å.

(Teppen, et al., 1997) developed CFF91 force field parameters for clay along with other minerals (quartz, gibbsite, kaolinite, pyrophyllite, and beidellite). (Teppen, et al., 1997) used a flexible clay lattice considering the effect of sliding capability of clay surface atoms on interlayer ions and water. Force constants developed for zeolites by (Hill and Sauer, 1995) using ab-initio

method were adopted by (Teppen, et al., 1997). In addition, quantum method was used to obtain the parameters for octahedrally coordinated aluminum and other atoms that were missing in zeolites (Schmidt, 2005, Schmidt, et al., 2005). The force field developed by (Teppen, et al., 1997) had been verified for pyrophyllite, kaolinite, and gibbsite and was found to be within 1% of experimental values for structural parameters of these minerals. In our study we used CHARMM force field parameter which had been obtained from force field developed by (Schmidt, et al., 2005).

In our previous studies, steered molecular dynamics simulation was used to study the mechanical response of Phyrophyllite and Na-MMT upon applied stress (Katti, et al., 2005, Schmidt, et al., 2005, Katti, et al., 2007). Molecular dynamics study of clay hydration had been conducted by (Schmidt, et al., 2005, Katti, et al., 2007). A multi scale modeling and experimental approach was taken to study the clay hydration by (Katti, et al., 2009) and interesting correlation were observed between the properties of swelling clays at different length scales.

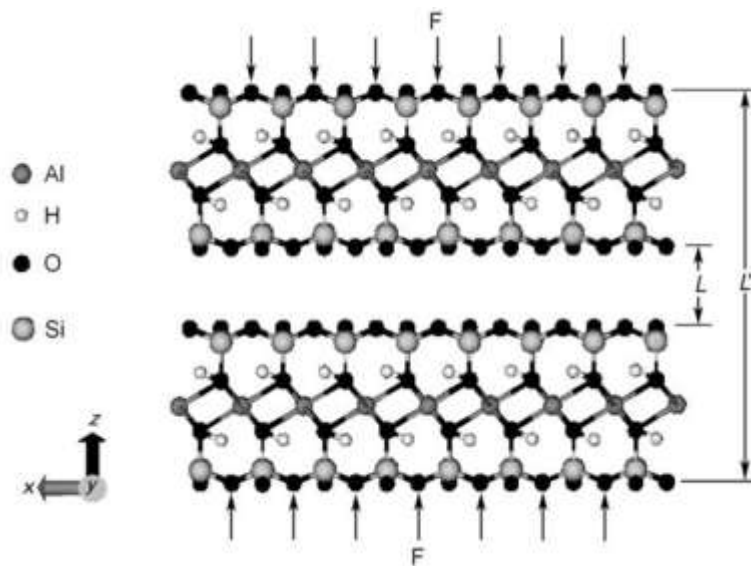


Figure 3.26: Mechanical response of pyrophyllite upon applied stress (Katti, et al., 2005).

Mechanical response and hydration studies of Na-MMT using steered molecular dynamics provided important molecular stress-strain behavior of swelling clays at different water content (Schmidt, et al., 2005, Katti, et al., 2007).

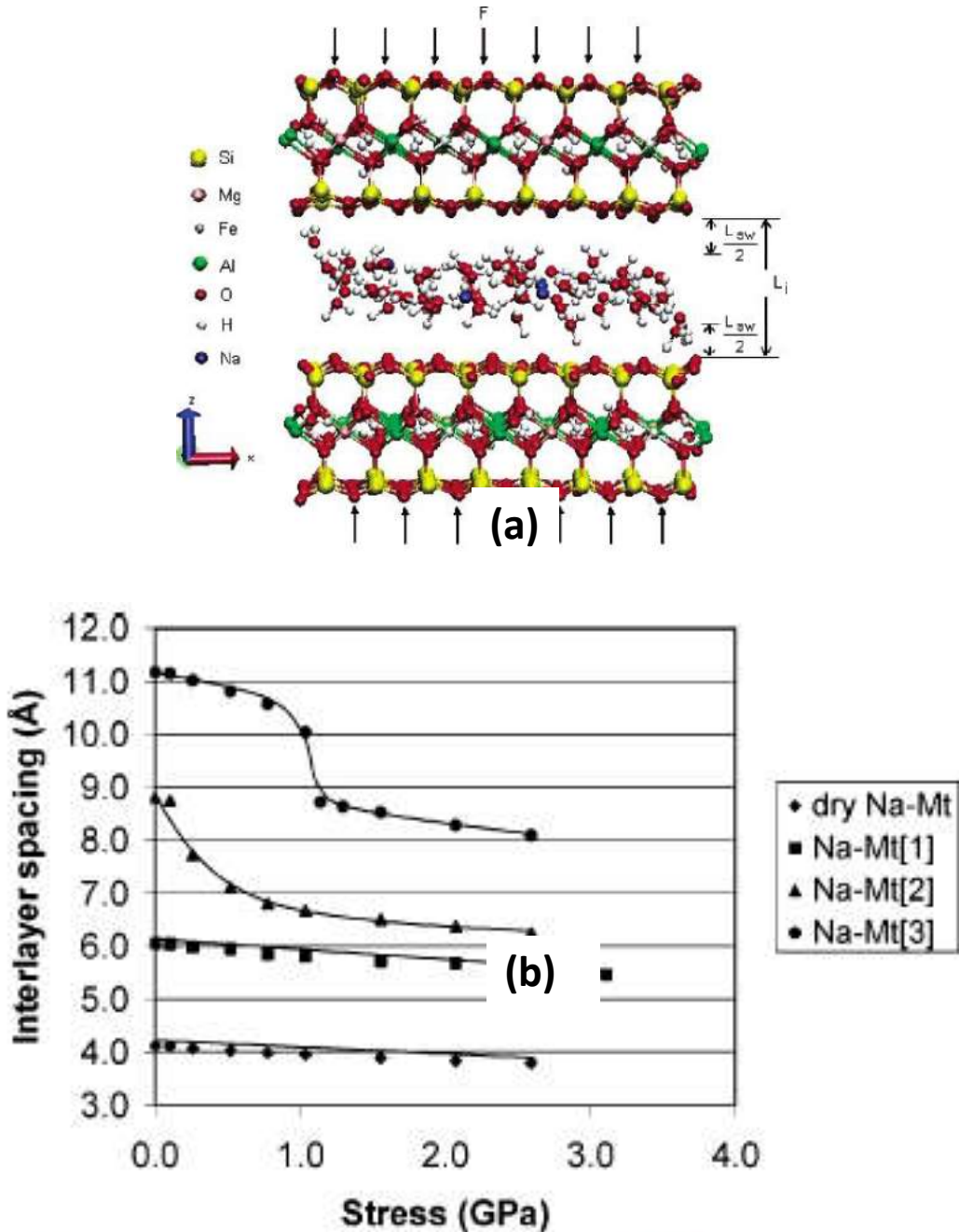


Figure 3.27: (a) Molecular model of sodium montmorillonite interlayer with two layers of water, (b) Stress Vs interlayer spacing for different water content in clays.

3.4 References

- [1] Amarasinghe, P. M. (2009). "Role of clay-fluid molecular interactions on fluid flow and mechanical behavior of swelling clays." PhD, North Dakota State University, ND, USA.
- [2] Essig, K., Urban, R. D., Birk, H., and Jones, H. (1993). "Diode-laser spectroscopy of nad, kd, rbd, and csd - determination of the mass-independent parameters and mass scaling coefficients of the alkali-metal hydrides." *Zeitschrift Fur Naturforschung Section a-a Journal of Physical Sciences*, 48(11), 1111-1114.
- [3] Katti, K. S., and Katti, D. R. (2006). "Relationship of swelling and swelling pressure on silica-water interactions in montmorillonite." *Langmuir*, 22(2), 532-537.
- [4] Johnston, C. T., and Premachandra, G. S. (2001). "Polarized ATR-FTIR study of smectite in aqueous suspension." *Langmuir*, 17(12), 3712-3718.
- [5] Leonard, R. A. (1970). "Infrared analysis of partially deuterated water adsorbed on clay." *Soil Science Society of America Proceedings*, 34(2), 339-&.
- [6] Sposito, G., and Anderson, D. M. (1975). "Infrared study of exchangeable cation hydration in montmorillonite." *Soil Science Society of America Journal*, 39(6), 1095-1099.
- [7] Katti, K. S., Sikdar, D., Katti, D. R., Ghosh, P., and Verma, D. (2006). "Molecular interactions in intercalated organically modified clay and clay-polycaprolactam nanocomposites: Experiments and modeling." *Polymer*, 47(1), 403-414.
- [8] Sikdar, D., Katti, D. R., and Katti, K. S. (2006). "A molecular model for epsilon-caprolactam-based intercalated polymer clay nanocomposite: Integrating modeling and experiments." *Langmuir*, 22(18), 7738-7747.

- [9] Sikdar, D., Katti, D., Katti, K., and Mohanty, B. (2007). "Effect of organic modifiers on dynamic and static nanomechanical properties and crystallinity of intercalated clay-polycaprolactam nanocomposites." *Journal of Applied Polymer Science*, 105(2), 790-802.
- [10] Sikdar, D., Katti, D. R., Katti, K. S., and Mohanty, B. (2009). "Influence of backbone chain length and functional groups of organic modifiers on crystallinity and nanomechanical properties of intercalated clay-polycaprolactam nanocomposites." *International Journal of Nanotechnology*, 6(5-6), 468-492.
- [11] Katti, D., and Shanmugasundaram, V. (2001). "Influence of swelling on the microstructure of expansive clays." *Canadian Geotechnical Journal*, 38(1), 175-182.
- [12] Amarasinghe, P. M., Katti, K. S., and Katti, D. R. (2009). "Nature of organic fluid-montmorillonite interactions: An FTIR spectroscopic study." *Journal of Colloid and Interface Science*, 337(1), 97-105.
- [13] Gleason, M. H., Daniel, D. E., and Eykholt, G. R. (1997). "Calcium and sodium bentonite for hydraulic containment applications." *Journal of Geotechnical and Geoenvironmental Engineering*, 123(5), 438-445.
- [14] Anandarajah, A. (1997). "Influence of particle orientation on one-dimensional compression of montmorillonite." *Journal of Colloid and Interface Science*, 194(1), 44-52.
- [15] Yao, M., and Anandarajah, A. (2003). "Three-dimensional discrete element method of analysis of clays." *Journal of Engineering Mechanics-Asce*, 129(6), 585-596.
- [16] Anandarajah, A. (2000). "On influence of fabric anisotropy on the stress-strain behavior of clays." *Computers and Geotechnics*, 27(1), 1-17.

- [17] Katti, D. R., Matar, M. I., Katti, K. S., and Amarasinghe, P. M. (2009). "Multiscale modeling of swelling clays: A computational and experimental approach." *Ksce Journal of Civil Engineering*, 13(4), 243-255.
- [18] Stillinger, F. H., and Rahman, A. (1974). "Molecular-dynamics study of liquid water under high compression." *Journal of Chemical Physics*, 61(12), 4973-4980.
- [19] Schmidt, S. R. (2005). "Evaluation of clay-water interactions : a quantitative determination of clayinterlayer forces with varying hydration by steered molecular dynamics." MS, North Dakota State University,, ND, USA.
- [20] Brooks, B. R., Bruccoleri, R. E., Olafson, B. D., States, D. J., Swaminathan, S., and Karplus, M. (1983). "CHARMM - A program for macromolecular energy, minimization, and dynamics calculations." *Journal of Computational Chemistry*, 4(2), 187-217.
- [21] Dinur, U., and Hagler, A. T. (1990). "A novel decomposition of torsional potentials into pairwise interactions - a study of energy 2nd derivatives." *Journal of Computational Chemistry*, 11(10), 1234-1246.
- [22] Skipper, N. T., Lock, P. A., Titiloye, J. O., Swenson, J., Mirza, Z. A., Howells, W. S., and Fernandez-Alonso, F. (2006). "The structure and dynamics of 2-dimensional fluids in swelling clays." *Chemical Geology*, 230(3-4), 182-196.
- [23] Hensen, E. J. M., Tambach, T. J., Blik, A., and Smit, B. (2001). "Adsorption isotherms of water in Li-, Na-, and K-montmorillonite by molecular simulation." *Journal of Chemical Physics*, 115(7), 3322-3329.
- [24] Park, S. H., and Sposito, G. (2003). "Do montmorillonite surfaces promote methane hydrate formation? Monte Carlo and molecular dynamics simulations." *Journal of Physical Chemistry B*, 107(10), 2281-2290.

- [25] Yu, C. H., Newton, S. Q., Norman, M. A., Schafer, L., and Miller, D. M. (2003). "Molecular dynamics simulations of adsorption of organic compounds at the clay mineral/aqueous solution interface." *Structural Chemistry*, 14(2), 175-185.
- [26] Yu, C. H., Newton, S. Q., Norman, M. A., Miller, D. M., Schafer, L., and Teppen, B. J. (2000). "Molecular dynamics simulations of the adsorption of methylene blue at clay mineral surfaces." *Clays and Clay Minerals*, 48(6), 665-681.
- [27] Sutton, R., and Sposito, G. (2002). "Animated molecular dynamics simulations of hydrated caesium-smectite interlayers." *Geochemical Transactions*, 3, 73-80.
- [28] Warne, M. R., Allan, N. L., and Cosgrove, T. (2000). "Computer simulation of water molecules at kaolinite and silica surfaces." *Physical Chemistry Chemical Physics*, 2(16), 3663-3668.
- [29] Shroll, R. M., and Smith, D. E. (1999). "Molecular dynamics simulations in the grand canonical ensemble: Application to clay mineral swelling." *Journal of Chemical Physics*, 111(19), 9025-9033.
- [30] Hwang, S., Blanco, M., Demiralp, E., Cagin, T., and Goddard, W. A. (2001). "The MS-Q force field for clay minerals: Application to oil production." *Journal of Physical Chemistry B*, 105(19), 4122-4127.
- [31] Newman, S. P., Di Cristina, T., Coveney, P. V., and Jones, W. (2002). "Molecular dynamics simulation of cationic and anionic clays containing amino acids." *Langmuir*, 18(7), 2933-2939.
- [32] Park, S., Fitch, A., and Wang, Y. L. (1997). "Computational studies compared to electrochemical measurements of intercalation of cationic compounds in wyoming montmorillonite." *Journal of Physical Chemistry B*, 101(25), 4889-4896.

- [33] Tunega, D., Benco, L., Haberhauer, G., Gerzabek, M. H., and Lischka, H. (2002). "Ab initio molecular dynamics study of adsorption sites on the (001) surfaces of 1 : 1 dioctahedral clay minerals." *Journal of Physical Chemistry B*, 106(44), 11515-11525.
- [34] Daniel Tunega*, M. H. G., and Hans Lischka (2004). "Ab Initio Molecular Dynamics Study of a Monomolecular Water Layer on Octahedral and Tetrahedral Kaolinite Surfaces." *J. Phys. Chem. B*, 108, 5930-5936.
- [35] Suter, J. L., Boek, E. S., and Sprik, M. (2008). "Adsorption of a Sodium Ion on a Smectite Clay from Constrained Ab Initio Molecular Dynamics Simulations." *Journal of Physical Chemistry C*, 112(48), 18832-18839.
- [36] Lock, P. A., and Skipper, N. T. (2007). "Computer simulation of the structure and dynamics of phenol in sodium montmorillonite hydrates." *European Journal of Soil Science*, 58(4), 958-966.
- [37] Tambach, T. J., Bolhuis, P. G., Hensen, E. J. M., and Smit, B. (2006). "Hysteresis in clay swelling induced by hydrogen bonding: Accurate prediction of swelling states." *Langmuir*, 22(3), 1223-1234.
- [38] Pintore, M., Deiana, S., Demontis, P., Manunza, B., Suffritti, G. B., and Gessa, C. (2001). "Simulations of interlayer methanol in Ca- and Na-saturated montmorillonites using molecular dynamics." *Clays and Clay Minerals*, 49(3), 255-262.
- [39] Chang, F. R. C., Skipper, N. T., and Sposito, G. (1995). "Computer-simulation of interlayer molecular-structure in sodium montmorillonite hydrates." *Langmuir*, 11(7), 2734-2741.
- [40] Smirnov, K. S., and Bougeard, D. (1999). "A molecular dynamics study of structure and short-time dynamics of water in kaolinite." *Journal of Physical Chemistry B*, 103(25), 5266-5273.

- [41] Schmidt, S. R., Katti, D. R., Ghosh, P., and Katti, K. S. (2005). "Evolution of mechanical response of sodium montmorillonite interlayer with increasing hydration by molecular dynamics." *Langmuir*, 21(17), 8069-8076.
- [42] Skipper, N. T., Chang, F. R. C., and Sposito, G. (1995). "Monte-carlo simulation of interlayer molecular-structure in swelling clay-minerals .1. Methodology." *Clays and Clay Minerals*, 43(3), 285-293.
- [43] Teppen, B. J., Rasmussen, K., Bertsch, P. M., Miller, D. M., and Schafer, L. (1997). "Molecular dynamics modeling of clay minerals .1. Gibbsite, kaolinite, pyrophyllite, and beidellite." *Journal of Physical Chemistry B*, 101(9), 1579-1587.
- [44] Hill, J. R., and Sauer, J. (1995). "Molecular mechanics potential for silica and zeolite catalysts based on ab-initio calculations .2. Aluminosilicates." *Journal of Physical Chemistry*, 99(23), 9536-9550.
- [45] Katti, D. R., Schmidt, S. R., Ghosh, P., and Katti, K. S. (2007). "Molecular modeling of the mechanical behavior and interactions in dry and slightly hydrated sodium montmorillonite interlayer." *Canadian Geotechnical Journal*, 44(4), 425-435.
- [46] Katti, D. R., Schmidt, S. R., Ghosh, P., and Katti, K. S. (2005). "Modeling the response of pyrophyllite interlayer to applied stress using steered molecular dynamics." *Clays and Clay Minerals*, 53(2), 171-178.

CHAPTER 4. EFFECT OF FLUID POLARITY ON PERMEABILITY CHARACTERISTICS IN NA-MONTMORILLONITE SWELLING CLAY

4.1 Introduction

In previous FTIR studies, we have observed that stronger of molecular interactions occur for high polar fluids with the same swelling clays. In this study, we are investigating the effect of fluid polarity on the flow properties of swelling clays. Swelling clays exhibits tremendous amount of volume expansions and exerts huge swelling pressure when the clays come in contact with water, thus clays cause tremendous damage to infrastructure. Montmorillonite swelling clays is widely used for landfill liners and other applications as barrier materials for due to very low permeability of fluids. Recent events of landfill failures and resulting increasing concern for health and environmental hazard indicate the necessity of a thorough investigation of flow properties of swelling clays, the major constituent of barrier materials. We have studied the flow properties of Na-montmorillonite swelling clays with a wide range of polarity fluids ranging from as high as formamide (Dielectric Constant 110) and as low as toluene (Dielectric Constant 2.4). The fluid used in this study has been chosen very carefully, these fluids are commonly found in landfill leachates and identified as highly toxic with potential for health hazard by US Environmental Protection Agency (EPA).

Permeability is sometimes termed as saturated hydraulic conductivity. Hydraulic conductivity is defined as the rate of flow of water or any other fluid under laminar flow condition through a cross sectional area of porous medium under a unit hydraulic gradient and standard temperature (20⁰C) (ASTM D5084). According to Darcy (Darcy, 1856) the mathematical form for hydraulic conductivity is

$$Q=kiA$$

Here, Q = rate of flow (cm^3/sec)

K = permeability or hydraulic conductivity

A = Cross sectional area (cm^2)

i = hydraulic gradient

The value of permeability depends on several factors for instance type of soil, particle size, and porosity. Permeability of fluids also depends on soil mineralogy especially for clays. Flow rate of water is an important aspect in designing earth dams, retaining structures, foundations, and slope stability analysis. Very low permeability of swelling clays in case of water is the reason for wide application as barrier materials in landfill liners, hazardous or nuclear waste management, also as protection barriers in transportation facilities. Swelling clays especially bentonite is used as geosynthetic clay liners. Geosynthetic clay liners are commonly made with a thin layer of bentonite clay that is sandwiched between two geotextile or geomembrane sheets as shown in Figure 4.1. Besides low permeability clay has other advantages for use in GCL's for example self-healing capacity and resistance to freeze thaw cycles.

Permeability of bentonite clays has been extensively studied by numerous researchers (Gleason, et al., 1997, Bowders, et al., 1997, Daniel, 1984, Hewitt and Daniel, 1997, Ruhl and Daniel, 1997). Due to the numerous occasions of failure of landfill liners, there are a necessity of revisiting landfill linear design technique or principals. From the studies of different researchers it was observed that constituents of landfill leachates have different flow behavior than water. Therefore, for the effective design of barrier systems, understanding the complex behavior of organic fluids on the clay component in landfill liners becomes very vital. Our study approached the problem in a very systematic way considering a wide range of polarity fluids present in

landfill leachates. The fluids studied in our investigation are identified as highly toxic by Environmental Protection Agency (EPA), USA, also commonly found in land leachates.

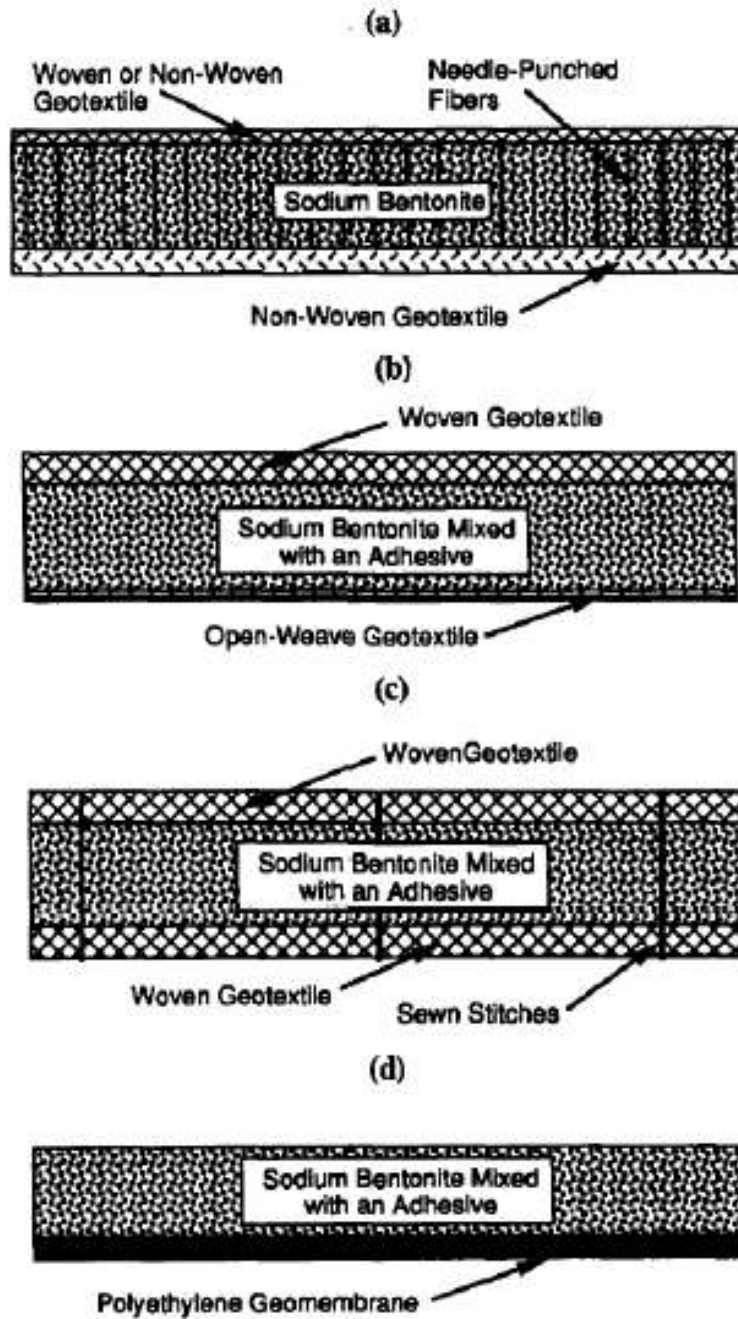


Figure 4.1: Different type of clay liners, (a) Needle-punched (b) adhesive-bonded (c) stitched bonded (d) composite GCL (LaGatta, et al., 1997 as cited by Amarasinghe, 2009).

4.2 Permeability Measuring Techniques

Constant head and falling head permeability tests are the most commonly used technique for measuring permeability of soils (shown in Figure 4.2). Constant head method is mainly used for fine to coarse grained soil (silt and sand) while falling head method is mainly used for permeability measurement of very fine grained soils that is for clays with very low permeability. In falling head method hydraulic head is allowed to fall as the liquid flow through the sample.

The mathematical representation provided by Tschébotarioff (Tschébotarioff, 1951),

$$dQ = -dh a = K h/L A dt \quad \dots\dots\dots(a)$$

Here, dQ = total discharge

dh = hydraulic head fall at time period dt

From the equation (a) hydraulic conductivity k can be derived as,

$$K = 2.3 La/At \log_e h_1/h_2$$

Here, k is the coefficient of permeability, L is the height of the sample, A is the cross sectional area of the sample and ‘ a ’ is the cross sectional area of glass tube.

In case of constant head method, hydraulic head is kept constant and amount of fluid flow through the sample is measured with time. The mathematical expression for permeability using constant head method is

$$K = \Delta Q L/ A h \Delta t$$

Here, k is the coefficient of permeability, L is the height of the sample, A is the cross sectional area of the and dQ is the amount of total flow at time period dt .

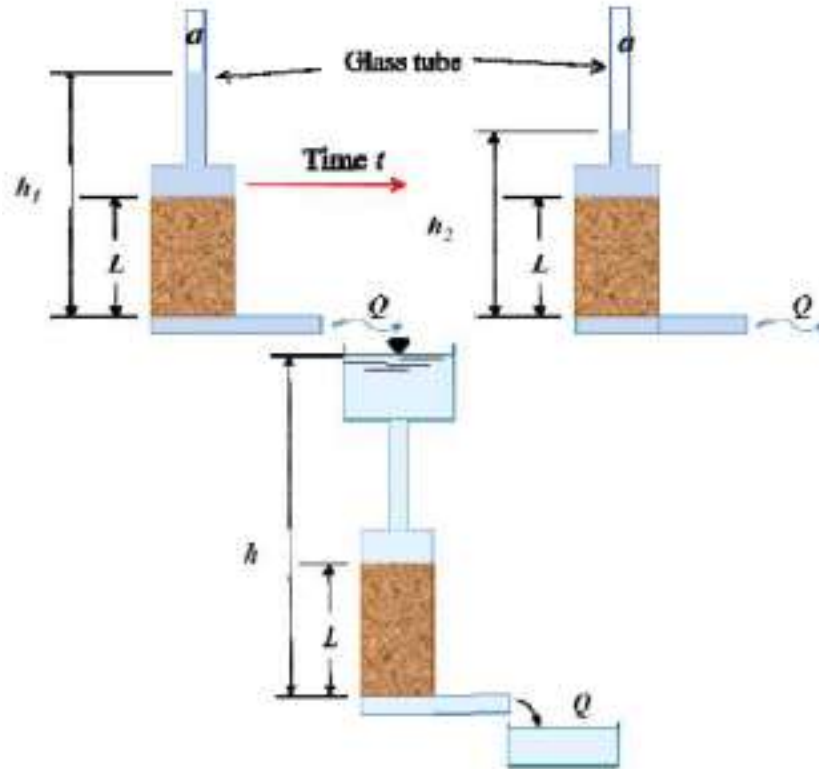


Figure 4.2: Constant head (bottom) and falling head permeability measuring device (top) (Amarasinghe, 2009).

4.3 Types of Permeability Cells

4.3.1. Rigid Wall Permeameter

Permeameters are mainly divided into two main categories according to the type of cells, rigid wall and flexible wall cells. In the case of rigid wall cells, soil sample is confined in a rigid usually stainless steel cylinder (as shown in Figure 4.3). These types of cells are mainly used for coarse grained soil with high permeability. They are not recommended for low permeability clayey soil due to potential for leakage along the interface between the sample and the walls. Restrains of this type of permeameter is not able to apply confining pressure to the sample for simulating field condition. Another problem is saturation of sample cannot be confirmed

accurately. This type of permeameter is used for coarse grained soils for its simplicity in set up and low cost of the cell.

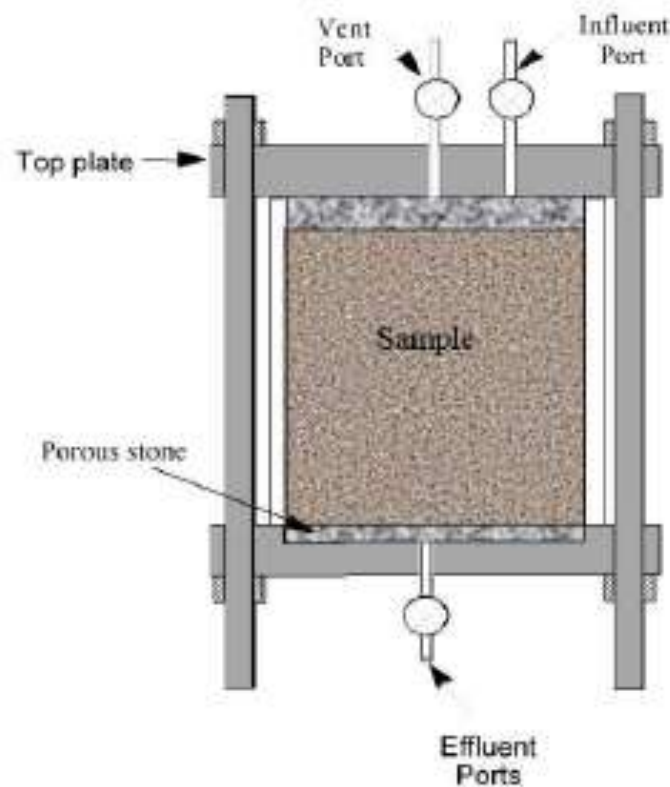


Figure 4.3: Rigid wall permeability meter cell (Amarasinghe, 2009).

4.3.2. Flexible Wall Permeameter

Flexible wall cells are currently commercially available and most popular type of permeameter especially for clay soils (Figure. 4.4). Due to the flexible membrane more contact between soil sample and cell was is possible, thus reduces the possibility of leakage. Moreover, flexible wall permeameter provides the scope of applying confining pressure for mimicking the field conditions. The main problem of flexible cell is that it cannot accurately measure permeability for swelling clays. Due to extremely high swelling, bulging of sample occurs and cause change in cross-sectional area, thus leading to inaccurate results. Swelling also alters the microstructure of the sample and thus, makes the test unreliable. However, accurate

measurement of permeability of swelling clays such as Na-Montmorillonite with water or other organic fluids is extremely important for effective design of barrier system. Na- Montmorillonite is an important component of GCLs.

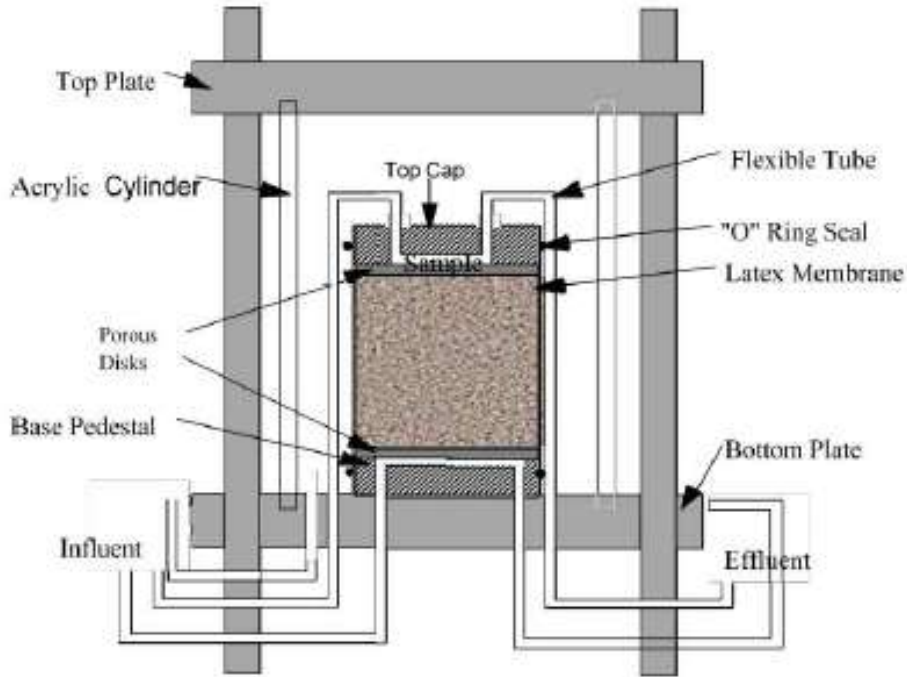


Figure 4.4: Flexible wall permeability meter cell (Amarasinghe, 2009).

4.4 New Integrated Porous Rigid Wall and Flexible Wall Permeameter

Rigid wall permeameter is more suitable for coarse grained soil with high permeability. Rigid wall permeameter was the only options until flexible wall permeameter was developed (Daniel et al. 1984). Flexible wall cell is commonly used for clayey soils by researchers (Bowders, et al., 1997, Hewitt and Daniel, 1997, Ruhl and Daniel, 1997). But from the findings of our previous work reveal that flexible wall permeameter cannot accurately measure permeability of swelling clays. Our prior work shows that swelling pressure causes change in microstructure of Na-MMT experimentally and results in particle breakdown of the sample (Amarasinghe, 2009, Katti and Katti, 2006, Katti and Shanmugasundaram, 2001). In our group, the particle breakdown due to swelling and swelling pressure is also numerically studied using

discrete element method (DEM) (Katti, et al., 2009). To understand the complete mechanism of swelling the study was extended to molecular scale. In the previous work by our group, the molecular hydraulic conductivity of the interlayer using Fourier Transform Infrared Spectroscopy (FTIR) and X-ray diffraction analysis (XRD) was evaluated (Amarasinghe, 2009, Amarasinghe, et al., 2008). The swelling pressure of bentonite has been studied experimentally by numerous researchers. The swelling pressure of bentonite clays had been reported in the range between 95- 575 KPa. (Windal and Shahrour, 2002) and have shown that if the swelling of clays is prevented in one direction, it causes increasing swelling in another direction. As in the traditional flexible wall permeameter (also known as triaxial cells) vertical swelling is prevented by locking rod, lateral swelling can rise even higher and cause bulging of samples.

Daniel (Daniel, 1984) addressed the use of cathetometers for measuring any volume change during permeability test by some researchers and apply confining pressure accordingly to keep the volume constant. This procedure will be tedious and we may be able to bring the volume back to original value, but the microstructure will be affected. According to ASTM D5084 (2003) permeability test procedure a confining pressure 1.5 times greater than swelling pressure of soil is suggested to maintain the volume unchanged. But the problem here is application of confining pressure before sample saturation or bulging of sample may cause disturbance to the soil sample. Again, the amount of confining pressure as 1.5 times the swelling pressure does not have any basis rather an approximation. Due to the vital importance of accurate measurement of permeability of swelling clays with different fluids our group designed and fabricated a new device for permeability of clays (Figure 4.5) (Amarasinghe, 2009). The name of the device termed as Integrated Porous Rigid Wall and Flexible Wall Permeameter (Provisional US Patent 2008).



Figure 4.5: Complete set up of new integrated porous rigid wall and flexible wall permeameter.

The device incorporates the good features of both rigid cell and flexible cell permeameter and especially suitable for accurate permeability measurement of swelling clays. The device consist of a rigid porous stone (split into two parts) that holds the swelling clay sample and whose surface is covered by a flexible impermeable membrane. Due to rigid porous stone, lateral swelling can be prevented and at the same time applying of confining pressure is also possible. As the porous stone is spliced of two parts, placement of undisturbed sample is also possible. The detailed designing and fabrication process can be found in (Amarasinghe, 2009). The device also open ups the scope of some experimental studies such as permeability of swelling clays at certain predefined amount of swelling or permeability at different magnitude of consolidations. Another advantage is consolidating stress can be applied both vertically and horizontally, that is three dimensional consolidation is possible. Split set up of porous stone also allows undisturbed sample removal after permeability or consolidation test for further experimental studies like X-ray diffraction (XRD), Infrared Spectroscopy (IR) and Scanning Electron Microscopic (SEM) Analysis.



Figure 4.6: Components of newly designed permeameter (1a) Porous stone cylinder (2a) Stainless steel porous stone holding cap (2c) porous stone with clamped holding cap.

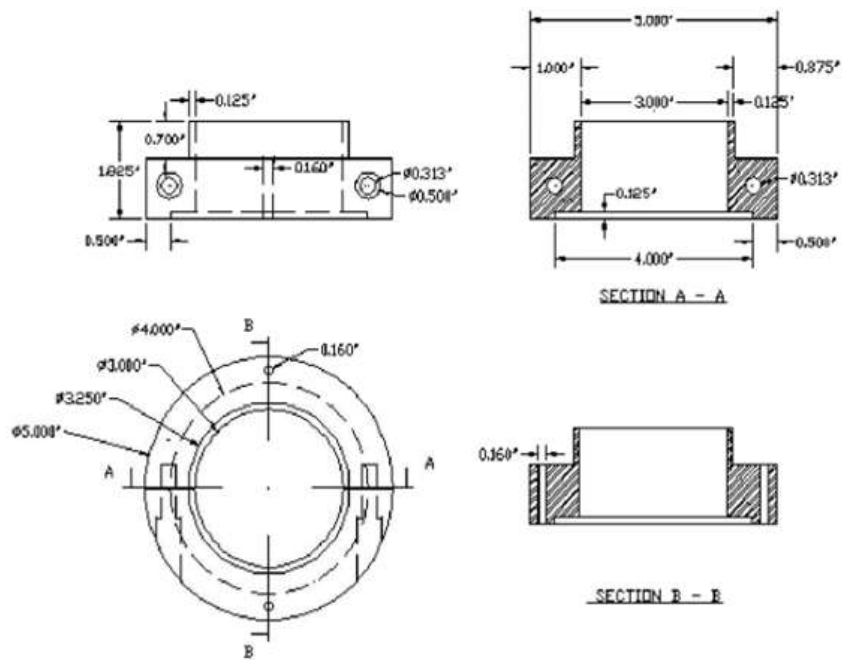


Figure 4.7: Design details of new permeameter (Amarasinghe, 2008).

4.5 Permeability Testing Procedure

The newly designed permeability testing device by our group is very simple for set up and testing method. The complete procedure for sample set up and testing method as follows (Amarasinghe, 2009)-

1. Wrap the triaxial cell base with flexible membrane. A little vacuum grease can be used for better sealing.
2. Place the two 'O' rings on the base.
3. Now place the bottom porous stone holding cap on the base surrounding the 'O' rings and membrane. Lightly tighten the screws of the bottom porous stone holding cap for placing the porous stone.
4. Fix the two bottom porous stone on the groove of the porous stone holding cap.
Completely tight the screws so that porous stone will not move around holding cap.
5. Assemble the top porous stone (two halves) on the bottom porous stone.
6. Fix the top porous stone holding cap, be sure to be porous stone fit perfectly with the holding cap. Tighten the porous stone holding cap so that porous stone will not move.
7. Fix the vertical screws that hold the bottom and top porous stone holding caps.
8. Stretch the flexible membrane and place over the top porous stone holding cap.
9. Place the porous stone (1/2 inch thick stone disc) on the base assembly until porous stone reach the edge of bottom porous stone holding cap. Insert a filter paper at bottom.
10. Place the sample and compact in the hollow area. In case of field sample place the sample inside the hollow area. Place a filter paper at the top of the sample.
11. Fix the top porous stone.
12. Assemble the top cap of the triaxial cell. For better a little vacuum grease can be used.

13. Unfold the flexible membrane and cover the triaxial cell cap.
14. Fix the two 'O' rings around the top cap.
15. Fix all other parts for example clear acrylic cylinder, quick release type rod and drainage lines.

4.6 Materials and Method

Na-MMT (SWy-2, Wyoming) used in this study was obtained from the clay mineral repository at the University of Missouri, Columbia. The cationic ex-change capacity of SWy-2 is 76.4 mequivalent/100g and the chemical formula is $\text{Na-Si}_{16}(\text{Al}_6\text{FeMg})\text{O}_{20}(\text{OH})_4$. Molecular structure and dielectric constant values of the fluids used are shown in figure 4.8. Consistency of particle size in all the samples Na-MMT was grounded and passed through No 200 sieve (Mesh size 76 μm). Formamide used in the experiment was obtained from Mallinckrodt Baker, Inc. NJ with 90-100% purity. Permeability and consolidation test for toluene, TCE, methanol and water was performed by previous graduate student (Amarasinghe, 2009). 99.7% toluene, 99.99% TCE were obtained from same company. 99.99% methanol was collected from Alpha Aesar, MA and deionized water was prepared in the laboratory.

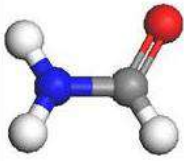
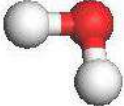
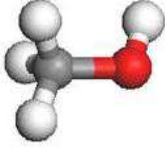
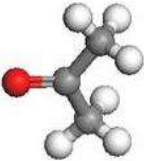
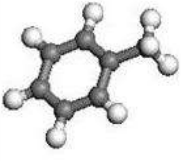
Fluid	Formamide	Water	Methanol	Acetone	Toluene
Structure					
Dielectric Constant	110	80	33	20	2.4

Figure 4.8: Molecular structures and dielectric constant values of solvents used in this study.

4.7 Permeability Test Results

The newly designed device by our group (Katti et al. provisional patent 2008) was used for calculating the permeability test of high swelling Na-Montmorillonite clays. The test method ASTM D5084 (2003) were followed and standard test method for flexible wall cells were used. The sample (Na-Montmorillonite) was compacted and achieved a unit weight of 849 kg/m^3 . The height and diameter of the same is 1 in (2.5 cm) and 2.9 inches (7.37 cm). Permeability was measured for Na-Montmorillonite clays with five different fluids. For each of the sample, saturation was confirmed. It took more than 6 month to saturate the clays in case of formamide and complete permeability experiment for formamide required more than a year. The reading of burette water reading was taken as shown in Figure 4.9. No significant absorption of formamide was observed after six month. Pressure difference between top and bottom of the sample was kept close to 4 KPa during the permeability test. Permeability test data for formamide sample is given in the table 4.1.

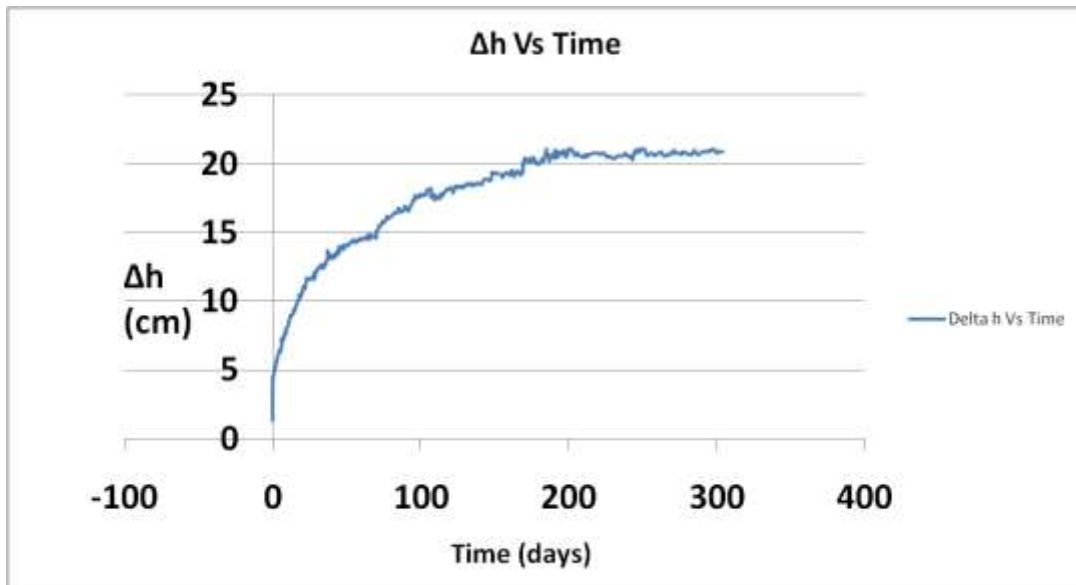


Figure 4.9: Amount of water absorbed by the sample over time.

Table 4.1: Calculation of permeability of clays in formamide-clay sample

Test	Δt (sec)	H_1	h_2	a (cm ²)	A (cm ²)	L (cm)	K (cm/sec)
1	691458	452.105	451.994	0.906	41	2.5	9.7538E ⁻¹²
2	691542	459.362	459.252	0.906	41	2.5	9.5985E ⁻¹²
3	691020	459.473	459.362	0.906	41	2.5	9.6035E ⁻¹²
4	691320	466.289	466.179	0.906	41	2.5	9.4589E ⁻¹²
Average permeability							9.6037E ⁻¹²

The permeability test of Na-Montmorillonite with TCE, toluene, methanol and water were performed by previous PhD student Pryanthi Amarasinghe (Amarasinghe, 2009) .

Permeability of Na-Montmorillonite with formamide took more than one year while all other lesser polarity fluids together took almost one year. From our experiment, permeability of water in Na-Montmorillonite with water was calculated as 3.77×10^{-10} which is very much agreeable with the existing literature (Gleason, et al., 1997) in terms of magnitude, still our results represents more accurate value due to newly designed device. The permeability equation used was-

$$K = a \cdot L / 2 \cdot A \cdot \Delta t \ln (h_1/h_2)$$

Here, h_1 , h_2 is the head loss across the sample at the beginning and end of the test, a is the burette cross sectional area (cm²), A is the sample cross sectional area (cm²), Δt is the time duration in seconds and L is the sample length in cm.

Our permeability studies show some interesting results which enabled us to correlate the fluid polarity with permeability of clays. We see that higher the polarity of the fluids, lower the permeability of that fluid with same swelling clay. We see that permeability of toluene in clay is million times greater than permeability of water in the same clay, while permeability of formamide is hundred times lesser than water for the same clay. In our previous FTIR studies qualitatively show that higher the polarity of fluids greater the molecular interactions (Amarasinghe, 2008, 2009). This permeability tests and previous results provide enough

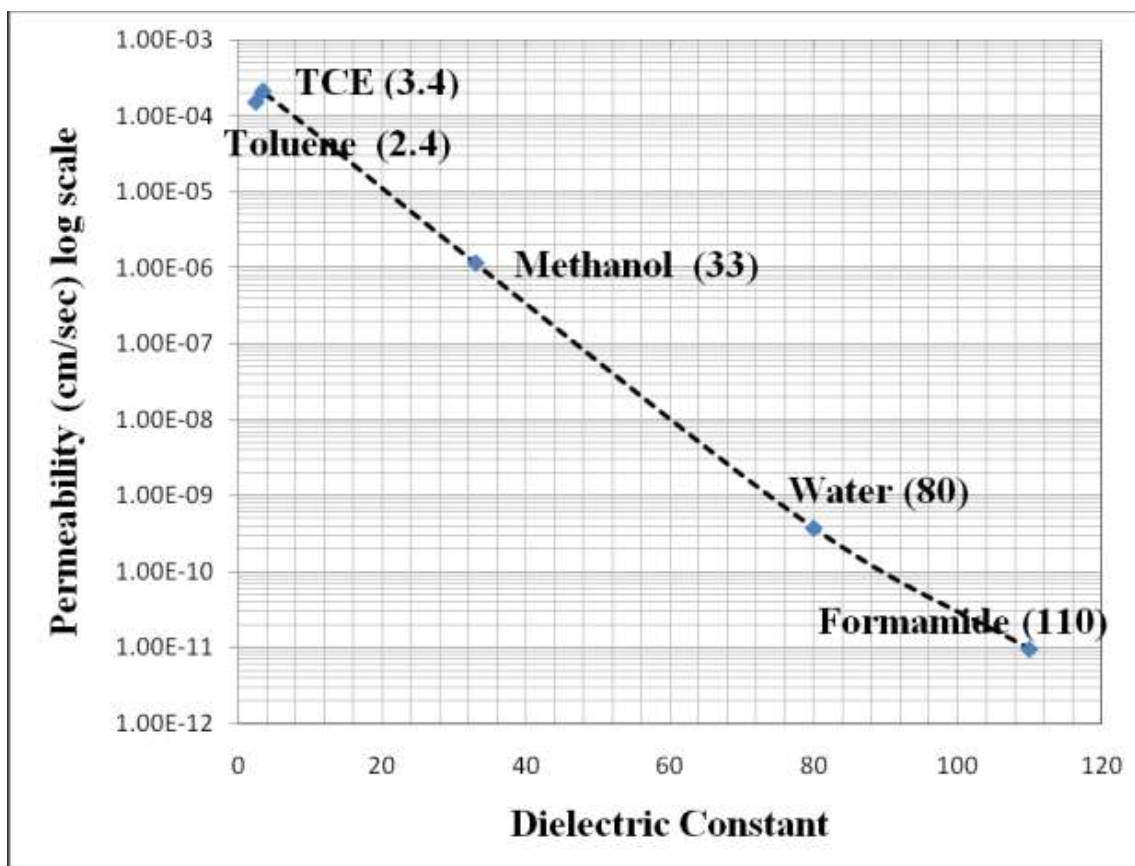


Figure 4.10: Permeability Vs dielectric constant graph showing higher permeability for low polar fluids.

Table 4.2: Permeability of sodium montmorillonite clays with different polarity solvents

Fluid	Dielectric Constant	Permeability of Na-MMT
Toluene	2.4	1.52x10 ⁻⁴
TCE	3.4	2.12x10 ⁻⁴
Methanol	30	1.16x10 ⁻⁶
Water	80	3.77x10 ⁻¹⁰
Formamide	110	0.9x10 ⁻¹¹

motivation for further molecular modeling investigation which presented in the chapter four.

These modeling and experimental studies provided us the opportunity to bridge the properties of swelling clays at different length scales.

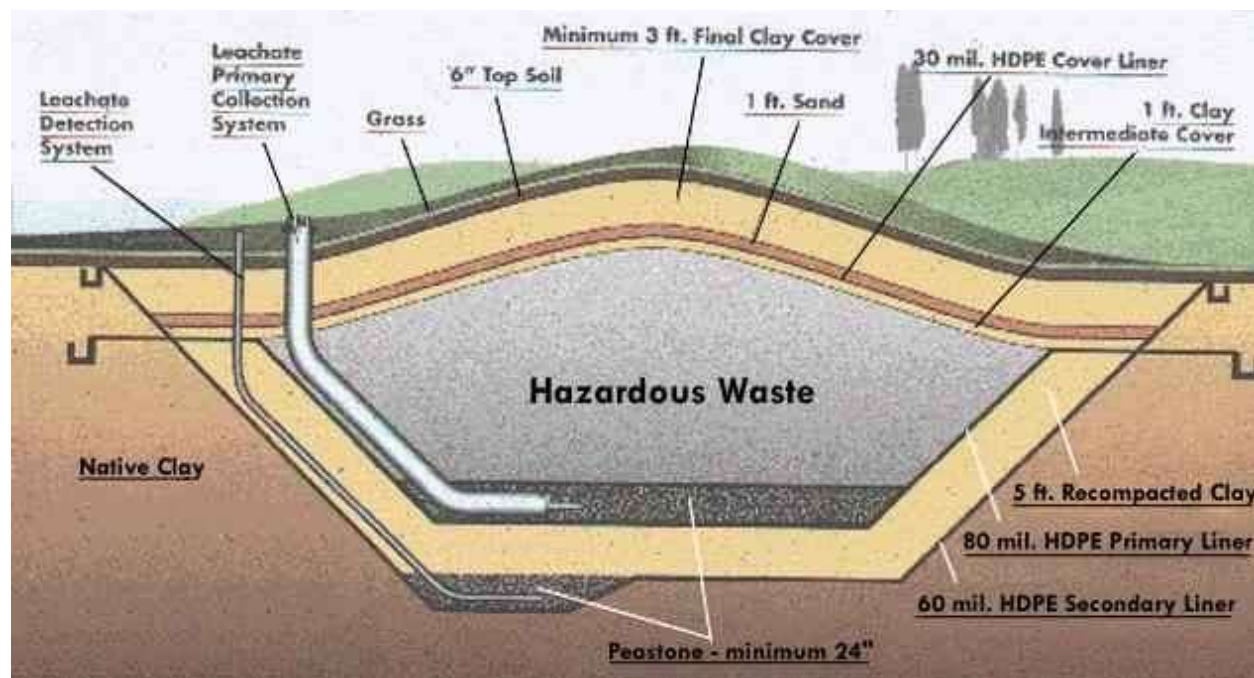


Figure 4.11: Schematic of landfill (www.ensoles.org).

One of the greatest concerns for health and environment is failure of landfill liners. A number of landfills have been reported to be failed in recent years. The constituents in landfill leachates are highly toxic and termed as hazardous for health and environment by EPA, USA. One of the fundamental problems with landfill design is permeability of leachates has been assumed to be as low as water which was found 10^{-8} to 10^{-10} cm/sec (Gleason, et al., 1997, Ruhl and Daniel, 1997, Ebina, et al., 2004). We studied some of the fluids that present in the landfill leachates such as toluene, TCE, methanol, water and formamide. We interestingly found that these fluids have very significant difference in permeability through montmorillonite clays, one of the main constituents of landfill liners. Since, the low polar fluids present in landfill leachates have much higher flow rate through clays, landfill liners designed to prevent leakage of leachates (assuming leachates have same permeability as water) are not sufficient for these fluids. Thus eventually causing entire failure of landfill liners. So, we recommend considering the permeability of all the possible constituents during landfill liner design.

4.8 References

- [1] Darcy, H. (1856). "Determination des lois d'e`coulement de l'eau a`travers." In *Les Fontaines Publiques de la Ville de Dijon*. Environmental Science, Policy and Management, 210 Hearst Memo- Victor Dalmont, Paris.
- [2] LaGatta, M. D., Boardman, B. T., Cooley, B. H., and David, D. E. (1997). "Geosynthetic clay liners subjected to differential settlement." *Journal of Geotechnical and Geoenvironmental Engineering*, 123(5), 402-410.
- [3] Bowders, J. J., Tan, J. P., and Daniel, D. E. (1997). "Expanded clay and shale aggregates for leachate collection systems." *Journal of Geotechnical and Geoenvironmental Engineering*, 123(11), 1030-1034.
- [4] Daniel, D. E. (1984). "Predicting hydraulic conductivity of clay liners." *Journal of Geotechnical Engineering-Asce*, 110(2), 285-300.
- [5] Hewitt, R. D., and Daniel, D. E. (1997). "Hydraulic conductivity of geosynthetic clay liners after freeze-thaw." *Journal of Geotechnical and Geoenvironmental Engineering*, 123(4), 305-313.
- [6] Ruhl, J. L., and Daniel, D. E. (1997). "Geosynthetic clay liners permeated with chemical solutions and leachates." *Journal of Geotechnical and Geoenvironmental Engineering*, 123(4), 369-381.
- [7] Gleason, M. H., Daniel, D. E., and Eykholt, G. R. (1997). "Calcium and sodium bentonite for hydraulic containment applications." *Journal of Geotechnical and Geoenvironmental Engineering*, 123(5), 438-445.
- [8] Tschebotarioff, G. (1951). *Soil Mechanics, Foundations, and Earth Structures* McGraw-Hill, New York.

- [9] Katti, K. S., and Katti, D. R. (2006). "Relationship of swelling and swelling pressure on silica-water interactions in montmorillonite." *Langmuir*, 22(2), 532-537.
- [10] Katti, D., and Shanmugasundaram, V. (2001). "Influence of swelling on the microstructure of expansive clays." *Canadian Geotechnical Journal*, 38(1), 175-182.
- [11] Amarasinghe, P. M. (2009). "Role of clay-fluid molecular interactions on fluid flow and mechanical behavior of swelling clays." PhD, North Dakota State University, ND, USA.
- [12] Katti, D. R., Matar, M. I., Katti, K. S., and Amarasinghe, P. M. (2009). "Multiscale modeling of swelling clays: A computational and experimental approach." *Ksce Journal of Civil Engineering*, 13(4), 243-255.
- [13] Amarasinghe, P. M., Katti, K. S., and Katti, D. R. (2008). "Molecular Hydraulic Properties of Montmorillonite: A Polarized Fourier Transform Infrared Spectroscopic Study." *Applied Spectroscopy*, 62(12), 1303-1313.
- [14] Windal, T., and Shahrour, I. (2002). "Study of the swelling behavior of a compacted soil using flexible odometer." *Mechanics Research Communications*, 29(5), 375-382.
- [15] Ebina, T., Minja, R. J. A., Nagase, A. T., Onodera, Y., and Chatterjee, A. (2004). "Correlation of hydraulic conductivity of clay-sand compacted specimens with clay properties." *Applied Clay Science*, 26(1-4), 3-12.

CHAPTER 5. ROLE OF MOLECULAR INTERACTIONS AND EFFECT OF FLUID POLARITY ON SWELLING AND FLOW PROPERTIES OF SWELLING CLAYS: A MOLECULAR DYNAMICS STUDY

The chapter describes the role of molecular interactions and fluid polarity on swelling and flow properties of swelling clays using molecular dynamics (MD) simulations. The content of this chapter is to be submitted in Journal of Engineering Mechanics, American Society of Civil Engineering (ASCE).

5.1 Introduction

Interesting findings were revealed from our experimental studies, also from the work by previous students in the research group. We approached the study of swelling clays very systematically with the help of multi-scale experiments and contemporary modeling. From our macroscale permeability and consolidation tests with a wide range of polarity fluids, we were able to correlate the effect of solvent polarity on flow properties of swelling clays. From our scanning electron microscopic (SEM) study we were able to see the effect of different polarity fluids on the microstructure of swelling clays. Evaluation of microstructure during swelling and swelling pressure was previously studied experimentally by (Katti and Shanmugasundaram, 2001) and numerically using a modified discrete element method (DEM) (Katti, et al., 2009). Mechanical response of pyrophyllite and montmorillonite were previously studied using steered molecular dynamics (SMD) simulation by (Katti, et al., 2005, Schmidt, et al., 2005, Katti, et al., 2007). Fourier Transform Infrared Spectroscopic (FTIR) studies on Na-montmorillonite with a wide range of fluids provided a very good qualitative idea about effect of molecular interactions between clay-fluids on swelling behavior (Amarasinghe, et al., 2009, Amarasinghe, et al., 2008). The main goal of our study was to provide a quantitative estimation of interlayer fluids at different level of swelling, and we found molecular modeling as the best tool for the study. Our study also provides a quantitative linkage between molecular interactions, evaluation of

microstructure, particle breakdown and flow rate (permeability) through clays. We were able to explain molecular mechanism of swelling and successfully linked up the correlations with micro or macro scale behavior.

5.2 Modeling Approach

Clay minerals or clay molecules are also sometimes known as clay layers (Cornelis and Dutrow, 2007). The clay layers are stacked one upon another and the gap or space between two clay layers is known as interlayer space. One mineralogical term widely will be used in this study is d_{001} spacing, defined as interlayer spacing plus layer thickness. Interlayer space can be filled with cations and fluid molecules. In dry Na-MMT clay interlayer, sodium ions present between two clay sheets balance the charge developed due to isomorphous substitution (Figure. 5.1). Fluid molecules enter into the interlayer start interacting with the interlayer sodium ions as well as clay surface causing the expansion of interlayer spacing. The extent of this interaction varies with nature and amount of interlayer solvents. In this work, we have started with small amount of interlayer fluid (10%, 20%, 30%, and 40%) and subsequently increased the amount of interlayer fluid until we achieved the experimental condition. The structure and dielectric constant values for the fluids used in this study are shown in Figure. 5.2.

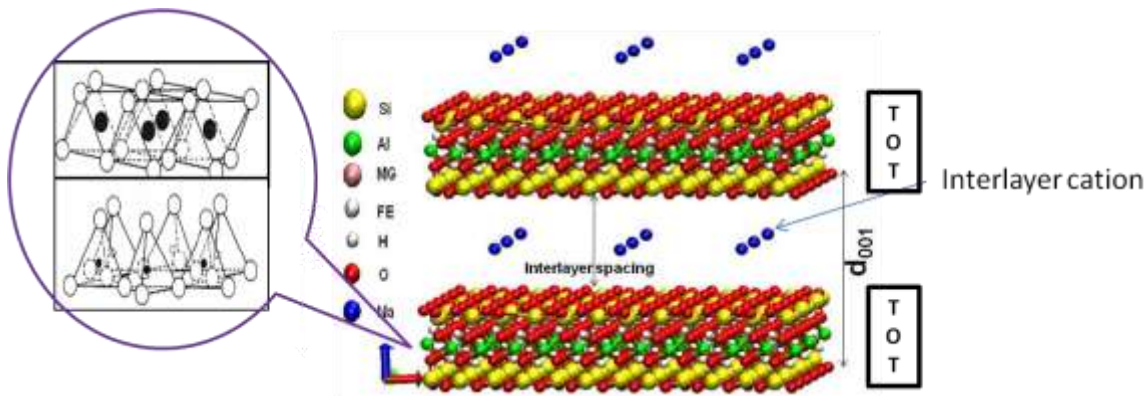


Figure 5.1: T-O-T structure and different components of Na-Montmorillonite model has been shown in 6x3 (with 18 unit cell) model used in this study.

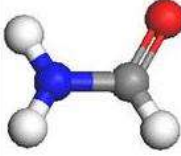
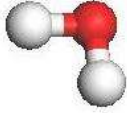
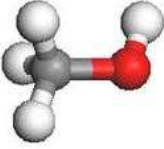
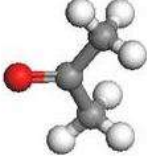

Fluid	Formamide	Water	Methanol	Acetone	Toluene
Structure					
Dielectric Constant	110	80	33	20	2.4

Figure. 5.2: Molecular structures and dielectric constants of the solvents used in this study.

Computational resources and mimicking the real system is one of the major challenges in molecular modeling. Some of the simulations especially for solvation, a large amount of computational time can be saved by not introducing explicit solvent molecules but rather introducing solvent effect as distance dependent dielectric constant. Another way of saving computational time is by applying restrains to the solvent molecules or considering a functional group or segment of molecule as one particle. By doing so, we are able to save computational time to some extent, but we also have to consider that by introducing these assumptions, we are modeling less realistic system. Especially conformational analysis using fully or partially restrained solvent molecules might be incorrect. In our current study, solvent molecules are free to move in three dimensions which is similar to the real experimental system that allows us to perform better conformational analysis.

In our study, isobaric-isothermal ensemble of MD was used. In isobaric-isothermal ensemble the number of atoms, pressure and temperature remain constant. The d_{001} spacing and interlayer spacing was measured for different model with varying amount of interlayer fluids when simulations reach room temperature and pressure. This work evaluates quantitatively the amount of fluid present between the interlayer at experimental condition causing a particular amount of swelling. When the simulation reached equilibrium, we calculated the d_{001} spacing by

tracing the coordinates of the oxygen atoms of the bottom clay layer. Relationships between dielectric constant and d_{001} spacing were developed for different amount of interlayer fluids.

5.3 Model Construction

The Na- Montmorillonite used in all of the previous studies by the authors (Katti and Shanmugasundaram, 2001); (Katti and Katti, 2006); (Amarasinghe, et al., 2008); (Amarasinghe, et al., 2009), SWy-2, was acquired the University of Missouri, Columbia, Missouri. The clay minerals repository at the University of Missouri, Columbia, Missouri provides the researchers a consistent composition for comparing the results. The chemical formula of the of the acquired Na- Montmorillonite is $(Ca_{0.12}Na_{0.32}K_{0.05})[Al_{3.01}Fe(III)_{0.41}Mn_{0.01}Mg_{0.54}Ti_{0.02}][Si_{7.98}Al_{0.02}]O_{20}(OH)_4$ (Van Olphen, 1979). (Schmidt, et al., 2005) for the first time constructed the Na-montmorillonite model with simplified formula $NaSi_{16}(Al_6FeMg)O_{20}(OH)_4$. Coordinates of the unit cells in Schmidt et al. model are based on those proposed by (Skipper, et al., 1995) and atomic charges were obtained from (Teppen, et al., 1997). Montmorillonite consist a tetrahedral-octahedral-tetrahedral (T-O-T) structure which is known as clay layers. Isomorphic substitution in the octahedral sheet causes charge development in clay layer. Due to each number of substitution 0.5e amount of charges develop in the clay sheet. The charge imbalance is balanced by introducing 0.5 Na cations in each unit cell at the interlayer.

The dimensions of unit cell in our clay mode are $5.28\text{\AA} \times 9.14\text{\AA} \times 6.56\text{\AA}$ ($1\text{\AA} = 10^{-10}$ m or 0.1 nm). The model used by (Schmidt, et al., 2005) is a 4x2 model, that is, each clay layer contains four unit cells in x direction and two unit cells in the y direction. So the overall dimension of (Schmidt, et al., 2005)'s model is $21.12\text{\AA} \times 18.28\text{\AA} \times 6.56\text{\AA}$. Later on, (Katti, et al., 2006) derived a 6x3 model for studying polymer clay nanocomposites with six unit cell in x direction and 3 unit cell in y direction and an overall dimension of $31.68\text{\AA} \times 27.44\text{\AA} \times 24.16\text{\AA}$ from (Schmidt, et

al., 2005)'s model. Katti et al. model did not contain interlayer Na ions as those were replaced by modifier and their concern was study the polymer clay nanocomposites. The montmorillonite clay model used in this study was created from (Katti, et al., 2006) model by introducing appropriate isomorphous substitution and interlayer sodium cations.

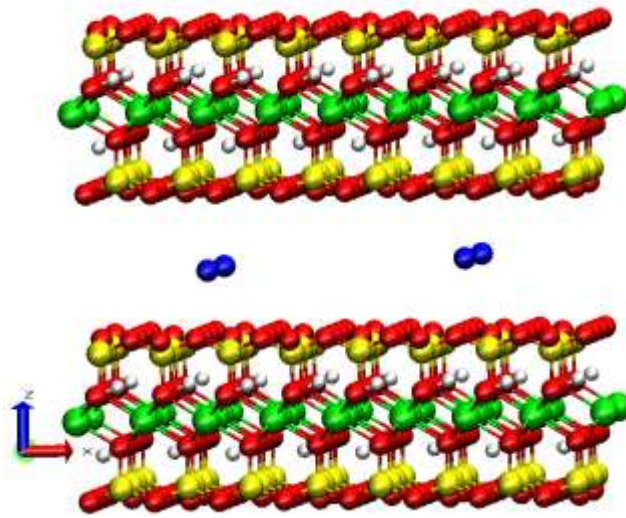


Figure 5.3: 4x2 Na-Montmorillonite model (with 8 unit cell) used in our previous study.

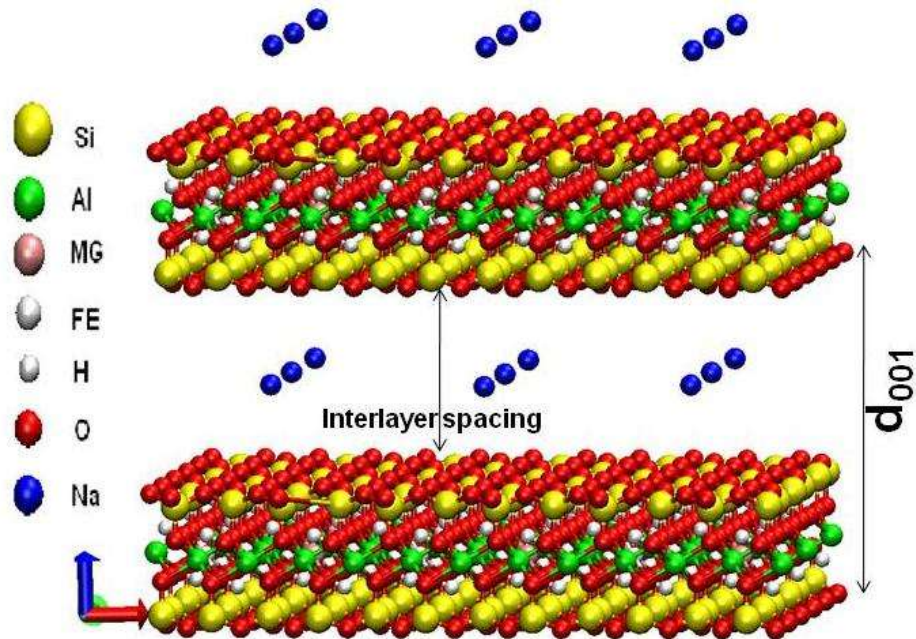


Figure 5.4: 6x3 Na-Montmorillonite model (with 18 unit cell) used in this study.

Fluids chosen for this study have a wide range of polarity, ranging from very high as formamide (DEC =110) to very low as toluene (DEC=2.4). Model of fluid molecules were constructed using Materials Studio and final coordinates of MMT-Fluid model obtained using PSFGEN plug in of Visual Molecular Dynamics (VMD) software (Humphrey, et al., 1996).

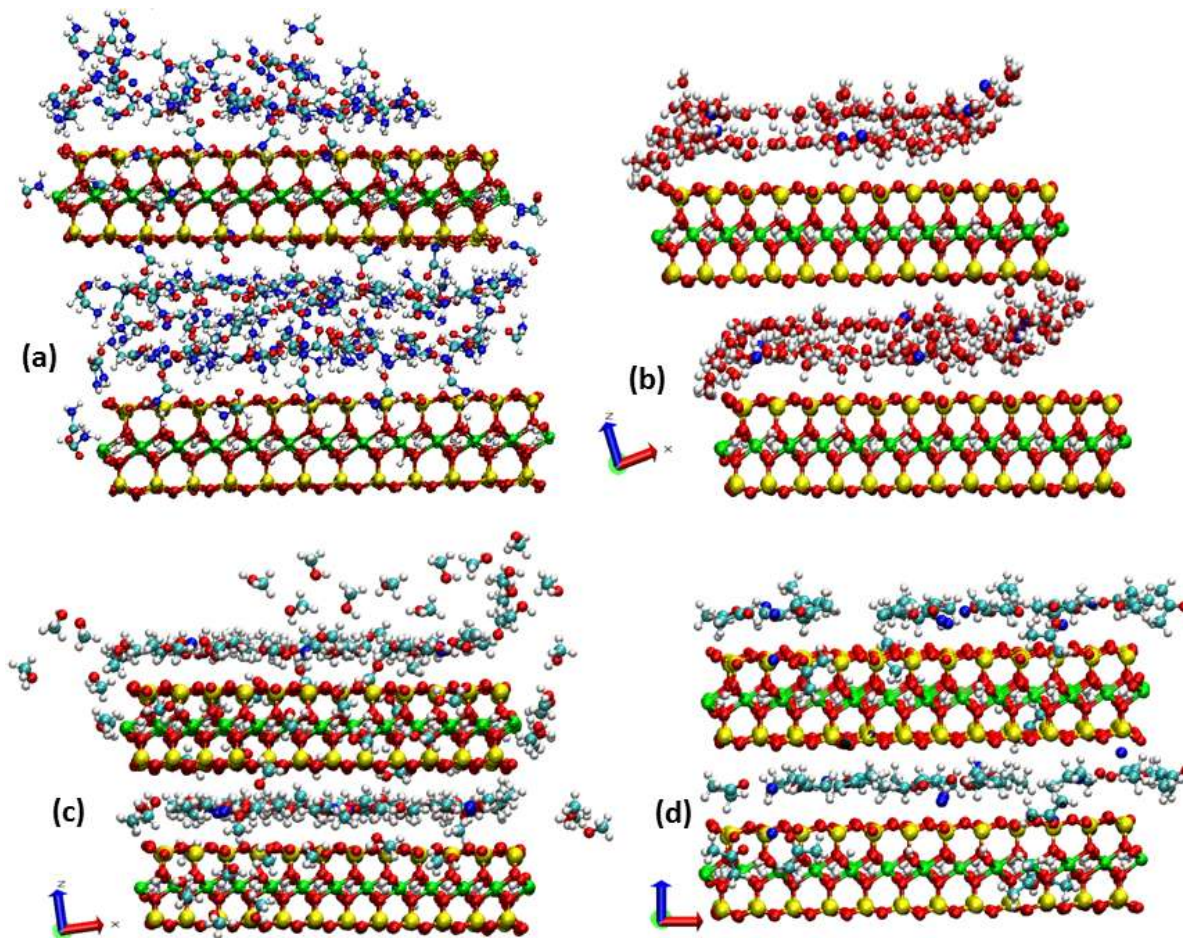


Figure. 5.5: Na-MMT with (a) 40 wt% interlayer formamide (b) 20% Water (c) 20% Methanol and (d) 10% Acetone (After Equilibration). Total thirteen models were prepared with 10%, 20%, 30%, 35% and 40% interlayer different fluids.

Different models (Figure. 5.5) were prepared for Na-MMT with 10%, 20%, 30%, 35%, 40% (% by weight) of fluids. 10% fluids were placed as a single layer between the interlayer. So 20%, 30%, 40% fluids were placed as two, three and four layers consequently. In model with 35%

water was placed as four layers between interlayer. As the molecular weight of different fluid is different, 10% fluid is equivalent to approximately 48 formamide, 72 water, 40 methanol, 24 acetone and 15 toluene molecules.

For our molecular dynamics (MD) simulations NAMD 2.7b2 software was used. NAMD (Phillips, et al., 2005) was developed by the Theoretical and Computational Biophysics Group in the Beckman Institute at the University of Illinois at Urbana-Champaign.

5.4 Force Field Parameters

MD was used to study the molecular interaction of clay with different pore fluids. NAMD 2.7b2 software was used in this study which supports CHARMM (Brooks, et al., 1983) and AMBER force fields. CHARMM force field parameters for montmorillonite were derived by Schmidt (Katti, et al., 2005) (Schmidt, et al., 2005, Katti, et al., 2007) from the CFF force field developed by (Teppen, et al., 1997). Formamide, methanol and acetone parameter was obtained from CHARMM GUI Archive - CHARMM Small Molecule Library (MacKerell, et al., 1998, Foloppe and MacKerell, 2000). Toluene force field parameters were taken from (Lopes, et al., 2007).

5.5 Simulation Details

We used NAMD 2.7b2 and visual molecular dynamics (VMD) for the simulations described in this study. 35-500 MHz Pentium processor were used to run the simulations in the 128-3 GHz Xeon processor parallel computing systems of the CHPC (Center for High Performance Computing system) at the North Dakota State University.

In the first step of MD simulations geometry was minimized, that is the model was brought to the minimum energy condition to achieve optimized geometric conformation. Minimization was performed to avoid any excessive energy in the system that might be released later on and could

cause the simulation to become unstable. All the models were minimized for 150,000 iterations. The convergence of the total energy was observed. The minimization was performed at simulated conditions of vacuum and 0 K. Conjugate gradient algorithm, an iterative method for finding the nearest local minima of a function has been used for minimization. During the entire simulation clay layers as well as interlayer sodium ions were restrained in x and y direction that is only can move in the z direction. One of the important features of this study is during the entire simulations fluid molecules were kept free in all three dimensions. In the previous studies water molecules were kept restrained in x and y direction. In this study fluid molecules are kept free in three dimensions thus have more freedom to orient in any direction which not only allowed us better conformational analysis but also mimicking the real experimental conditions.

MD simulations are usually conducted at atmospheric pressure and temperature. Temperature and pressure were raised to 300K and 1 atmosphere in a step by step procedure. Temperature was raised from 0 to 100K, 100 to 200K, 200 to 300 k and pressure raised from 0 to 0.25 atm, 0.25 to 0.5 atm, 0.5 to 0.75 atm and finally 0.75 to 1 atm. We utilized langevin dynamics for controlling temperature and heat energy of the system. The Nose- Hoover Langevin piston method (Martyna, et al., 1994) was used for raising pressure.

NAMD uses Verlet algorithm, a commonly used time integration algorithm for the integration of the MD equations. The step size was used as 0.5 fs (10^{-15} s) for all the simulations performed in this study. The duration of each steps is 75 ps (10^{-12} s) or 150000 steps resulting a total simulation time as 0.525 ns (10^{-9} s) or 1050,000 steps. Convergence of total potential energy was reached sufficiently before end of each simulation. In reality, the size of clay sheet is much bigger than our clay model and surrounded by clay sheets. Periodic boundary conditions were applied which create copies of model in all three dimensions to solve the problem. If we

study an individual small model then edge effect will be dominating, by applying periodic boundary we were able to avoid the edge effect. Particle Mesh Ewald (PME) method was utilized to calculate the electrostatic interaction between atom pairs which is the most appropriate method for calculating a large number of electrostatic energies between atom groups in a crystal structure.

The d_{001} spacing and position of atoms were calculated by averaging the data collected over last 20 ps (40000 steps) of the simulation. Simulation took 7-10 hour in each step (Total 56-80 hours) using a 16 processors at distributed-memory cluster located in NDSU Center for High Performance Computing System (CHPC).

5.6 Results and Discussion

We developed the model for different clay-fluid system with different weight % of fluids to achieve the experimental d_{001} spacing. d_{001} spacing at experimental condition and corresponding from modeling is shown in table. 1. During experiment we were not able to achieve slurry condition for water and formamide. Experimental d_{001} spacing reported for formamide contains 40% formamide, water contains 60% water and clay slurry was prepared using rest of the fluids. From the molecular simulations we found that at experimental condition interlayer contained 40% formamide, 35% water, 20% methanol, 10% acetone and very small or no toluene molecules. Therefore, we see that at experimental condition clay interlayer holds all the formamide, 35% water out of 60%, 20% methanol, 10% acetone and no or very little toluene. This indicates that interlayer contains greater amount of higher polarity fluids. The presence of greater amount of solvents for high polar fluids can be correlated with increased swelling, swelling pressure, particle breakdown and low permeability from the understanding of our previous studies. Results of the previous study (Amarasinghe, et al., 2009, Amarasinghe, et al.,

2008) shows that higher polar fluids will cause greater amount of swelling, similar results also observed in XRD analysis by the authors. (Katti and Shanmugasundaram, 2001). They have shown that greater amount of swelling will cause more particle breakdown thus cause more swelling pressure. So, it is expected that high polar fluids will show greater swelling pressure. Again, greater amount of particle breakdown will cause decrease in size of voids, increase in surface area which will provide for more clay-fluid interactions and thus will lead to low flow rate as we observed in macro scale permeability tests. Schematic showing the correlation of greater amount of interlayer fluids for higher polarity fluids with their lower permeability is shown in the Figure. 5.6.

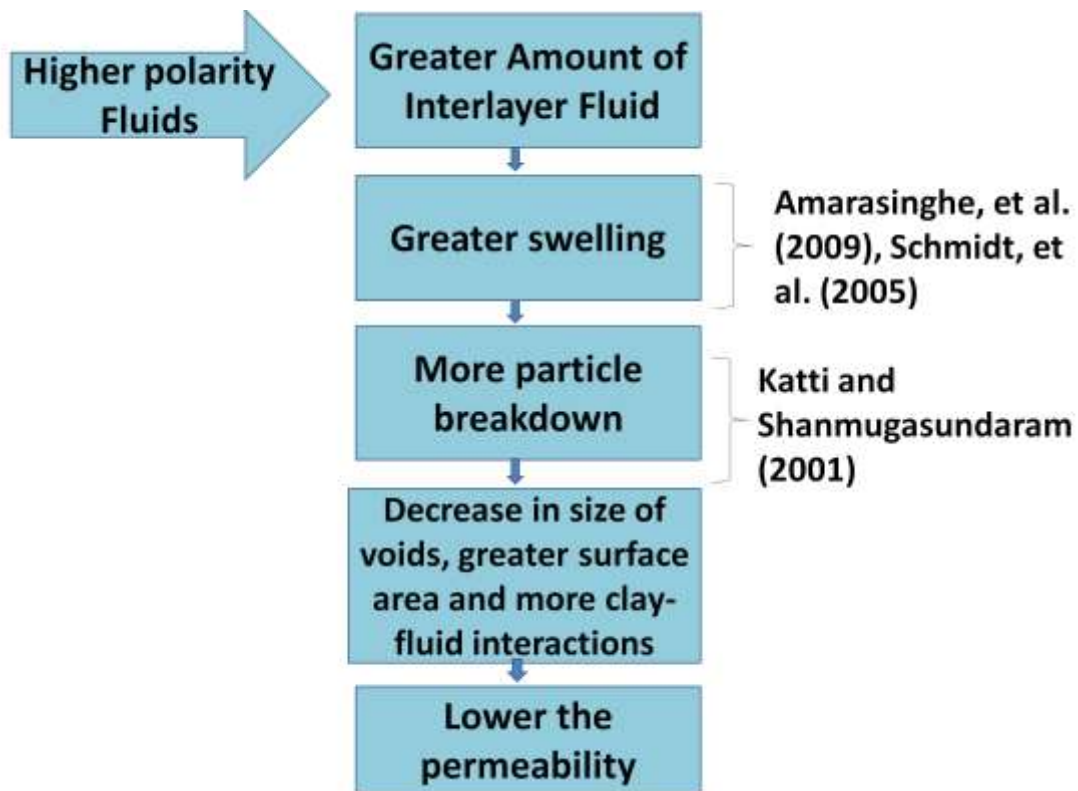


Figure. 5.6: Correlation of fluid polarity, amount of interlayer fluid and permeability of fluids.

Table 5.1: d_{001} spacing from experiments and molecular dynamics simulations

Fluid	D.C	d_{001} spacing					d_{001} spacing (Experimental)
		10%	20%	30%	35%	40%	
Formamide	110	13.345	14.77	16.9		18.91	18.99
Water	80	12.7	15.65	17.79	18.03		18.32
Methanol	33	13.14	17.69				17.14
Acetone	20	13.32					12.98
Toluene	2.4						9.74

From the experimental studies, we see that there is no increase in d_{001} spacing for toluene. But we were not able to achieve experimental d_{001} spacing with even small amount (10%) of toluene, which indicates that very few or no toluene molecules present in the interlayer at experimental condition. Again, looking at the Na-MMT toluene conformation (Figure. 5.7) suggests that toluene molecules tend to come out from interlayer in comparison to other molecules with greater dielectric constant. This indicates that lower interactions of low polar fluids with the clay sheet which leading to a higher value of permeability for low polar fluids.

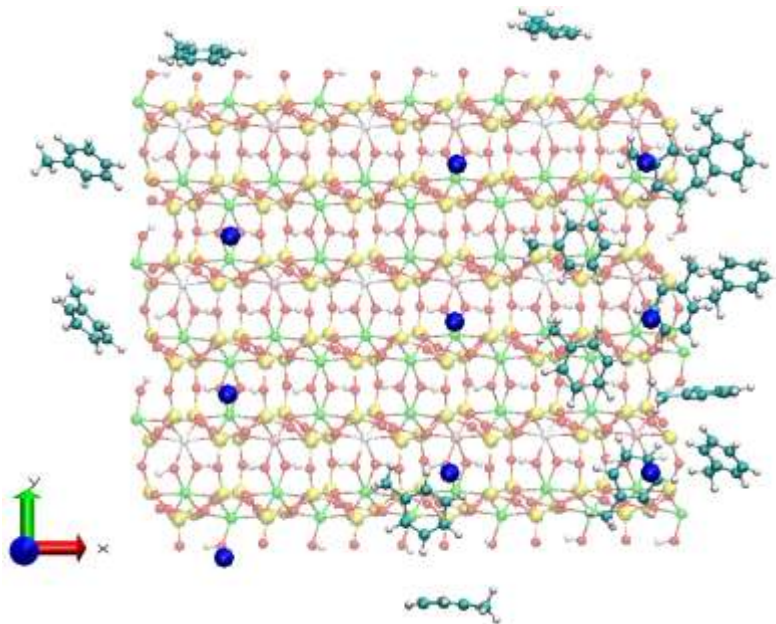


Figure. 5.7: Na-MMT with 10% toluene (conformation).

From our interaction energy values we see clay-clay electrostatic interaction is only 1-6 % of total clay fluid or Na⁺ ions fluid interactions. In dry clays, electrostatic repulsion due to negative charged clay surface is balanced by the attraction of counter ions and clay sheet. But as the fluid molecules come into the interlayer they are the dominating factor. So, we can say that the contribution of electrostatic repulsion of clay surfaces is small for clay swelling in compare to the hydration of clay surface and counter ions. Similar observation was also seen qualitatively for clay-water system by (Lupe, 1997). Although structure and charge distribution of organic molecules is complex, still we see much strong interaction between fluid molecules and Na⁺ ions than clay-clay or clay-fluid interactions (Figure. 5.8). The conformation of water molecules in MMT-10% water model shows clustering of water molecules around the Na⁺ ions, as the amount of interlayer fluid increases they start forming layer. For experimental condition model, 55% of total water molecules present in the 3 Å mid region of interlayer near sodium ions (Interlayer spacing is 11.5 Å). For other fluids a higher fluid concentration around sodium ions also has been observed. From the interaction energies and conformation analysis, a higher interactions of Na⁺ ions with the fluid molecules has been observed, followed by clay-fluid interactions and comparatively very small clay-clay interactions are observed. Therefore we can conclude that clay-fluid interactions are initiated by hydration (solvation) of Na⁺ ions following by hydration of clay sheets. Absence of interlayer counter ions is the reason for poor interactions of talc with water molecules as explained in the study by (Delville and Sokolowski, 1993).

When fluid molecules introduce into the interlayer clay-clay interaction decreases (Figure. 5.9). As the amount of interlayer fluid increases, it causes further reduction in clay-clay interaction energies (Figure. 5.9, Figure 5.10). We see in case of higher polarity fluids more reduction in clay-clay interaction (Figure. 5.11). As fluid molecules introduced into the

interlayer, clay-sodium ion interactions also decreases and with increasing amount of interlayer fluid we see more reduction in clay-sodium ion interactions (Figure. 5.12, Figure. 5.13). We see higher polarity fluids cause more reduction in clay-sodium ion interactions, as also seen in case of clay-clay interactions. The reduction of clay-sodium ion interactions may be due the results of both attractive interactions of clay sheet for surrounding fluids and interactions of sodium ions for surrounding fluid molecules (hydration of clay sheet and sodium ions for water). So, clay sheets and sodium ions are not able to attract each other as strongly as in dry clay.

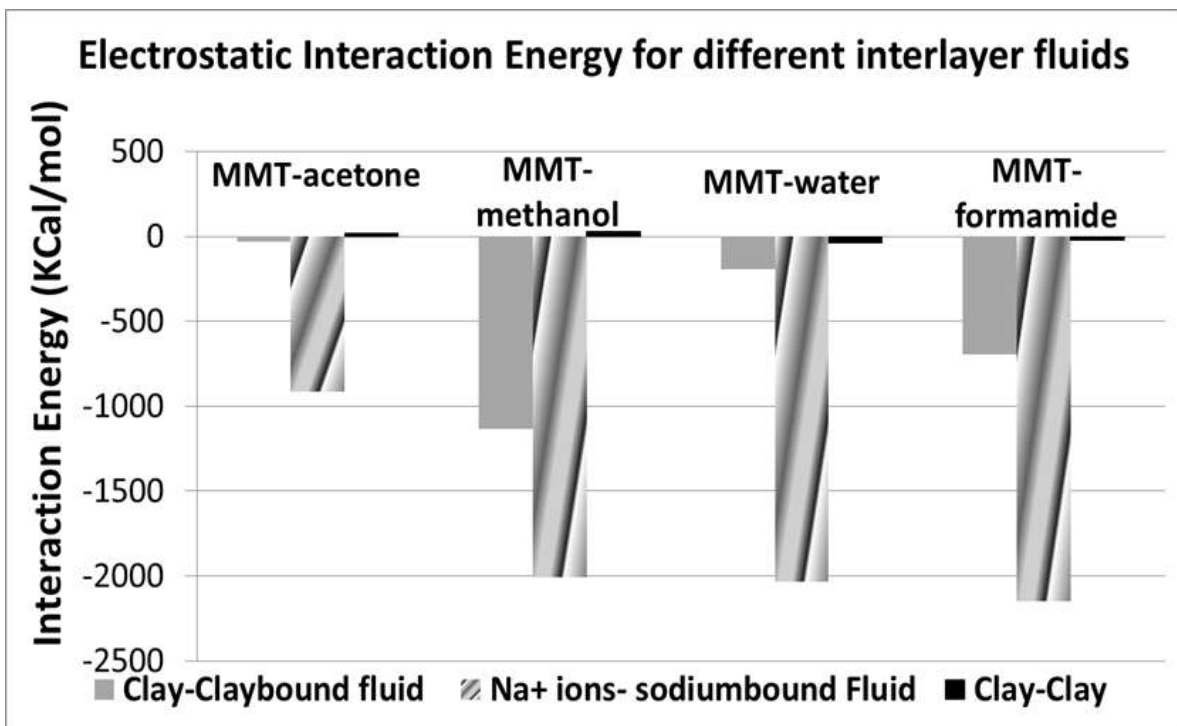


Figure. 5.8: Interaction Energies between clay-claybound fluid, Na+-sodiumbound fluids and clay-clay at experimental condition.

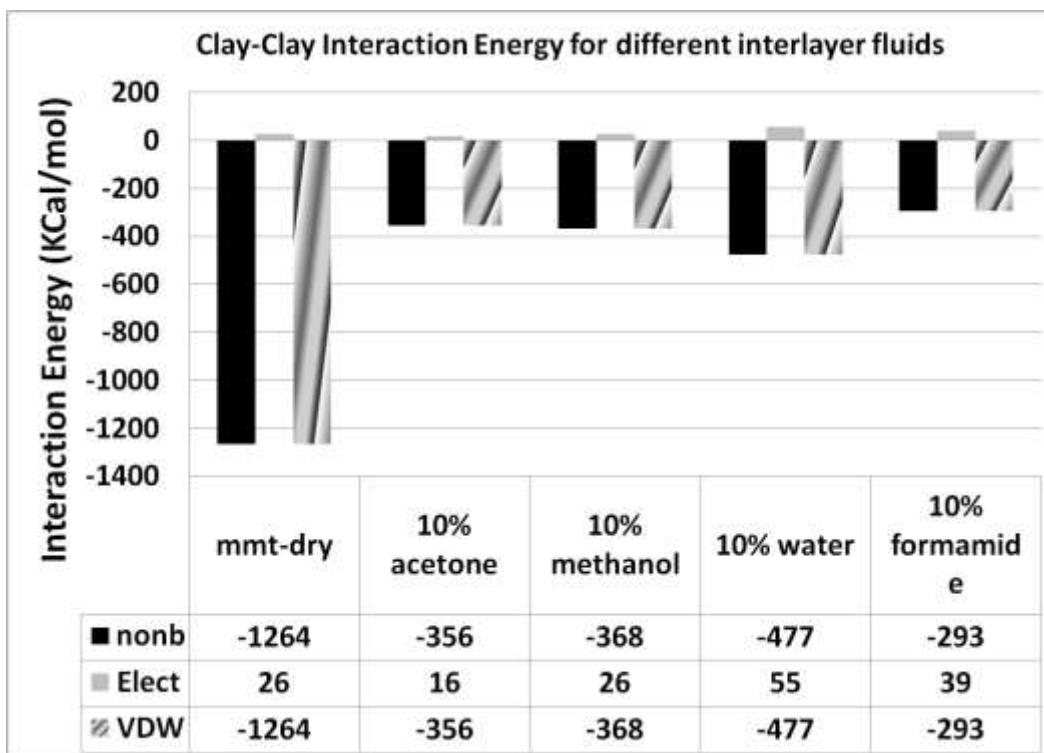


Figure. 5.9: Interaction Energy between two clay sheets for 10 wt% different polarity fluids.

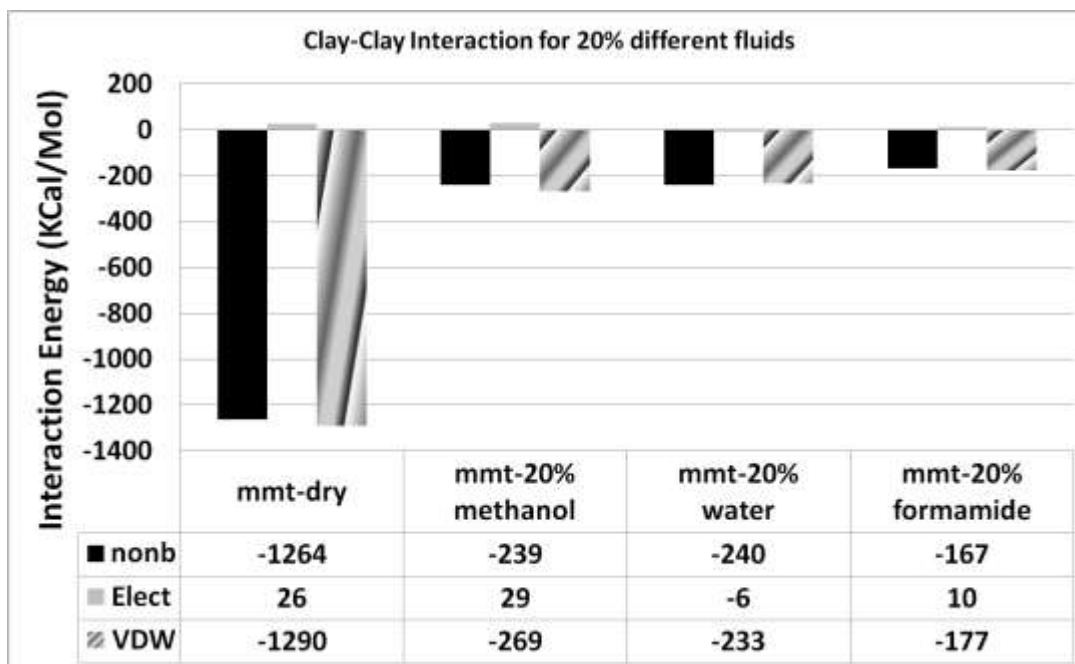


Figure. 5.10: Interaction Energy between two clay sheets for 20 wt% different polarity fluids.

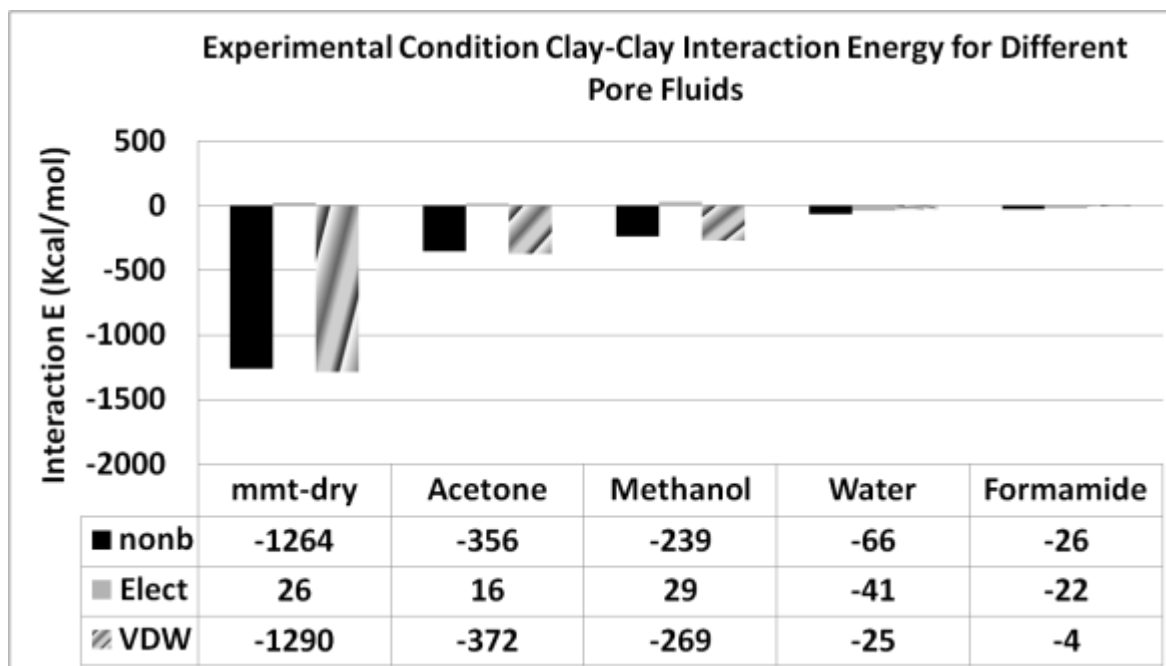


Figure. 5.11: Interaction Energy between two clay sheets at experimental condition for different polarity fluids.

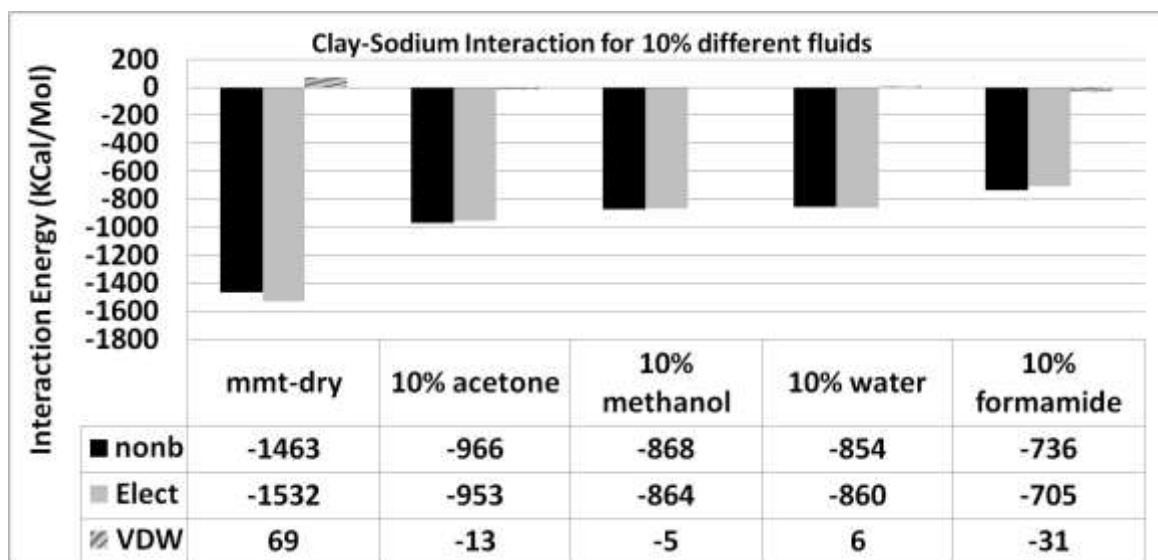


Figure. 5.12: Interaction Energy between clay sheets and sodium ions for 10 wt% different polarity fluids.

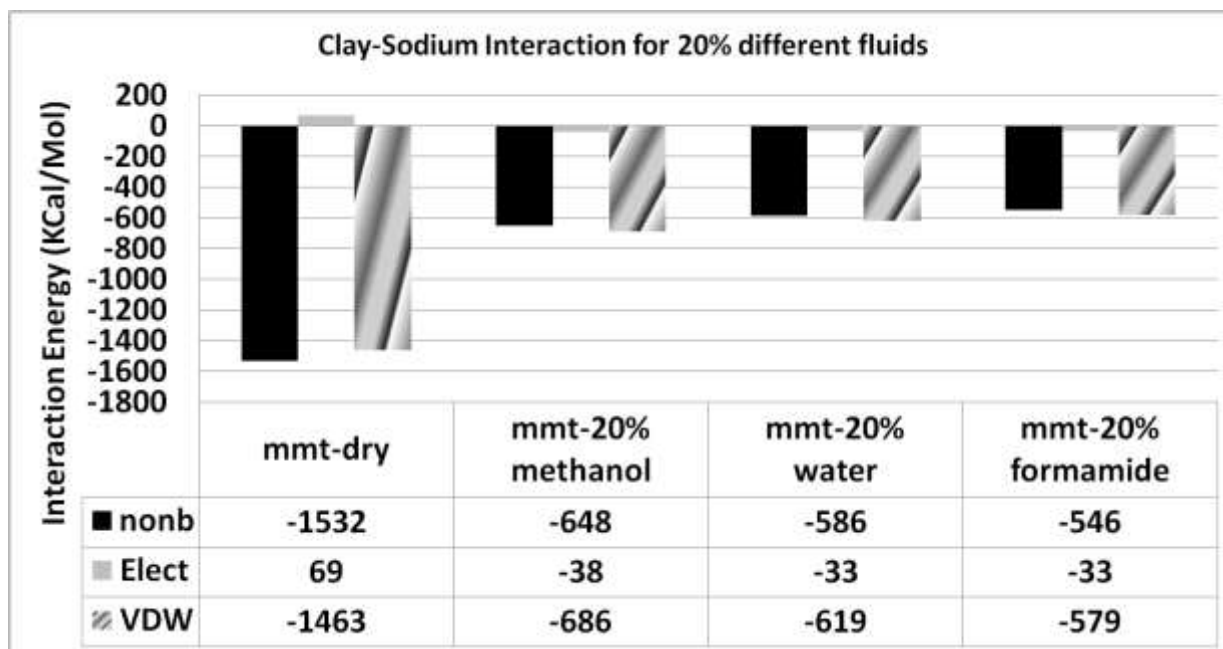


Figure. 5.13: Interaction Energy between clay sheets and sodium ions for 20 wt% different polarity fluids.

The conformation of the interlayer fluid depends on several factors including surface charge density, type of interlayer cations and nature of interlayer fluid. An increase in charge density will cause more orientation along the surface and show strong layering phenomenon. This is the reason behind mica and vermiculate with greater charge density show more layering than montmorillonite (Delville, 1992). The ratio of tetrahedral to octahedral substitution also affects the layering, higher the ration more layering is expected. The ratio of tetrahedral to octahedral substitution in montmorillonite is low in compare to some other clays (like beidelite) having only tetrahedral substitution. Another important factor is type of interlayer cations. Interlayer cations highly disturb the layering phenomenon. Li^+ ion show more attracts the water molecules more strongly than Na^+ ion hence show less layering phenomenon, while K^+ , Cs^+ ions attract the water molecules less strongly than Na^+ ions and show more layering. For our Na-MMT-water system it is expected weak layering phenomenon as we see for 10% water content

(Figure. 5.14). As the water content increases it starts forming layer. The layering phenomenon for organic fluid molecules is much complex to explain, we see fluid molecules have higher concentration around the plane of counter ions. We calculated the average direction of dipole moments for clay bound fluids (fluids within 3.5 Å of clay surface) from where we see the conformation of clay bound fluid molecules show strong orientation towards clay surface with increasing amount of interlayer fluids (Figure 5.15, Figure 5.16). This may be due to less influence of exchangeable cations on clay bound fluid with increasing interlayer fluid. Another observation is higher polarity fluid molecules show strong orientation as we see in Figure. 5.17 for clay bound fluids.

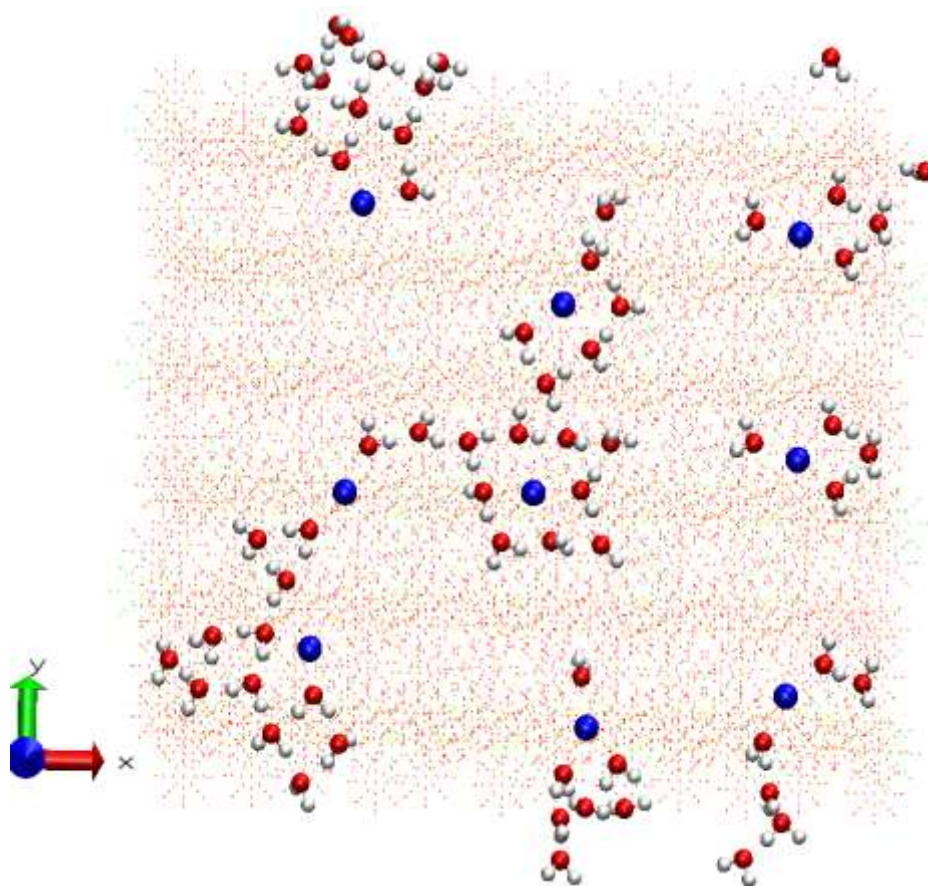


Figure. 5.14: Na-MMT with 10% water (After Equilibration).

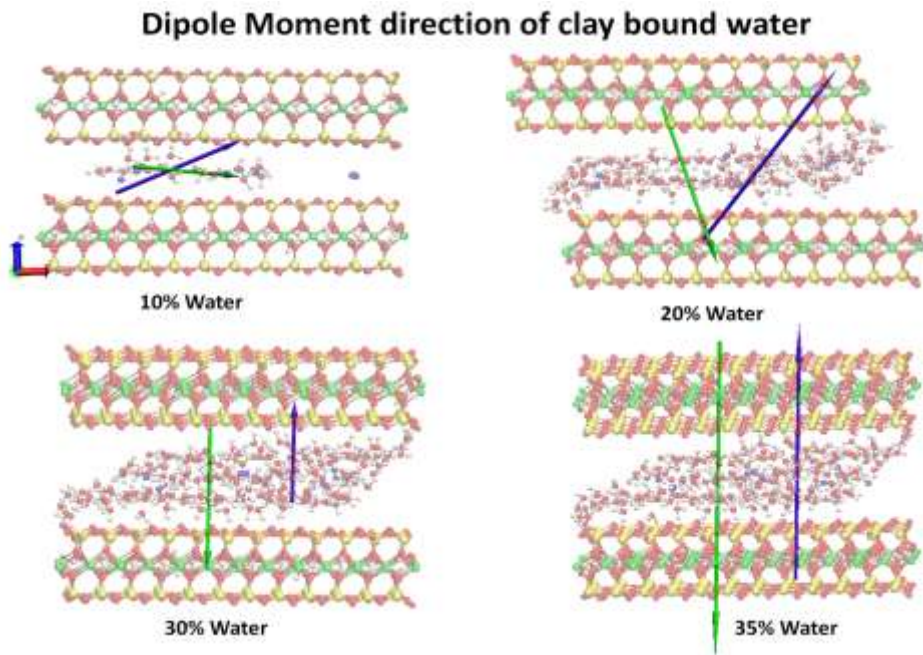


Figure. 5.15: Dipole moment direction of clay bound water.

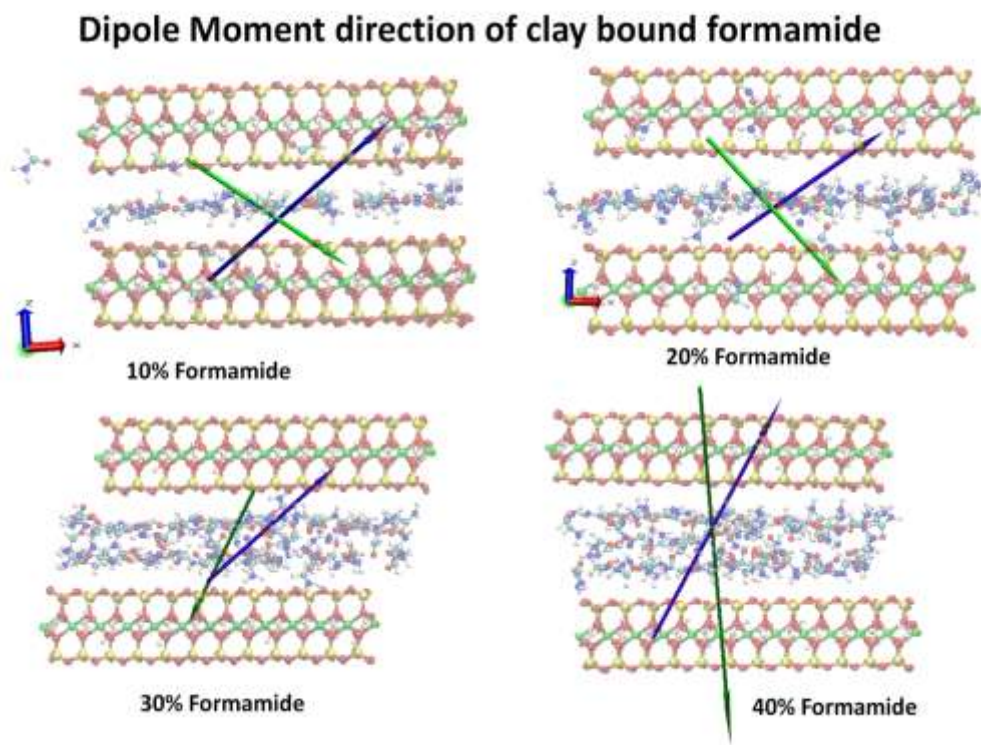


Figure. 5.16: Dipole moment direction of clay bound formamide.

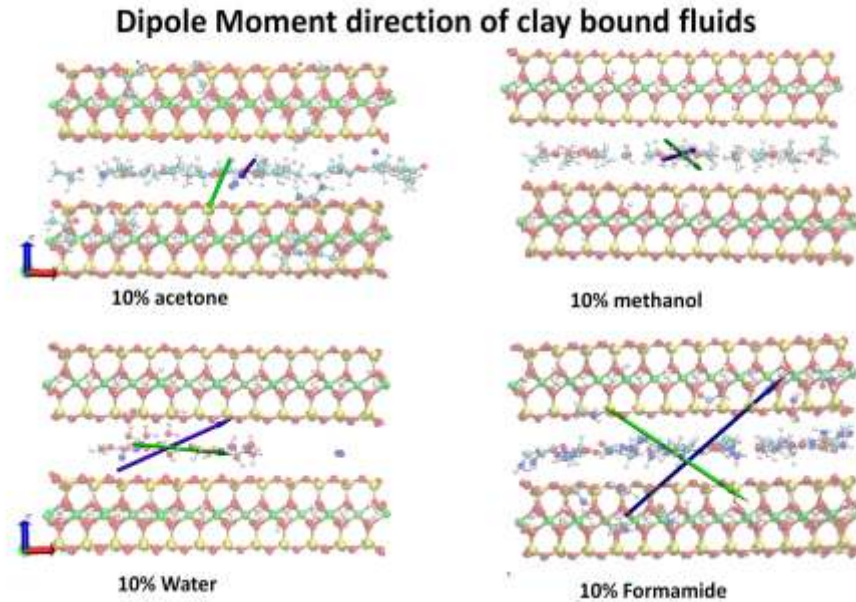


Figure. 5.17: Dipole moment direction of clay bound fluids.

From the conformation of fluid molecules, we see oxygen atoms in fluid molecules are always directed towards sodium ions and hydrogen atoms towards oxygen atoms in the clay surface. At small amount of interlayer fluid, fluid molecules oriented around the sodium ions in a arranged pattern and maximum four oxygen atoms (of fluid molecule) heading towards sodium ions (Figure 5.18, Figure 5.19). For 20 % formamide and methanol we see, fluid molecules still maintain their organized pattern. At 10% interlayer methanol we see maximum 2/3 methanol molecules around sodium ions and for 20% interlayer methanol we observe maximum four methanol molecule around a sodium ion (Figure. 5.19, Figure. 5.20). Four methanol molecules for multilayer solvation and two methanol molecules for monolayer solvation were observed by (Pintore, et al., 2001) where CH_3 chain were kept rigid.

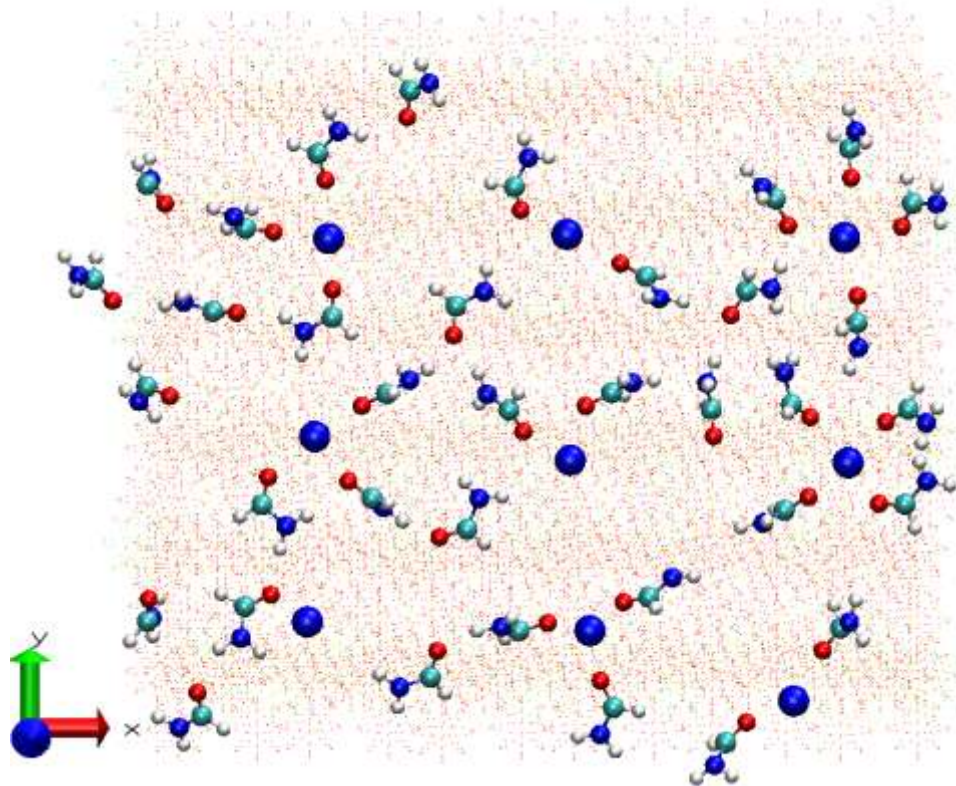


Figure. 5.18: Perspective view of Na-MMT with 20% formamide (conformation).

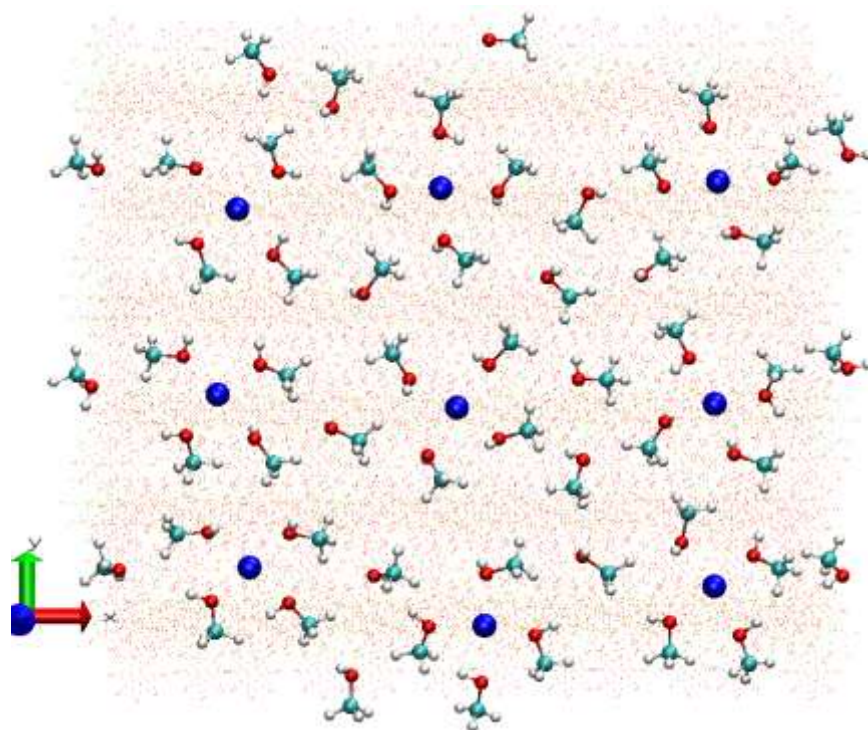


Figure. 5.19: Perspective view of Na-MMT with 20% methanol (conformation).

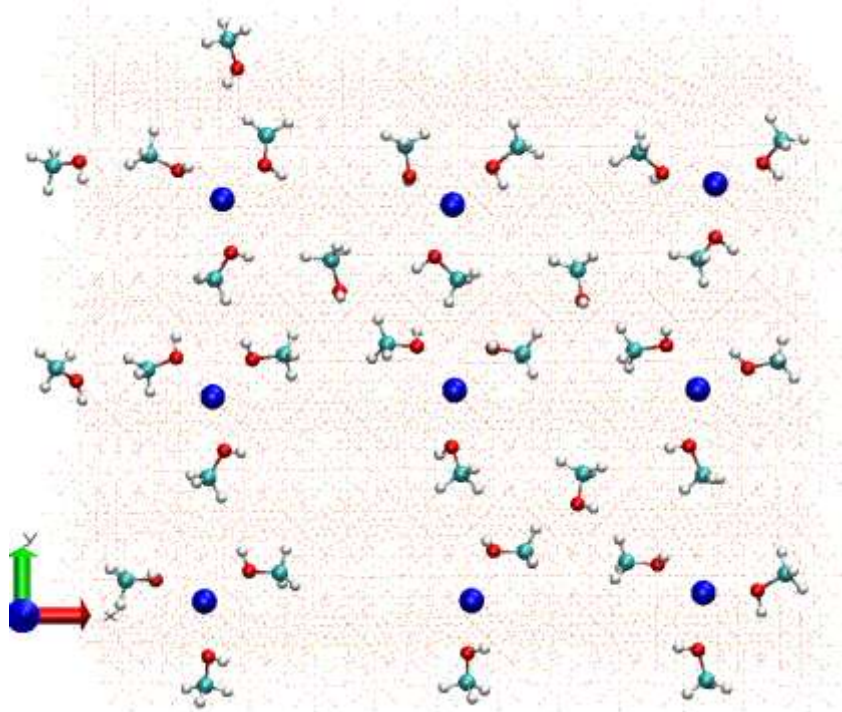


Figure 5.20: Perspective view of Na-MMT with 10% methanol (conformation).

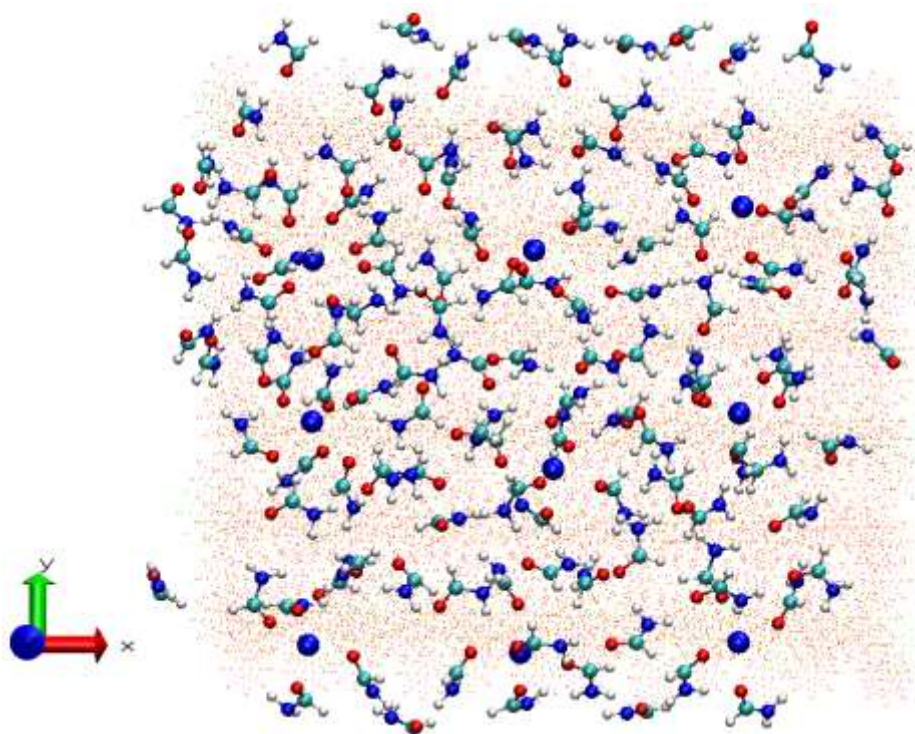


Figure. 5.21: Perspective view of Na-MMT with 40% formamide (conformation).

As the amount of interlayer fluid increases, fluid molecules start losing their arranged pattern (Figure 5.21). Toluene conformation shows random orientation of toluene molecules without showing affinity towards a particular group of atoms in the clay sheet (Figure. 5.7). This is may be the reason for toluene having a high permeability through clay.

5.7 Conclusion

Molecular models have been developed for Na-MMT clay with a wide range of interlayer fluids for the study of clay fluid interactions at molecular level. We performed molecular dynamics simulations to quantitatively evaluate the amount of interlayer fluid at different level of swelling as well as to investigate the influence of fluid properties on swelling. From our modeling results we were able to estimate the quantitative amount of fluid molecules went to interlayer during the experimental studies performed earlier. From the current studies we see that all of formamide (40 wt%) introduced went to interlayer, 35% out of 60% water, 20% methanol, 10% acetone and no or very few toluene molecules went into the interlayer at experimental condition. The study shows that greater the polarity of fluids, less the mobility of fluids and hence remain at interlayer causing greater swelling. From the current study along with previous experimental studies (Amarasinghe, et al., 2009, Amarasinghe, et al., 2008) we see that higher polarity fluids show greater swelling and swelling pressure. Our interaction energy values show that clay-clay electrostatic interactions are only 1-6 % of total clay fluid or Na^+ ions fluid interactions which indicate that the hydration (solvation) of clay surface and counter ions is the dominating factor for clay swelling rather interaction between negatively charged clay sheets. From the interaction energies and conformation a higher interaction of Na^+ ions with fluid molecules followed by clay-fluid and comparatively very small clay-clay interactions were observed. So, we can say that hydration (solvation) of clay is initiated by hydration (solvation) of

Na⁺ ions followed by hydration of clay sheets. From the conformational analysis we see, at lower fluid concentration interlayer fluids show organized orientation and as the amount of fluid increases fluids orientation is more random. From the average direction of dipole moments of fluid molecules, we see with increasing interlayer fluid, fluid molecules strongly orient towards clay sheets. This study along with the previous experimental studies provides a quantitative estimation of interlayer fluids at particular level of swelling as well as shows the effects of solvent polarity on flow properties, swelling and swelling pressure of clays. This study also provides an insight into molecular mechanism that lead to macro scale behavior of swelling clays. Significant variation in flow properties and swelling of clays with different polarity fluids is very important for landfill liner design as well as other geotechnical and geo-environmental applications indicates that current state of art of designs may be adequate for water or a particular type of fluid, but may not be adequate for other fluids present in the site specific condition.

5.8 References

- [1] Katti, D., and Shanmugasundaram, V. (2001). "Influence of swelling on the microstructure of expansive clays." *Canadian Geotechnical Journal*, 38(1), 175-182.
- [2] Katti, D. R., Matar, M. I., Katti, K. S., and Amarasinghe, P. M. (2009). "Multiscale modeling of swelling clays: A computational and experimental approach." *Ksce Journal of Civil Engineering*, 13(4), 243-255.
- [3] Katti, D. R., Schmidt, S. R., Ghosh, P., and Katti, K. S. (2005). "Modeling the response of pyrophyllite interlayer to applied stress using steered molecular dynamics." *Clays and Clay Minerals*, 53(2), 171-178.

- [4] Schmidt, S. R., Katti, D. R., Ghosh, P., and Katti, K. S. (2005). "Evolution of mechanical response of sodium montmorillonite interlayer with increasing hydration by molecular dynamics." *Langmuir*, 21(17), 8069-8076.
- [5] Katti, D. R., Schmidt, S. R., Ghosh, P., and Katti, K. S. (2007). "Molecular modeling of the mechanical behavior and interactions in dry and slightly hydrated sodium montmorillonite interlayer." *Canadian Geotechnical Journal*, 44(4), 425-435.
- [6] Amarasinghe, P. M., Katti, K. S., and Katti, D. R. (2008). "Molecular Hydraulic Properties of Montmorillonite: A Polarized Fourier Transform Infrared Spectroscopic Study." *Applied Spectroscopy*, 62(12), 1303-1313.
- [7] Amarasinghe, P. M., Katti, K. S., and Katti, D. R. (2009). "Nature of organic fluid-montmorillonite interactions: An FTIR spectroscopic study." *Journal of Colloid and Interface Science*, 337(1), 97-105.
- [8] Cornelis, K., and Dutrow, B. (2007). *Manual of Mineral Science*, John Wiley & Sons, Inc.
- [9] Katti, K. S., and Katti, D. R. (2006). "Relationship of swelling and swelling pressure on silica-water interactions in montmorillonite." *Langmuir*, 22(2), 532-537.
- [10] Van Olphen, H. a. F., J. J (1979). *Data handbook for clay materials and other non-metallic minerals*, Pergamon Press, New York.
- [11] Skipper, N. T., Chang, F. R. C., and Sposito, G. (1995). "Monte-carlo simulation of interlayer molecular-structure in swelling clay-minerals .1. Methodology." *Clays and Clay Minerals*, 43(3), 285-293.
- [12] Teppen, B. J., Rasmussen, K., Bertsch, P. M., Miller, D. M., and Schafer, L. (1997). "Molecular dynamics modeling of clay minerals .1. Gibbsite, kaolinite, pyrophyllite, and beidellite." *Journal of Physical Chemistry B*, 101(9), 1579-1587.

- [13] Katti, K. S., Sikdar, D., Katti, D. R., Ghosh, P., and Verma, D. (2006). "Molecular interactions in intercalated organically modified clay and clay-polycaprolactam nanocomposites: Experiments and modeling." *Polymer*, 47(1), 403-414.
- [14] Humphrey, W., Dalke, A., and Schulten, K. (1996). "VMD: Visual molecular dynamics." *Journal of Molecular Graphics*, 14(1), 33-&.
- [15] Phillips, J. C., Braun, R., Wang, W., Gumbart, J., Tajkhorshid, E., Villa, E., Chipot, C., Skeel, R. D., Kale, L., and Schulten, K. (2005). "Scalable molecular dynamics with NAMD." *Journal of Computational Chemistry*, 26(16), 1781-1802.
- [16] Brooks, B. R., Bruccoleri, R. E., Olafson, B. D., States, D. J., Swaminathan, S., and Karplus, M. (1983). "Charmm - a program for macromolecular energy, minimization, and dynamics calculations." *Journal of Computational Chemistry*, 4(2), 187-217.
- [17] MacKerell, A. D., Bashford, D., Bellott, M., Dunbrack, R. L., Evanseck, J. D., Field, M. J., Fischer, S., Gao, J., Guo, H., Ha, S., Joseph-McCarthy, D., Kuchnir, L., Kuczera, K., Lau, F. T. K., Mattos, C., Michnick, S., Ngo, T., Nguyen, D. T., Prodhom, B., Reiher, W. E., Roux, B., Schlenkrich, M., Smith, J. C., Stote, R., Straub, J., Watanabe, M., Wiorkiewicz-Kuczera, J., Yin, D., and Karplus, M. (1998). "All-atom empirical potential for molecular modeling and dynamics studies of proteins." *Journal of Physical Chemistry B*, 102(18), 3586-3616.
- [18] Foloppe, N., and MacKerell, A. D. (2000). "All-atom empirical force field for nucleic acids: I. Parameter optimization based on small molecule and condensed phase macromolecular target data." *Journal of Computational Chemistry*, 21(2), 86-104.
- [19] Lopes, P. E. M., Lamoureux, G., Roux, B., and MacKerell, A. D. (2007). "Polarizable empirical force field for aromatic compounds based on the classical drude oscillator." *Journal of Physical Chemistry B*, 111(11), 2873-2885.

- [20] Martyna, G. J., Tobias, D. J., and Klein, M. L. (1994). "Constant-pressure molecular-dynamics algorithms." *Journal of Chemical Physics*, 101(5), 4177-4189.
- [21] Lupe, M. B. M. (1997). "Molecular Atomistic Simulations of Clay Swelling in Water Dispersions." *Molecular Engineering*, Volume 7(Numbers 3-4), 367-383.
- [22] Delville, A., and Sokolowski, S. (1993). "Adsorption of vapor at a solid interface - a molecular-model of clay wetting." *Journal of Physical Chemistry*, 97(23), 6261-6271.
- [23] Delville, A. (1992). "Structure of liquids at a solid interface - an application to the swelling of clay by water." *Langmuir*, 8(7), 1796-1805.
- [24] Pintore, M., Deiana, S., Demontis, P., Manunza, B., Suffritti, G. B., and Gessa, C. (2001). "Simulations of interlayer methanol in Ca- and Na-saturated montmorillonites using molecular dynamics." *Clays and Clay Minerals*, 49(3), 255-262.

CHAPTER 6. STUDY THE DOUBLE LAYER THEORY FOR SWELLING CLAYS

6.1 Introduction

Clay swelling can be divided into two main categories, crystalline swelling and osmotic swelling or free swelling. Many researchers tried to explain clay swelling in terms of double layer theory. The fundamental assumptions in most of the double layer theories as an infinite negative charged clay surface is the first layer and distribution of oppositely charged ions as second layer. Different scientists tried to represent this distribution of oppositely charged ions in different way, and came up with modified versions of double layer theories. Although these theories have some success explaining certain phenomenon in clays, cannot explain swelling mechanism and have significant limitations. For example, non-swelling behavior of some highly charged clay particles and interlayer swelling they cannot be explained with these theories. We see some fundamental problems associated with the assumptions associated with double layer theory for example uniform charged surface, point charge, infinite plates, etc.

The swelling of clays is of great interest in engineering, soil chemistry and other fields of science. Among the different mineral type smectite group shows significant amount of swelling. Swellings of clays occur in two main form called crystalline swelling and osmotic swelling. Although numerous numbers of studies had been performed on swelling clays, very few of the studies addressed the behavior of interlayer fluids using molecular dynamics and Monte Carlo simulations. But most of these studies are within the range of crystalline swelling which has been reported in the range of 17-20 Å (Schmidt, et al., 2005, Katti, et al., 2007, Quirk and Marcelja, 1997). There is a lack of understanding for the complete swelling mechanism. Many researchers tried to explain swelling in terms of double layer theories for example DLVO (Derjaguin-Landau-Verwey-Overbeek) theory, Gouy-Chapman double layer theory, modified Gouy-

Chapman double layer theory, and Stern theory. Most of these theories have limitations explaining swelling clays and the assumptions associated with each of the theories need to be justified for swelling clays. DLVO theory cannot explain the non-swelling behavior of some highly charged clays minerals such as mica and vermiculate (Kleijn and Oster, 1982). According to the double layer theory, first layer of the double layer is formed by the negative charge on the clay surface. Associated assumption in all the double layer theories is that charge distribution is homogeneous over the surface of the particles where in reality charge distribution in clay surface is discrete in nature. The second layer is formed by the excess of oppositely charged ions in the solution. These counter ions were assumed as of point charges thus occupy no space and may reach excessively high concentrations at the clay surface-liquid interface. This assumption has significant limitations as in reality ions are of finite size. Later on finite ion size had been incorporated in Stern theory (1924). Gouy-Chapman double layer theory assumes ions follows the Boltzmann distribution, where the activity is proportional to molar concentration (<http://pubpages.unh.edu>). This is may be a reasonable assumption for bulk solution, but have significant limitations for confined fluids between two charged surface. Again, experimentally reported double layer thickness was found to be greater than calculated from the theory, which is may be due to the associated assumptions. In case of very dilute solutions, the error associated with neglecting finite size is small but in case concentrated solutions size effect is vital. In this case, Guoy-Chapman theory predicts impossibly high ion concentrations next to the surface (Yeung and Mitchell, 1993). Therefore, the actual concentration next to the clay surface will be less than predicted by Guoy-Chapman. Moreover, interaction between the surface, counter ions and solvents cannot explain completely using the theory. Stern (1924) developed an improved version of double layer theory that takes into account the finite dimensions of the ions.

According to Stern theory, first layer is similar to that of Gouy-Chapman theory. However, the second layer divides into two layers, (1) a tightly packed sublayer near the colloid surface called Stern layer, and (2) a diffuse layer. The potential distribution in Stern theory appears to be a combination of the Helmholtz and the Gouy-Chapman diffuse double layer. In the Stern layer, the potential decreases with distance from the surface according to the Helmholtz theory. After that (in the diffuse layer), decrease in potential with distance follows the Gouy-Chapman theory. The first ions of the Gouy-Chapman diffused double layer are not at the surface, but at some distance δ away from the surface. The maximum possible concentration will be determined by the hydrated radii of the cations. Stern considered that the distance of the closest counter ion to the charged surface is determined by the size of the ions.

The double layer theories are developed on some fundamental assumptions. One of the assumptions is uniformly distributed charged surface, while in reality swelling clays consist of discrete charge distribution due to isomorphic substitution. Experimentally reported double layer thickness found to be greater than evaluated from theory (<http://pubpages.unh.edu>). The goal of this work is to perform a molecular level study of swelling clays, and interpretation of the applicability double layer theory for swelling clays.

6.2 Double Layer Theory

Due to the electronegative charge clay particle in suspension can absorb cations. The distribution of cations is not uniform in suspension rather a higher concentration is observed near clay surface. A layer of oppositely charged ions and negatively charged clay surface are together called as double layer. First layer is the negatively charged clay surface and layer of cations on clay surface is described as second layer. Although the charge is located at the point of isomorphic substations, double layer theories considered first layer as of uniformly charged

plates. Although the positively charged ions are attracted by the negatively charged clay surface, these are free to move in the suspension. In fact, equilibrium exists between two opposite processes, one is potential energy due to negatively charged clay surface and another is free Brownian motion of the cations.

Double layer also sometimes described as electrical double layer refers to a parallel layer of opposite charge on a negative or positively charged surface. The charged surface is known as first layer. The second layer is the layer of oppositely charged ions. The distribution of second layer ions have been described differently by different researchers, but in general can be termed as double layer theories. The double layer theories have been using widely to explain different physical phenomenon in many real-world problems. Many researchers also tried to explain clay swelling in terms of double layer theories.

The double layer theory was first proposed by Helmholtz in 1853. Helmholtz described the physical model of ion absorption on a charged surface (double layer) mathematically as a simple capacitor. Later on Gouy-Chapman (G., 1910, Gouy, 1909, Gouy, 1910, D.L, 1913, Chapman, 1913) came up with improved double layer theory known as diffuse double layer theory. Gouy- Chapman's model is known as called as diffuse double layer theory because counter ions are dispersed in the liquid layer, as are the gas molecule in the earth's atmosphere. In both Helmholtz and Gouy-Chapman theory, ions were considered as point charges. Stern theory (1924) for the first time considered ionic dimension (Stern, 1924). The influence of ionic dimension is greatest near the colloidal surface. In Stern theory, first layer is similar to that of Gouy Chapman theory. However, the second layer is divided into two sub-layers, one near the colloidal surface and a diffuse layer. With some limitations, the combined Gouy-Chapman-Stern model is up to now the most commonly used.

In smectite clays, negative charge at clay surface is balanced by interlayer cations. As the water enters into the interlayer, these cations try to go into the solution as bulk solution contains very less number of cations. This distribution of ions due to Brownian motion is restrained due to the negatively charged clay surface (Anderson, et al., 2000). So, it is expected that the concentration of cations near the clay particle will be higher in comparison to bulk solution. Therefore, maximum electrical potential is located at clay surface, decrease as one travel away from clay surface and become zero at infinite distance (Papelis, et al., 1996). Many researchers tried to explain ion distribution around a clay surface in terms of double layer theory (Figure 2.11). Potential distribution from clay surface depends on several factors including surface charge density, concentrations and valence of cations, dielectric constant of fluids, etc. A typical potential distribution had been shown in Figure 6.1 after (Mitchell, 1993).

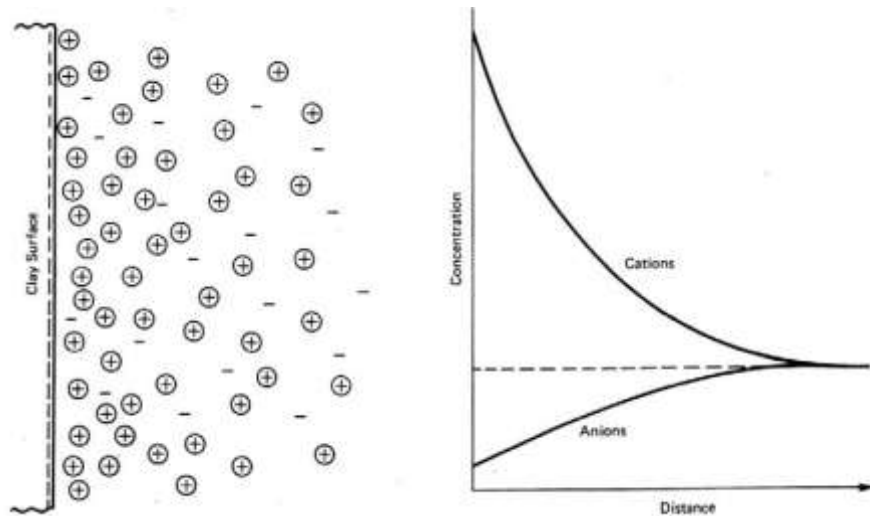


Figure 6.1: Distribution of ions from clay surface according to diffused double layer theory (Mitchell, 1993).

6.3 Helmholtz Double Layer Theory

The Helmholtz double layer theory is one of the earliest double layer theories (Tan, 1998). In Helmholtz theory negative charge on the colloid is considered to be evenly distributed

over the surface (charge density σ). The distribution of counter ions in the second layer is considered to be concentrated in a plane parallel to the surface at a distance χ . The dielectric constant (D) of the medium considered being constant, thus Helmholtz theory calculates the electrokinetic potential ζ is the same as the total potential Ψ . The electrochemical potential is the maximum at colloidal surface and drops linearly with increasing distance (χ) from the surface within the double layer. This is because the value for σ is decreasing very fast with distance from the surface, and reaches zero at the border of the double layer.

Helmholtz theory consists of certain limitations for example, hypothesizes of rigid layer of opposite charges that does not occur in nature. The consideration of linear potential distribution with distance also has limitations. Like all other double layer theories colloid surface was considered as uniformly distributed infinite charge plates.

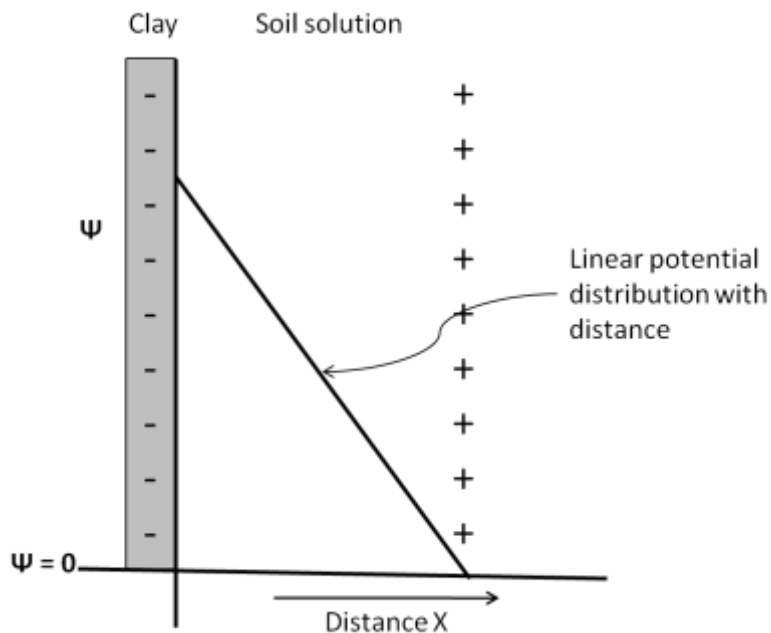


Figure 6.2: Graphical representation or potential distribution according to Helmholtz double layer theory.

6.4 Gouy-Chapman Double Layer Theory

Gouy-Chapman double layer theory also known as diffused double layer theory is one of the widely used theories. In this theory, negative charge on the colloid surface again considered as uniformly distributed. The counter ions dispersed in the liquid layer as are the gas molecule in the earth's atmosphere. For this it is called as diffuse double layer theory. According to Gouy-Chapman double layer theory the concentration distribution in the liquid zone follows the Boltzmann equation i.e,

$$C_x = C_x^0 \exp (-ze\Psi/kT)$$

Where C_x = concentration of cations (mol/L) at distance x from surface, C_x^0 = concentration of cations in the bulk solution (mol/L), z = valence of cations, e = charge of electron, Ψ = electrical potential, k = Boltzmann constant, T = absolute temperature.

In this theory, counter ions are considered as point charges. Solvent is treated as continuous medium with non-variant DEC with position in the double layer. A deficit of anions is usually present at the colloidal surface and the total charge of the surface is considered to be balanced by excess cations.

The electric potential at the colloidal surface is maximum, and decreases exponentially with distance from the surface. The distribution of potential follows the following equation

$$\Psi_x = \Psi_0 \exp (-Kx)$$

Here, Ψ_x = electrical potential at x distance from surface, Ψ_0 = electrical potential at surface, K = constant associated with concentration, valence of cations, dielectric constant, and temperature.

At room temperature,

$$K = 3 \times 10^7 z^{\pm} \sqrt{C}$$

Where, Z = valence of the ion, C = concentration of the bulk solution in moles/lit

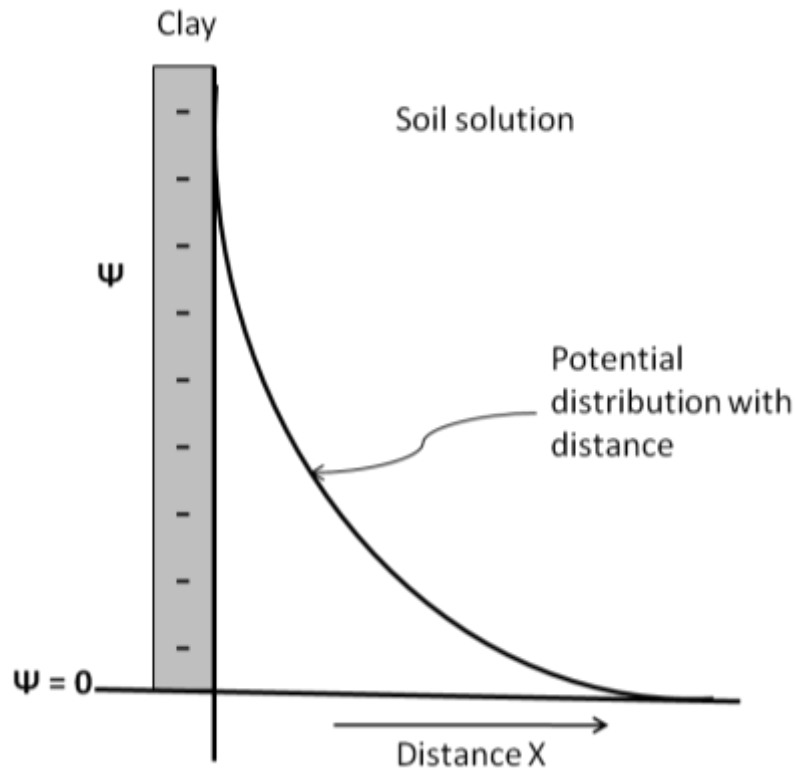


Figure 6.3: Graphical representation of potential distribution according to Gouy-Chapman double layer theory.

The value of $1/K$ is usually used as a measure of the thickness of the double layer (Verwey and Overbeek, 1948). Gouy-Chapman double layer theory consists of several limitations. For example like Helmholtz theory, the negative charge was considered to be evenly distributed over the surface. Another major problem is that the counter ions are assumed as point charges, therefore occupy no spaces and may reach excessively high concentrations at the liquid interface. But in reality, ions are of finite sizes, so cannot reach extensively. According to Stern (Stern, 1924) ions cannot approach more closely than allowed by their effective radii. The distribution of counter ions was assumed to follow the Boltzmann distribution. But the problem associated with Boltzmann distribution is that it assumes activity as equal to molar concentration. This may be a reasonable assumption for the bulk solution, but certainly have limitations near a

charged surface. Again literature shows that experimentally obtained double layer thickness is generally found to be somewhat greater than calculated. This may relate to the error incorporated in assuming activity equals molar concentration when using the desired form of the Boltzman distribution. Another problem with Gouy-Chapman theory is, specific interactions between the surface, the counterions and the medium were not considered. This limitation particularly applies to variable charge surfaces (Sparks, 1999).

6.5 Stern Theory

Stern modification of double layer theory for the first time considered the ionic dimensions of cations. The influence of ionic dimension is the maximum close to colloidal surface. According to Stern theory, the first layer of double layer is similar to that of Gouy-Chapman theory, but the second layer represented as divided into layers, (1) a sub-layer near the colloidal surface and (2) a diffuse layer. The first sub-layer with tightly packed cations is called the Stern layer. In Stern theory, potential distribution is seems to be a combination of the Helmholtz and the Gouy-Chapman diffuse double layer. In the Stern layer, the potential decreases with distance from the surface according to the Helmholtz theory. After that (in the diffuse layer), decrease in potential with distance follows the Gouy-Chapman theory. According to Stern theory, the first layer of ions are not at the surface as proposed in the Gouy-Chapman diffuse double layer theory, rather located at a distance ' δ ' away from the surface. This δ depends on hydrated radius of the cations.

6.6 Triple Layer Theory

The double layer theory had been developed for the study of surface absorption-reaction and ion exchange behavior of silicate clays. The negative charge that develops due to isomorphous substitutions are assumed to be on the clay surface and defined as first layer in

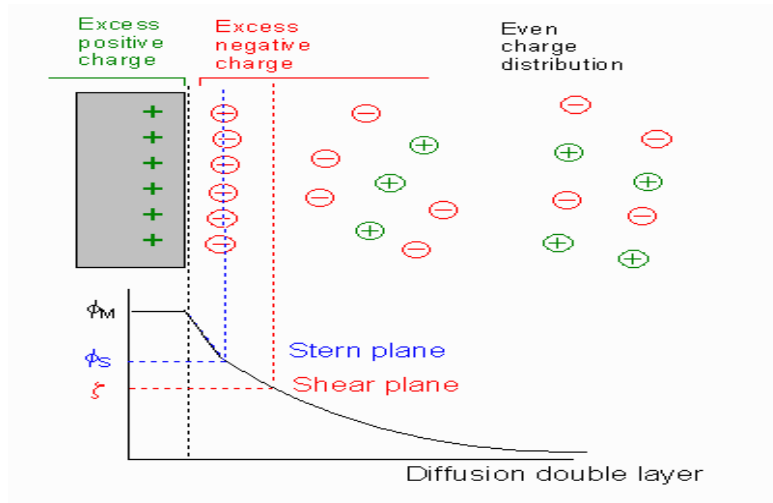


Figure 6.4: Potential and ion distribution according to Stern double layer theory (Chemistry lab, New Mexico State University).

double layer theory. But some of the clays show oxy-hydroxyl surfaces which is different from silicate clays (Tan, 1998). Triple layer theory considers the different planes where potential determining ions (primarily H^+ , OH^- and OH^{2+} ions) shields the permanent charge of the oxide clays. The presence of these potential determining ions move the counter ions further outward from the clay surfaces. This model is known as triple layer model or theory and first proposed by (Tan, 1998, Yates, et al., 1974). Later on other modified triple layer model was presented by (Kleijn and Oster, 1982, Bowden, et al., 1977). Potential determining ions has been proposed as integral part of the solid surface by (Kleijn and Oster, 1982), but in reality this layer is located at liquid phase (Tan, 1998). The next layer can be divided into two phase-inner Helmholtz layer and outer Helmholtz layer, and also located in the liquid phase. The inner Helmholtz layer is the zone where the counter ions adsorption occurs while the outer Helmholtz layer is the zone which gradually changes into a diffuse layer. Triple layer will develop only if there is a presence of potential determining ions. Triple layer model have some similarity with Stern double layer theory and in case of absence of potential determining ions Stern theory should be applied.

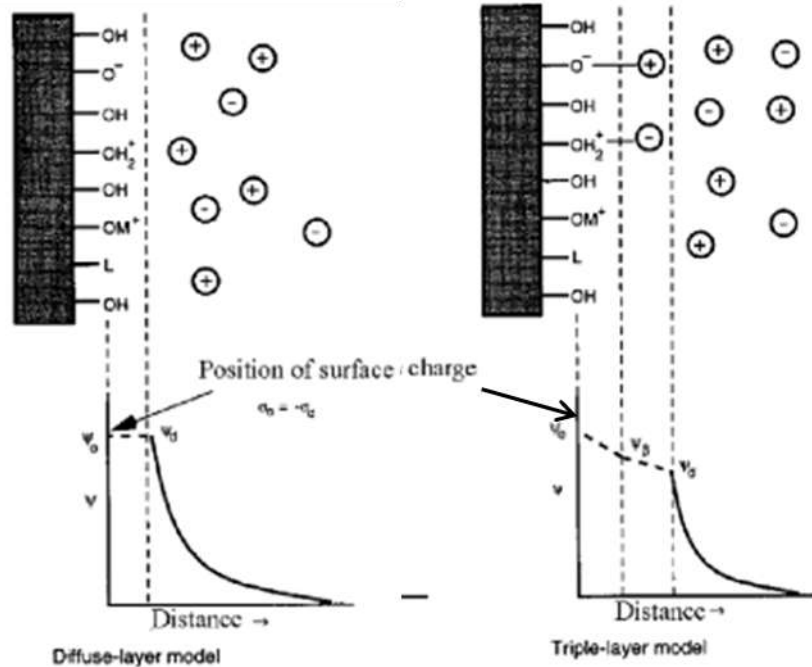


Figure 6.5: Schematic of diffuse double layer and Triple layer model (Broder et al. 2008).

6.7 Zeta Potential (ζ)

Zeta potential is the electrical potential at the solid-liquid interface of a colloidal system. If an electrical field is introduced in a colloidal suspension, colloidal particles and counter ions will move in opposite direction which develops the potential at the solid-liquid interface. The seat of the zeta potential is located at the shearing or slippage plane between the bulk liquid and the diffused layer of liquid moving with the particle. The position of the shearing plane is a theoretical term. Since the exact position of the shearing or slippage plane is not known, zeta potential represents the potential at an unknown distance from colloidal surface (Tan, 1998). Zeta potential is not the same as colloidal surface potential (Van Olphen, 1979).

6.7.1 Effect of Electrolyte Concentrations on Zeta Potential

Zeta potential has significant correlation with the thickness of the double layer. With the increase of electrolyte concentration zeta potential decreases so as the double layer thickness. If the electrolyte concentration continues to increase it reaches a critical point where zeta potential

is zero. This point is known as isoelectric point. The repulsive force of particles and double layer thickness are the lowest at isoelectric point (Tan, 1998). At and below isoelectric point flocculation will occur due to low repulsive force between particles. Zeta potential is not a unique property of colloid rather a property of colloidal solution, and also depends on the surface potential (ψ) of the colloid.

Mathematically, $V_e = (D \zeta E) / (4\pi\eta)$

Here, V_e is the Electro-kinetic velocity, D is the dielectric constant, E is the applied electric field strength and η is the viscosity of fluid.

6.8 Double Layer Thickness

The double layer thickness can be defined as a measure of the typical range of the electrostatic potential that propagates from the surface of the particle into the liquid and depends on the electrolyte concentration and valence (Debye and Huckel, 1924).

The electrolyte concentration in colloidal solution highly influences the thickness of the diffuse double layer. The thickness of the diffused double layer decrease with an increase in the electrolyte concentration. Thickness of the double layer also depends on the nature of counter ions. The diffuse double layer is thinner for divalent cations than monovalent. The thickness of double layer decreases with increasing counter ion valence. Hence double layer thickness for different counter ions can be expressed as: mono-valent ions > divalent ions > trivalent ions. Correlation between electrolyte concentration, valences of counter ions and thickness of double layer had been quantitatively shown by (Overbeek, 1948, Verwey and Overbeek, 1948) as presented in table:6.1. Similar observation also has been reported by (Tan, 1998, Sridharan and Satyamurty, 1996) as shown in Figure 6.6, 6.7 and 6.8.

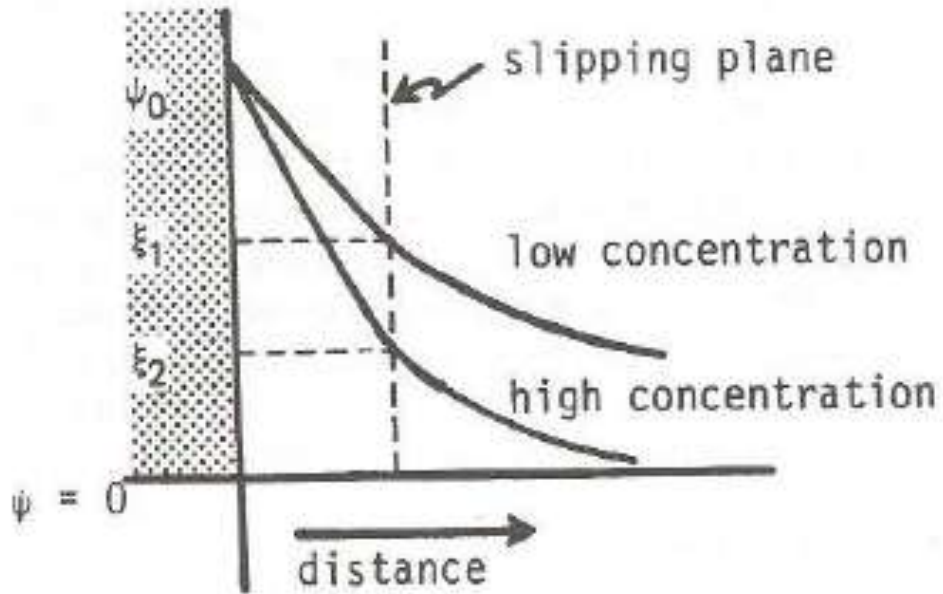


Figure 6.6: Potential distribution at different electrolyte concentration showing lower the concentration, greater the thickness of double layer (Tan, 1998, Sridharan and Satyamurty, 1996).

Table 6.1: Effect of electrolyte concentration and ion valences on double layer thickness (Verwey and Overbeek, 1948)

Electrolite Concentration (Mol/L)	Thickness of Double Layer, (1/K) cm	
	Monovalent ions	Divalent ions
1x10 ⁻⁵	1x10 ⁻⁵	0.5x10 ⁻⁵
1x10 ⁻³	1x10 ⁻⁶	0.5x10 ⁻⁶
1x10 ⁻¹	1x10 ⁻⁷	0.5x10 ⁻⁷

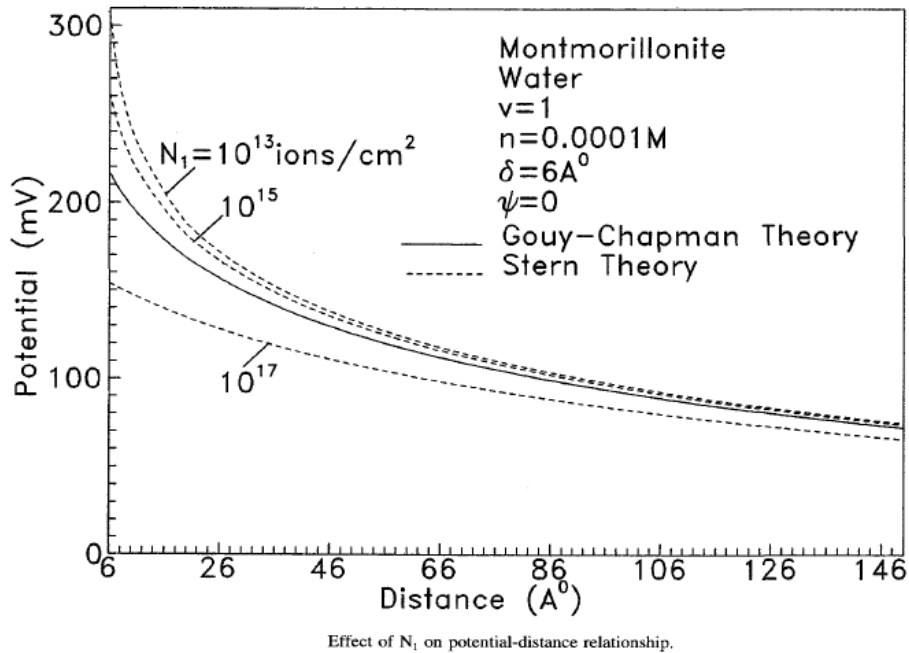


Figure 6.7: Potential Vs distance plot for montmorillonite with different electrolyte concentration showing potential decreases with increasing cation concentration (Sridharan and Satyamurty, 1996).

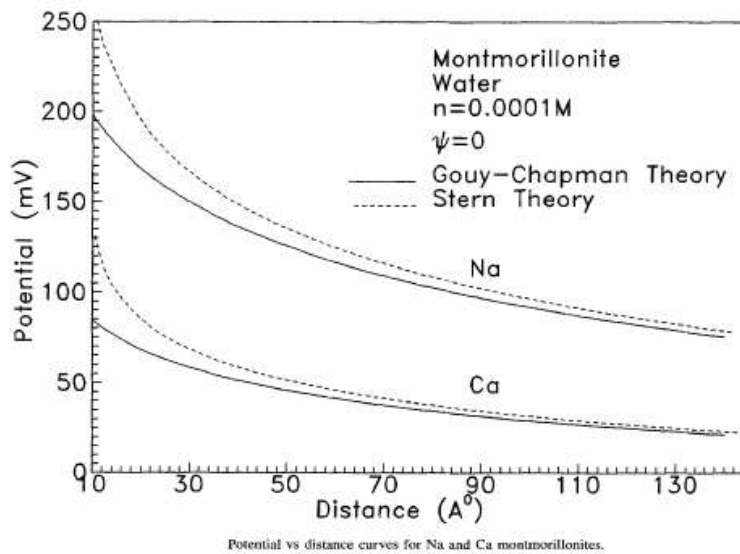


Figure 6.8: Potential vs. distance curves for Na and Ca montmorillonites showing potential decreases with increasing cation valence (Sridharan and Satyamurty, 1996).

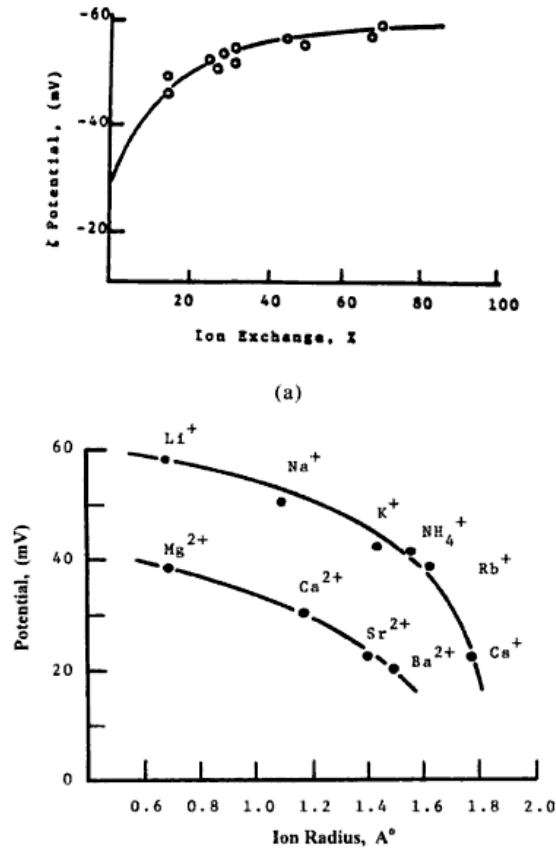


Figure 6.9: Zeta potential Vs characteristics of ions. (a) Ion-exchange capacity and (b) ionic radius (Jenny and Reitemeier, 1935 as shown in (Fang, 1997)).

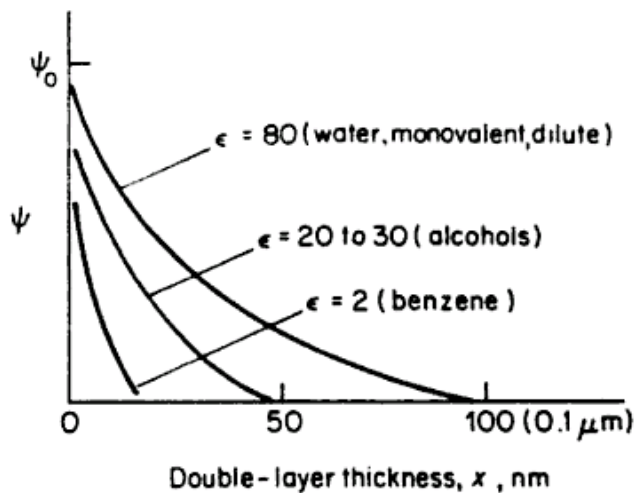


Figure 6.10: Effect of pore fluid dielectric constant on the thickness of double layer (Hsai-Yang-Fang, 1997).

6.9 DLVO Theory

DLVO theory provides a quantitative estimation of interactions between clay particles. The DLVO theory is based on the mutual repulsion of overlapping electrical double layers and attractive interactions due to London-Wander walls forces (Shingo, et al., 1988). The theory was independently proposed by (Derjaguin and Landau, 1945) and (Verwey and Overbeek, 1948). Verwey and Overbeek (1948) used energy method while force was considered by Derjaguin and Landau (1945) although they come up with the same results.

6.9.1 Potential Energy Due to Two Interacting Double Layers

In the discussion on double layer theories we described the thickness of double layer. The first layer is the charged surface of particle and second layer is the zone up to which the effect of charged surface is present. Now let's assume, if double layer of two plate type particles come close to each other within the zones of influence they will repel each other. These types of double layers are called interacting double layers.

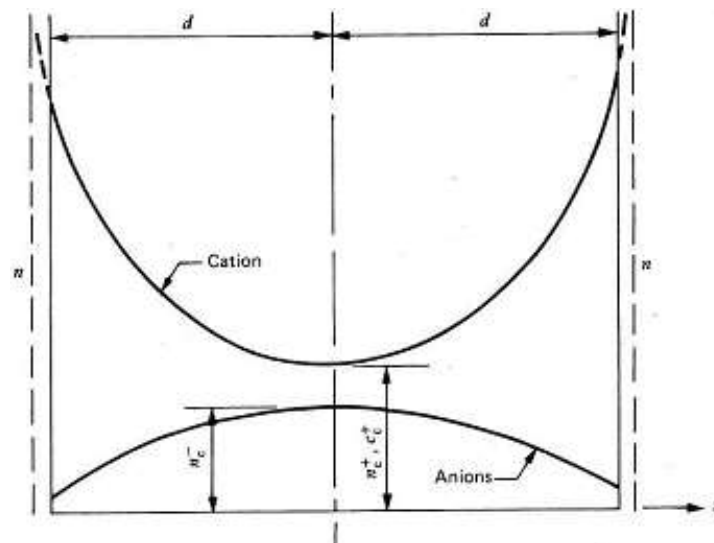


Figure 6.11: Charge distribution in interacting double layers between two plates (Mitchell, 1993).

If the plates are separated by a distance $2d$ then potential energy can be calculated mathematically as,

$$V_R = 2 \int_{-\infty}^d p dz \dots\dots\dots(6.1)$$

Here, P = external pressure required to keep the plates together.

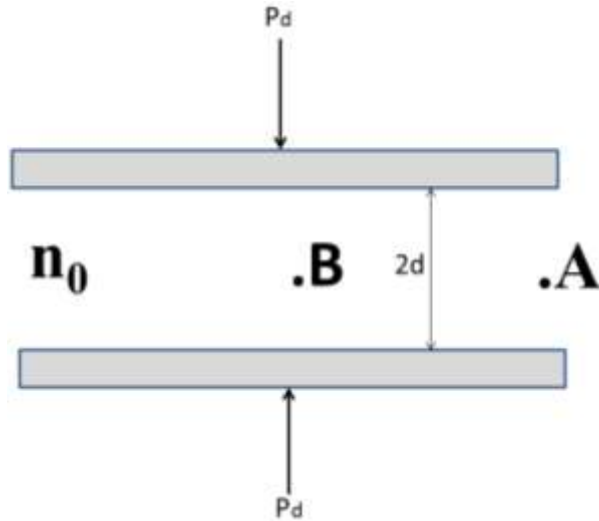


Figure 6.12: Schematic for repulsion between two interacting charged plates.

Let's assume two plates are in a symmetrical electrolyte solution of water at $2d$ separation. The pressure required is P_d (dyne/cm²), total number of ions is $2n_0$, surface potential is ψ_0 and mid-plane potential is ψ_d . Then, chemical potential of water at any point A outside the two plates can be calculated as presented by (Shingo, et al., 1988).

$$\begin{aligned} \mu_A &= \mu_0 + Z_A g = -\frac{RT}{M} \sum (X_i) + Z_A g \\ &= -\frac{RT}{M} \sum \left(\frac{2n_0}{1/M} \times \frac{1}{N} \right) + Z_A g \\ &= -2kTn_0 + Z_A g \dots\dots\dots(6.2) \end{aligned}$$

Here, M = Molecular weight of water, Z_A = distance (standard height) of point A, N = Avogadro's no and μ_0 = Chemical potential decrease due to ions

Similarly, chemical potential of water at any point B inside the two plates can be calculated as,

$$\mu_B = -kTn_0(e^{-e\psi_d/kT} + e^{-e\psi_d/kT}) + P_d + Z_B g \quad \dots\dots\dots(6.3)$$

Here, k = Boltzman constant, T = absolute temperature

For an equilibrium system, $\mu_A = \mu_B$

$$-2kTn_0 + Z_A g = -kTn_0(e^{-e\psi_d/kT} + e^{-e\psi_d/kT}) + P_d + Z_B g$$

If $Z_A = Z_B$, then we get

$$-2kTn_0 = -kTn_0(e^{-\frac{e\psi_d}{kT}} + e^{-\frac{e\psi_d}{kT}}) + P_d$$

$$\text{So, } P_d = n_0kT(e^{-\frac{e\psi_d}{kT}} + e^{-\frac{e\psi_d}{kT}} - 2) = 2n_0kT(e^{-\frac{e\psi_d}{kT}} - 1) \quad \dots\dots\dots(6.4)$$

In equation 6.4, P_d represents the repulsive force between two charged plates at 2d separation distance. P_d has been termed as disjoining pressure by (Derjaguin, et al., 1964, Derjaguin and Churaev, 1976, Derjaguin and Churaev, 1977, Derjaguin and Churaev, 1978).

Disjoining pressure is a function of d and defined as,

$$P_d(d) = \frac{\mu_f - \mu_0}{\bar{v}}$$

By substituting the value of P_d in equation 6.4, we can obtain potential energy due to repulsive force from equation 6.1,

$$V_R = 2 \int_{-\infty}^d p dz = 2 \int_{-\infty}^d [2n_0kT(e^{-\frac{e\psi_d}{kT}} - 1)] dz \quad \dots\dots\dots(6.5)$$

6.9.2 Potential Energy Due to Van der Waals Forces Between Two Particles

Van der Waal potential between two atoms as given in London theory is (Shingo, et al., 1988), $\psi = -\frac{C}{r^6}$ (6.6)

Here, r = separation between two atoms and C can be expressed as,

$$C_L = \frac{3}{2} \alpha_1 \alpha_2 \frac{h\lambda_1 \lambda_2}{\lambda_1 + \lambda_2} \approx \frac{3}{2} \alpha_1 \alpha_2 \frac{I_1 I_2}{I_1 + I_2} \quad \dots\dots\dots(6.7)$$

Here, α = polarization capability, h = Plank's constant, I = ionization energy and λ = frequency

Differentiating the equation (6.6) we get the force,

$$f = \frac{6C}{r^n}$$

If the atoms are separated by a distance apart, the time required for electric field to travel from one instantaneous dipole to neighboring dipoles is called the life time of the dipole. This type of interaction is known as out of phase interactions (Shingo, et al., 1988, Casimir and Polder, 1948). (Casimir and Polder, 1948) described Van der Waals force is proportional to r^{-8} for out of phase dipoles.

The attraction potential of multi-atomic condition can be calculated as summation of individual interatomic forces. For two flat plates separating at $2d$ distance attraction potential can be calculated as

$$V_A = -\frac{A}{48\pi} \left[\frac{1}{d^2} + \frac{1}{(d+\delta)^2} - \frac{2}{(d+\delta/2)^2} \right] \dots\dots\dots(6.8)$$

Here δ = thickness of plate and A = Hemakar constant can be represented as,

$$A = \pi^2 q^2 C$$

Here, q = number of atoms in unit volume of the particle. If $\delta \gg d$, then equation (6.8) can be rewritten as,

$$V_A = -\frac{A}{48\pi} \frac{1}{d^2} = -\frac{A}{12\pi} \frac{1}{D^2} \dots\dots\dots(6.9)$$

Here, $D = 2d$ = distance between the plates.

Differentiating the equation (6.8) and (6.9) we can obtain the attractive force per unit area,

$$F_A = -\frac{A}{24\pi} \left[\frac{1}{d^3} + \frac{1}{(d+\delta)^3} - \frac{2}{(d+\delta/2)^3} \right]$$

$$F_A = -\frac{A}{6\pi} \frac{1}{D^3}$$

6.9.3 Total Potential Energy

The total potential energy (V_t) between two charged particles will be the sum of the attractive potential energy (V_A) and repulsive energy (V_R).

$$V_t = V_A + V_B$$

V_t depends on d , n_0 , v , δ and T as V_R is a function of these parameters.

6.9.4 Hamaker Constant

Hamaker constant, can be represented as $A = \pi^2 q^2 \lambda$, is the constant used in calculating the attractive energy between two particles. Here, q represents the number of atoms present per unit volume (cm^3) and λ is the London-van der Waals constant (Shingo, et al., 1988). This simplified equation is only applicable to calculate the attractive interaction between two particles when they are in vacuum. For particles in medium other than vacuum Hamaker constant can be represented as,

$$A = A_{11} + A_{22} - 2A_{12}$$

Here, A_{11} , A_{22} and A_{12} represent the Hamaker constant for particle-particle, fluid-fluid and particle-fluid respectively. A good approximation for A_{12} can be $(A_{11} \cdot A_{22})^{1/2}$.

For two different substance particles Hamaker constant can be represented as, $A = \pi^2 q_1 q_2 \lambda_{12}$.

Hamaker constant is a function of separation distance and can be evaluated from atomic density, polarizability, and the medium present (Van Olphen, 1979). The typical values of Hamaker constant for two same substance particles as presented by Hamaker, 1937 as, higher end value is 3×10^{-12} erg, average value is 0.7×10^{-12} erg and lower end value is 0.7×10^{-14} erg.

For mica-air-mica system Hamaker constant was measured by (Tabor and Winterto.Rh, 1969, Tabor and Winterto.Rh, 1968) as $(1.07 \pm 0.05A) \times 10^{-12}$ erg and calculated as

$(1.35 \pm 0.15A) \times 10^{-12}$ by (Israelac.Jn and Tabor, 1972). (Shingo, et al., 1988) suggested that

Hamaker constant for mica-air-mica system can be used as reasonable assumption for clays.

Hamaker constants for kaolinite, illite, and montmorillonite with nine different organic fluids had been computed by (Chen, et al., 1996) and for montmorillonite-water system Hamaker constant

was found to be 0.870×10^{-20} J or 0.0870×10^{-12} erg. (Verwey and Overbeek, 1948) reported Hamaker constant for water-water interactions (A_{22}) as 6×10^{-13} erg while A_{22} had been reported as 3.4×10^{-13} erg by (Tabor and Winterto.Rh, 1969). Once we know the Hamaker constant for Clay-Clay in air and hamaker constant for fluid-fluid, we can compute the Hamakar constant for Clay-fluid syatem.

Thus, Hamaker constant for clay-water-clay system is,

$$A_{12} = 1 \times 10^{-13} \text{ erg (Assuming, Hamaker constant between water-water is as } 3.4 \times 10^{-13}\text{)}$$

$$A_{12} = 2 \times 10^{-13} \text{ erg (Assuming, Hamaker constant between water-water is as } 3.4 \times 10^{-13}\text{)}$$

Hamaker constant for mica-electrolite solution (10^{-13} to 10^{-13} mol KNO₃/mica) had been computed by (Israelachvili and Adams, 1978); and found to be 2.2×10^{-13} erg.

6.10 Application and Limitations of DLVO Theory

DLVO theory considers the total potential energy is the summation of repulsive force due to interacting double layers and attractive force due to Van der Waal forces. (Israelachvili and Adams, 1978, Israelachvili, 1978) had been studied the forces acting between mica surfaces in different aqueous electrolyte solution and observed four different types forces acting between at contact to 200 nm separation. The first two forces are same as addressed in DLVO theory; Van der Waal and double layer force. (Israelachvili and Adams, 1978, Israelachvili, 1978) proposed the Van der Waal force active zones as about 6.5 nm from clay surfaces (Shingo, et al., 1988). The double layer repulsive force had been studied for different concentration of electrolyte solutions (1:1, 1:2 and 2:2). At lower concentration repulsive force calculated was somehow in agreement with DLVO theory but at concentration above 10^{-3} mol/dm³ the difference was significant, especially for 2:1 electrolytes.

(Israelachvili, 1978) proposed that there are some additional repulsive forces acting in clay-aqueous electrolyte system and termed as ‘hydration forces’. Hydration forces act over a range of 1 nm and decay exponentially with distance. The hydration forces are complex, cannot be directly extrapolate from separation distance, varies between different clay types and may the reason of mystery of swelling clays. These forces are independent of electrolyte types and dependent on lots of factors such as type of electrolyte cations, pH, particle orientation, and so on (Israelachvili, 1978).

The disjoining pressure caused due to repulsion of interaction double layers, electromagnetic field fluctuation, and structural modification of liquids due to influence of charged surface. The three components of disjoining pressure are: ionic-electrolitatic, molecular and structural; although the first two components of disjoining pressure had been considered in DLVO theory, structural modification in fluid layer had been neglected in DLVO theory (Shingo, et al., 1988). The ions had been considered as point charges in DLVO theory. Therefore DLVO theory will be valid only if the separation distance between particles is large enough (more than 30 to 40 Å) to ignore the ionic size (Shingo, et al., 1988). The concept used for surface charge density in DLVO theory is only valid when the distance from charged surface is lesser than the average distance of neighboring charged surfaces (Shingo, et al., 1988).

Repulsive force between particles and interlayer water had been neglected in DLVO theory. In case of montmorillonite this repulsive force act when the inter spacing is less than 100 Å (Shingo, et al., 1988).

6.11 References

[1] Katti, D. R., Schmidt, S. R., Ghosh, P., and Katti, K. S. (2007). "Molecular modeling of the mechanical behavior and interactions in dry and slightly hydrated sodium montmorillonite

- interlayer." *Canadian Geotechnical Journal*, 44(4), 425-435.
- [2] Schmidt, S. R., Katti, D. R., Ghosh, P., and Katti, K. S. (2005). "Evolution of mechanical response of sodium montmorillonite interlayer with increasing hydration by molecular dynamics." *Langmuir*, 21(17), 8069-8076.
- [3] Quirk, J. P., and Marcelja, S. (1997). "Application of double-layer theories to the extensive crystalline swelling of Li-montmorillonite." *Langmuir*, 13(23), 6241-6248.
- [4] Kleijn, W. B., and Oster, J. D. (1982). "A model of clay swelling and tactoid formation." *Clays and Clay Minerals*, 30(5), 383-390.
- [5] Yeung, A. T., and Mitchell, J. K. (1993). "Coupled fluid, electrical and chemical flows in soil." *Geotechnique*, 43(1), 121-134.
- [6] G., G. (1910). *J. Phys*, 9, 457.
- [7] Gouy (1909). "On the constitution of the electric charge at the surface of an electrolyte." *Comptes Rendus Hebdomadaires Des Seances De L Academie Des Sciences*, 149, 654-657.
- [8] Gouy, G. (1910). *J. Phys*, 457.
- [9] D.L, C. (1913). *Phil. Mag*, 25, 475.
- [10] Chapman, D. L. (1913). *Phil. Mag.*, 25, 475.
- [11] Stern, O. (1924). *Z.Electrochem*, 508.
- [12] Anderson, A. N., Crawford, J. W., and McBratney, A. B. (2000). "On diffusion in fractal soil structures." *Soil Science Society of America Journal*, 64(1), 19-24.
- [13] Papelis, C., Chen, C. C., and Hayes, K. F. (1996). "Effects of cation and sorption site type on metal ion sorption on clay minerals: An X-ray absorption spectroscopic study." *Abstracts of Papers of the American Chemical Society*, 211, 101-GEOC.

- [14] Mitchell, J. K. (1993). *Fundamentals of Soil Behavior*, Second Edition, John Wiley Sons, Inc.
- [15] Tan, K. H. (1998). *Principles of soil chemistry*, Marcel Dekker, Inc.
- [16] Verwey, E. J. W., and Overbeek, J. T. G. (1948). "Theory of the Stability of Lyophobic Colloids."
- [17] Sparks, D. L. (1999). *Soil Physical Chemistry*, CRC Press LLC.
- [18] Yates, D. E., Levine, S., and Healy, T. W. (1974). "Site-binding model of electrical double-layer at oxide-water interface." *Journal of the Chemical Society-Faraday Transactions I*, 70, 1807-1818.
- [19] Bowden, W. L., Bonnar, P., Brown, D. B., and Geiger, W. E. (1977). "Electrochemistry of nitroprusside ion in non-aqueous solvents." *Inorganic Chemistry*, 16(1), 41-43.
- [20] Van Olphen, H. a. F., J. J (1979). *Data handbook for clay materials and other non-metallic minerals*, Pergamon Press, New York.
- [21] Debye, P., and Huckel, E. (1924). "Remarks on a rate concerning cataphoretic appearances in suspended parts." *Physikalische Zeitschrift*, 25, 49-52.
- [22] Overbeek, V. a. J. T. G. (1948). "Theory of the Stability of Lyophobic Colloids." Elsevier, Amsterdam.
- [23] Sridharan, A., and Satyamurty, P. V. (1996). "Potential-distance relationships of clay-water systems considering the Stern theory." *Clays and Clay Minerals*, 44(4), 479-484.
- [24] Fang, H.-Y. (1997). *Introduction to environmental geotechnology*, CRC Press.
- [25] Shingo, I., Toshio, T., and Benno, W. (1988). *Soil-Water Interactions*, Marcel Dekker, Inc.

- [26] Derjaguin, B., and Landau, L. (1945). "Theory of stability of highly charged liophobic sols and adhesion of highly charged particles in solutions of electrolytes." *Zhurnal Eksperimentalnoi I Teoreticheskoi Fiziki*, 15(11), 663-682.
- [27] Derjaguin, B. V., Kabanov, B. N., Voropaye.Tn, and Titiyevs.As (1964). "Surface forces + stability of colloids + disperse systems." *Journal of Colloid Science*, 19(2), 113-&.
- [28] Derjaguin, B. V., and Churaev, N. V. (1976). "Polymolecular adsorption and capillary condensation in narrow slit pores." *Journal of Colloid and Interface Science*, 54(2), 157-175.
- [29] Derjaguin, B. V., and Churaev, N. V. (1977). "Disjoining pressure of thin-layers of binary-solutions." *Journal of Colloid and Interface Science*, 62(3), 369-380.
- [30] Derjaguin, B. V., and Churaev, N. V. (1978). "Question of determining concept of disjoining pressure and its role in equilibrium and flow of thin-films." *Journal of Colloid and Interface Science*, 66(3), 389-398.
- [31] Casimir, H. B. G., and Polder, D. (1948). "The influence of retardation on the london-vanderwaals forces." *Physical Review*, 73(4), 360-372.
- [32] Tabor, D., and Winterto.Rh (1969). "Direct measurement of normal and retarded van der waals forces." *Proceedings of the Royal Society of London Series a-Mathematical and Physical Sciences*, 312(1511), 435-&.
- [33] Tabor, D., and Winterto.Rh (1968). "Surface forces - direct measurement of normal and retarded van der waals forces." *Nature*, 219(5159), 1120-&.
- [34] Israelac.Jn, and Tabor, D. (1972). "Measurement of van-der-waals dispersion forces in range 1.4 to 130 nm." *Nature-Physical Science*, 236(68), 106-&.
- [35] Chen, S. Y., Ambe, S., Takematsu, N., and Ambe, F. (1996). "Multitracer study on removal mechanisms of metal elements from seawater." *Analytical Sciences*, 12(1), 1-6.

[36] Israelachvili, J. N., and Adams, G. E. (1978). "Measurement of forces between 2 mica surfaces in aqueous-electrolyte solutions in range 0-100 nm." *Journal of the Chemical Society-Faraday Transactions I*, 74, 975-&.

[37] Israelachvili, J. N. (1978). "Measurement of forces between surfaces immersed in electrolyte-solutions." *Faraday Discussions*, 65, 20-24.

CHAPTER 7. SOLVATION OF NA-MONTMORILLONITE (NA-MMT) CLAYS: EFFECT OF ATOMS AT THE EDGE AND DISCRETE CHARGE DISTRIBUTION IN CLAYSHEET

The chapter describes the effect of broken bonds at the edge and discrete charge distribution in clay sheet using molecular dynamics (MD) simulations. This chapter also discusses the fundamental assumptions in double layer theory, applicability and limitations in describing swelling mechanism. The content of this chapter is to be submitted in Journal of Engineering Mechanics, American Society of Civil Engineering (ASCE).

7.1 Introduction

Molecular dynamics (MD) simulations were performed with two different sized Na-MMT clay sheets to study the behavior at molecular scale. Distribution of relative density of water molecules and clay-water interaction energies at different distance from claysheet were calculated. Distance dependent orientation and distribution of water molecules were also analyzed. Greater attraction of water molecules towards the zones of isomorphic substitutions has been observed from the conformational analysis. Therefore, consideration of discrete charge distribution and charges at the clay edges is very vital in calculating the potential energy for clay particles.

The swelling of clays is of great interest in engineering, soil chemistry, and other fields of science. Among the different mineral type smectite group shows significant amount of swelling. Swellings of clays occur in two main form called crystalline swelling and osmotic swelling. Although numerous numbers of studies had been performed on swelling clays, very few of the studies addressed the behavior of interlayer fluids using Molecular dynamics and Monte Carlo simulations. But most of these studies are within the range of crystalline swelling which has been reported in the range of 17-20 Å (Katti, et al., 2007); (Schmidt, et al., 2005); (Quirk and Marcelja, 1997), (Skipper, et al., 1995). There is a lack of understanding for the complete

swelling mechanism. Many researchers tried to explain swelling in terms of double layer theories for example DLVO (Derjaguin-Landau-Verwey-Overbeek) theory, Gouy-Chapman double layer theory, Modified Gouy-Chapman double layer theory and Stern theory (Schmidt, 2005). Most of these theories have limitations explaining swelling clays and the assumptions associated with each of the theories need to be justified for swelling clays. DLVO theory cannot explain the non-swelling behavior of some highly charged clays minerals such as mica and vermiculate (Kleijn and Oster, 1982). According to the double layer theory, first layer of the double layer is formed by the negative charge in the clay surface. Associated assumption in all the double layer theories is that charge distribution is homogeneous over the surface of the particles where in reality charge distribution in clay surface is discrete in nature. The second layer is formed by the excess of oppositely charged ions in the solution. These counter ions were assumed as of point charges thus occupy no space and may reach excessively at the clay surface-liquid interface. This assumption has significant limitations as in reality ions are of finite size which have been considered in Stern theory. Gouy-Chapman double layer assumes Boltzmann distribution where the activity is proportional to molar concentration. This is may be true for bulk solution, but have limitations for a confined fluids between two charged surface. Again, experimentally reported double layer thickness was found to be greater than calculated from the theory (Tan, 1998), which is may be due to the associated assumptions. In case of very dilute solutions, the error associated with neglecting finite size is small but in case concentrated solutions size effect is vital. In this case, Guoy-Chapman theory predicts impossibly high ion concentrations next to the surface (Yeung and Mitchell, 1993). Therefore, the actual concentration next to the clay surface will be less than predicted by Guoy-Chapman. Moreover, interaction between the surface, counter ions and solvents cannot explain completely using the theory. Stern (Stern, 1924) came

up with an improved theory where finite dimensions of the ions were taken into account. According to Stern theory, first layer is similar to that of Gouy-Chapman theory. However, the second layer divides into two layers, (1) a tightly packed sub-layer near the colloid surface called Stern layer, (2) a diffuse layer. The potential distribution in Stern theory appears to be a combination of the Helmholtz and the Gouy-Chapman diffuse double layer. In the Stern layer, the potential decreases with distance from the surface according to the Helmholtz theory. After that (in the diffuse layer), decrease in potential with distance follows the Gouy-Chapman theory. The first layer of ions are not at the surface as assumed in the Gouy-Chapman diffuse double layer, rather at a distance 'δ' away from the surface. The maximum possible concentration will be determined by the hydrated radii of the cations. Stern considered that the distance of the closest counter ion to the charged surface is determined by the size of the ions.

The double layer theory is developed on some fundamental assumptions. One of the assumptions is uniformly distributed charged surface while swelling clays consist of discrete charge distribution due to isomorphic substitution. Experimentally reported double layer thickness from the literature found to be greater than evaluated from theory. The focus of this work is to perform a molecular level study of two different sized swelling clay particles and evaluate the effect of charges due to edges and discrete distribution of charges at the claysheet.

7.2 Modeling Approach

In this work we performed molecular level simulation of solvation model with two different sized Na-montmorillonite claysheet. Na-montmorillonite used in our previous experimental studies had been collected from the clay mineral repository at the University of Missouri, Columbia, Missouri had a chemical formula $(\text{Ca}_{0.12}\text{Na}_{0.32}\text{K}_{0.05})[\text{Al}_{3.01}\text{Fe(III)}_{0.41}\text{Mn}_{0.01}$

$\text{Mg}_{0.54}\text{Ti}_{0.02} [\text{Si}_{7.98}\text{Al}_{0.02}]\text{O}_{20}(\text{OH})_4$ (Van Olphen, 1979). The molecular model of clay sheet as well as Na-MMT model in our previous studies have a simplified chemical $\text{NaSi}_{16}(\text{Al}_6\text{FeMg})\text{O}_{40}(\text{OH})_8$. The model of Na-MMT was first created by (Schmidt, et al., 2005). (Schmidt, et al., 2005) derived the coordinates of the unit cells in their model from (Skipper, et al., 1995) and obtained the atomic charges from (Teppen, et al., 1997). The model developed by (Schmidt, et al., 2005) contains 8 unit cells (4x2). Later on, a larger Na-MMT model with 18 unit cells (6x3) was developed by the authors for the study of solvent polarity on swelling clays. Clay sheet used in this study (6x3) was derived from the Na-MMT model used in the previous study by the authors.

The main focus of our study is to study the finite size effect of claysheet on distribution of water molecules or ions around the claysheet. For this we prepared solvation model with two different sized claysheet. Firstly, with 6x3 claysheet (claysheet with 18 unit cell and dimensions are 31.68 Å x 27.42 Å x 6.56 Å) having a solvation box size as 100 Åx100 Åx100 Å. Another model was with 4x2 claysheet (claysheet with 8 unit cell and dimensions are 21.12 Å x 18.28 Å x 6.56 Å) having a solvation box size 70 Åx70 Åx110 Å. Solvation model with 6x3 claysheet contains 31809 numbers of water molecules and total 96147 atoms. Solvation model with 4x2 claysheet contains 16346 numbers of water molecules and total 49358 atoms. Accelrys® Materials Studio V4.4 software and PSFGEN plug-in of VMD package was used for creating the solvation model for the simulation (Humphrey, et al., 1996).

7.3 Simulation Details

NAMD, version 2.7b2 software was used for MD simulations and VMD package was used for visualization (Phillips, et al., 2005). CHARMM force field parameters were used. CHARMM force field for Na-MMT was developed by Schmidt (Schmidt, et al., 2005). Isobaric-

isothermal ensemble, that is constant number, pressure, and temperature (NPT), were applied for molecular dynamics (MD) simulations.

Simulations were run on National Center for Supercomputing Applications (NCSA-Teragrid) using 24 processors. At the first step minimization was performed which brings the model to a geometric conformation with minimum energy condition. Minimization was performed to avoid any excess energy in the system that might be released at subsequent step of MD simulation causing the simulation unstable. The model was minimized for 150000 iterations. Convergence of the total energy was confirmed to ensure that corresponding run time was sufficient for the minimization. The minimization was performed at simulated conditions of 0 K and vacuum. Conjugate gradient algorithm, an iterative method to find the nearest local minima of a function, was used for minimization. During the entire simulation clay sheet was restrained in x and y direction that is only allowed to move in z direction. Equilibration of the model was performed at atmospheric pressure and temperature. A step by step method was applied for raising the temperature and pressure; the final temperature was 300K and final pressure was atmospheric (1bar) pressure. Steps for temperature raise was from 0 to 100K, 100 to 200K, 200 to 300 k and pressure raise was from 0 to 0.25 atm, 0.25 to 0.5 atm, 0.5 to 0.75 atm and finally 0.75 to 1 atm. Langevin dynamics were applied for controlling temperature and heat energy of the system. The Nose- Hoover Langevin piston method (Martyna, et al., 1994) was applied for raising the pressure. The software package NAMD uses Verlet algorithm to integrate the MD equations. All simulations done in this study used a step size 0.5 fs (10^{-15} s). The duration of each steps is 75 ps (10^{-12} s) or 150000 steps resulting a total simulation time as 0.525 ns (10^{-9} s) or 1050,000 steps. Convergence of total potential energy was reached sufficiently before end of each simulation. Periodic boundary conditions were applied in the simulations. Particle Mesh

Ewald (PME) method was utilized for the calculation of electrostatic interactions between atom pairs, an appropriate method for sum up a large number of electrostatic energies between pairs of atoms in a crystal structure. After the simulation came to equilibrium, interactions of the clay sheet with water molecules and conformational analysis was performed. Simulation took approximately 60 hours in each step (Total 20-30 days) using a 24 processors at distributed-memory cluster located at National Center for Supercomputing Applications (NCSA-Teragrid) at University of Illinois at Urbana Champaign (UIUC).

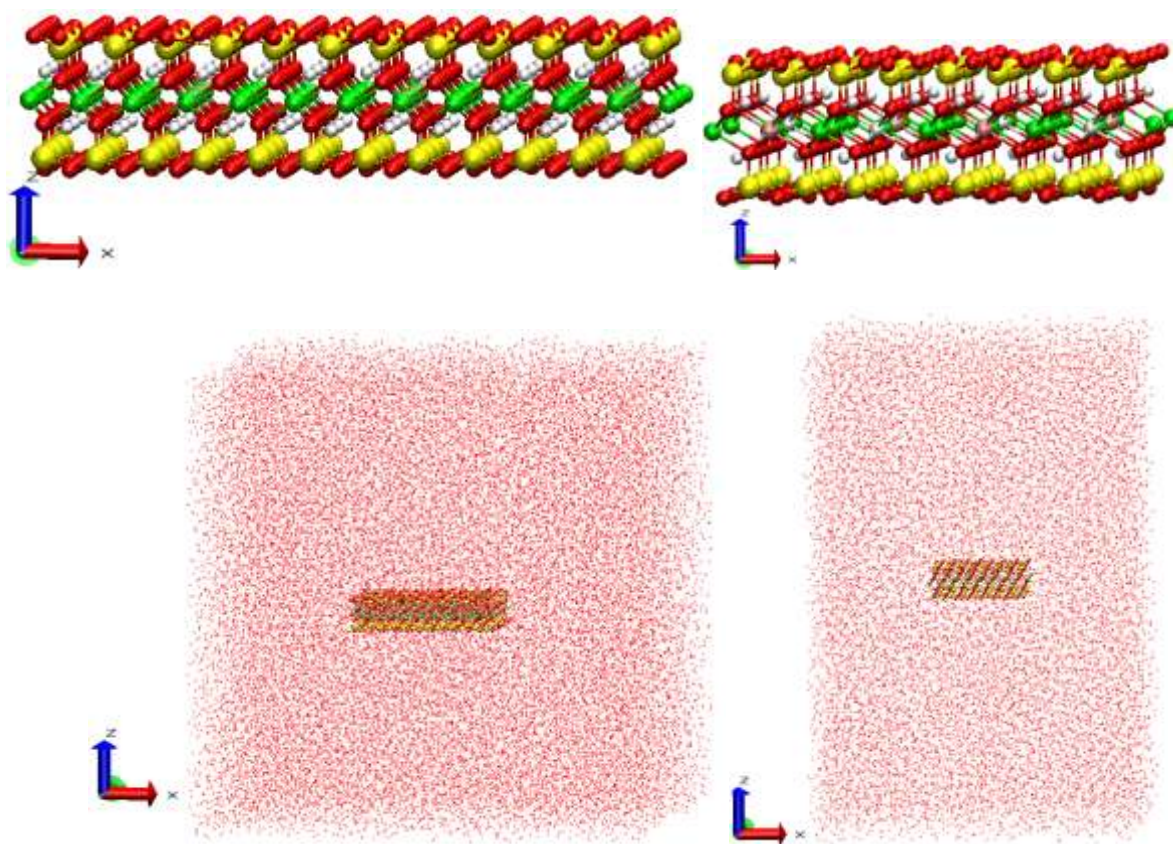


Figure 7.1: 6x3 claysheet (18 unit cell) and solvation model (left); 4x2 claysheet (8 unit cell) and solvation model (right).

7.4 Results and Discussions

We developed the solvation models with two different sized claysheet to study the size effect of claysheet on distribution of water molecules and interactions with water molecules.

From our previous studies (Katti and Shanmugasundaram, 2001), we have observed experimentally that particles breakdown as a result of swelling and swelling pressure. It is expected that potential distribution in an infinite surface with an edge charge will be quite different than a finite surface with edge charge, hence the assumptions of infinite charged surface as in double layer theories are questionable. For a full sized claysheet (say $2 \times 2 \mu\text{m}$) if we want to calculate the potential or ions distribution at the mid plane, the error may be less due to neglecting edge charges. But modeling an actual size clay sheet requires tremendous amount of computational resources. So the error associated with model increases as we use smaller claysheet model. If we consider the mineralogical aspect of charge development in claysheet we see, the charges in a clay sheet come from isomorphous substitutions and contribution from the edge. For montmorillonite isomorphous substitutions are dominating charge contributors than (Shingo, et al., 1988). If we use smaller claysheet model ratio of edge to surface area increases. This is may be the reason for higher per unit cell potential as seen for 4×2 claysheet than 6×3 claysheet.

For example, if we assume two different sized clay models, one $1 \mu\text{m} \times 1 \mu\text{m}$ and another one is $30\text{\AA} \times 30\text{\AA}$. From the montmorillonite model (developed based on simplified formula of standard SWy_2 clay) we found that isomorphous substitutions occur at alternate unit cells of claysheet. So, we can easily calculate the number of isomorphous substitutions and associated charges due to isomorphous substitution for a particular size of claysheet. (Shingo, et al., 1988) have shown the charge developed due to oxygen and hydroxyl ions with unsatisfied valences at the broken edge (broken bonds), also presented the equation for chemical reactions at different pH condition of outer solution.

According to (Shingo, et al., 1988) charges at edge comes from the following broken bonds-

$$\text{Si}-\text{O}^-$$

Si]

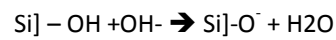
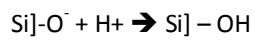
> O^{1/2-}

Al]

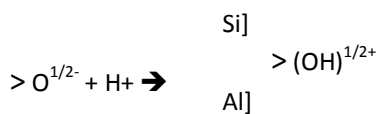
Al]- O^{1/2-}

Al]- (OH)^{1/2-}

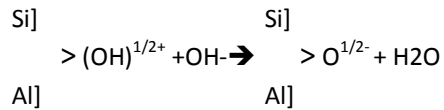
The chemical reaction at different pH of the outer solution is as follows-



Si]



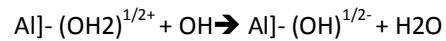
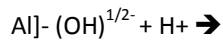
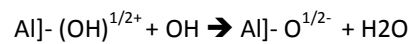
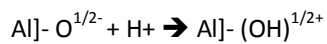
Si]



Al]

Al]

Al]



From the equation, we can see that if the pH in the solution increases, the right side reactions will dominate and the negative charges due to broken bonds will increase. The opposite situation will occur for a decrease in pH. From our 4x2 and 6x3 models we calculated an average negative charge of 0.034/square Å area. Let's assume 0.03 negative charge per square Å for our comparison for 1 μm x 1 μm and 30Å x 30Å particle sizes.

For 1 μm x 1 μm claysheet model:

$$\text{Surface area} = 1 \mu\text{m} \times 1 \mu\text{m} = 100,000,000 \text{ square } \text{\AA}$$

$$\text{Edge area} = 2(1 \mu\text{m} + 1 \mu\text{m}) \times 6.54 \text{\AA} = 261,600 \text{ square } \text{\AA}$$

$$\frac{\text{Area}_{\text{surface}}}{\text{Area}_{\text{edge}}} = 382.263$$

$$\text{Area of a unit cell} = 5.28 \text{\AA} \times 9.14 \text{\AA} = 48.26 \text{ square } \text{\AA}$$

$$\text{No of unit cell in } 1 \mu\text{m} \times 1 \mu\text{m} \text{ clay particle} = 100,000,000/48.26 = 2,0721,10$$

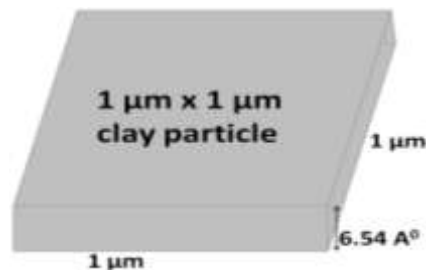
No of isomorphous substitutions in 1 μm x 1 μm clay particle = 20721010/2 = 1036055 (same as no of negative charge)

$$\text{Edge charge} = \text{Area}_{\text{edge}} \times \text{charge per unit area} = 261,600 \times 0.03 = 7848$$

$$\text{Total charge} = 1,043,903$$

Charge due to isomorphous substitutions = 99.25% of total charge

Charge due to broken bonds at the edge = 0.75% of total charge (hence can be neglected)



For 30 Å x 30 Å claysheet model:

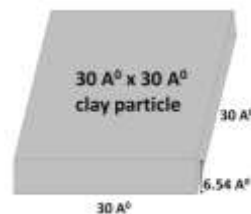
$$\text{Surface area} = 30 \text{\AA} \times 30 \text{\AA} = 900 \text{ square } \text{\AA}$$

$$\text{Edge area} = 2(30 \text{\AA} + 30 \text{\AA}) \times 6.54 \text{\AA} = 784.8 \text{ square } \text{\AA}$$

$$\frac{\text{Area}_{\text{surface}}}{\text{Area}_{\text{edge}}} = 1.1467$$

$$\text{Area of a unit cell} = 5.28 \text{\AA} \times 9.14 \text{\AA} = 48.26 \text{ square } \text{\AA}$$

$$\text{No of unit cell in } 30 \text{\AA} \times 30 \text{\AA} \text{ clay particle} = 900/48.26 = 18$$



No of isomorphous substitutions in $30 \text{ \AA} \times 30 \text{ \AA}$ clay particle = $18/2 = 9$ (same as no of negative charge)

Edge charge = $\text{Area}_{\text{edge}} \times \text{charge per unit area} = 784.8 \times 0.03 = 23.54$

Total charge = 32.54

Charge due to isomorphous substitutions = 27.66% of total charge

Charge due to broken bonds at the edge = 72.34% of total charge (hence very much significant)

We performed molecular dynamics simulations for solvation model of two different sized claysheets (6x3 and 4x2). Number of water molecules at different distance from clay sheet has been calculated (can be represented as relative density) for both 6x3 and 4x2 solvation models. We observed a highest density of water molecules at certain distance from claysheet in case of 6x3 model and decreases after then coming to an almost uniform density (can be considered as bulk solution) (Figure. 7.2). We need to remember here that we used a cutoff distance of 32 \AA which is significantly higher than cutoff used in literature. The common practice of using a smaller cutoff is due to mainly two reasons; one is limitations of computational resources, secondly small size of models used to mimic the infinite clay sheet. Those models could be appropriate for the study of clay interlayer, but not for the study of solvation of claysheet.

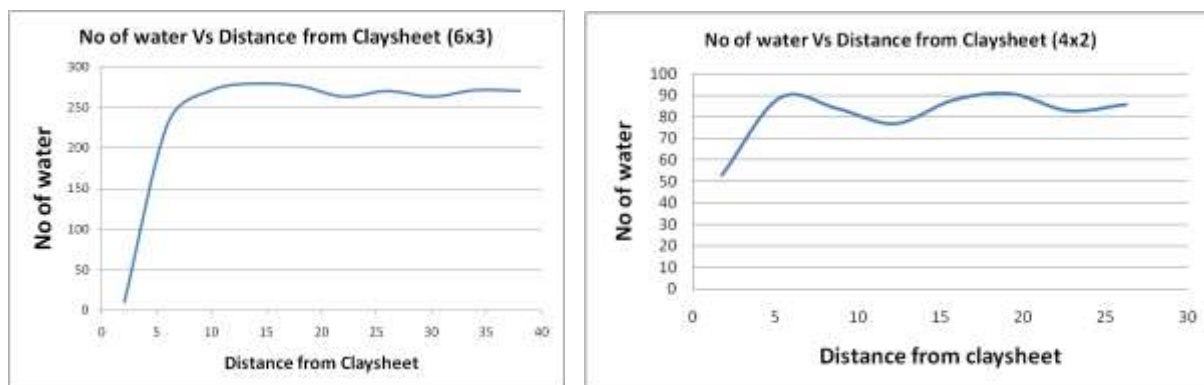


Figure 7.2: Relative density of water molecules at different distance from clay sheet for 6x3 solvation model (left) and 4x2 solvation model (right).

The non-uniform density distribution may be due to complex potential distribution as a result of higher influence of edge charges. In our future work, density distribution of water molecules with a larger claysheet can answer the questions. The conformation of water molecules around the claysheet shows that a higher concentration of water molecules at the zones of isomorphous substitutions (Figure. 7.3).

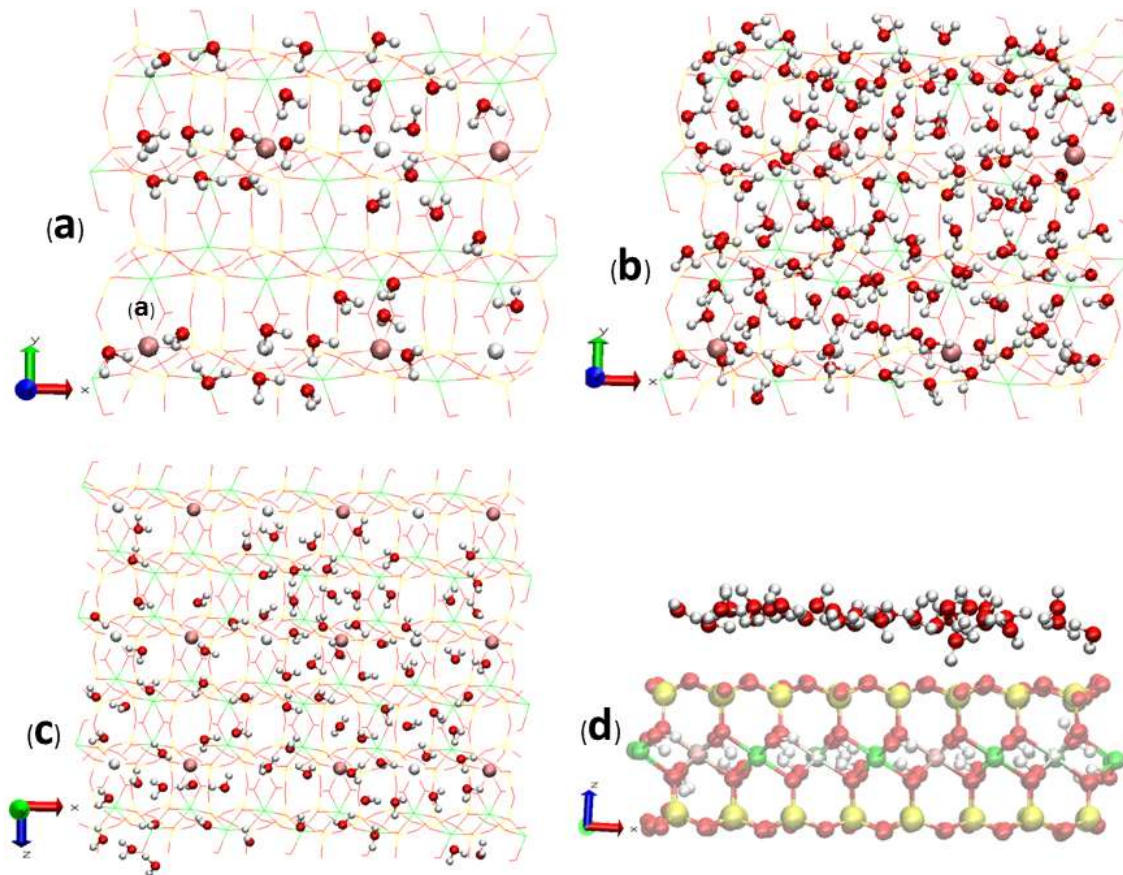


Figure. 7.3: Conformation in water molecules near clay surface shown for solvation model with 4x2 claysheet (a,b,d) and in 6x3 claysheet (c). Figure shows that a higher concentration of water molecules at the zones of isomorphous substitutions (purple atom represents Mg).

From our interaction energy plot (Figure. 7.4) we see that the distribution of Van der Waals interactions energy is identical for both 4x2 and 6x3 claysheet. But the shape of electrostatic interaction energy plot for 6x3 and 4x2 is completely different. Another observation

is the influence of Van der Waal interactions comes to zero at distance between 15-18 Å, while electrostatic interactions act over a much larger distance. So, using a larger cutoff distance allows us to perform better electrostatic interaction energy calculation and better conformational analysis.

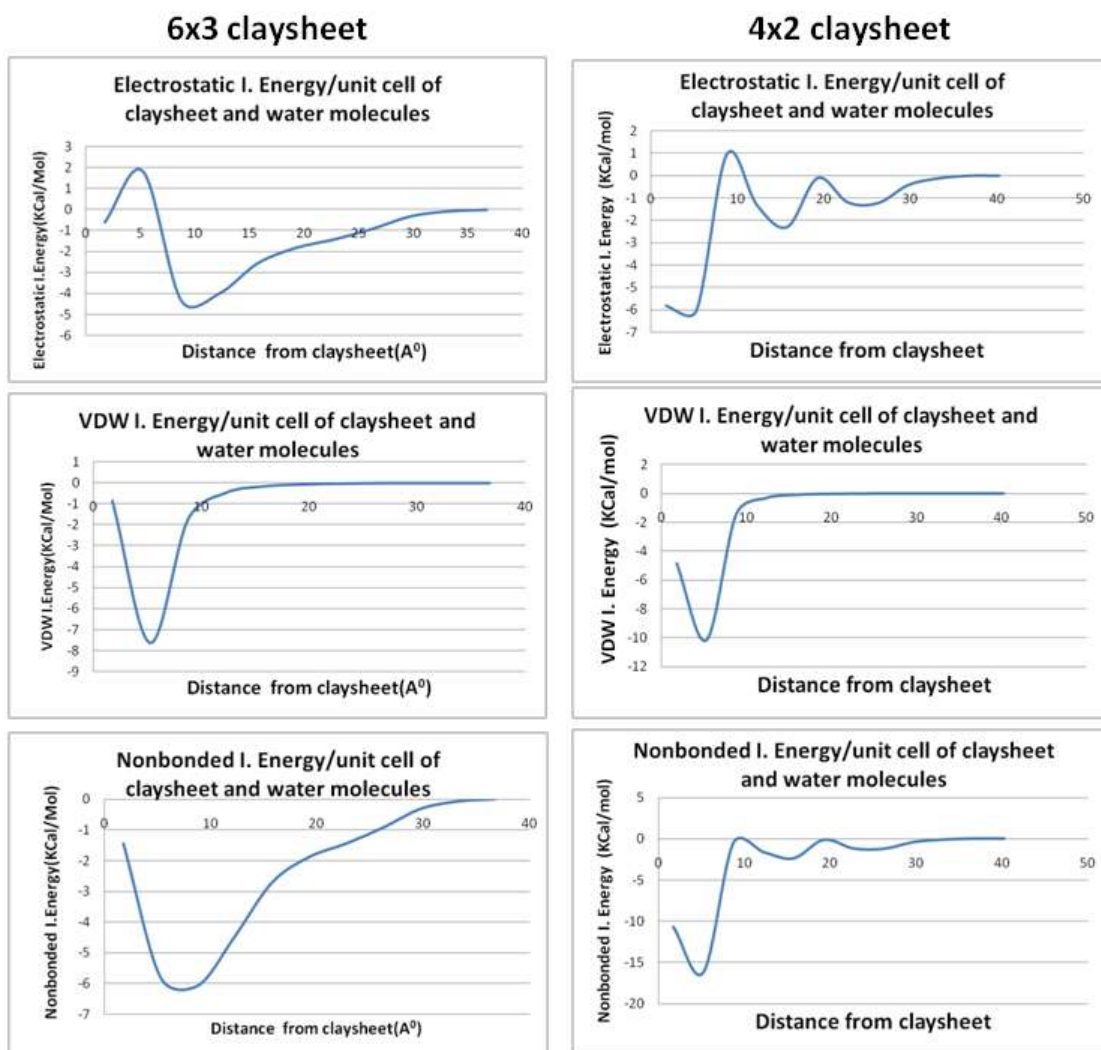


Figure. 7.4: Interaction energies between water molecules and per unit cell of clay sheet.

We also calculated the dipole moment distribution of water molecules at different distance from clay sheet. The average dipole moment direction shows that as we go further away from the clay sheet, less strong orientation of water molecules towards clay sheet i.e. less the influence of clay sheet on water molecules. Yoshida and Iwata, 1970 (as cited by (Shingo, et al.,

1988) reported the variation of pH at different distance from clay sheet. However they were not able to explain the reason for the phenomenon. Later on researchers observed the distance dependence of dielectric of fluids from clay surface. As we go away from the clay surface the dielectric constant of water increases and at some distance comes equal to the bulk water where no influence of claysheet present. (Sridharan and Satyamurty, 1996) showed that dielectric constant of water at Stern layer as 6 whereas bulk water has a dielectric constant 80. The dipole moment of water molecules depends on the ease of their orientation capacity. As near the clay surface water molecules are highly oriented towards claysheet their free rotation restrained. As we go away from the claysheet this restraint of free rotation diminishes. This is may be the reason for fluids showing low dielectric constant near clay surface.

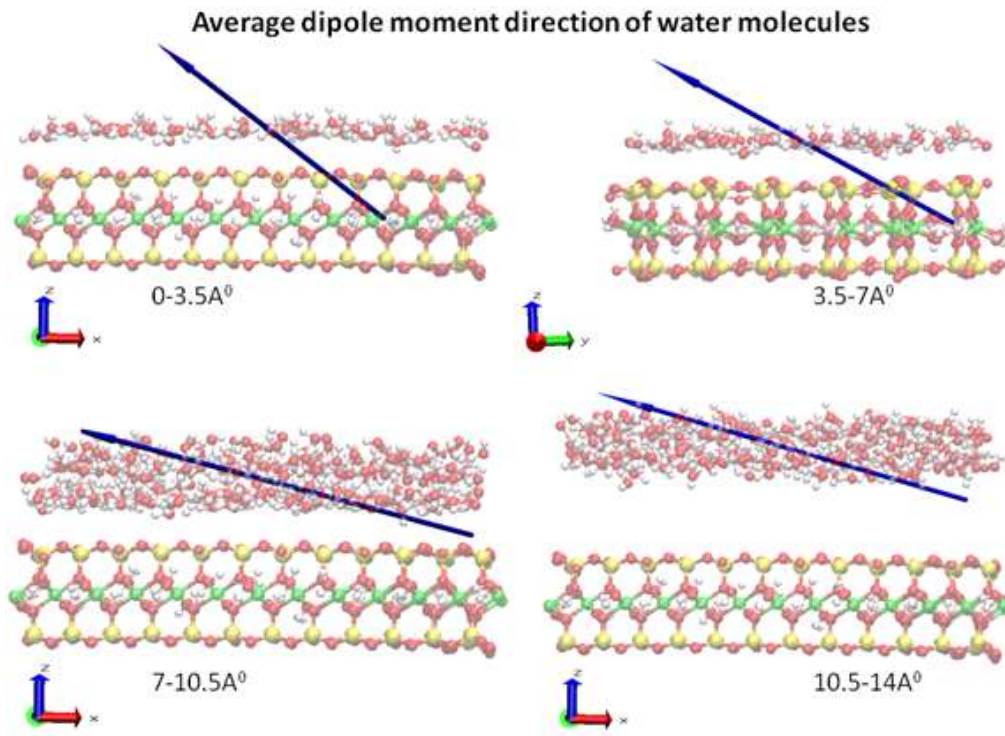


Figure. 7.5: Dipole moment direction showing near clay surface water molecules strongly oriented towards claysheet, as we go away from claysheet orientation of water molecules decreases.

Conformation analysis shows that distribution of water molecules are affected by the discrete charge distribution in the claysheet. So, the assumption of uniform charge distribution comes into question. We see that the first layer of water molecules adsorb on clay sheet at the hexagonal cavity of claysheet, while second layer also has organized pattern rather than randomly.

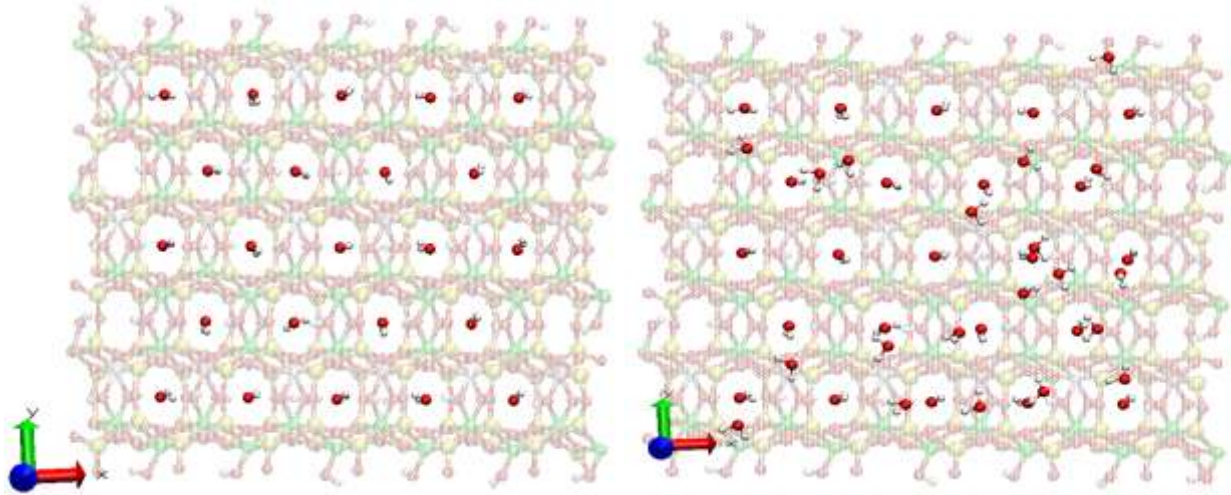


Figure. 7.6: Distribution of 1st and 2nd layer of water molecules on claysheet.

Most of the double layer theories are based on the cation concentrations in soil solution. The reason may be the focus of these studies for soil science or plant science. With the advancement of science, engineers and scientist can no longer depend on empirical methods. Moreover, some complicated problems for example swelling mechanism cannot be solved. For a pure soil-water condition, the applicability of double layer theories needs to be revisited. If we try to explain pure clay-water system with double layer theory, assumption as soil solution with very low ionic concentration will certainly introduced some error. This gives extremely high double layer thickness, thus excessive repulsive force due to interactive double layers. So, for the complete understanding of swelling mechanism of expansive clays simple potential distribution for flat surface may lead to erroneous conclusions. For complete understanding of swelling

behavior molecular level study need to be performed considering particle breakdown and contribution of charges due to broken bonds.

7.5 Conclusion

We performed molecular dynamics study for solvation of two different sized claysheet models. The interaction energies and density distribution is quite different not only in terms of magnitude but also trends of interaction energy curves. We observed higher interaction energy per unit cell in case of smaller claysheet model as a result of higher edge charge per unit cell in case of smaller claysheet model. The non-uniform density distribution in case of smaller clay particle may be due to complex potential distribution at different distance from claysheet. Conformation of water molecules shows a significant affinity of water molecules towards zones of isomorphic substitutions which lead to the importance of discrete charge distribution consideration in clay sheet while calculating potentials.

7.6 References

- [1] Katti, D. R., Schmidt, S. Corrected R., Ghosh, P., and Katti, K. S. (2007). "Molecular modeling of the mechanical behavior and interactions in dry and slightly hydrated sodium montmorillonite interlayer." *Canadian Geotechnical Journal*, 44(4), 425-435.
- [2] Schmidt, S. R., Katti, D. R., Ghosh, P., and Katti, K. S. (2005). "Evolution of mechanical response of sodium montmorillonite interlayer with increasing hydration by molecular dynamics." *Langmuir*, 21(17), 8069-8076.
- [3] Quirk, J. P., and Marcelja, S. (1997). "Application of double-layer theories to the extensive crystalline swelling of Li-montmorillonite." *Langmuir*, 13(23), 6241-6248.

- [4] Skipper, N. T., Chang, F. R. C., and Sposito, G. (1995). "Monte-c Corrected arlo simulation of interlayer molecular-structure in swelling clay-minerals .1. Methodology." *Clays and Clay Minerals*, 43(3), 285-293.
- [5] Schmidt, S. R. (2005). "Evaluation of clay-water interactions : a quantitative determination of clayinterlayer forces with varying hydration by steered molecular dynamics." MS, North Dakota State University,, ND, USA.
- [6] Kleijn, W. B., and Oster, J. D. (1982). "A model of clay swelling and tactoid formation." *Clays and Clay Minerals*, 30(5), 383-390.
- [7] Tan, K. H. (1998). *Principles of soil chemistry*, Marcel Dekker, Inc.
- [8] Yeung, A. T., and Mitchell, J. K. (1993). "Coupled fluid, electrical and chemical flows in soil." *Geotechnique*, 43(1), 121-134.
- [9] Stern, O. (1924). *Z.Electrochem*, 508.
- [10] Van Olphen, H. a. F., J. J (1979). *Data handbook for clay materials and other non-metallic minerals*, Pergamon Press, New York.
- [11] Teppen, B. J., Rasmussen, K., Bertsch, P. M., Miller, D. M., and Schafer, L. (1997). "Molecular dynamics modeling of clay minerals .1. Gibbsite, kaolinite, pyrophyllite, and beidellite." *Journal of Physical Chemistry B*, 101(9), 1579-1587.
- [12] Humphrey, W., Dalke, A., and Schulten, K. (1996). "VMD: Visual molecular dynamics." *Journal of Molecular Graphics*, 14(1), 33-&.
- [13] Phillips, J. C., Braun, R., Wang, W., Gumbart, J., Tajkhorshid, E., Villa, E., Chipot, C., Skeel, R. D., Kale, L., and Schulten, K. (2005). "Scalable molecular dynamics with NAMD." *Journal of Computational Chemistry*, 26(16), 1781-1802.

- [14] Martyna, G. J., Tobias, D. J., and Klein, M. L. (1994). "Constant-pressure molecular-dynamics algorithms." *Journal of Chemical Physics*, 101(5), 4177-4189.
- [15] Katti, D., and Shanmugasundaram, V. (2001). "Influence of swelling on the microstructure of expansive clays." *Canadian Geotechnical Journal*, 38(1), 175-182.
- [16] Shingo, I., Toshio, T., and Benno, W. (1988). *Soil-Water Interactions*, Marcel Dekker, Inc.
- [17] Sridharan, A., and Satyamurty, P. V. (1996). "Potential-distance relationships of clay-water systems considering the Stern theory." *Clays and Clay Minerals*, 44(4), 479-484.

CHAPTER 8. SUMMARY AND CONCLUSIONS

In this chapter we summarize the systematic experimental and modeling study conducted from molecular scale to macro scale to investigate the clay fluid interactions. This study provides important correlation between clay swelling and polarity of fluids; also provide an insight into the molecular mechanism of swelling.

8.1 Summary and Conclusions

From the understanding of this study along with the previous studies, we were able to develop important linkage between molecular level interactions with particle breakdown, evaluation of microstructure and macro scale swelling and flow properties.

This study along with previous studies provides an insight into the clay swelling behavior. Although research has been conducted on swelling clays on a particulate scale, for the first time we attempted a multiscale approach to tie the properties at different length scales. Our previous Scanning Electron Microscopic (SEM) study revealed the particle breakdown during swelling and correlation was developed between swelling and swelling pressure. Later on particles breakdown was also simulated using a modified discrete element method. In previous FTIR studies, we have seen qualitatively that greater amount of molecular interactions occur for high polar fluids with the same swelling clay. A new device for accurate measurement of permeability for swelling clays had been designed and fabricated by the group. Macroscale flow properties such as permeability, consolidation and triaxial tests were conducted using the new device.

In this study, we studied the effect of fluid polarity on flow properties of swelling clays using molecular modeling and experimental approach. We have studied the flow properties of Na-montmorillonite swelling clays with a wide range of polarity fluids ranging from as high as

formamide (Dielectric Constant 110) and as low as toluene (Dielectric Constant 2). The fluid used in this study has been chosen very carefully, these fluids are commonly found in landfill leachates and identified as highly toxic with potential for health hazard by US Environmental Protection Agency (EPA). Secondly and most importantly, we were able to tie the properties of swelling clays at different length scales. Thirdly, we performed solvation of clay sheets, discrete charge distribution, and contribution of edge charges on swelling clays and addressed some fundamental assumptions associated with double layer theories.

For the first time, effect of fluid polarity on swelling behavior has been studied using molecular modeling and complementary experimental studies. From our previous FTIR study, we were qualitatively able to show the effect of fluid polarity on clay-fluid molecular interactions. Using molecular modeling technique in this study we were able to provide a quantitative estimation of molecular level interactions at a particular level of swelling as well as able to develop quantitative correlation between clay-fluid molecular interactions and polarity of fluids. In the second part of this study, solvation of Na-Montmorillonite clay sheets had been studied, which provide interesting findings on the effect of atoms at the edge of clay sheet and discrete charge distribution in claysheet on swelling behavior of clays. This study also introduces fundamental discussions on assumptions associated with double layer theory.

We have developed the model for different clay-fluid system with different weight % of fluids to achieve the experimental d_{001} spacing. In this work, we started with small amount of interlayer fluid (10%, 20%, 30%, 40%) and subsequently increased the amount of interlayer fluid until we achieved the experimental condition. Experimental condition correspond to clay slurry in case of low polar fluids, 40 wt% formamide, and 60 wt% water (slurry condition was not achievable during experiments for formamide and water as complete exfoliation might occur for

high polar fluids). From molecular simulation we were able to quantify the amount of interlayer fluids present at experimental condition. Interestingly we see, all the formamide (40%) molecules in the clay entered into interlayer, 35% water out of 60%, 20% methanol, 10% acetone and very small or no toluene molecules went into interlayer. This indicates that interlayer contains greater amount of higher polarity fluids. We were able to correlate the presence of greater amount of solvents at interlayer for high polar fluids with increased swelling, swelling pressure, particle breakdown and low permeability from the understanding of our previous studies. Results of the previous study by (Amarasinghe, et al., 2009) shows that high polar fluids will cause greater amount of swelling, also observed in XRD study by the authors. (Katti and Shanmugasundaram, 2001) experimentally had shown that greater amount of swelling will cause more particle breakdown thus cause more swelling pressure. So it is expected that high polar fluids will show greater swelling pressure. Again, greater amount of particle breakdown will cause decrease in size of voids, increase in surface area which will provide for more clay-fluid interactions and thus will lead to low flow rate as we observed in macro scale permeability tests.

Interesting phenomenon was revealed from our conformational analysis of molecules. Conformation of clay-toluene sample shows that that toluene molecules tend to come out from interlayer in comparison to high polar fluid molecules. Again, we were not able to achieve experimental d_{001} spacing with even small amount (10%) of toluene, which indicates that very few or no toluene molecules present in the interlayer at experimental condition. This explains the non-swelling or very low swelling behavior in case of low polar fluids, associated lower clay-fluid molecular interactions, less particle breakdown, low swelling pressure and higher permeability for low polar fluids.

In contrary to popular idea of swelling due to repulsion of negatively charged clay sheets our study shows that interactions between interlayer cations and fluid molecules is the dominating cause for clay swelling. A result of this study provides new insight into our understanding of molecular mechanism of swelling. Our study suggests that swelling initiates by solvating interlayer cations following solvation of clay sheets. From our interaction energy values we see clay-clay electrostatic interaction is only 1-6 % of total clay fluid or Na⁺ ions fluid interactions. For dry clay electrostatic repulsion due to negative charged clay surface is balanced by the attraction of counter ions and clay sheet. But as the fluid molecules come into the interlayer they are the dominating factor. So, we can say that the contribution of electrostatic repulsion of clay surfaces is small for clay swelling in compare to the hydration of clay surface and counter ions. Similar observation was also seen qualitatively for clay-water system by (Lupe, 1997). Our conformational analysis show that 55% of total water molecules present in the 3 Å mid region of interlayer near sodium ions (Interlayer spacing is 11.5 Å; due to smaller size water molecules shows better conformation change) while a greater concentration of fluid molecules around sodium ions were observed for other fluids. From the interaction energies and conformation a higher interaction of Na⁺ ions with fluid molecules followed by clay-fluid and comparatively very small clay-clay interactions were observed.

Clay-clay and clay-sodium interactions decreases as the fluid molecules enter into the interlayer. As the amount of interlayer fluid increases more reduction in clay-clay and clay-sodium interactions occurs. Higher polarity fluids cause greater magnitude of reduction in both clay-clay and clay-sodium interactions. With increasing interaction between clay-fluid and interlayer sodium-fluid, clay sheets and sodium ions are not able to attract each other as strongly as in dry clay.

In the previous studies, a new permeability testing device was designed and fabricated as none of the commercially available permeameters can accurately measure the permeability of swelling clays. Using this newly designed permeability testing device we measured the permeability of Na-montmorillonite clays with different polarity fluids. Interestingly we see that permeability in case of high polar formamide is hundred times less than water, at the same time for the same clays shows permeability in case of low polar toluene million times greater than water. Moreover, we were able to tie this very useful macroscale phenomenon with molecular level interactions and evaluation of microstructure. Our molecular modeling study shows that greater amount of high polar fluid molecules enter into the interlayer causing high swelling and swelling pressure, consequently results in a greater amount of particle breakdown. On the other hand, low polar fluid show less swelling and swelling pressure; consequently have less influence on clay microstructure. As the swelling occurs, for high polar fluids, clay particles breakdown resulting a decrease in void spaces and more clay-fluid interaction take place which results a low permeability of high polar fluids. For low polar fluids since small amount of fluids enter into the interlayer, pore size remain same as less amount of particle breakdown occurs hence have a high permeability for low polar fluids.

In the second part of the study, theoretical and molecular modeling approaches were taken on some fundamental understanding on swelling mechanism. We performed molecular dynamics study for solvation of two different sized clay particles. The interaction energies and density distribution is quite different not only in terms of magnitude but also trends of interaction energy curves. Our study reveals that although for montmorillonite swelling clays isomorphous substitutions are the main contributor for charge in clay particle, broken bonds at the edge become very significant. We observed higher interaction energy per unit cell in case of smaller

clay particle as a result of higher edge charge per unit cell in case of smaller clay particle. The non-uniform density distribution in case of smaller clay particle may be due to complex potential distribution at different distance from claysheet.

We also addressed some fundamental assumptions associated with double layer theories. From our conformation of water molecules we see a significant affinity of water molecules towards zones of isomorphic substitutions while uniform charge distribution was assumed in double layer theories. The conformation and higher affinity at the zones of isomorphic substitutions lead to the importance of discrete charge distribution consideration in clay sheet while calculating potentials. Edge charges in clays had been neglected in double layer theories; the error associated with neglecting edge charges may be small for infinite clay sheets but may be significant for finite particle size. For kaolinites the main contributor of charge is broken bonds. For montmorillonite isomorphic substitution dominates the contribution from broken bonds. For montmorillonite isomorphous substitutions dominating charge contributor than broken bonds (Shingo, et al., 1988). But our previous study shows that particle breaks down due to swelling and deswelling (Katti and Shanmugasundaram, 2001). Mathematically, we were able to show that for regular sized clay sheet (assumed size) charge due to isomorphic substitutions is 99.25% of total charge and charge due to broken bonds at the edge is only 0.75% of total charge; hence may be neglected. Mathematically we were able to show that contribution from edge charge can be about 75% or even more with particle size approximately $21 \text{ \AA} \times 21 \text{ \AA}$.

We performed molecular dynamics simulations for solvation model of two different sized claysheets (6x3 and 4x2). Number of water molecules at different distance from clay sheet were calculated (can be represented as relative density) for both 6x3 and 4x2 solvation models. We observed a highest density of water molecules at certain distance from claysheet in case of 6x3

model and decreases after then coming to an almost uniform density which can be considered as bulk solution. We used a higher cutoff distance of 32 Å than used in literature which allows us better conformational analysis for solvation of claysheet. Our average dipole moment calculation for water molecules direction shows that as we go further away from the clay sheet, less strong orientation of water molecules towards claysheet i.e. less the influence of claysheet on water molecules. Yoshida and Iwata, (1970) (as cited by (Shingo, et al., 1988) previously reported variation of pH with distance from clay sheet although they were not able to explain the reason for the phenomenon at that time; Later on researchers observed the distance dependence of dielectric of fluids from clay surface. As we go away from the clay surface the dielectric constant of water increases and at some distance comes equal to the bulk water where no influence of claysheet present. (Sridharan and Satyamurty, 1996) showed that dielectric constant of water at Stern layer as “6” whereas bulk water has a dielectric constant 80. The dipole moment of water molecules depends on the ease of their orientation capacity. Our study shows that near the clay surface water molecules are highly oriented towards claysheet their free rotation restrained. As we go away from the claysheet this restrain of free rotation diminishes. This is may be the reason for fluids showing low dielectric constant near clay surface.

Most of the double layer theories are based on the cation concentrations in soil solution. The reason may be the focus of these studies for soil science or plant science. With the advancement of science, civil engineers can no longer depend on empirical methods. Moreover, some complicated problems for example swelling mechanism cannot be solved. For a pure soil-water condition, the applicability of double layer theories needs to be revisited. If we try to explain pure clay-water system with double layer theory, assumption as soil solution with very low ionic concentration will certainly introduced some error. This gives extremely high double

layer thickness, thus excessive repulsive force due to interactive double layers. So, for the complete understanding of swelling mechanism of expansive clays simple potential distribution for flat surface may lead to erroneous conclusions. These errors may accumulate as the particle break down due to swelling and swelling pressure. For complete understanding of swelling behavior molecular level study need to be performed considering particle breakdown.

The following are the major contribution coming out of this study:

1. Correlation has been developed for effect of fluid polarity on swelling and flow properties of swelling clays using molecular modeling and conjugate experiments.
2. Molecular model developed and simulation performed for five different clay-fluid systems at different level of swelling.
3. A quantitative estimation was made for interlayer fluids at different level of swelling for a wide range of polarity fluids.
4. Correlation has been developed for properties of swelling clays at different length scales. Molecular level clay-fluid interactions have been bridged with evaluation of microstructure, particle breakdown and macroscale swelling and flow properties.
5. Solvation of clay sheets studied using molecular dynamics simulation. The effect of discrete charge distribution, contribution of edge charges on swelling clays were investigated and discussed some fundamental assumptions associated with double layer theories.
6. Effect of discrete charge distribution and significance of edge charges with increasing swelling has been shown mathematically and using molecular simulations.
7. Finally and most importantly, this study incorporates the findings from this study and previous studies over a decade in the group which correlates the properties of swelling

clays at different length scales and provide an insight to molecular mechanism of swelling.

8.2 References

- [1] W.W. Olive, A. F. C., C.W. Frahme, Julius Schlocker, R.R. Schneider, and R.L Shuster (1989). "Swelling Clays Map Of The Conterminous United States." U. S. G. S. publication, ed.
- [2] Cornelis, K., and Dutrow, B. (2007). Manual of Mineral Science, John Wiley & Sons, Inc.
- [3] Guggenheim, S., and Martin, R. T. (1995). "Definition of clay and clay mineral - joint report of the aipea and cms nomenclature committees." Clay Minerals, 30(3), 257-259.
- [4] Jo, H. Y., Katsumi, T., Benson, C. H., and Edil, T. B. (2001). "Hydraulic conductivity and swelling of nonprehydrated GCLs permeated with single-species salt solutions." Journal of Geotechnical and Geoenvironmental Engineering, 127(7), 557-567.
- [5] M. Elimelech, J. G., Xiadong Jia, Richard Williams (1998). Particle deposition and aggregation: measurement, modelling and simulation, Butterworth-Heinemann.
- [6] Tan, K. H. (1998). Principles of soil chemistry, Marcel Dekker, Inc.
- [7] Overbeek, V. a. J. T. G. (1948). "Theory of the Stability of Lyophobic Colloids." Elsevier, Amsterdam.
- [8] Delville, A. (1991). "Modeling the clay water interface." langmuir, 7(3), 547-555.
- [9] delville, a. (1992). "structure of liquids at a solid interface - an application to the swelling of clay by water." Langmuir, 8(7), 1796-1805.
- [10] Delville, A., and Sokolowski, S. (1993). "Adsorption of vapor at a solid interface - a molecular-model of clay wetting." Journal of Physical Chemistry, 97(23), 6261-6271.

- [11] Velde, B. (1995). "Use of the smectite to illite conversion reaction model - effects of order of magnitude." Bulletin Des Centres De Recherches Exploration-Production Elf Aquitaine, 19(1), 235-242.
- [12] Schmidt, S. R. (2005). "Evaluation of clay-water interactions : a quantitative determination of clayinterlayer forces with varying hydration by steered molecular dynamics." MS, North Dakota State University,, ND, USA.
- [13] Birkeland, P. W. (1999). Soils and geomorphology, Oxford University Press, New York.
- [14] Bleam, W. F. (1993). "Atomic theories of phyllosilicates - quantum-chemistry, statistical-mechanics, electrostatic theory, and crystal-chemistry." Reviews of Geophysics, 31(1), 51-73.
- [15] Van Olphen, H. a. F., J. J (1979). Data handbook for clay materials and other non-metallic minerals, Pergamon Press, New York.
- [16] Mitchell, J. K. (1993). Fundamentals of Soil Behavior, Second Edition, John Wiley Sons, Inc.
- [17] Mitchell, J. (1993). Fundamentals of Soil Behavior, Second Edition, John Wiley & Sons, Inc., New York.
- [18] Grim, R. (1968). Clay mineralogy, 2nd Edition, McGraw-Hill, New York.
- [19] Sposito, G., Skipper, N. T., Sutton, R., Park, S. H., Soper, A. K., and Greathouse, J. A. (1999). "Surface geochemistry of the clay minerals." Proceedings of the National Academy of Sciences of the United States of America, 96(7), 3358-3364.
- [20] Dixon, J. a. W., SB (1989). Minerals in Soil Environments, 2nd Edition, Soil Science Society of America, Madison, WI.

- [21] Katti, D. R., Schmidt, S. R., Ghosh, P., and Katti, K. S. (2005). "Modeling the response of pyrophyllite interlayer to applied stress using steered molecular dynamics." *Clays and Clay Minerals*, 53(2), 171-178.
- [22] Smith, D. E., Wang, Y., and Whitley, H. D. (2004). "Molecular simulations of hydration and swelling in clay minerals." *Fluid Phase Equilibria*, 222, 189-194.
- [23] Schultz, L. G. (1969). "Lithium and potassium absorption, dehydroxylation temperature, and structural water content of aluminous smectites." *Clays and Clay Minerals*, 17(3), 115-&.
- [24] Katti, D. R., Tang, J. P., and Yazdani, S. (2003). "Undrained response of clays to varying strain rate." *Journal of Geotechnical and Geoenvironmental Engineering*, 129(3), 278-282.
- [25] Newman, A. C. D. (1987). *Chemistry of Clays and Clay Minerals*. Mineralogical Society Monograph, Longman Scientific and Technical, Harlow, Essex, England.
- [26] Low, P. F. "Fundamental mechanisms involved in the extension of clays and shales in highway design and construction." *Proc., Workshop on expansive clays and shales in highway design and construction*.
- [27] Israelachvili, J. N. (1985). "Intermolecular and Surface Forces." Academic Press: London.
- [28] Overbeek, J. T. G. (1952). "Electrokinetic phenomena." *Colloidal Science*, Vol 1, Elsevier, Amsterdam, Netherlands, 1952.
- [29] Anandarajah, A. (1997). "Influence of particle orientation on one-dimensional compression of montmorillonite." *Journal of Colloid and Interface Science*, 194(1), 44-52.
- [30] Amarasinghe, P. M. (2009). "Role of clay-fluid molecular interactions on fluid flow and mechanical behavior of swelling clays." PhD, North Dakota State University, ND, USA.
- [31] Essig, K., Urban, R. D., Birk, H., and Jones, H. (1993). "Diode-laser spectroscopy of NAD, KD, RBD, AND CSD - determination of the mass-independent parameters and mass scaling

coefficients of the alkali-metal hydrides." *Zeitschrift Fur Naturforschung Section a-a Journal of Physical Sciences*, 48(11), 1111-1114.

[32] Katti, K. S., and Katti, D. R. (2006). "Relationship of swelling and swelling pressure on silica-water interactions in montmorillonite." *Langmuir*, 22(2), 532-537.

[33] Johnston, C. T., and Premachandra, G. S. (2001). "Polarized ATR-FTIR study of smectite in aqueous suspension." *Langmuir*, 17(12), 3712-3718.

[34] Leonard, R. A. (1970). "Infrared analysis of partially deuterated water adsorbed on clay." *Soil Science Society of America Proceedings*, 34(2), 339-&.

[35] Sposito, G., and Anderson, D. M. (1975). "Infrared study of exchangeable cation hydration in montmorillonite." *Soil Science Society of America Journal*, 39(6), 1095-1099.

[36] Katti, K. S., Sikdar, D., Katti, D. R., Ghosh, P., and Verma, D. (2006). "Molecular interactions in intercalated organically modified clay and clay-polycaprolactam nanocomposites: Experiments and modeling." *Polymer*, 47(1), 403-414.

[37] Sikdar, D., Katti, D. R., and Katti, K. S. (2006). "A molecular model for epsilon-caprolactam-based intercalated polymer clay nanocomposite: Integrating modeling and experiments." *Langmuir*, 22(18), 7738-7747.

[38] Sikdar, D., Katti, D., Katti, K., and Mohanty, B. (2007). "Effect of organic modifiers on dynamic and static nanomechanical properties and crystallinity of intercalated clay-polycaprolactam nanocomposites." *Journal of Applied Polymer Science*, 105(2), 790-802.

[39] Sikdar, D., Katti, D. R., Katti, K. S., and Mohanty, B. (2009). "Influence of backbone chain length and functional groups of organic modifiers on crystallinity and nanomechanical properties of intercalated clay-polycaprolactam nanocomposites." *International Journal of Nanotechnology*, 6(5-6), 468-492.

- [40] Katti, D., and Shanmugasundaram, V. (2001). "Influence of swelling on the microstructure of expansive clays." *Canadian Geotechnical Journal*, 38(1), 175-182.
- [41] Amarasinghe, P. M., Katti, K. S., and Katti, D. R. (2009). "Nature of organic fluid-montmorillonite interactions: An FTIR spectroscopic study." *Journal of Colloid and Interface Science*, 337(1), 97-105.
- [42] Gleason, M. H., Daniel, D. E., and Eykholt, G. R. (1997). "Calcium and sodium bentonite for hydraulic containment applications." *Journal of Geotechnical and Geoenvironmental Engineering*, 123(5), 438-445.
- [43] Yao, M., and Anandarajah, A. (2003). "Three-dimensional discrete element method of analysis of clays." *Journal of Engineering Mechanics-Asce*, 129(6), 585-596.
- [44] Anandarajah, A. (2000). "On influence of fabric anisotropy on the stress-strain behavior of clays." *Computers and Geotechnics*, 27(1), 1-17.
- [45] Katti, D. R., Matar, M. I., Katti, K. S., and Amarasinghe, P. M. (2009). "Multiscale modeling of swelling clays: A computational and experimental approach." *Ksce Journal of Civil Engineering*, 13(4), 243-255.
- [46] Stillinger, F. H., and Rahman, A. (1974). "Molecular-dynamics study of liquid water under high compression." *Journal of Chemical Physics*, 61(12), 4973-4980.
- [47] Brooks, B. R., Bruccoleri, R. E., Olafson, B. D., States, D. J., Swaminathan, S., and Karplus, M. (1983). "Charmm - a program for macromolecular energy, minimization, and dynamics calculations." *Journal of Computational Chemistry*, 4(2), 187-217.
- [48] Dinur, U., and Hagler, A. T. (1990). "A Novel decomposition of torsional potentials into pairwise interactions - a study of energy 2nd derivatives." *Journal of Computational Chemistry*, 11(10), 1234-1246.

- [49] Skipper, N. T., Lock, P. A., Titiloye, J. O., Swenson, J., Mirza, Z. A., Howells, W. S., and Fernandez-Alonso, F. (2006). "The structure and dynamics of 2-dimensional fluids in swelling clays." *Chemical Geology*, 230(3-4), 182-196.
- [50] Hensen, E. J. M., Tambach, T. J., Blik, A., and Smit, B. (2001). "Adsorption isotherms of water in Li-, Na-, and K-montmorillonite by molecular simulation." *Journal of Chemical Physics*, 115(7), 3322-3329.
- [51] Park, S. H., and Sposito, G. (2003). "Do montmorillonite surfaces promote methane hydrate formation? Monte Carlo and molecular dynamics simulations." *Journal of Physical Chemistry B*, 107(10), 2281-2290.
- [52] Yu, C. H., Newton, S. Q., Norman, M. A., Schafer, L., and Miller, D. M. (2003). "Molecular dynamics simulations of adsorption of organic compounds at the clay mineral/aqueous solution interface." *Structural Chemistry*, 14(2), 175-185.
- [53] Yu, C. H., Newton, S. Q., Norman, M. A., Miller, D. M., Schafer, L., and Teppen, B. J. (2000). "Molecular dynamics simulations of the adsorption of methylene blue at clay mineral surfaces." *Clays and Clay Minerals*, 48(6), 665-681.
- [54] Sutton, R., and Sposito, G. (2002). "Animated molecular dynamics simulations of hydrated caesium-smectite interlayers." *Geochemical Transactions*, 3, 73-80.
- [55] Warne, M. R., Allan, N. L., and Cosgrove, T. (2000). "Computer simulation of water molecules at kaolinite and silica surfaces." *Physical Chemistry Chemical Physics*, 2(16), 3663-3668.
- [56] Shroll, R. M., and Smith, D. E. (1999). "Molecular dynamics simulations in the grand canonical ensemble: Application to clay mineral swelling." *Journal of Chemical Physics*, 111(19), 9025-9033.

- [57] Hwang, S., Blanco, M., Demiralp, E., Cagin, T., and Goddard, W. A. (2001). "The MS-Q force field for clay minerals: Application to oil production." *Journal of Physical Chemistry B*, 105(19), 4122-4127.
- [58] Newman, S. P., Di Cristina, T., Coveney, P. V., and Jones, W. (2002). "Molecular dynamics simulation of cationic and anionic clays containing amino acids." *Langmuir*, 18(7), 2933-2939.
- [59] Park, S., Fitch, A., and Wang, Y. L. (1997). "Computational studies compared to electrochemical measurements of intercalation of cationic compounds in wyoming montmorillonite." *Journal of Physical Chemistry B*, 101(25), 4889-4896.
- [60] Tunega, D., Benco, L., Haberhauer, G., Gerzabek, M. H., and Lischka, H. (2002). "Ab initio molecular dynamics study of adsorption sites on the (001) surfaces of 1 : 1 dioctahedral clay minerals." *Journal of Physical Chemistry B*, 106(44), 11515-11525.
- [61] Daniel Tunega*, M. H. G., and Hans Lischka (2004). "Ab Initio Molecular Dynamics Study of a Monomolecular Water Layer on Octahedral and Tetrahedral Kaolinite Surfaces." *J. Phys. Chem. B*, 108, 5930-5936.
- [62] Suter, J. L., Boek, E. S., and Sprik, M. (2008). "Adsorption of a Sodium Ion on a Smectite Clay from Constrained Ab Initio Molecular Dynamics Simulations." *Journal of Physical Chemistry C*, 112(48), 18832-18839.
- [63] Lock, P. A., and Skipper, N. T. (2007). "Computer simulation of the structure and dynamics of phenol in sodium montmorillonite hydrates." *European Journal of Soil Science*, 58(4), 958-966.
- [64] Tambach, T. J., Bolhuis, P. G., Hensen, E. J. M., and Smit, B. (2006). "Hysteresis in clay swelling induced by hydrogen bonding: Accurate prediction of swelling states." *Langmuir*, 22(3), 1223-1234.

- [65] Pintore, M., Deiana, S., Demontis, P., Manunza, B., Suffritti, G. B., and Gessa, C. (2001). "Simulations of interlayer methanol in Ca- and Na-saturated montmorillonites using molecular dynamics." *Clays and Clay Minerals*, 49(3), 255-262.
- [66] Chang, F. R. C., Skipper, N. T., and Sposito, G. (1995). "Computer-simulation of interlayer molecular-structure in sodium montmorillonite hydrates." *Langmuir*, 11(7), 2734-2741.
- [67] Smirnov, K. S., and Bougeard, D. (1999). "A molecular dynamics study of structure and short-time dynamics of water in kaolinite." *Journal of Physical Chemistry B*, 103(25), 5266-5273.
- [68] Schmidt, S. R., Katti, D. R., Ghosh, P., and Katti, K. S. (2005). "Evolution of mechanical response of sodium montmorillonite interlayer with increasing hydration by molecular dynamics." *Langmuir*, 21(17), 8069-8076.
- [69] Skipper, N. T., Chang, F. R. C., and Sposito, G. (1995). "Monte-carlo simulation of interlayer molecular-structure in swelling clay-minerals .1. Methodology." *Clays and Clay Minerals*, 43(3), 285-293.
- [70] Teppen, B. J., Rasmussen, K., Bertsch, P. M., Miller, D. M., and Schafer, L. (1997). "Molecular dynamics modeling of clay minerals .1. Gibbsite, kaolinite, pyrophyllite, and beidellite." *Journal of Physical Chemistry B*, 101(9), 1579-1587.
- [71] Hill, J. R., and Sauer, J. (1995). "Molecular mechanics potential for silica and zeolite catalysts based on ab-initio calculations .2. Aluminosilicates." *Journal of Physical Chemistry*, 99(23), 9536-9550.
- [72] Katti, D. R., Schmidt, S. R., Ghosh, P., and Katti, K. S. (2007). "Molecular modeling of the mechanical behavior and interactions in dry and slightly hydrated sodium montmorillonite interlayer." *Canadian Geotechnical Journal*, 44(4), 425-435.

- [73] Darcy, H. (1856). "Determination des lois d'écoulement de l'eau à travers." In Les Fontaines Publiques de la Ville de Dijon. Environmental Science, Policy and Management, 210 Hearst Memo- Victor Dalmont, Paris.
- [74] LaGatta, M. D., Boardman, B. T., Cooley, B. H., and David, D. E. (1997). "Geosynthetic clay liners subjected to differential settlement." Journal of Geotechnical and Geoenvironmental Engineering, 123(5), 402-410.
- [75] Bowders, J. J., Tan, J. P., and Daniel, D. E. (1997). "Expanded clay and shale aggregates for leachate collection systems." Journal of Geotechnical and Geoenvironmental Engineering, 123(11), 1030-1034.
- [76] Daniel, D. E. (1984). "Predicting hydraulic conductivity of clay liners." Journal of Geotechnical Engineering-Asce, 110(2), 285-300.
- [77] Hewitt, R. D., and Daniel, D. E. (1997). "Hydraulic conductivity of geosynthetic clay liners after freeze-thaw." Journal of Geotechnical and Geoenvironmental Engineering, 123(4), 305-313.
- [78] Ruhl, J. L., and Daniel, D. E. (1997). "Geosynthetic clay liners permeated with chemical solutions and leachates." Journal of Geotechnical and Geoenvironmental Engineering, 123(4), 369-381.
- [79] Tschebotarioff, G. (1951). Soil Mechanics, Foundations, and Earth Structures McGraw-Hill, New York.
- [80] Amarasinghe, P. M., Katti, K. S., and Katti, D. R. (2008). "Molecular Hydraulic Properties of Montmorillonite: A Polarized Fourier Transform Infrared Spectroscopic Study." Applied Spectroscopy, 62(12), 1303-1313.

- [81] Windal, T., and Shahrour, I. (2002). "Study of the swelling behavior of a compacted soil using flexible odometer." *Mechanics Research Communications*, 29(5), 375-382.
- [82] Ebina, T., Minja, R. J. A., Nagase, A. T., Onodera, Y., and Chatterjee, A. (2004). "Correlation of hydraulic conductivity of clay-sand compacted specimens with clay properties." *Applied Clay Science*, 26(1-4), 3-12.
- [83] Humphrey, W., Dalke, A., and Schulten, K. (1996). "VMD: Visual molecular dynamics." *Journal of Molecular Graphics*, 14(1), 33-&.
- [84] Phillips, J. C., Braun, R., Wang, W., Gumbart, J., Tajkhorshid, E., Villa, E., Chipot, C., Skeel, R. D., Kale, L., and Schulten, K. (2005). "Scalable molecular dynamics with NAMD." *Journal of Computational Chemistry*, 26(16), 1781-1802.
- [85] MacKerell, A. D., Bashford, D., Bellott, M., Dunbrack, R. L., Evanseck, J. D., Field, M. J., Fischer, S., Gao, J., Guo, H., Ha, S., Joseph-McCarthy, D., Kuchnir, L., Kuczera, K., Lau, F. T. K., Mattos, C., Michnick, S., Ngo, T., Nguyen, D. T., Prodhom, B., Reiher, W. E., Roux, B., Schlenkrich, M., Smith, J. C., Stote, R., Straub, J., Watanabe, M., Wiorkiewicz-Kuczera, J., Yin, D., and Karplus, M. (1998). "All-atom empirical potential for molecular modeling and dynamics studies of proteins." *Journal of Physical Chemistry B*, 102(18), 3586-3616.
- [86] Foloppe, N., and MacKerell, A. D. (2000). "All-atom empirical force field for nucleic acids: I. Parameter optimization based on small molecule and condensed phase macromolecular target data." *Journal of Computational Chemistry*, 21(2), 86-104.
- [87] Lopes, P. E. M., Lamoureux, G., Roux, B., and MacKerell, A. D. (2007). "Polarizable empirical force field for aromatic compounds based on the classical drude oscillator." *Journal of Physical Chemistry B*, 111(11), 2873-2885.

- [88] Martyna, G. J., Tobias, D. J., and Klein, M. L. (1994). "Constant-pressure molecular-dynamics algorithms." *Journal of Chemical Physics*, 101(5), 4177-4189.
- [89] Lupe, M. B. M. (1997). "Molecular Atomistic Simulations of Clay Swelling in Water Dispersions." *Molecular Engineering*, Volume 7(Numbers 3-4), 367-383.
- [90] Quirk, J. P., and Marcelja, S. (1997). "Application of double-layer theories to the extensive crystalline swelling of Li-montmorillonite." *Langmuir*, 13(23), 6241-6248.
- [91] Kleijn, W. B., and Oster, J. D. (1982). "A model of clay swelling and tactoid formation." *Clays and Clay Minerals*, 30(5), 383-390.
- [92] Yeung, A. T., and Mitchell, J. K. (1993). "Coupled fluid, electrical and chemical flows in soil." *Geotechnique*, 43(1), 121-134.
- [93] G., G. (1910). *J. Phys*, 9, 457.
- [94] Gouy (1909). "On the constitution of the electric charge at the surface of an electrolyte." *Comptes Rendus Hebdomadaires Des Seances De L Academie Des Sciences*, 149, 654-657.
- [95] Gouy, G. (1910). *J. Phys*, 457.
- [96] D.L, C. (1913). *Phil. Mag*, 25, 475.
- [97] Chapman, D. L. (1913). *Phil. Mag.*, 25, 475.
- [98] Stern, O. (1924). *Z.Electrochem*, 508.
- [99] Anderson, A. N., Crawford, J. W., and McBratney, A. B. (2000). "On diffusion in fractal soil structures." *Soil Science Society of America Journal*, 64(1), 19-24.
- [100] Papelis, C., Chen, C. C., and Hayes, K. F. (1996). "Effects of cation and sorption site type on metal ion sorption on clay minerals: An X-ray absorption spectroscopic study." *Abstracts of Papers of the American Chemical Society*, 211, 101-GEOC.

- [101] Verwey, E. J. W., and Overbeek, J. T. G. (1948). "Theory of the Stability of Lyophobic Colloids."
- [102] Sparks, D. L. (1999). Soil Physical Chemistry, CRC Press LLC.
- [103] Yates, D. E., Levine, S., and Healy, T. W. (1974). "Site-binding model of electrical double-layer at oxide-water interface." *Journal of the Chemical Society-Faraday Transactions I*, 70, 1807-1818.
- [104] Bowden, W. L., Bonnar, P., Brown, D. B., and Geiger, W. E. (1977). "Electrochemistry of nitroprusside ion in non-aqueous solvents." *Inorganic Chemistry*, 16(1), 41-43.
- [105] Debye, P., and Huckel, E. (1924). "Remarks on a note concerning cataphoretic appearances in suspended parts." *Physikalische Zeitschrift*, 25, 49-52.
- [106] Sridharan, A., and Satyamurty, P. V. (1996). "Potential-distance relationships of clay-water systems considering the Stern theory." *Clays and Clay Minerals*, 44(4), 479-484.
- [107] Fang, H.-Y. (1997). Introduction to environmental geotechnology, CRC Press.
- [108] Shingo, I., Toshio, T., and Benno, W. (1988). Soil-Water Interactions, Marcel Dekker, Inc.
- [109] Derjaguin, B., and Landau, L. (1945). "Theory of stability of highly charged lyophobic sols and adhesion of highly charged particles in solutions of electrolytes." *Zhurnal Eksperimentalnoi i Teoreticheskoi Fiziki*, 15(11), 663-682.
- [110] Derjaguin, B. V., Kabanov, B. N., Voropayev, Tn, and Titiyevs, As (1964). "Surface forces + stability of colloids + disperse systems." *Journal of Colloid Science*, 19(2), 113-&.
- [111] Derjaguin, B. V., and Churaev, N. V. (1976). "Polymolecular adsorption and capillary condensation in narrow slit pores." *Journal of Colloid and Interface Science*, 54(2), 157-175.
- [112] Derjaguin, B. V., and Churaev, N. V. (1977). "Disjoining pressure of thin-layers of binary-solutions." *Journal of Colloid and Interface Science*, 62(3), 369-380.

- [113] Derjaguin, B. V., and Churaev, N. V. (1978). "Question of determining concept of disjoining pressure and its role in equilibrium and flow of thin-films." *Journal of Colloid and Interface Science*, 66(3), 389-398.
- [114] Casimir, H. B. G., and Polder, D. (1948). "The influence of retardation on the london-vanderwaals forces." *Physical Review*, 73(4), 360-372.
- [115] Tabor, D., and Winterto.Rh (1969). "Direct measurement of normal and retarded van der waals forces." *Proceedings of the Royal Society of London Series a-Mathematical and Physical Sciences*, 312(1511), 435-&.
- [116] Tabor, D., and Winterto.Rh (1968). "Surface forces - direct measurement of normal and retarded van der waals forces." *Nature*, 219(5159), 1120-&.
- [117] Israelac.Jn, and Tabor, D. (1972). "Measurement of van-der-waals dispersion forces in range 1.4 to 130 nm." *Nature-Physical Science*, 236(68), 106-&.
- [118] Chen, S. Y., Ambe, S., Takematsu, N., and Ambe, F. (1996). "Multitracer study on removal mechanisms of metal elements from seawater." *Analytical Sciences*, 12(1), 1-6.
- [119] Israelachvili, J. N., and Adams, G. E. (1978). "Measurement of forces between 2 mica surfaces in aqueous-electrolyte solutions in range 0-100 nm." *Journal of the Chemical Society-Faraday Transactions I*, 74, 975-&.
- [120] Israelachvili, J. N. (1978). "Measurement of forces between surfaces immersed in electrolyte-solutions." *Faraday Discussions*, 65, 20-24.

CHAPTER 9. FUTURE WORKS

We recommend the following directions for the future study on clay fluid molecular interactions which we believe will be helpful for complete understanding of swelling mechanism as well as for engineering design. Also, these future studies may provide the opportunity to provide a new look on the existing theories and may reveal the mystery of clay swelling.

9.1 Experimental Works

1. Flow properties (permeability, consolidation, etc.) can be investigated for different clay-fluid samples with different amount of initial hydration which may provide important information for clay barrier system.
2. Microstructure analysis can be performed for different clay-fluid samples with different initial moisture contents.
3. Effect of initial moisture content on swelling can be investigated experimentally.

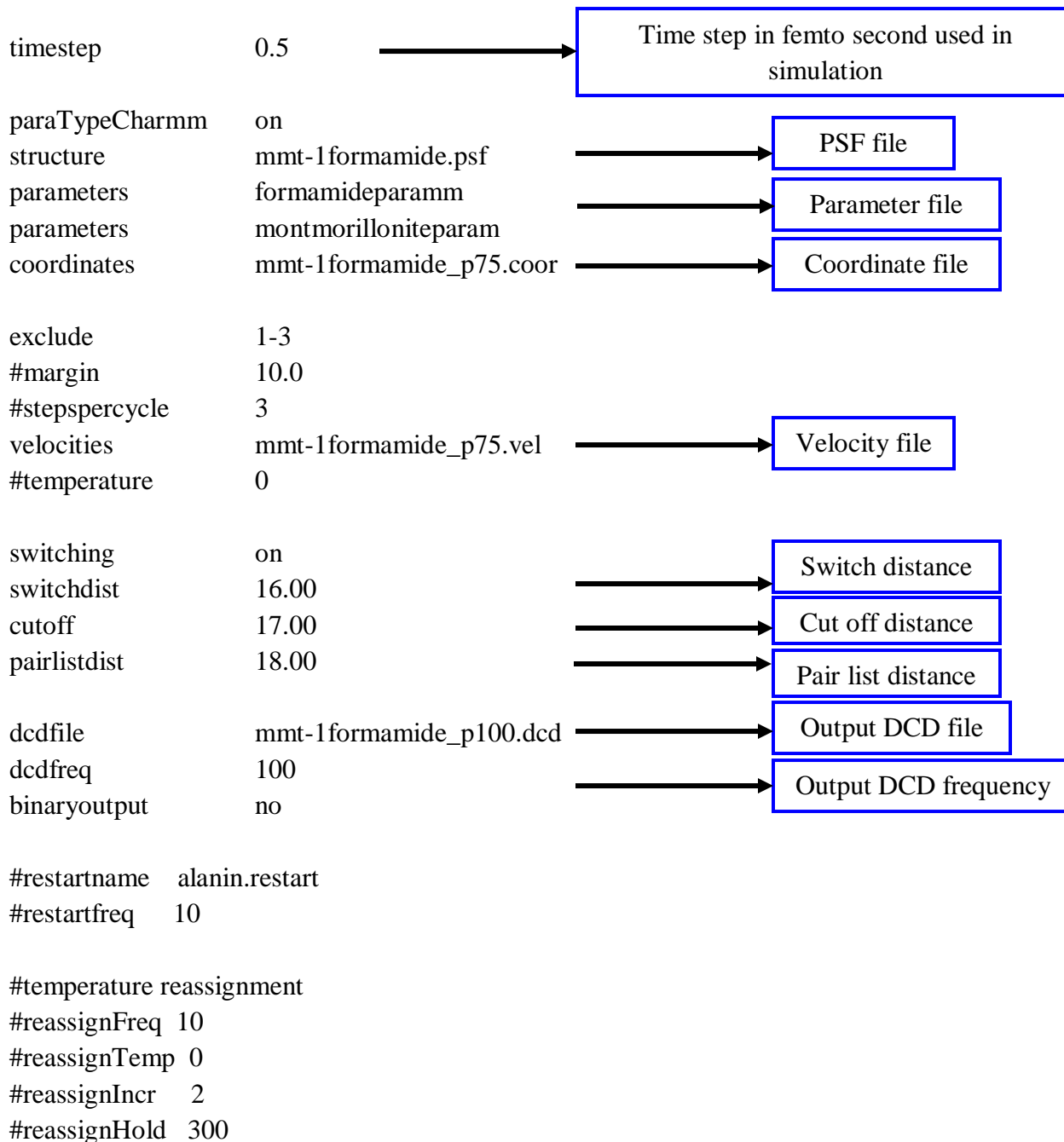
9.2 Computational Works

1. Solvation model can be prepared and simulation performed for clay with a wide range polarity fluids. Molecular level flow rate can be found for different fluids.
2. Solvation simulations can be performed to investigate the effect of ion concentration in soil solution on swelling and flow properties of swelling clays.
3. Effect of fluid polarity on pH can be investigated for different fluids at different distance from clay sheets.

CHAPTER 10. APPENDICES

10.1. Configuration files in NAMD for Molecular Dynamics Simulation

This is a test namd configuration file



langevin	on	→	Temperature used in MD simulation
langevinTemp	300		
langevinDamping	1		

langevinPiston	on	→	Pressure used in MD simulation
langevinPistonTarget	1.01325		
langevinPistonPeriod	200		
langevinPistonDecay	100		
langevinPistonTemp	300		
useFlexibleCell	yes		
useConstantArea	yes		

#IMD information

IMDon	no	→	Command of using VMD port for visualization of MD simulation
IMDport	2030		
IMDfreq	1		
IMDwait	off		

#constantforce yes
#consforcefile debaforcetest.pdb

#periodic boundary conditions

cellBasisVector1	40 0 0	→	Periodic boundary in X direction
cellBasisVector2	0 34 0	→	Periodic boundary in X direction
cellBasisVector3	0 0 34	→	Periodic boundary in X direction

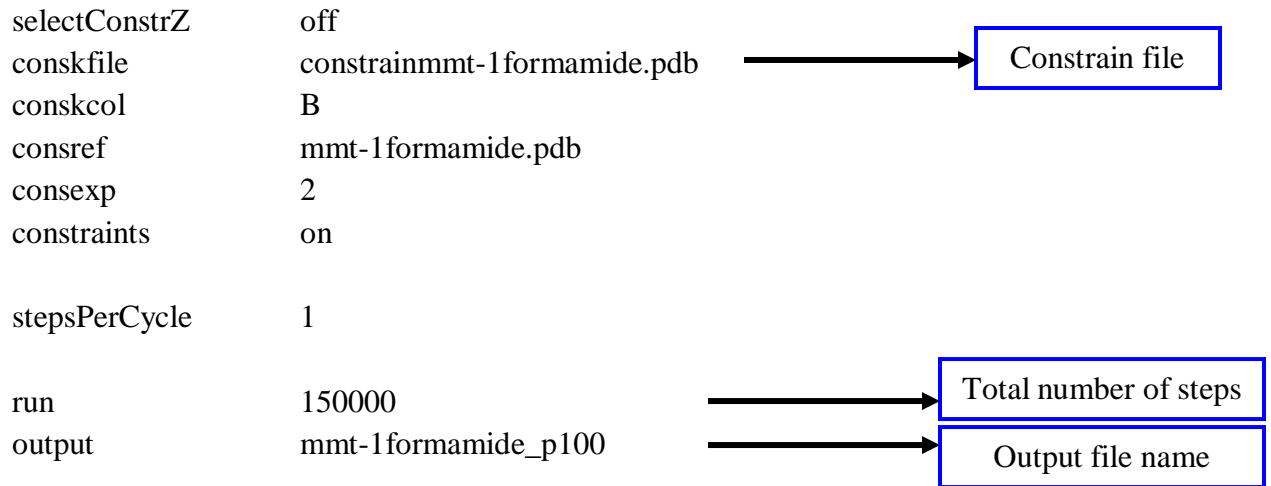
#cellOrigin 9.967 -4.228 9.720

#PME

PME	on	→	PME grid in X, Y, Z direction
PMEGridSizeX	40		
PMEGridSizeY	34		
PMEGridSizeZ	34		

#selectconstraints

selectConstraints	on
selectConstrX	on
selectConstrY	on



10.2. NAMD Generated Coordinate File (Shown Part Only)

REMARK original generated coordinate pdb file

Atom Serial	Atom Name	Residue Name	Atom Sl. No	Atom Coordinates			Column for applying force/constrain		Segment Name	
				X	X	X				
ATOM	1	AL1	PYR	1	-0.214	-14.904	-15.026	1.00	0.00	B
ATOM	2	FE2	PYR	1	2.426	-16.434	-14.988	1.00	0.00	B
ATOM	3	AL3	PYR	1	2.426	-19.474	-14.980	1.00	0.00	B
ATOM	4	AL4	PYR	1	5.066	-21.003	-14.942	1.00	0.00	B
ATOM	5	SI1	PYR	1	0.701	-19.482	-17.732	1.00	0.00	B
ATOM	6	SI2	PYR	1	0.701	-16.442	-17.740	1.00	0.00	B
ATOM	7	SI3	PYR	1	3.340	-14.912	-17.711	1.00	0.00	B
ATOM	8	SI4	PYR	1	3.341	-21.012	-17.694	1.00	0.00	B
ATOM	9	SI5	PYR	1	4.151	-16.426	-12.236	1.00	0.00	B
ATOM	10	SI6	PYR	1	1.512	-14.896	-12.274	1.00	0.00	B
ATOM	11	SI7	PYR	1	4.152	-19.466	-12.228	1.00	0.00	B
ATOM	12	SI8	PYR	1	1.512	-20.996	-12.256	1.00	0.00	B
ATOM	713	O6	PYR	18	29.715	3.377	-15.761	1.00	0.00	B
ATOM	714	O10	PYR	18	29.716	-2.723	-15.743	1.00	0.00	B
ATOM	715	O13	PYR	18	30.569	1.853	-13.625	1.00	0.00	B
ATOM	716	O14	PYR	18	27.929	3.383	-13.663	1.00	0.00	B
ATOM	717	O17	PYR	18	30.569	-1.187	-13.617	1.00	0.00	B
ATOM	718	O19	PYR	18	27.929	-2.717	-13.646	1.00	0.00	B
ATOM	719	O23	PYR	18	30.569	-4.237	-13.608	1.00	0.00	B
ATOM	720	O24	PYR	18	27.076	4.896	-15.799	1.00	0.00	B
ATOM	721	AL1	PYR	1	0.024	-14.977	1.702	1.00	0.00	C
ATOM	722	FE2	PYR	1	2.664	-16.507	1.740	1.00	0.00	C
ATOM	723	AL3	PYR	1	2.664	-19.547	1.748	1.00	0.00	C
ATOM	724	AL4	PYR	1	5.304	-21.076	1.786	1.00	0.00	C
ATOM	725	SI1	PYR	1	0.939	-19.555	-1.004	1.00	0.00	C
ATOM	726	SI2	PYR	1	0.939	-16.515	-1.012	1.00	0.00	C
ATOM	727	SI3	PYR	1	3.578	-14.985	-0.983	1.00	0.00	C
ATOM	728	SI4	PYR	1	3.579	-21.085	-0.966	1.00	0.00	C
ATOM	729	SI5	PYR	1	4.389	-16.499	4.492	1.00	0.00	C
ATOM	730	SI6	PYR	1	1.750	-14.969	4.454	1.00	0.00	C
ATOM	731	SI7	PYR	1	4.390	-19.539	4.500	1.00	0.00	C
ATOM	732	SI8	PYR	1	1.750	-21.069	4.472	1.00	0.00	C
ATOM	1432	O4	PYR	18	27.314	1.773	0.938	1.00	0.00	C
ATOM	1433	O6	PYR	18	29.953	3.304	0.967	1.00	0.00	C
ATOM	1434	O10	PYR	18	29.954	-2.796	0.985	1.00	0.00	C
ATOM	1435	O13	PYR	18	30.807	1.780	3.103	1.00	0.00	C
ATOM	1436	O14	PYR	18	28.167	3.310	3.065	1.00	0.00	C
ATOM	1437	O17	PYR	18	30.807	-1.260	3.111	1.00	0.00	C
ATOM	1438	O19	PYR	18	28.167	-2.790	3.082	1.00	0.00	C
ATOM	1439	O23	PYR	18	30.807	-4.310	3.120	1.00	0.00	C
ATOM	1440	O24	PYR	18	27.314	4.823	0.929	1.00	0.00	C

ATOM	1441	NA1	SOD	1	6.014	-17.680	-6.252	1.00	0.00	S
ATOM	1442	NA1	SOD	2	6.056	-10.317	-6.231	1.00	0.00	S
ATOM	1443	NA1	SOD	3	6.098	-1.994	-6.213	1.00	0.00	S
ATOM	1444	NA1	SOD	4	16.540	-17.694	-6.169	1.00	0.00	S
ATOM	1445	NA1	SOD	5	16.582	-10.331	-6.148	1.00	0.00	S
ATOM	1446	NA1	SOD	6	16.625	-2.009	-6.130	1.00	0.00	S
ATOM	1447	NA1	SOD	7	26.735	-17.707	-5.929	1.00	0.00	S
ATOM	1448	NA1	SOD	8	26.777	-10.343	-5.907	1.00	0.00	S
ATOM	1449	NA1	SOD	9	26.820	-2.021	-5.889	1.00	0.00	S
ATOM	1450	NA1	SOD	1	6.039	-17.686	9.739	1.00	0.00	R
ATOM	1451	NA1	SOD	2	6.081	-10.323	9.739	1.00	0.00	R
ATOM	1452	NA1	SOD	3	6.123	-2.000	9.739	1.00	0.00	R
ATOM	1453	NA1	SOD	4	16.565	-17.700	9.819	1.00	0.00	R
ATOM	1454	NA1	SOD	5	16.607	-10.337	9.819	1.00	0.00	R
ATOM	1455	NA1	SOD	6	16.650	-2.015	9.819	1.00	0.00	R
ATOM	1456	NA1	SOD	7	26.760	-17.713	9.819	1.00	0.00	R
ATOM	1457	NA1	SOD	8	26.802	-10.349	9.819	1.00	0.00	R
ATOM	1458	NA1	SOD	9	26.845	-2.027	9.819	1.00	0.00	R
ATOM	1459	HA	MOL C	1	3.319	-15.778	12.109	1.00	0.00	O1
ATOM	1460	C	MOL C	1	2.328	-15.216	12.090	1.00	0.00	O1
ATOM	1461	N	MOL C	1	2.315	-13.710	11.986	1.00	0.00	O1
ATOM	1462	H1	MOL C	1	3.271	-13.149	11.928	1.00	0.00	O1
ATOM	1463	H2	MOL C	1	1.350	-13.163	11.967	1.00	0.00	O1
ATOM	1464	O	MOL C	1	1.026	-15.976	12.171	1.00	0.00	O1
ATOM	1465	HA	MOL C	2	3.372	-21.220	12.034	1.00	0.00	O1
ATOM	1466	C	MOL C	2	2.381	-20.657	12.016	1.00	0.00	O1
ATOM	1467	N	MOL C	2	2.368	-19.152	11.911	1.00	0.00	O1
ATOM	1468	H1	MOL C	2	3.324	-18.590	11.854	1.00	0.00	O1
ATOM	1469	H2	MOL C	2	1.402	-18.605	11.892	1.00	0.00	O1
ATOM	1470	O	MOL C	2	1.079	-21.418	12.096	1.00	0.00	O1
ATOM	1471	HA	MOL C	3	3.300	-10.574	12.097	1.00	0.00	O1
ATOM	1472	C	MOL C	3	2.309	-10.012	12.078	1.00	0.00	O1
ATOM	1473	N	MOL C	3	2.296	-8.506	11.974	1.00	0.00	O1
ATOM	1474	H1	MOL C	3	3.252	-7.945	11.916	1.00	0.00	O1
ATOM	1475	H2	MOL C	3	1.330	-7.959	11.955	1.00	0.00	O1
ATOM	1476	O	MOL C	3	1.007	-10.772	12.159	1.00	0.00	O1
ATOM	1477	HA	MOL C	4	3.234	-4.688	12.102	1.00	0.00	O1
ATOM	1478	C	MOL C	4	2.243	-4.126	12.084	1.00	0.00	O1
ATOM	1479	N	MOL C	4	2.230	-2.620	11.979	1.00	0.00	O1
ATOM	1480	H1	MOL C	4	3.186	-2.059	11.921	1.00	0.00	O1
ATOM	1481	H2	MOL C	4	1.265	-2.073	11.960	1.00	0.00	O1
ATOM	1482	O	MOL C	4	0.941	-4.887	12.164	1.00	0.00	O1
END										

10.3. Part of a NAMD Generated Velocity File (Shown Part Only)

```

REMARK    FINAL VELOCITIES WRITTEN BY NAMD AT TIMESTEP 150000
ATOM      1  AL1  PYR      1      6.025  -1.639   3.457   1.00   0.00      B
ATOM      2  FE2  PYR      1     -1.373   3.326   0.943   1.00   0.00      B
ATOM      3  AL3  PYR      1     -0.535  -2.923  -3.337   1.00   0.00      B
ATOM      4  AL4  PYR      1     -1.083  -2.248   0.578   1.00   0.00      B
ATOM      5  SI1  PYR      1      3.645   3.788   4.709   1.00   0.00      B
ATOM      6  SI2  PYR      1     -2.828  -5.522   2.179   1.00   0.00      B
ATOM      7  SI3  PYR      1      5.887  -2.108  -1.142   1.00   0.00      B
ATOM      8  SI4  PYR      1     -0.750   3.075  -3.390   1.00   0.00      B
ATOM      9  SI5  PYR      1     -0.152   0.397  -1.404   1.00   0.00      B
ATOM     10  SI6  PYR      1      0.616   3.551   2.485   1.00   0.00      B
ATOM     11  SI7  PYR      1     -2.467  -0.062   1.571   1.00   0.00      B
ATOM     12  SI8  PYR      1      1.888   3.831  -1.807   1.00   0.00      B
ATOM     13  H1   PYR      1      7.542   5.221  11.195   1.00   0.00      B
ATOM     14  H2   PYR      1     19.400  -0.761   2.062   1.00   0.00      B
ATOM     15  H3   PYR      1     11.415   3.394  18.417   1.00   0.00      B
ATOM     16  H4   PYR      1     -2.317  -6.019 -20.024   1.00   0.00      B

ATOM     716  O14  PYR     18     -0.498   0.539   2.314   1.00   0.00      B
ATOM     717  O17  PYR     18     -4.081   4.575  -0.432   1.00   0.00      B
ATOM     718  O19  PYR     18      1.263   4.693  -2.311   1.00   0.00      B
ATOM     719  O23  PYR     18     -4.911  -2.177  -4.793   1.00   0.00      B
ATOM     720  O24  PYR     18      0.744  -0.047   6.448   1.00   0.00      B
ATOM     721  AL1  PYR      1     -1.791   4.093  -2.686   1.00   0.00      C
ATOM     722  FE2  PYR      1      0.748  -0.052  -0.728   1.00   0.00      C
ATOM     723  AL3  PYR      1     -1.874   4.332   3.341   1.00   0.00      C
ATOM     724  AL4  PYR      1      0.622  -1.165   2.751   1.00   0.00      C
ATOM     725  SI1  PYR      1      1.927  -0.259  -1.947   1.00   0.00      C
ATOM     726  SI2  PYR      1      1.718   0.885   0.139   1.00   0.00      C
ATOM     727  SI3  PYR      1     -0.265   4.082   0.223   1.00   0.00      C
ATOM     728  SI4  PYR      1     -1.650  -5.837  -2.103   1.00   0.00      C
ATOM     729  SI5  PYR      1      0.113   1.471  -2.511   1.00   0.00      C
ATOM     730  SI6  PYR      1     -1.337   0.714   6.896   1.00   0.00      C
ATOM     731  SI7  PYR      1      8.518   3.924  -0.082   1.00   0.00      C
ATOM     732  SI8  PYR      1      1.066  -2.682  -1.029   1.00   0.00      C
ATOM     733  H1   PYR      1      1.965 -22.787   9.293   1.00   0.00      C
ATOM     734  H2   PYR      1    -18.637  18.378   3.000   1.00   0.00      C
ATOM     735  H3   PYR      1      1.967 -17.986   1.457   1.00   0.00      C

ATOM    1436  O14  PYR     18     -0.301  -3.121  -4.149   1.00   0.00      C
ATOM    1437  O17  PYR     18     -2.033   0.430  -1.330   1.00   0.00      C
ATOM    1438  O19  PYR     18     -2.941   4.349   0.044   1.00   0.00      C
ATOM    1439  O23  PYR     18      3.934  -5.102  -2.010   1.00   0.00      C
ATOM    1440  O24  PYR     18      1.926  -0.831   0.880   1.00   0.00      C
ATOM    1441  NA1  SOD      1     -3.437   0.539   3.185   1.00   0.00      S
ATOM    1442  NA1  SOD      2     -0.997  -4.278   1.596   1.00   0.00      S
ATOM    1443  NA1  SOD      3     -3.409  -4.053   0.057   1.00   0.00      S
ATOM    1444  NA1  SOD      4     -1.939  -1.156   0.874   1.00   0.00      S
ATOM    1445  NA1  SOD      5      2.202  -2.151   4.391   1.00   0.00      S
ATOM    1446  NA1  SOD      6      2.116   2.150  -0.632   1.00   0.00      S
ATOM    1447  NA1  SOD      7     -1.293   2.404   2.493   1.00   0.00      S
ATOM    1448  NA1  SOD      8      0.289   0.724   8.036   1.00   0.00      S
ATOM    1449  NA1  SOD      9     -5.025  -8.363   3.362   1.00   0.00      S

```

ATOM	1450	NA1	SOD	1	-5.438	-1.043	4.674	1.00	0.00	R
ATOM	1451	NA1	SOD	2	0.310	-0.788	-3.570	1.00	0.00	R
ATOM	1452	NA1	SOD	3	-3.515	-0.774	1.700	1.00	0.00	R
ATOM	1453	NA1	SOD	4	-1.072	3.627	4.246	1.00	0.00	R
ATOM	1454	NA1	SOD	5	4.065	1.308	4.648	1.00	0.00	R
ATOM	1455	NA1	SOD	6	-2.137	1.085	-0.138	1.00	0.00	R
ATOM	1456	NA1	SOD	7	0.597	3.654	0.119	1.00	0.00	R
ATOM	1457	NA1	SOD	8	-4.742	2.371	3.237	1.00	0.00	R
ATOM	1458	NA1	SOD	9	-4.194	-6.180	-1.098	1.00	0.00	R
ATOM	1459	HA	MOL C	1	-7.017	25.561	11.795	1.00	0.00	O1
ATOM	1460	C	MOL C	1	-3.526	6.557	3.604	1.00	0.00	O1
ATOM	1461	N	MOL C	1	-3.761	-1.600	2.177	1.00	0.00	O1
ATOM	1462	H1	MOL C	1	1.448	5.072	-18.271	1.00	0.00	O1
ATOM	1463	H2	MOL C	1	-7.903	-8.850	32.664	1.00	0.00	O1
ATOM	1464	O	MOL C	1	2.738	7.156	-2.619	1.00	0.00	O1
ATOM	1465	HA	MOL C	2	-25.300	-18.200	-18.342	1.00	0.00	O1
ATOM	1466	C	MOL C	2	-4.633	-3.641	-3.461	1.00	0.00	O1
ATOM	1467	N	MOL C	2	-3.120	-1.680	-8.391	1.00	0.00	O1
ATOM	1468	H1	MOL C	2	23.723	-6.437	22.491	1.00	0.00	O1
ATOM	1469	H2	MOL C	2	8.689	-21.325	-10.931	1.00	0.00	O1
ATOM	1470	O	MOL C	2	-3.244	-4.057	5.854	1.00	0.00	O1
ATOM	1471	HA	MOL C	3	15.439	6.884	11.449	1.00	0.00	O1
ATOM	1472	C	MOL C	3	2.361	-3.439	-9.032	1.00	0.00	O1
ATOM	1473	N	MOL C	3	-5.203	5.803	1.168	1.00	0.00	O1
ATOM	1474	H1	MOL C	3	-9.386	7.722	28.527	1.00	0.00	O1
ATOM	1475	H2	MOL C	3	8.675	6.586	24.032	1.00	0.00	O1
ATOM	1476	O	MOL C	3	7.051	-5.341	-0.107	1.00	0.00	O1
ATOM	1477	HA	MOL C	4	18.428	8.322	-1.425	1.00	0.00	O1
ATOM	1478	C	MOL C	4	2.567	0.549	8.982	1.00	0.00	O1
ATOM	1479	N	MOL C	4	-7.526	-3.189	-10.276	1.00	0.00	O1
ATOM	1480	H1	MOL C	4	30.303	-19.394	20.885	1.00	0.00	O1
ATOM	1481	H2	MOL C	4	23.976	-32.271	-4.060	1.00	0.00	O1
ATOM	1482	O	MOL C	4	3.536	3.861	-12.515	1.00	0.00	O1
ATOM	2173	HA	MOL C	35	15.268	5.832	-34.397	1.00	0.00	O24
ATOM	2174	C	MOL C	35	1.457	-3.589	-1.002	1.00	0.00	O24
ATOM	2175	N	MOL C	35	1.992	-2.453	-3.202	1.00	0.00	O24
ATOM	2176	H1	MOL C	35	12.040	31.017	-10.160	1.00	0.00	O24
ATOM	2177	H2	MOL C	35	7.609	-16.936	-2.490	1.00	0.00	O24
ATOM	2178	O	MOL C	35	-6.661	-4.575	-6.451	1.00	0.00	O24
END										

10.4. NAMD Generated PSF Structure File (Shown Part Only)

PSF

```

1 !NTITLE
REMARKS original generated structure x-plor psf file

2034 !NATOM
  1 B 1 PYR AL1 AL 1.680000 26.9815 0
  2 B 1 PYR FE2 FE 1.680000 55.8470 0
  3 B 1 PYR AL3 AL 1.680000 26.9815 0
  4 B 1 PYR AL4 AL 1.680000 26.9815 0
  5 B 1 PYR SI1 SI 1.400000 28.0855 0
  6 B 1 PYR SI2 SI 1.400000 28.0855 0
  7 B 1 PYR SI3 SI 1.400000 28.0855 0
  8 B 1 PYR SI4 SI 1.400000 28.0855 0
  9 B 1 PYR SI5 SI 1.400000 28.0855 0
 10 B 1 PYR SI6 SI 1.400000 28.0855 0
 11 B 1 PYR SI7 SI 1.400000 28.0855 0
 12 B 1 PYR SI8 SI 1.400000 28.0855 0
 13 B 1 PYR H1 HX 0.400000 1.0079 0
 14 B 1 PYR H2 HX 0.400000 1.0079 0
 15 B 1 PYR H3 HX 0.400000 1.0079 0
 719 B 18 PYR O23 OC -0.960000 15.9994 0
 720 B 18 PYR O24 OB -0.960000 15.9994 0

 721 C 1 PYR AL1 AL 1.680000 26.9815 0
 722 C 1 PYR FE2 FE 1.680000 55.8470 0
 723 C 1 PYR AL3 AL 1.680000 26.9815 0
 724 C 1 PYR AL4 AL 1.680000 26.9815 0
 725 C 1 PYR SI1 SI 1.400000 28.0855 0
 726 C 1 PYR SI2 SI 1.400000 28.0855 0
 727 C 1 PYR SI3 SI 1.400000 28.0855 0
 728 C 1 PYR SI4 SI 1.400000 28.0855 0
 729 C 1 PYR SI5 SI 1.400000 28.0855 0
 730 C 1 PYR SI6 SI 1.400000 28.0855 0
1438 C 18 PYR O19 OC -0.910000 15.9994 0
1439 C 18 PYR O23 OC -0.960000 15.9994 0
1440 C 18 PYR O24 OB -0.960000 15.9994 0

1441 S 1 SOD NA1 NA 1.000000 22.9898 0
1442 S 2 SOD NA1 NA 1.000000 22.9898 0
1443 S 3 SOD NA1 NA 1.000000 22.9898 0
1444 S 4 SOD NA1 NA 1.000000 22.9898 0
1445 S 5 SOD NA1 NA 1.000000 22.9898 0
1453 R 4 SOD NA1 NA 1.000000 22.9898 0
1454 R 5 SOD NA1 NA 1.000000 22.9898 0
1455 R 6 SOD NA1 NA 1.000000 22.9898 0
1456 R 7 SOD NA1 NA 1.000000 22.9898 0
1457 R 8 SOD NA1 NA 1.000000 22.9898 0
1458 R 9 SOD NA1 NA 1.000000 22.9898 0

1459 O1 1 MOL HA HA 0.080000 1.0079 0
1460 O1 1 MOL C CC 0.420000 12.0067 0
1461 O1 1 MOL N NH2 -0.690000 14.0067 0

```

1462	O1	1	MOL	H1	H	0.350000	1.0079	0
1463	O1	1	MOL	H2	H	0.350000	1.0079	0
1464	O1	1	MOL	O	O	-0.510000	15.9994	0
1465	O1	2	MOL	HA	HA	0.080000	1.0079	0
1466	O1	2	MOL	C	CC	0.420000	12.0067	0
1467	O1	2	MOL	N	NH2	-0.690000	14.0067	0
1468	O1	2	MOL	H1	H	0.350000	1.0079	0
1469	O1	2	MOL	H2	H	0.350000	1.0079	0
1470	O1	2	MOL	O	O	-0.510000	15.9994	0
1471	O1	3	MOL	HA	HA	0.080000	1.0079	0
1472	O1	3	MOL	C	CC	0.420000	12.0067	0
1473	O1	3	MOL	N	NH2	-0.690000	14.0067	0
1474	O1	3	MOL	H1	H	0.350000	1.0079	0
1475	O1	3	MOL	H2	H	0.350000	1.0079	0
1476	O1	3	MOL	O	O	-0.510000	15.9994	0
1477	O1	4	MOL	HA	HA	0.080000	1.0079	0
1478	O1	4	MOL	C	CC	0.420000	12.0067	0
1479	O1	4	MOL	N	NH2	-0.690000	14.0067	0
1480	O1	4	MOL	H1	H	0.350000	1.0079	0
1481	O1	4	MOL	H2	H	0.350000	1.0079	0
1482	O1	4	MOL	O	O	-0.510000	15.9994	0
1483	O1	5	MOL	HA	HA	0.080000	1.0079	0
1484	O1	5	MOL	C	CC	0.420000	12.0067	0
1485	O1	5	MOL	N	NH2	-0.690000	14.0067	0
1486	O1	5	MOL	H1	H	0.350000	1.0079	0
1487	O1	5	MOL	H2	H	0.350000	1.0079	0

2536 !NBOND: bonds

1	32	1	36	1	40	4	78
4	71	5	31	5	20	5	21
6	32	6	18	6	20	7	17
7	33	7	18	7	19	8	34
8	21	8	22	9	63	9	35
9	24	9	25	10	267	10	24
11	66	11	37	11	25	11	28
12	38	12	26	12	27	12	28
13	29	14	30	15	39	16	40
17	248	19	46	22	45	23	10
29	2	29	3	30	2	30	3
31	3	32	2	33	41	33	2

5504 !NTHETA: angles

1	40	16	1	36	2	1	36	10
1	32	2	1	32	6	2	35	41
2	33	41	2	30	3	2	29	3
3	37	4	3	34	4	4	78	43
4	71	43	4	78	52	4	71	45
5	31	3	5	21	8	5	20	6
6	32	2	6	18	7	7	17	248
7	33	41	7	19	46	7	33	2
8	22	45	8	34	4	8	34	3
9	63	50	9	35	41	9	35	2
9	25	11	9	24	10	10	267	252
10	36	2	11	66	52	11	37	4
11	37	3	11	28	12	12	38	3

10.5. Part of a NAMD Constrain File (Shown Part Only)

REMARK original generated coordinate pdb file

Constrain applied on
claysheet, segment
'B' and 'C'



ATOM	1	AL1	PYR	1	-0.214	-14.904	-15.026	1.00	1	B
ATOM	2	FE2	PYR	1	2.426	-16.434	-14.988	1.00	1	B
ATOM	3	AL3	PYR	1	2.426	-19.474	-14.980	1.00	1	B
ATOM	4	AL4	PYR	1	5.066	-21.003	-14.942	1.00	1	B
ATOM	5	SI1	PYR	1	0.701	-19.482	-17.732	1.00	1	B
ATOM	6	SI2	PYR	1	0.701	-16.442	-17.740	1.00	1	B
ATOM	7	SI3	PYR	1	3.340	-14.912	-17.711	1.00	1	B
ATOM	8	SI4	PYR	1	3.341	-21.012	-17.694	1.00	1	B
ATOM	9	SI5	PYR	1	4.151	-16.426	-12.236	1.00	1	B
ATOM	10	SI6	PYR	1	1.512	-14.896	-12.274	1.00	1	B
ATOM	11	SI7	PYR	1	4.152	-19.466	-12.228	1.00	1	B
ATOM	12	SI8	PYR	1	1.512	-20.996	-12.256	1.00	1	B
ATOM	13	H1	PYR	1	4.206	-17.958	-16.396	1.00	1	B
ATOM	14	H2	PYR	1	0.646	-17.950	-13.572	1.00	1	B
ATOM	718	O19	PYR	18	27.929	-2.717	-13.646	1.00	1	B
ATOM	719	O23	PYR	18	30.569	-4.237	-13.608	1.00	1	B
ATOM	720	O24	PYR	18	27.076	4.896	-15.799	1.00	1	B
ATOM	721	AL1	PYR	1	0.024	-14.977	1.702	1.00	1	C
ATOM	722	FE2	PYR	1	2.664	-16.507	1.740	1.00	1	C
ATOM	723	AL3	PYR	1	2.664	-19.547	1.748	1.00	1	C
ATOM	724	AL4	PYR	1	5.304	-21.076	1.786	1.00	1	C
ATOM	725	SI1	PYR	1	0.939	-19.555	-1.004	1.00	1	C
ATOM	726	SI2	PYR	1	0.939	-16.515	-1.012	1.00	1	C
ATOM	727	SI3	PYR	1	3.578	-14.985	-0.983	1.00	1	C
ATOM	728	SI4	PYR	1	3.579	-21.085	-0.966	1.00	1	C
ATOM	729	SI5	PYR	1	4.389	-16.499	4.492	1.00	1	C
ATOM	730	SI6	PYR	1	1.750	-14.969	4.454	1.00	1	C
ATOM	1441	NA1	SOD	1	6.055	-17.690	-8.618	1.00	1	S
ATOM	1442	NA1	SOD	2	6.097	-10.327	-8.597	1.00	1	S
ATOM	1443	NA1	SOD	3	6.139	-2.004	-8.579	1.00	1	S
ATOM	1444	NA1	SOD	4	16.581	-17.704	-8.535	1.00	1	S
ATOM	1445	NA1	SOD	5	16.623	-10.341	-8.514	1.00	1	S
ATOM	1446	NA1	SOD	6	16.666	-2.019	-8.496	1.00	1	S
ATOM	1452	NA1	SOD	3	6.139	-2.004	8.800	1.00	1	R
ATOM	1453	NA1	SOD	4	16.581	-17.704	8.880	1.00	1	R
ATOM	1454	NA1	SOD	5	16.623	-10.341	8.880	1.00	1	R
ATOM	1455	NA1	SOD	6	16.666	-2.019	8.880	1.00	1	R
ATOM	1456	NA1	SOD	7	26.776	-17.717	8.880	1.00	1	R
ATOM	1457	NA1	SOD	8	26.818	-10.353	8.880	1.00	1	R
ATOM	1458	NA1	SOD	9	26.861	-2.031	8.880	1.00	1	R

Constrain applied on
claysheet, segment
'B' and 'C'



ATOM	1459	HA	MOL	C	1	10.673	-16.756	-4.992	1.00	0.00	O1
ATOM	1460	C	MOL	C	1	9.682	-16.194	-5.010	1.00	0.00	O1
ATOM	1461	N	MOL	C	1	9.669	-14.688	-5.115	1.00	0.00	O1
ATOM	1462	H1	MOL	C	1	10.625	-14.127	-5.172	1.00	0.00	O1
ATOM	1463	H2	MOL	C	1	8.703	-14.141	-5.134	1.00	0.00	O1
ATOM	1464	O	MOL	C	1	8.380	-16.954	-4.930	1.00	0.00	O1
ATOM	1465	HA	MOL	C	2	10.729	-21.134	-5.035	1.00	0.00	O1
ATOM	1466	C	MOL	C	2	9.739	-20.572	-5.053	1.00	0.00	O1
ATOM	1467	N	MOL	C	2	9.726	-19.066	-5.157	1.00	0.00	O1
ATOM	1468	H1	MOL	C	2	10.682	-18.505	-5.215	1.00	0.00	O1
ATOM	1469	H2	MOL	C	2	8.760	-18.519	-5.177	1.00	0.00	O1
ATOM	1470	O	MOL	C	2	8.437	-21.332	-4.973	1.00	0.00	O1
ATOM	1471	HA	MOL	C	3	10.648	-12.415	-5.101	1.00	0.00	O1
ATOM	1472	C	MOL	C	3	9.657	-11.853	-5.119	1.00	0.00	O1
ATOM	1473	N	MOL	C	3	9.644	-10.347	-5.224	1.00	0.00	O1
ATOM	1474	H1	MOL	C	3	10.601	-9.786	-5.281	1.00	0.00	O1
ATOM	1475	H2	MOL	C	3	8.679	-9.800	-5.243	1.00	0.00	O1
ATOM	1476	O	MOL	C	3	8.355	-12.614	-5.039	1.00	0.00	O1
ATOM	1477	HA	MOL	C	4	10.606	-7.857	-5.136	1.00	0.00	O1
ATOM	1478	C	MOL	C	4	9.615	-7.294	-5.154	1.00	0.00	O1

OS	SI	OC	100	110.6		
OS	SI	OA	100	110.6		
OS	SI	OB	100	110.6		
OS	SI	OS	100	135		
SI	OS	SI	34.933	120		
HT	OT	HT	34.933	104.52		
HT	HT	OT	0	127.74		
OC	MG	OC	80	180		
OA	MG	OA	80	180		
OB	MG	OB	80	180		
OC	MG	OA	80	90		
OC	MG	OB	80	90		
OA	MG	OB	80	90		
MG	OC	AL	198.27	109.5		
MG	OA	AL	198.27	109.5		
MG	OB	AL	198.27	109.5		
SI	OC	MG	155.74	124.5		
SI	OA	MG	155.74	124.5		
SI	OB	MG	155.74	124.5		
MG	OC	HX	34.933	118		
MG	OA	HX	34.933	118		
MG	OB	HX	34.933	118		
OC	FE	OC	80	180		
OA	FE	OA	80	180		
OB	FE	OB	80	180		
OC	FE	OA	80	90		
OC	FE	OB	80	90		
OA	FE	OB	80	90		
FE	OC	AL	198.27	109.5		
FE	OA	AL	198.27	109.5		
FE	OB	AL	198.27	109.5		
SI	OC	FE	155.74	124.5		
SI	OA	FE	155.74	124.5		
SI	OB	FE	155.74	124.5		
FE	OC	HX	34.933	118		
FE	OA	HX	34.933	118		
FE	OB	HX	34.933	118		
H	NH2	CC	50.000	120.0000		
H	NH2	H	23.000	120.0000		
NH2	CC	HA	44.000	111.00	50.00	1.98000
O	CC	HA	44.000	122.0000		
O	CC	NH2	75.000	122.50	50.00	2.37000

! DIHEDRAL PARAMETERS
DIHEDRALS

X	OS	SI	X	0	1	180	} → Dihedral Parameters
X	AL	OC	X	0	1	180	
X	AL	OA	X	0	1	180	
X	AL	OB	X	0	1	180	
X	SI	OC	X	0.722	1	180	
X	SI	OA	X	0.722	1	180	
X	SI	OB	X	0.722	1	180	

```

X   OS   AL   X   0   1   180
X   MG   OC   X   0   1   180
X   MG   OA   X   0   1   180
X     MG     OB   X   0   1 180
X     OS     MG   X   0   1 180
X     FE     OC   X   0   1 180
X     FE     OA   X   0   1 180
X     FE     OB   X   0   1 180
X     OS     FE   X   0   1 180
X     OS     OA   X   0   1 180
X     OS     OB   X   0   1 180
X     OS     OC   X   0   1 180

```

```

HA  CC  NH2  H      1.4000  2  180.00
O   CC  NH2  H      1.4000  2  180.00

```

! IMPROPER PARAMETERS

```

!IMPROPER          SI   X   X   OS   0   0
!IMPROPER          SI   X   X   OC   0   0

```

```

NONBONDED nbxmod 5 atom cdie1 shift vatom vdistance vswitch -
cutnb 14.0 ctofnb 12.0 ctonnb 10.0 eps 1.0 e14fac 1.0 wmin 1.5

```

! NON-BONDED LIST OPTIONS

```

!          eps      sigma      eps(1:4) sigma(1:4)
!          (kcal/mol) (A)
!          -----
AL  0.000 -0.150000  3.5357 ! 6.300000
OS  0.000 -1.000000  1.6837 ! 3.000000
OC  0.000 -6.000000  1.5714 ! 2.800000
OA  0.000 -6.000000  1.5714 ! 2.800000
OB  0.000 -6.000000  1.5714 ! 2.800000
SI  0.000 -0.001000  4.1531 ! 7.400000
HX  0.000 -0.000100  1.3469 ! 2.400000
HT  0.000 -0.020000  0.4770 ! 0.850000
OT  0.000 -0.300000  1.4030 ! 2.500000
NA  0.000 -0.250000  1.4030 ! 2.500000
MG  0.000 -0.150000  3.5357 ! 6.300000
FE  0.000 -0.150000  3.5357 ! 6.300000

O   0.000000 -0.120000  1.700000
CC  0.000000 -0.070000  2.000000
H   0.000000 -0.046000  0.224500
HA  0.000000 -0.022000  1.320000
NH2 0.000000 -0.200000  1.850000

```

Nonbonded Parameters

10.7. Topology File

!Topology file of 12-aminolauric acid and Montmorillonite clay sheet jointly.

!Mass file of Montmorillonite

!(Mass) (Sl.#) (Atom type) (Atomic Weight) (Periodic table representation)

Sl.#	Atom type	Atomic Weight	Periodic table representation
22	1		
MASS 1	AL	26.98154	AL
MASS 2	H	1.00794	H
MASS 3	SI	28.0855	SI
MASS 4	OS	15.9994	O
MASS 5	OC	15.9994	O
MASS 6	OT	15.9994	O
MASS 7	HT	1.00794	H
MASS 8	NA	22.98977	NA
MASS 9	FE	55.8470	FE
MASS 10	MG	24.3050	MG
MASS 11	NL	14.0067	N
MASS 12	HL	1.00794	H
MASS 13	HP	1.00794	H
MASS 14	HA	1.00794	H
MASS 15	CL	12.0067	C
MASS 16	C	12.0067	C
MASS 17	CA	12.0067	C
MASS 18	CB	12.0067	C
MASS 19	OL	15.9994	O
MASS 20	OA	15.9994	O

AUTO ANGLES DIHE

RESI SOD 1.000 ! sodium ion

GROUP

ATOM NA1 NA 1.000

RESI WAT 0.000 ! tip3p water model, generate using noangle nodihedral
GROUP

ATOM O1 OT -0.834

ATOM H1 HT 0.417

ATOM H2 HT 0.417

BOND O1 H1 O1 H2 ! H1 H2 ! removed the H-H bond ! the last bond (H-H) is
needed for shake

! ANGLE H1 O1 H2 ! required

ACCEPTOR O1

RESI PYR

ATOM AL1 AL 1.68

ATOM AL2 AL 1.68

ATOM AL3 AL 1.68

ATOM AL4 AL 1.68

ATOM SI1 SI 1.40

ATOM SI2 SI 1.40

ATOM SI3 SI 1.40

```

ATOM SI4 SI 1.40
ATOM SI5 SI 1.40
ATOM SI6 SI 1.40
ATOM SI7 SI 1.40
ATOM SI8 SI 1.40
ATOM H1 H 0.40
ATOM H2 H 0.40
ATOM H3 H 0.40
ATOM H4 H 0.40
ATOM O5 OS -0.70
ATOM O7 OS -0.70
ATOM O8 OS -0.70
ATOM O9 OS -0.70
ATOM O11 OS -0.70
ATOM O12 OS -0.70
ATOM O15 OS -0.70
ATOM O16 OS -0.70
ATOM O18 OS -0.70
ATOM O20 OS -0.70
ATOM O21 OS -0.70

```

Partial charges on the atoms
of residue 'PYR'

!Patching of bonds

```

BOND AL1 O4
BOND AL1 O14
BOND AL1 O24
BOND H1 O1
BOND O1 AL2
BOND O1 AL3
BOND H2 O2
BOND O2 AL2
BOND O2 AL3
BOND SI1 O3
BOND SI1 O9
BOND SI1 O11
BOND O3 AL3
BOND SI2 O4
BOND SI2 O7
BOND SI2 O9
BOND O4 AL2
BOND SI3 O5
BOND SI3 O6
BOND 1SI7 2O20
BOND 1SI5 2O15

```

Connectivity between the
atoms of residue 'PYR'

!Patching of angles

```

ANGLE 1O22 1SI7 2O20
ANGLE 1O18 1SI7 2O20
ANGLE 1SI7 2O20 2SI8
ANGLE 1O16 1SI5 2O15
ANGLE 1O18 1SI5 2O15
ANGLE 1SI5 2O15 2SI6
ANGLE 1O17 1SI7 2O20
ANGLE 1O13 1SI5 2O15
ANGLE 1O23 1AL4 2O19
ANGLE 1O10 1AL4 2O19

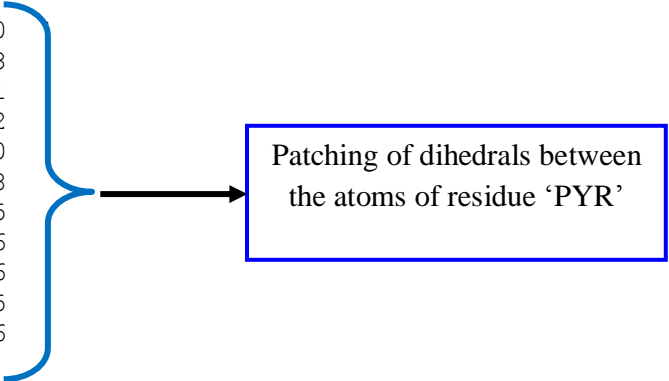
```

Patching of angles between
the atoms of residue 'PYR'

ANGLE 1017 1AL4 2019

!Patching of dihedrals

DIHE	1SI8	1O22	1SI7	2O20
DIHE	1O22	1SI7	2O20	2SI8
DIHE	1SI7	2O20	2SI8	2O21
DIHE	1SI7	2O20	2SI8	2O22
DIHE	1SI5	1O18	1SI7	2O20
DIHE	1O18	1SI7	2O20	2SI8
DIHE	1SI6	1O16	1SI5	2O15
DIHE	1O16	1SI5	2O15	2SI6
DIHE	1SI5	2O15	2SI6	2O16
DIHE	1SI7	1O18	1SI5	2O15
DIHE	1O18	1SI5	2O15	2SI6



Patching of dihedrals between
the atoms of residue 'PYR'